

# **EXPERIMENTAL AND NUMERICAL STUDIES ON SPRINGBACK OF 2-PLY AND 3-PLY LAMINATE COMPOSITES OF ALUMINIUM AND STAINLESS STEEL**

**PANKAJ KUMAR SHARMA**



**DEPARTMENT OF MECHANICAL ENGINEERING**

**DELHI TECHNOLOGICAL UNIVERSITY, DELHI**

**OCTOBER 2023**

# **EXPERIMENTAL AND NUMERICAL STUDIES ON SPRINGBACK OF 2-PLY AND 3-PLY LAMINATE COMPOSITES OF ALUMINIUM AND STAINLESS STEEL**

by

Pankaj Kumar Sharma

Under the Supervision of

Prof. Vijay Gautam

Prof. Atul Kumar Agrawal

**Department of Mechanical Engineering**

Submitted

in fulfillment of the requirements of the degree of

**Doctor of Philosophy**

to the



**DEPARTMENT OF MECHANICAL ENGINEERING**

**DELHI TECHNOLOGICAL UNIVERSITY, DELHI**

**OCTOBER 2023**

***Dedicated***

***to***

***my beloved Mother Smt. Aruna Sharma for her unconditional  
love and Blessings***

***and***

***my dear wife Vinita Sharma***

# **DELHI TECHNOLOGICAL UNIVERSITY**

(Formerly Delhi College of Engineering)

## **CANDIDATE'S DECLARATION**

I hereby declare that the thesis entitled “**Experimental and Numerical Studies on Springback of 2-Ply and 3-Ply Laminate Composites of Aluminium and Stainless Steel**” submitted by me for the award of the degree of *Doctor of Philosophy* to **Delhi Technological University (Formerly Delhi College of Engineering)** is a record of bonafide work carried out by me under the guidance of **Prof. Vijay Gautam, DTU & Prof. Atul Kumar Agrawal, DTU.**

I further declare that the work reported in this thesis has not been submitted and will not be submitted, either in part or in full, for the award of any other degree or diploma in this Institute or any other Institute or University.

**Pankaj Kumar Sharma**

Reg No. 2K16/PhD/ME/63

Department of Mechanical Engineering

Delhi Technological University, Delhi

Place. Delhi

Date

# **MECHANICAL ENGINEERING DEPARTMENT**

**DELHI TECHNOLOGICAL UNIVERSITY**

(Formerly Delhi College of Engineering)

## **CERTIFICATE**

This is to certify that the thesis entitled “**Experimental and Numerical Studies on Springback of 2-Ply and 3-Ply Laminate Composites of Aluminium and Stainless Steel**” submitted by **Mr. Pankaj Kumar Sharma** to **Delhi Technological University (Formerly DCE)**, for the award of the degree of “*Doctor of Philosophy*” in Mechanical engineering is a record of *bonafide* work carried out by him. Pankaj Kumar Sharma has worked under our guidance and supervision and has fulfilled the requirements for the submission of this thesis, which to our knowledge has reached requisite standards.

The results contained in this thesis are original and have not been submitted to any other university or institute for an award of any degree or diploma.

**Prof. Vijay Gautam**

Professor

Department of Mechanical Engineering

Delhi Technological University (DTU)

Bawana, Delhi-110042

**Prof. Atul Kumar Agrawal**

Professor

Department of Mechanical Engineering

Delhi Technological University (DTU)

Bawana, Delhi-110042

## ACKNOWLEDGEMENTS

I would like to convey my deep sense of gratitude and sincere thanks to my guides **Professor Vijay Gautam** and **Professor Atul Kumar Agrawal**, Department of Mechanical Engineering, Delhi Technological University, for giving me an opportunity to pursue this research work under their guidance. Both have been a tremendous mentor for me. Perseverance, exuberance, positive approaches are just some of the traits they have imprinted on my personality.

They steered me through this journey with his invaluable advice, positive criticism, stimulating discussions and consistent encouragement. If I will stand proud of my achievements, then undeniably they are the main creditor. It is my privilege to be under their tutelage. Their advice on both research as well as on my career have been priceless. Words are short to suffice their favour and cooperation. I am grateful to them in all respects.

I would like to express my gratitude to **Prof. S. Indu**, Vice chancellor, Delhi Technological University, Delhi for providing this opportunity to carry out this work in this prestigious institute.

I would like to thank **Prof. S.K Garg**, DRC Chairman and Head of the department Mechanical engineering, for his support to finish this work.

I wish to record my thanks and gratitude to our all Internal and External SRC experts, **Prof. Amit Kumar Srivastava** Department of Civil Engineering (Delhi Technological University), **Prof. D. Ravi** (IIT Delhi) and **Prof. Mohammed Suhaib** (Jamia Millia Islamia, New Delhi) for their valuable guidance, critical and constructive discussion during this work.

I would like to thank my fellow research scholar especially **Subhajit, Nanak Ram, Ravi, Rakesh, Bijendra and Praveen** for helping and encouraging me throughout my research. Mr. Subhajit help me a lot in my research work. Without his motivation and encouragement, pursuit of this Ph.D work would have never been possible.

I would like to thank lab assistant **Mr. OM Prakash and Mr. Tek Chand** for their help and support during the experimental work.

I take this opportunity to thank my faculty colleague especially **Dr. Ashok Kumar Yadav, Mr. Neeraj Kumar Prasad, and Mrs. Priya Sharma** who helped me directly or indirectly during this research work.

I also convey my sincere thanks to **Mr. Kuldeep Sharma**, Vice Chairman of PK Precision Tools and **Mr. Rohtas Sharma**, Chairman of PK Precision Tools for their kind support for the experimental work carried out at PK Precision Tools, Greater Noida, Uttar Pradesh, India.

I sincerely thank the anonymous reviewers whose insightful and constructive comments and suggested revisions improved the organization and clarity of the research.

I am greatly indebted to my parents for their love and blessings to see me scaling greater heights of life.

With immense pleasure and delight, I would like to thank my wife **Vinita Sharma** for giving me mental and moral support in my highs and lows of this Ph.D. journey. I appreciate my two little sons **Dhruv and Shaurya** for abiding by my neglect and the patience they showed during my Ph.D. work would never say how grateful I am to both of you.

I express my unfailing gratitude towards Raj Kumar Goel Institute of

Technology, Ghaziabad, Uttar Pradesh, for allowing me to conduct research work as a part-time scholar. I heartily thank **Prof. Ravi Shankar Prasad**, Department of Mechanical Engineering, RKGIT, for his constant and immeasurable support and encouragement.

Finally, I would like to express my thanks to Almighty 'ॐ' for giving me patience and strength to overcome all types of hindrances.

**(Pankaj Kumar Sharma)**



## **ABSTRACT**

To meet the requirement of materials having higher tensile strength to weight ratio along with corrosion resistance, the 2-ply and 3-ply clad sheets of aluminium and stainless steel are being utilized in domestic applications, manufacturing of automotive sheet metal parts, shipbuilding, and other industries. Metal clad sheet composites are a different kind of composite material where alternating metal layers are bonded together with inter-metallic bond.

The sheet metal components manufactured by forming processes may undergo some geometrical changes due to the phenomenon of springback. The behaviour of springback during bending of 2-ply and 3-ply clad sheet metals is very complex due to the combination of sheets of different mechanical properties and thicknesses.

Accurate prediction of springback in clad sheets in a bending operation will help in improving the die design by involving springback compensation. It would facilitate the optimum selection of materials, blank design, and other design variables so as to manufacture parts with minimum springback. In the present work, an analytical method has been developed that predicts the amount of springback in bending of clad sheet using input parameters from stress-strain diagrams of sheet materials like tensile properties, strain hardening exponent and anisotropy of parent sheets. The total bending moment in the analytical model at a cross sectional plane is calculated from the bending stresses for different layers. Springback is calculated by superimposing the effect of a negative bending moment of the same magnitude so as to simulate the unloading phenomenon. Numerical simulations have also been done for the simulation of V-bending of clad sheet using Abaqus software based on FEM (finite element method). Experimental work has also been carried out and compared with the simulation and

analytical results. The data from stress-strain plots for the parent and clad sheets was generated using computerized UTM. The parent and clad sheets are characterized using tensile properties, strain hardening exponent and anisotropy. The typical yield strengths (0.2% offset) of clad sheets for the tensile specimens oriented at  $0^\circ$ ,  $45^\circ$  and  $90^\circ$  are observed to be 115MPa, 117MPa and 114MPa for a 2-ply and 153.5MPa, 174MPa and 176 MPa for a 3-ply sheet, respectively. A set of three punch profile radii was used to conduct V-bending experiments for the measurement of springback on a computerized UTM. The results from the analytical model and FEM simulation are seen found to be in close agreement with the experimental results. It is observed that an increase in punch profile radius causes a significant increase in springback for both 2-ply and 3-ply clad sheets. For a 2-ply clad sheet, the bend samples (with AA1050 as inner layer ) which are oriented at  $45^\circ$  to the rolling direction, the experimental values of springback, higher than the other two orientations, are observed to be 4.12 and 4.88 with punch profile radii of 15mm and 20mm, respectively. In case of a 3-ply clad sheet, the bend samples (with SS304 as inner layer) oriented at  $90^\circ$  to the rolling direction, the experimental values of springback higher than the other two orientations, are found to be  $5.15^\circ$  and  $6.10^\circ$  with punch radii of 15mm and 20mm, respectively. Similar trend of results is obtained with analytical and simulation techniques. FE simulation results are closer to the values of experimental results than the analytical model results. The analytical model assumes a plane strain condition and neglects the neutral axis shift. These assumptions are not made for the simulation. Also, a more robust material model is used in FE simulations.

The effect of sheet setting on the die is also investigated in this work. Effect of the position of aluminium sheet at both inner and outer layers is studied. Sheet setting

conditions affect the values of springback due to the tensile strength variations and different bending radii during V-bending operations. For both the sheet settings, the residual stresses as predicted Abaqus simulations are in good agreement with the experimental results except for a few cases.

***Keywords:*** *Clad sheets, Springback, V-bending, Anisotropy, Analytical Model, FE Simulation.*

## TABLE OF CONTENT

| <b>Topics</b>   | <b>Page no</b> |
|---|----------------|
| Candidate's Declaration   | i              |
| Certificate   | ii             |
| Acknowledgement   | iii-v          |
| Abstract  | vi-viii        |
| Table of Contents   | ix-xii         |
| List of Figures   | xiii-xx        |
| List of Tables  | xxi-xxii       |
| List of Abbreviations   | xxiii          |
| Nomenclatures   | xxiv-xxv       |
| <b>Chapter 1 Introduction</b>   | <b>1-19</b>    |
| 1.1 Sheet metal forming   | 1              |
| 1.2 Bending   | 5              |
| 1.3 Clad sheet metals   | 11             |
| 1.3.1 Manufacturing of clad sheet metals                                  | 12             |
| 1.3.2 2-ply and 3-ply laminate composite of aluminium and stainless steel | 17             |
| 1.3.3 Advantages of aluminium/ stainless steel-clad sheets                | 17             |
| 1.3.4 Application of aluminium/ stainless steel-clad sheets               | 18             |
| <b>Chapter 2 Literature Review</b>  | <b>20 - 32</b> |
| 2.1 Springback in conventional blanks/monolithic Sheets                   | 20             |
| 2.2 Springback in clad sheet  | 24             |
| 2.3 Springback influencing factors  | 28             |

|   |  |                |
|---|--|----------------|
| 2.3.1   | Modulus of elasticity or Young's modulus (E)                             | 28             |
| 2.3.2   | Sheet thickness (t)  | 29             |
| 2.3.3   | Flow stress ( $\sigma_0$ ) or yield stress and strain hardening exponent | 29             |
| 2.3.4   | Anisotropy   | 30             |
| 2.4   | Research gaps and motivation   | 31             |
| 2.4.1   | Research gaps  | 31             |
| 2.4.2   | Research objectives  | 31             |
| <b>Chapter 3 Development of Analytical Model</b>                    |  | <b>33 - 54</b> |
| 3.1   | Development of the analytical model for 2-ply sheet                      | 33             |
| 3.1.1   | Case-I Bending of the two-ply sheet with SS430 as the inner layer        | 38             |
| 3.1.2   | Case-II Bending of a two-ply sheet with AA1050 as the inner layer        | 40             |
| 3.2   | Development of the analytical model for 3-ply sheet                      | 43             |
| 3.2.1   | Case-I Bending of three-ply sheet with SS430 as the inner layer          | 47             |
| 3.2.2   | Case-II Bending of three-ply sheet with SS304 as the inner layer         | 50             |
| 3.3   | Summary of the chapter   | 52             |
| <b>Chapter 4 Springback Prediction by Finite Element Simulation</b> |  | <b>55 - 69</b> |
| 4.1   | About the software   | 56             |
| 4.2   | Modelling and simulations of bending process                             | 56             |
| 4.3   | Numerical simulations of clad sheet                                      | 58             |
| 4.3.1   | Modelling and meshing  | 58             |
| 4.3.2   | Boundary conditions and simulations                                      | 63             |
| 4.4   | Measurement of residual stress numerically                               | 68             |

|                  |  |                |
|------------------|--|----------------|
| <b>Chapter 5</b> | <b>Experimental Procedure</b>  | <b>70 - 93</b> |
| 5.1              | Material selection   | 71             |
| 5.1.1            | Microstructural examination of 2-ply and 3-ply clad sheets                                     | 71             |
| 5.2              | Determination of tensile properties and anisotropy   | 73             |
| 5.3              | Microhardness measurement  | 83             |
| 5.4              | Determination of springback for clad sheet   | 84             |
| 5.5              | Measurement of residual stress   | 92             |
| <b>Chapter 6</b> | <b>Results and Discussion</b>  | <b>94 -151</b> |
| 6.1              | Chemical compositions of two-ply and three-ply clad sheet                                      | 94             |
| 6.1.1            | Chemical composition of 2-ply clad sheet   | 94             |
| 6.1.2            | Chemical composition of three-ply clad sheet   | 94             |
| 6.2              | Microstructural analysis of the 3-ply and 2-ply clad sheets                                    | 95             |
| 6.3              | Tensile properties   | 96             |
| 6.3.1            | Tensile properties of 2-ply sheet  | 96             |
| 6.3.2            | Tensile properties of 3-ply sheet  | 99             |
| 6.4              | Microhardness  | 101            |
| 6.4.1            | Microhardness of 2-ply clad sheet  | 101            |
| 6.4.2            | Microhardness of 3-ply clad Sheet  | 102            |
| 6.5              | Springback characteristics   | 103            |
| 6.5.1            | Springback analysis of 2-ply clad sheet  | 103            |
| 6.5.2            | Springback analysis of 3-ply clad sheet  | 110            |
| 6.5.3            | Springback analysis for varying punch radius   | 114            |
| 6.6              | Distribution of longitudinal and residual stress through the thickness<br>for 2-ply clad sheet | 123            |

|  |   |                  |
|--|---|------------------|
| 6.7  | Distribution of longitudinal and residual stress through the thickness for 3-ply clad sheet | 131              |
| 6.8  | Industrial significance of the present research work  | 141              |
| 6.9  | Other people's work and discussion  | 142              |
| 6.10   | Limitations of present research work  | 150              |
| <b>Chapter 7 Conclusions and Future Research Scope</b> |   | <b>152 - 156</b> |
| 7.1  | Summary   | 152              |
| 7.2  | Conclusions   | 153              |
| 7.3  | Future research work  | 155              |
| <b>References</b>                                      |   | <b>157 - 167</b> |

## LIST OF FIGURES

| <b>Fig. No</b> | <b>Title</b>   | <b>Page No</b> |
|----------------|--|----------------|
| Fig. 1.1       | Deep drawing process   | 2              |
| Fig. 1.2       | A complete deep drawing process to get a final product   | 3              |
| Fig. 1.3       | Roll forming line  | 4              |
| Fig. 1.4       | Stretch forming  | 5              |
| Fig. 1.5       | V-bending operation  | 7              |
| Fig. 1.6       | Common bending operations  | 7              |
| Fig. 1.7       | Springback in bending showing stress distribution before and after springback through thickness                    | 9              |
| Fig. 1.8       | Springback reducing methods in V-bending   | 10             |
| Fig. 1.9       | Schematic representation of diffusion bonding  | 13             |
| Fig. 1.10      | Schematic representation of explosive cladding   | 14             |
| Fig. 1.11      | Schematic of cold roll bonding process   | 15             |
| Fig. 1.12      | Manufacturing process for AlZn4SiPb/steel laminated sheet  | 16             |
| Fig. 1.13      | Representation of mechanical properties by the cladding of SS and Al metal   | 17             |
| Fig. 1.14      | Various components manufactured by using aluminium/stainless steel-clad sheets                                     | 19             |
| Fig. 2.1       | Comparison of (a) elastic recovery in two different steels and (b) springback in U-bending of two different steels | 30             |
| Fig. 3.1       | Schematic of plane-strain bending of two-ply sheet   | 34             |



|          |  |    |
|----------|--|----|
| Fig. 3.2 | (a) Transverse section of a two-ply sheet AA 1050/SS 430) (b) Transformed section      | 37 |
| Fig. 3.3 | Transverse section of a two-ply sheet with SS430 as the inner layer                    | 38 |
| Fig.3.4  | Transverse section of a two-ply sheet with an AA1050 as the inner layer                | 41 |
| Fig.3.5  | Change in bend angle after springback  | 43 |
| Fig.3.6  | Plane strain bending of a three-ply clad sheet   | 44 |
| Fig.3.7  | (a) Cross-section of a three-ply clad sheet and (b) Equivalent transformed section     | 46 |
| Fig.3.8  | Cross-section of a clad sheet with SS430 as the inner layer                            | 47 |
| Fig. 3.9 | Cross-section of a three-ply clad sheet with a SS304 as the inner layer during bending | 50 |
| Fig.4.1  | CAD model of (a) Punch and (b) Die for blank of 2-ply clad sheet                       | 58 |
| Fig.4.2  | CAD model of blank of 2-ply clad sheet   | 59 |
| Fig.4.3  | Meshed model of blank of 2-ply clad sheet  | 59 |
| Fig.4.4  | CAD model of (a) Punch and (b) Die for blank of 3-ply clad                             | 61 |
| Fig.4.5  | CAD model of blank of 3-ply clad sheet   | 61 |
| Fig.4.6  | Meshed model of blank of 3-ply clad sheet  | 62 |
| Fig.4.7  | Assembly of die, punch, and 2-ply blank  | 63 |
| Fig.4.8  | Boundary conditions for simulation of bending of 2-ply blank                           | 64 |

|          |  |    |
|----------|--|----|
| Fig.4.9  | Loaded and unloaded frames after springback of a 2-ply sheet (oriented 45° w.r.t. R.D.) with SS430 as an inner layer for punch radius 15mm   | 65 |
| Fig.4.10 | Loaded and unloaded frames after springback of a 2-ply sheet (oriented 45° w.r.t. R.D.) with AA1050 as an inner layer for punch radius 15 mm | 66 |
| Fig.4.11 | Loaded and unloaded frames after springback of a 3-ply sheet for punch radius 15 mm  | 66 |
| Fig.4.12 | Surfaces of blank plotted using CAE interface before and after springback  | 67 |
| Fig.4.13 | Loaded and unloaded frames after springback of AA1050 specimen (oriented 0° w.r.t. R.D.) for punch radius 15 mm                              | 68 |
| Fig.4.14 | Loaded and unloaded frames after springback of SS430 specimen (oriented 0° w.r.t. R.D.) for punch radius 15 mm                               | 68 |
| Fig. 5.1 | Schematic diagram of the whole experimental plan   | 70 |
| Fig. 5.2 | Laser cutting of tensile samples in progress   | 73 |
| Fig. 5.3 | Tensile samples of 3-ply sheet with different orientations   | 73 |
| Fig. 5.4 | Tensile samples of 2-ply sheet with different orientations   | 74 |
| Fig. 5.5 | Anisotropy samples of 2-ply sheet with different orientations  | 74 |
| Fig. 5.6 | Separation process of SS430 and SS304 from 3-ply sheet by immersing into NaOH Solution   | 75 |
| Fig. 5.7 | Tensile samples of SS430 sheet with different orientations   | 75 |
| Fig. 5.8 | Tensile samples of SS304 sheet with different orientations   | 76 |

|           |   |    |
|-----------|---|----|
| Fig. 5.9  | Experimental setup used for removal of SS430 from 2-ply clad sheet  | 77 |
| Fig. 5.10 | Tensile samples of AA1050 separated from 2-ply sheet  | 78 |
| Fig. 5.11 | Anisotropy samples of AA1050 separated from 2-ply sheet   | 78 |
| Fig. 5.12 | Size description of sample of tensile and anisotropic test (All dimensions are in mm)   | 79 |
| Fig. 5.13 | Size description of sub size sample of tensile and anisotropic test for AA1050 (All dimensions are in mm)   | 79 |
| Fig. 5.14 | Performing tensile test on 50kN table top UTM (make: Tenius Olsen)  | 80 |
| Fig. 5.15 | ln (true stress)-ln (true strain) plots of AA1050 at (a) 0°, (b) 45° and (c) 90° to R.D.  | 82 |
| Fig. 5.16 | Duramin 40 Microhardness tester   | 84 |
| Fig. 5.17 | Design of punches and dies for V-bending experiments (dimensions in mm): (a)-(e) Dies for a punch profile radius of 15mm, (f) Punch with profile radius of 15mm, (g)-(k) Dies for a punch profile radius of 17.5mm, (l) Punch with profile radius of 17.5mm, (m)-(q) Dies for a punch profile radius of 20mm and (r) Punch with profile radius of 20 mm | 87 |
| Fig. 5.18 | Experimental setup for V-bending operation  | 88 |
| Fig. 5.19 | Cutting of bending samples on Wire-Cut EDM  | 89 |
| Fig. 5.20 | Bending samples of 2-ply sheet with different orientations  | 90 |
| Fig. 5.21 | Bent samples of AA1050, SS430 and SS304   | 91 |

|           |  |     |
|-----------|--|-----|
| Fig. 5.22 | Bent samples of 2-ply and 3-ply clad sheets  | 91  |
| Fig. 5.23 | Sensor-based vision inspection machine for angle measurement   | 92  |
| Fig. 5.24 | (a) Experimental set-up for residual stress measurement using an X-ray machine and (b) Measurement of residual stress in progress                                      | 92  |
| Fig. 6.1  | Microstructure of 3-ply clad sheet (SS430/AA1050/SS304) at 600X  | 96  |
| Fig. 6.2  | Microstructure of 2-ply clad sheet (SS430/AA1050) at 600X  | 96  |
| Fig. 6.3  | True stress-true strain plots of a 2-ply clad, SS430 and AA1050 sheet samples  | 99  |
| Fig. 6.4  | True stress-true strain plots of three-ply clad sheet and individual layers  | 101 |
| Fig. 6.5  | Impressions of hardness tester (DURAMIN-40 M1) in SS430/AA1050/SS304 clad sheet  | 103 |
| Fig. 6.6  | Surfaces of blank of AA1050 (oriented 0° to R.D.) plotted using CAE interface before and after springback  | 105 |
| Fig. 6.7  | Comparison of predicted springback results with experimental in bending operation of a 2-ply sheet for punch radius 15 mm (a) inner layer SS430 (b) inner layer AA1050 | 107 |
| Fig. 6.8  | Central part of laminated sheets during V-bending for 45-degree orientation: (a) AA_out/SS_in and (b) AA_in/SS_out (c) actual image of AA_out/SS_in and AA_in/SS_out   | 109 |

|           |  |     |
|-----------|--|-----|
| Fig. 6.9  | Stress distribution in 2-ply sample with varying thickness and bending radius  | 109 |
| Fig. 6.10 | Comparison of experimental values of springback of individual layers for punch radius 15 mm  | 111 |
| Fig. 6.11 | Stress distribution in 3-ply sample with varying bending radius  | 113 |
| Fig. 6.12 | Springback results of a 3-ply clad sheet for punch radius 15 mm (a) inner layer SS430 and (b) inner layer SS304  | 114 |
| Fig. 6.13 | Experimental and simulated springback results of a 2-ply clad sheets, oriented at (a) 0°, (b) 45° and (c) 90° for varying punch radius when SS430 taken as an inner layer  | 116 |
| Fig. 6.14 | Experimental and simulated springback results of a 2-ply clad sheets, oriented at (a) 0°, (b) 45° and (c) 90° for varying punch radius when AA1050 taken as an inner layer | 117 |
| Fig. 6.15 | Experimental and simulated springback results of a 3-ply clad sheet, oriented at (a) 0°, (b) 45° and (c) 90° for varying punch radius when SS430 taken as an inner layer   | 119 |
| Fig. 6.16 | Experimental and simulated springback results of a 3-ply clad sheet, oriented at (a) 0°, (b) 45° and (c) 90° for varying punch radius when SS304 taken as an inner layer   | 120 |
| Fig. 6.17 | Experimental and analytical springback results of a 3-ply sheet oriented at (a) 0°, (b) 45° and (c) 90° for varying punch radius when SS 430 taken as an inner layer       | 122 |

|           |  |     |
|-----------|--|-----|
| Fig. 6.18 | Experimental and analytical springback results of a 3-ply sheet oriented at (a) 0°, (b) 45° and (c) 90° for varying punch radius when SS 304 taken as an inner layer   | 123 |
| Fig. 6.19 | Variation of longitudinal and residual stress through thickness (a), (c) and (e) with SS430 as inner layer; and (b), (d) and (f) with AA1050 as inner layer for three different orientations at 15 mm punch profile radius   | 126 |
| Fig. 6.20 | Variation of longitudinal and residual stress through thickness (a), (c) and (e) with SS430 as inner layer; and (b), (d) and (f) with AA1050 as inner layer for three different orientations at 17.5 mm punch profile radius | 129 |
| Fig. 6.21 | Variation of longitudinal and residual stress through thickness (a), (c) and (e) with SS430 as inner layer; and (b), (d) and (f) with AA1050 as inner layer for three different orientations at 20 mm punch profile radius   | 131 |
| Fig. 6.22 | Distribution of longitudinal and residual stress through thickness (a), (c) and (e) with SS430 as inner layer; (b), (d) and (f) with SS304 as inner layer for three different orientations at 15 mm punch profile radius     | 136 |
| Fig. 6.23 | Distribution of longitudinal and residual stress through thickness (a), (c) and (e) with SS430 as inner layer; (b), (d) and (f) with SS304 as inner layer for three different orientations at 17.5 mm punch profile radius   | 138 |

Fig. 6.24                      Distribution of longitudinal and residual stress through thickness    140  
(a), (c) and (e) with SS430 as inner layer; (b), (d) and (f) with  
SS304 as inner layer for three different orientations at 20 mm  
punch profile radius

## LIST OF TABLES

| <b>Table No</b> | <b>Titles</b>   | <b>Page No</b> |
|-----------------|---|----------------|
| Table 3.1       | Comparison of analytical models for monolithic sheets.  | 53             |
| Table 3.2       | Comparison of analytical models of laminated sheets   | 53             |
| Table 4.1       | Details of elements and nodes for the simulations of 2-ply clad sheet   | 60             |
| Table 4.2       | Details of elements and nodes for the simulations of 3-ply clad sheet   | 62             |
| Table 4.3       | List of fixed and variable parameters   | 65             |
| Table 4.4       | Captured coordinates from loaded and unloaded frames of 2-ply clad blank oriented at 45° w.r.t. R.D. for 15 mm punch radius | 67             |
| Table 6.1       | Chemical composition of individual layers of the 2-ply sheet in wt%.  | 94             |
| Table 6.2       | Chemical composition of individual layers of the clad sheet in wt%.   | 95             |
| Table 6.3       | Tensile properties of 2-ply sheet   | 97             |
| Table 6.4       | Tensile properties of AA1050 layer  | 98             |
| Table 6.5       | Tensile properties of SS430 layer   | 98             |
| Table 6.6       | Tensile properties of a 3-ply clad sheet  | 99             |
| Table 6.7       | Tensile properties of individual layers   | 100            |
| Table 6.8       | Microhardness of individual layers of the 2-ply clad sheet  | 101            |
| Table 6.9       | Microhardness of individual layers of the 3-ply clad sheet  | 102            |
| Table 6.10      | Springback results of SS430 and AA1050 for punch radius 15 mm   | 103            |
| Table 6.11      | Captured coordinates from loaded and unloaded frames of AA1050 blank oriented at 0° w.r.t. R.D. for 15 mm punch radius      | 104            |
| Table 6.12      | Comparison of predicted springback results with experimental in bending operation of a 2-ply sheet for punch radius 15 mm   | 106            |



|            |  |     |
|------------|--|-----|
| Table 6.13 | Thickness and max punch load for V-bent laminated sheet when punch having 15 mm radius       | 110 |
| Table 6.14 | Springback results of a 3-ply clad sheet for punch radius 15 mm                              | 113 |
| Table 6.15 | Experimental and simulated springback results of a 2-ply clad sheet for varying punch radius | 115 |
| Table 6.16 | Numerical and Experimental springback results of a 3-ply sheet for varying bending radius    | 118 |
| Table 6.17 | Analytical and Experimental springback results of a 3-ply sheet for varying bending radius   | 121 |
| Table 6.18 | Comparison of experimental and simulation results for 3-ply clad sheet                       | 132 |
| Table 6.19 | Comparison of bending and springback studies   | 142 |

## LIST OF ABBREVIATIONS

|      |  |
|------|--|
| AHSS | Advanced High Strength Steel               |
| ASTM | American Society for Testing and Materials |
| CAE  | Computer Aided Engineering                 |
| EAM  | Equivalent Area Method                     |
| FE   | Finite Element                             |
| FEA  | Finite Element Analysis                    |
| FEM  | Finite Element Method                      |
| HSLA | High Strength Low Alloy                    |
| HV   | Vickers Hardness                           |
| PPR  | Punch Profile radius                       |
| RD   | Rolling Direction                          |
| TWBs | Tailor Welded Blanks                       |
| UTM  | Universal Testing Machine                  |
| UTS  | Ultimate Tensile Strength                  |
| YS   | Yield Strength                             |

## NOMENCLATURES

|   |  |
|---|--|
| $dF_x$                                      | Elemental bending force along x-axis                             |
| $dz$  | Thickness of the element   |
| $\sigma_{x(elastic)}, \sigma_{x1(plastic)}$ | Bending stress along x-axis in elastic region and plastic region |
| $\sigma_{0x}$                               | Yield stress along x-axis  |
| $\sigma'_0$                                 | Yield stress in plane strain condition                           |
| $w$   | Width of the bending sample                                      |
| $t_1, t_2, t_3$                             | Thickness of the AA1050, SS430 and SS304 sheets<br>respectively  |
| $r, r'$                                     | Initial and final radii of curvature                             |
| $z$   | Distance of the element from neutral plane                       |
| $z_e$                                       | Distance of the elastic core from neutral plane                  |
| $\epsilon_x$                                | True strain along x-axis   |
| $\epsilon_{0x}$                             | Strain at yield along x-axis (parallel to rolling direction)     |
| $E$   | Elastic modulus  |
| $E'$  | Modulus of elasticity in plane-strain condition                  |
| $\nu$                                       | Poisson's ratio  |
| $n$   | Strain hardening exponent  |
| $K$   | Strength coefficient   |
| $K'$  | Strength coefficient in plane-strain condition<br>respectively   |
| $M_1, M_2$ and $M_3$                        | Bending moments of AA1050, SS430, and SS304 respectively         |

|                                |  |
|--------------------------------|--|
| $M$                            | Total bending moment   |
| $R_0, R_{90}$                  | Plastic strain ratio in rolling and transverse directions respectively |
| $C_1, C_2$                     | Constants depending on $R_0$ and $R_{90}$                              |
| $\bar{\sigma}, \bar{\epsilon}$ | Effective stress and effective strain                                  |
| $\theta$                       | Included bend angle  |
| $\theta_{sb}$                  | Springback   |
| $\theta_i, \theta_f$           | Initial and final included bend angle                                  |
| $\alpha_i, \alpha_f$           | Initial and final bend angle   |
| $K_s$                          | Springback ratio   |

# CHAPTER 01

## INTRODUCTION

### 1.1 Sheet metal forming

Several metallic parts of home appliances, aircraft, automobiles and building products are manufactured by deformation routes. This comprises well known manufacturing methods like sheet metal forming, forging, extrusion, rolling and hydroforming. The increasing competitiveness between industries and the demand of fuel-efficient lightweight automobiles have prompted the industries to think upon the introduction of new materials and increasing accuracy of manufacture by low-cost production processes. Several parts of a vehicle body are made by forming processes. B. Osgurg (2012) reported that the number of hot stamping parts in a Volvo car body have increased by 50 times in the last few decades. These forming processes include rolling, extrusion, forging and sheet metal forming.

Sheet metal forming is a process in which a thin sheet metal blank undergoes a permanent change in shape due to plastic deformation without failure. In today's era, sheet metal forming is playing an important role in modern manufacturing industries as it allows the production of high-quality sheet metal parts with complex shape at a low cost to fulfil the demands of design and manufacturing engineers in the field of automobiles, ship building, aviation, building products and home appliances etc. The important sheet metal forming processes which are widely used in industries are deep drawing, roll forming, stretching, and bending.

In sheet metal forming, deep drawing is a process where the sheet metal blank is stretched into a desired shape. A punch moves downward towards the sheet metal blank and try to pushes it into a die cavity so that it can achieve the desired shape. In deep drawing process, tensile forces deform the sheet metal blank plastically into a cup-shaped part. The deep drawn components having drawing depth more than half of the punch diameter. In deep drawing

process, parts are drawn in various cross-sections with curved, tapered, or straight walls but rectangular, square, and cylindrical parts are more common in actual practices. Ductile sheet metals like steel, brass, copper, and aluminum alloys are widely used in deep drawing processes to make various parts such as kitchen sinks, cups, cans, fuel tanks and automotive bodies etc. The deep drawing operation needs a tool and a die, a blank and blank holder as shown in Fig.1.1.

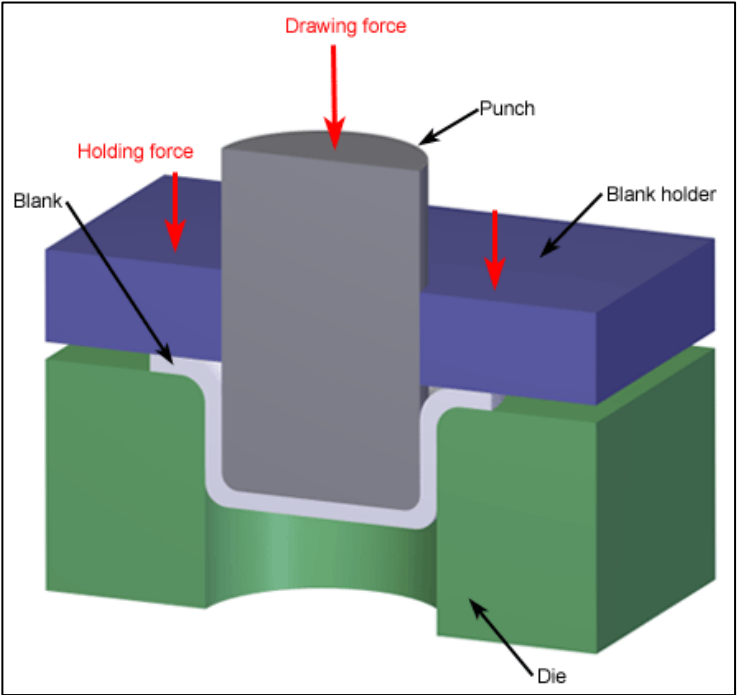


Fig. 1.1 Deep drawing process [Custompartnet.com, 2018]

The blank holder is used to clamp the blank on the die, having cavity centrally. The tool which is known as punch, pushes the blank towards die cavity and stretches the blank into cavity. Generally, punch is hydraulically powered so that sufficient force can be applied to the blank. During the application of forces by the punch on the sheet metal blank, both punch and die are affected by wear and tear, hence these are made of tool steels. Sometimes the entire drawing process is completed in a series of operations, known as draw reduction. In each step, a punch or tool pushes the sheet metal blank into a different die and stretching the sheet metal blank to a greater depth each time.

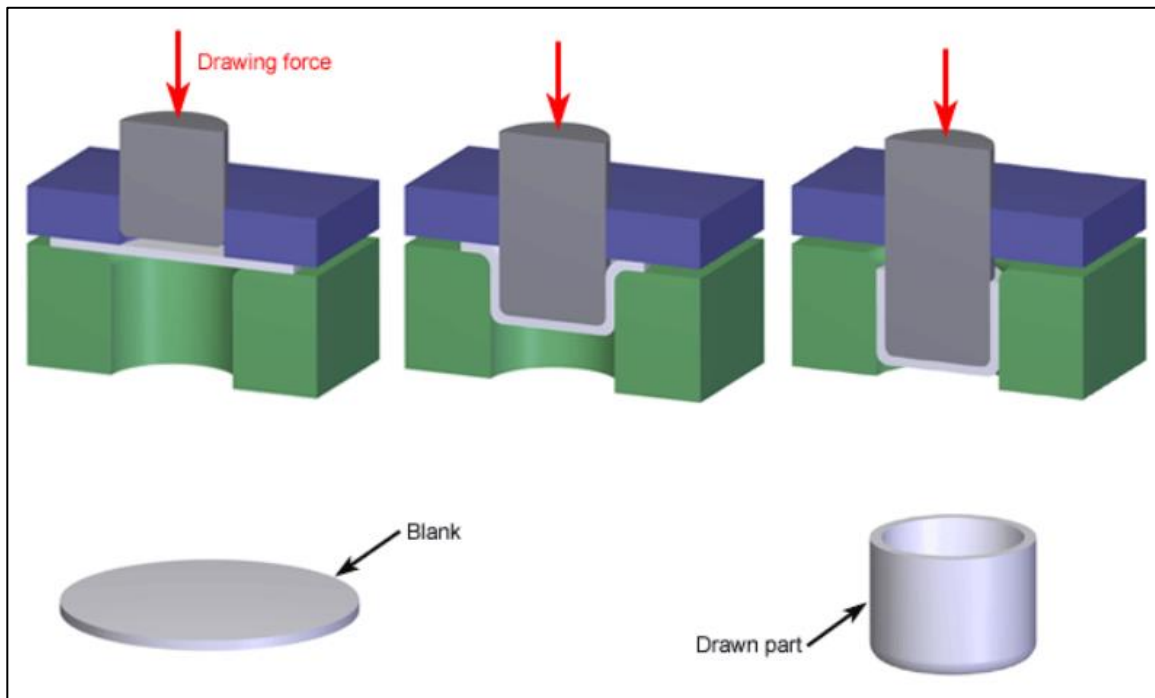


Fig. 1.2 A complete deep drawing process to get a final product [Custompartnet.com, 2018]

After the complete drawing of the part, the blank holder and punch can be relieved and the sheet metal part removed from the cavity of die. A complete deep drawing process of getting final product has been shown in Fig. 1.2. Due to clamping of sheet metal blank by blank holder, some portion of the sheet metal blank which is under the blank holder, may form a flange around the sheet metal part which can be cut or removed.

Roll forming is a metal forming operation in which a sheet metal is progressively shaped through a sequence of bending operations. This forming process or operation is executed on the roll forming line which consists of a series of roll stations as shown in Fig.1.3. Through all these roll stations, sheet metal stock is passed. Each roll station includes rollers or roller dies which are established on both sides of the sheet metal stock. In general, the roller's shape and size may be unique to a particular station. The position of the roller dies can be arranged below and above the sheet, along both sides of the sheet or at an angle etc. When sheet metal stock is entered forcefully through the roller dies in each roll station, it first deforms plastically and then consequently bends. Each roll station performs one stage in the complete bending of the sheet to form the desired part. To reduce the tool wear, lubrication of roller dies is done so that friction between the die and the sheet can be minimized. Lubricant is also helpful for higher production

rate. Material thickness, radius of each bend and no. of roll stations can be optimized for a higher rate of production. The roll forming line may also involve some other type of sheet metal forming operations, such as shearing or punching before or after the roll forming. A large number of ferrous metals like mild steel, stainless steel, alloy steel and non-ferrous metals like aluminium, copper, brass etc. are widely used in roll forming. The main features of roll forming include speed, flexibility, cost saving, energy savings and reduced scrap.

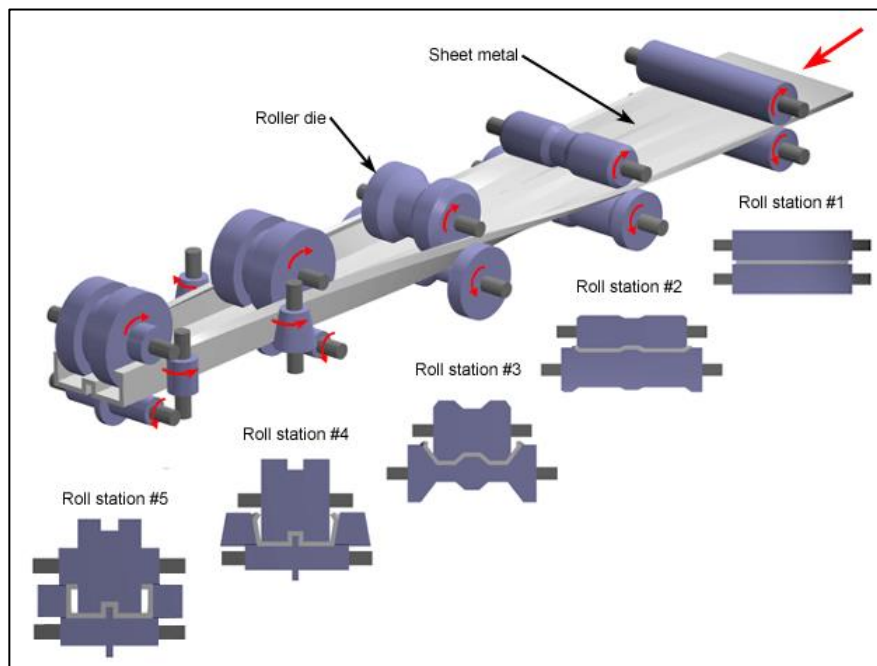


Fig. 1.3 Roll forming line [Custompartnet.com, 2018]

In metal forming, stretch forming is widely used to produce large contoured parts. In stretch forming, a sheet metal piece is stretched and bent over a form die simultaneously. In stretch forming, stretch press is used. Over the stretch press, sheet metal piece is safely gripped along its ends by gripping jaws as shown in Fig.1.4. To stretch the piece of sheet metal, each gripping jaw is attached to a carriage. These carriages are pulled by hydraulic force or pneumatic force so that the sheet metal piece can be stretched safely and securely. The main tooling of this process is a stretch form block which is known as a form die. The stretch form die or stretch form block is a contoured shape solid against which the piece of metal sheet is pressed. In stretch forming there are two types of stretch presses used, one is called as vertical stretch press and another one is called as horizontal stretch press. Mostly vertical stretch presses



are used in which form block or form die is placed on a press table, which may be lifted upward towards the metal sheet with the help of pneumatic or hydraulic ram. As the form block or form die moves upward towards the sheet metal, which is gripped rigidly by its ends, the tensile stresses increase and the piece of sheet metal deforms plastically and convert into a new shape. In horizontal stretch presses, the piece of sheet metal is pulled by gripping jaws around the form die horizontally.

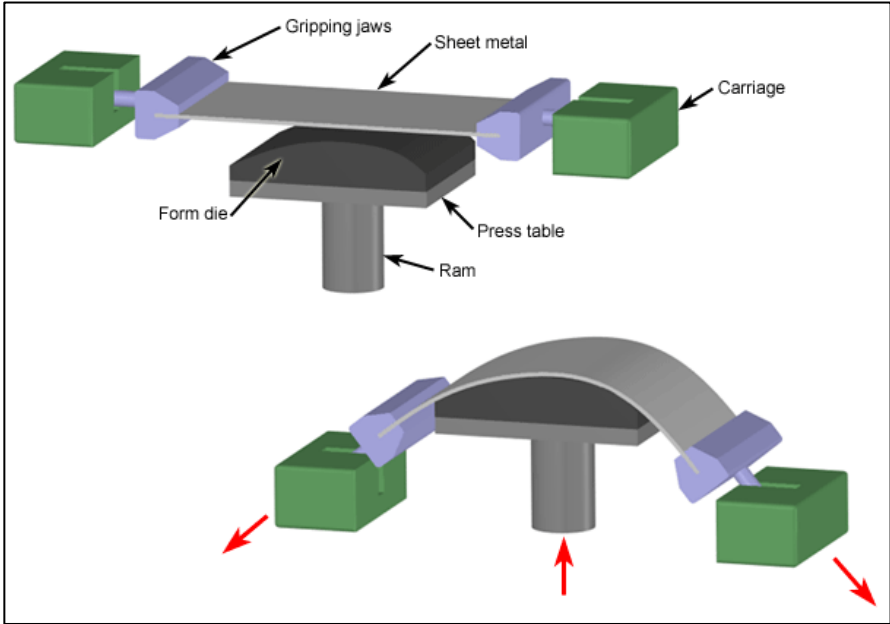


Fig. 1.4 Stretch forming [Custompartnet.com, 2018]

Stretch forming parts have large bend radius and are typically large in size. Their shapes can vary from surfaces having uniform curved cross-sections to a very complex non-uniform cross-section. Stretch forming parts are highly accurate and contain very smooth surfaces. Stretch forming prefers ductile sheet metals. The most commonly used ductile sheet metals are titanium, steel, aluminium and its alloys. Typical stretch forming parts can be found in a car as door panels or in aircrafts as wing panels. Enclosures and window frames also come under the category of stretch formed parts.

**1.2 Bending**

The bending is an important sheet metal forming process in manufacturing of aircraft, spacecraft, automobiles, and home appliances etc. To produce a bend in any part, bending force

should produce stresses beyond the yield limit of the material so that a permanent bend could be established after removing the load. When the forming load is removed, elastic recovery or springback occurs (Buang,2015-Dilip, 2014). Springback is the elastic recovery in the plastically deformed sheet after removal of punch which causes loss of dimensional accuracy and distortion of geometry. (Kalpakjian,2014-Kartik,2017)

In bending, fibers on the outer side of the neutral surface are subjected to tensile stress and fibers on the inner side are subjective to compressive stress. The value of strain on the neutral surface is zero. As per bending theory (Dieter and Bacon, 1986), in elastic bending, the position of neutral axis remains at the center and the compressive strain on inner side is equal to the tensile strain on outer side and hence thickness remains constant. In case of bending with large plastic strains, since the plastic strain is proportional to the distance from the neutral axis, the neutral axis shifts significantly towards the inner surface to maintain force equilibrium. The net strain in the bend region is tensile.

Sheet metals bending, as shown in Fig. 1.5, is a very popular and commonly used process for producing sheet metal parts with curved sections.

In the case of corrugated sheets, bending increases the stiffness of the part by raising its moment of inertia. Stiffness is defined as load applied per unit deflection. When a beam is bent, the general equation for elastic curve during bending is given by  $\frac{d^2y}{dx^2} = \frac{M}{EI}$ , where M is the bending moment, I is the moment of inertia, E is the modulus of elasticity, y is the deflection and x is the distance measured along the length of the member to the section where deflection is to be determined. It is clear from the above equation that the larger the moment of inertia, the smaller the deflection and hence greater the stiffness. For example, when a blank is transformed into a corrugated sheet by bending operation, the corrugated sheet has a higher moment of inertia than the flat sheet in the direction transverse to the corrugation and hence a higher stiffness

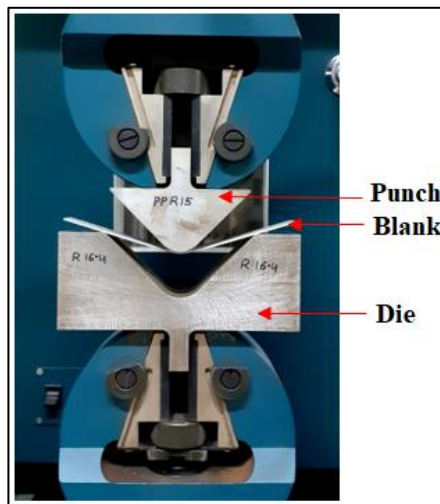


Fig. 1.5 V-bending operation

Some of the common bending operations such as V-bending, U-bending, U-draw bending and wipe bending are shown in Fig. 1.6(a)-(d). The V bending process is accomplished by a V-block for a die and a wedge-shaped punch to force the metal into die as shown in Fig. 1.6 (a).

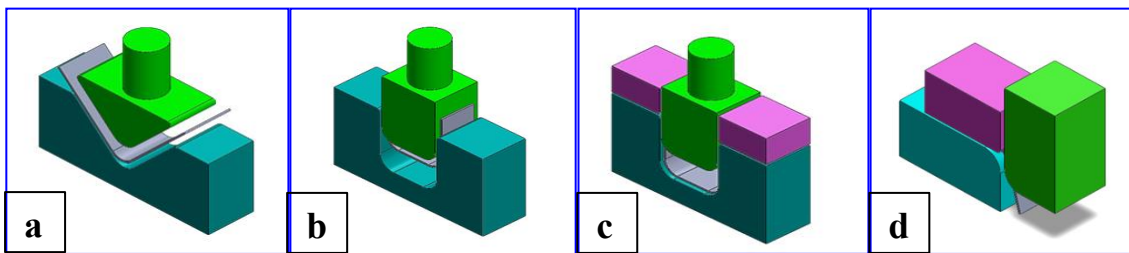


Fig. 1.6 Common bending operations (a) V bending (b) U bending (c) U Draw bending (d) Wipe bending

The V bending process is accomplished by a V-block for a die and a wedge-shaped punch to force the metal into die as shown in Fig. 1.6 (a). In V-die bending the die punch clearance is constant (equal to sheet thickness). This bending process is widely used. The sheet thickness ranging from 0.5 mm to 25 mm can be used for V bending.

The U shape in U-die bending is obtained by bending the sheet in such a way that in the same operation two parallel bending axes are formed as shown in Fig. 1.6 (b). To have contact with the bottom punch a backing pad is used. The use of backing pad needs around 30% more bending force to press the sheet contacting the punch. The use of a backing pad in U-bending is recommended because it offers multiple advantages, including improved material integrity,

better surface quality, enhanced accuracy, reduced springback, extended tool life. While it may require slightly more bending force, these benefits make it a worthwhile choice in many sheet metal bending applications, particularly when the quality and integrity of the final product are essential. Also, it helps in ejection of the formed components. In U draw bending the blank is clamped with the help of two holding pads as shown in Fig. 1.6 (c).

In Wipe bending, the sheet metal part is clamped to the block of die by a pressure pad which is basically spring loaded or hydraulically loaded and an extended sheet metal part over one edge of die block is wiped by the punch. The edge of the die block is provided with a bend radius along with the punch which is also provided with a chamfer or bend radius on its leading edge. This geometry is done to avoid severe wiping action between die block and punch as shown in Fig. 1.6 (d). This bending is also called as flanging. In this bending one edge of the sheet is bent to  $90^\circ$  while the other edge is retained by the material itself under the force of pad and blank-holder. The length of flange can be changed as per requirement and the bending angle can be controlled by changing the stroke position of punch.

When the bend angle decreases and bend radius increases, the plastic strain increases and the neutral layer moves significantly towards the compressive zone. Due to the shifting of neutral layer towards compressive side, the deformation zone contains tensile strain in the form of net strain causing thinning which will be finally responsible for fracture when the strain exceeds beyond failure limit. A more ductile material allows smaller magnitude of radius of curvature as such a type of material can withstand larger outer fiber stretch of the bend before fracture. The minimum bend radius for a specific material is the bend radius at which a crack emerges on the outer surface (subjected to tensile stress), and it is commonly defined in terms of multiples of thickness. It is a measure of a sheet's bendability. The stress concentration issue at rough edges results in decreased bendability. Residual stress is reciprocal to the bend radius. At smaller bend radius, greater residual stresses will be set-up in the thickness of sheet. Material properties, bend length and bend angle are also the key factors in determining minimum bend

radius. For soft annealed sheet metals, the minimum bend radius is equal to sheet thickness (Donaldson et al., 2012).

The term "springback" refers to the change in bend angle caused by elastic recovery following the removal of the forming load, which is particularly noticeable in the case of sheet metal bending. As illustrated in Fig. 1.7, a sheet specimen is bent with an initial bend radius ' $r_i$ ' through an angle ' $\theta_i$ ', when the load is removed, as a result of springback, the final bend radius increases to ' $r_f$ ' and bend angle decreases to ' $\theta_f$ '.

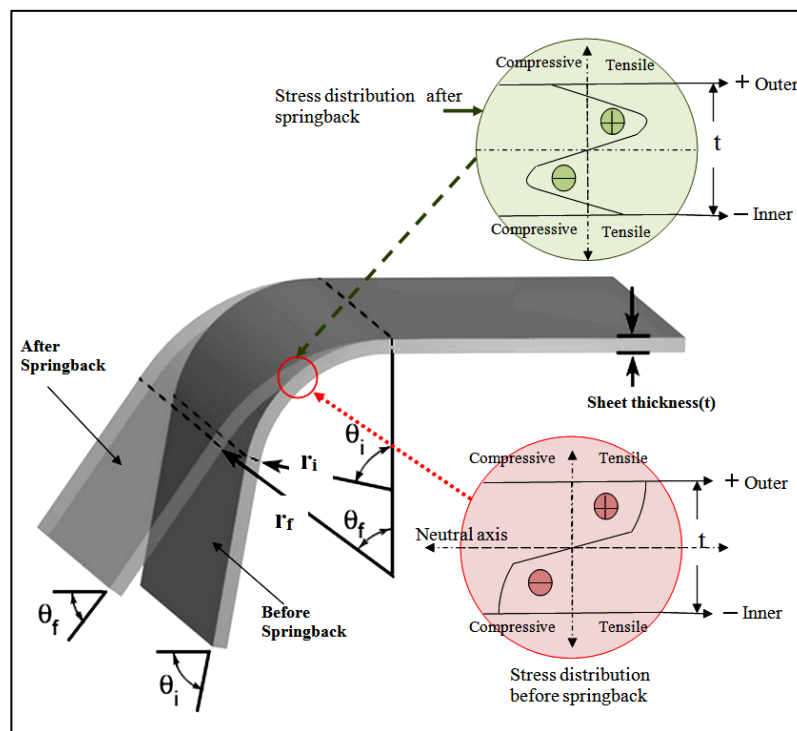


Fig. 1.7 Springback in bending showing stress distribution before and after springback through thickness (Custompartnet.com, 2018)

This change in angle is referred to as springback and the ratio of final angle to initial angle is called springback ratio ( $K_s$ ). The value of springback ratio or springback factor can vary from 0 to 1. Zero value of  $K_s$  indicates fully elastic bending i.e. there is complete elastic recovery, whereas the  $K_s$  value of one indicates zero springback

In the deformed cross section of the part, which is made up of elastic and plastic areas, the entire stress-strain curve (both compression and tension) below and above the neutral axis is traversed during bending in such a way that only the neutral surface preserves its original

length. As a result of springback, residual stresses are developed such that the outer portion, which was deformed under tension, displays compressive residual stress and the inner portion, which was deformed under compression, displays tensile residual stress as also shown in Fig. 1.7. Unsatisfactory bending is frequently caused by a lack of dimensional control brought on by springback and thinning. As it causes dimensional and geometrical changes in the formed parts or components, springback in sheet metal forming is a significant problem. Despite its apparent simplicity, the parameters affecting the bending process and springback should be understood thoroughly to produce the products with high geometrical and dimensional accuracy. In the sheet metal forming, springback is a significant quality issue.

Because of springback, the die's bend angle does not match to the final required angle. Serious issues during assembly operations may arise if the final shape of the component deviates from the planned tolerance. Springback has been seen in all sorts of bending processes, including press bending, roll bending, folding and roll forming. In practice, springback is compensated, by overbending the workpiece by a specified amount as shown in Fig. 1.8 (a). Springback allowance may be granted on either the die or the punch when overbending. Springback can be reduced or eliminated by keeping the workpiece to highly localized compressive stresses after the bending is completed and before the load is released.

This can also be achieved by coining or a counter punch as shown in Fig. 1.8 (b) and 1.8 (c) respectively.

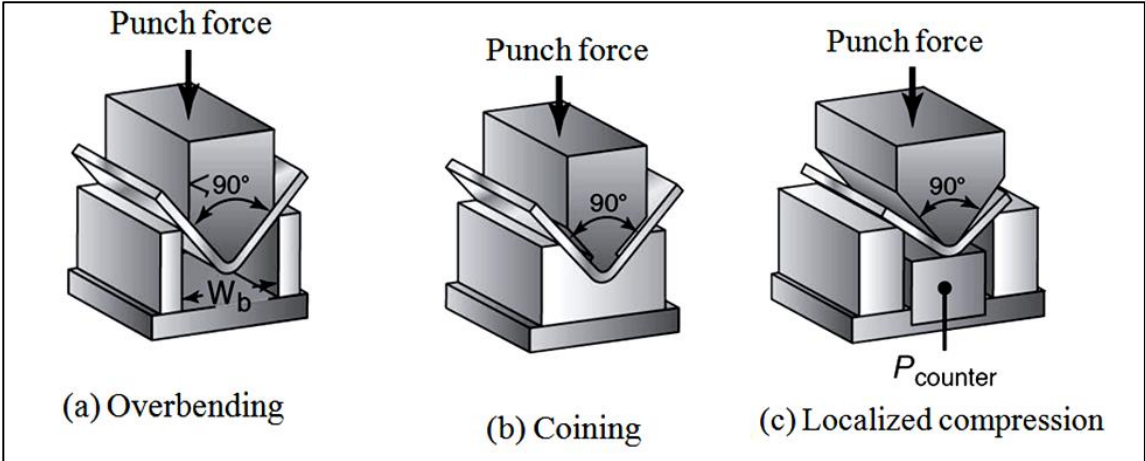


Fig. 1.8 Springback reducing methods in V-bending (Kalpakjian et al., 2008)

Another key approach for overcoming springback is stretch bending, which involves applying homogeneous plastic strain to the cross-section of the sheet metal using grips. This minimises the bending moment used to plastically deform the sheet, and the neutral axis moves fully out of the cross section of the specimen being bent. Furthermore, applying tensile stresses by stretching during deformation decreases the generation of residual stresses in the specimen's cross section. (Siegert and Wagner, 1994).

Springback compensation through punch/die allowance requires correct springback prediction and plays an important role in getting the final form of the component. This is determined by a variety of factors that impact springback. Springback prediction is required to allow die design with springback compensation as a corrective mechanism. The process of springback compensation has been simplified and made more effective by computer-aided compensation, but it still needs further analysis and optimization before and after compensation. (Banabic, 2010).

In the case of forming with clad composites or laminates, the complex behaviour during plastic deformation of a clad sheet metal depends upon the properties of individual materials, thickness ratio, stacking arrangement of materials in the thickness direction, surface properties, bonding parameters, and heat treatment. In the bending operation of clad sheets, springback evaluation and control becomes more complex and challenging. The bending operation of clad sheet metal is associated with a highly complex springback problem different from those of monolith sheets which also reduces the bending precision and accuracy in the formed components. The details of manufacturing and applications of clad sheets have been discussed as below.

### **1.3 Clad sheet metals**

There are various metals such as aluminium alloys, steel, brass, copper, titanium, tin, and nickel which are used for making skin panels of automobiles & aeroplane, building roofs, domestic home appliances, cans, and a number of other applications. Nowadays, laminated sheets/clad

sheets are getting huge popularity in the automobile and manufacturing industries. These materials are capable of solving engineering challenges which need superior metal properties. Metal clad sheet composites are a unique form of composite material in which alternating metal or metal containing layers are bonded together with inter-metal bonding. Different types of clad sheet metals are progressively employed in various industrial applications such as automotive, aerospace, and electrical industries due to their unique mechanical properties.

### **1.3.1 Manufacturing of clad sheet metals**

The process of design and development of the clad composite materials comprises of the selection of optimum level of various properties and stacking the layers of various thicknesses of different materials and interface structures (Kim, 2013). Clad sheets have also been produced by several solid-state bonding methods such as cold roll bonding, explosive and diffusion bonding. Though CRB (cold roll bonding) is the cost effective and most efficient method to manufacture the clad sheets (Kim, 2013-Manesh, 2003).

Diffusion bonding is a process of joining layers of sheet metal together with heat and pressure as shown in Fig.1.9. This process involves stacking of thin metal sheets together in a vacuum followed by raising the temperature as high as 50-80% of the melting point of the base material and the pressure is applied simultaneously. This simultaneous application of heat and applying pressure, makes some of the electrons from each metal sheet to transfer to its neighbouring metal sheet until internal joints in stacks formed. The products of diffusion bonding retain all the properties of the parent metal and are strong too.



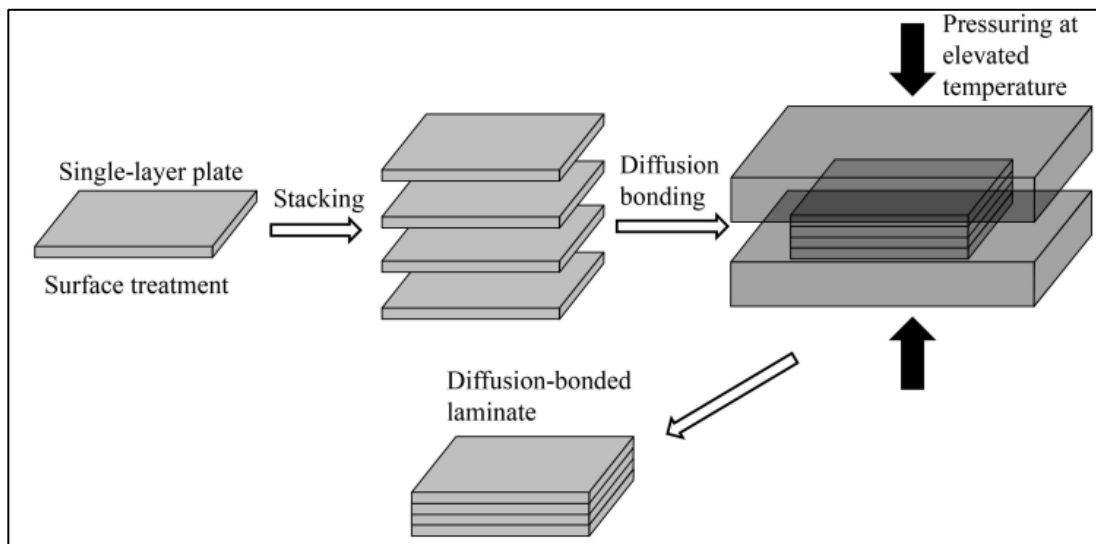


Fig.1.9 Schematic representation of diffusion bonding (He et. al., 2018)

### *Steps for Diffusion Bonding*

There are several steps to the diffusion bonding process, including:

*Part Preparation:* The pre-etched component's surface must be clean, straight and have a suggested finish of less than  $0.4\mu\text{m}$  RA. This prevents the surface from being contaminated. Stainless steel, Copper, Gold, Silver, Aluminium, Inconel, Moly, Nickel, Titanium etc. can all be utilised in diffusion bonding.

*Heat Applied:* Heat is applied in the form of induction, radiation, direct or indirect resistance in controlled environment or vacuum.

*Pressure Applied:* The range of the applying pressure is 3-10 MPa in a single direction. Pressure is applied along with application of heat.

*Part Finishing:* To confirm the surface of the final part is free from any type of residues, the part will go for a simple cleaning process after the completion of bonding process.

Explosion bonding, cladding, or welding, is a solid-state welding operation in which metallurgical joining of metals as performed. In explosion bonding, a controlled detonation of explosives is performed in such a manner so that one metal can accelerate into another metal and fuse together properly at their interfaces. An angular collision caused by the explosion's force results in an ejected plasma. Prior to the impact, the plasma jet acts to clear both the metal surfaces of impurities, leaving clean metal behind for joining.

Due to the high pressure along the collision front, the solid metals are forced to behave as viscous fluids. The pressures along the collision front are high enough to force the solid metals to act as viscous fluids. The significant bond line wave pattern in an explosive weld is created by the fluid-like behaviour of solid metals. If too much energy is applied, the solid metals may melt together, resulting in potentially brittle intermetallics. Also, the insufficient energy will not be able to make a proper bond between solid metals. Due to this, calculating the correct amount of force at the time of bonding between solid metals is one of the most critical challenges in the explosive welding process.

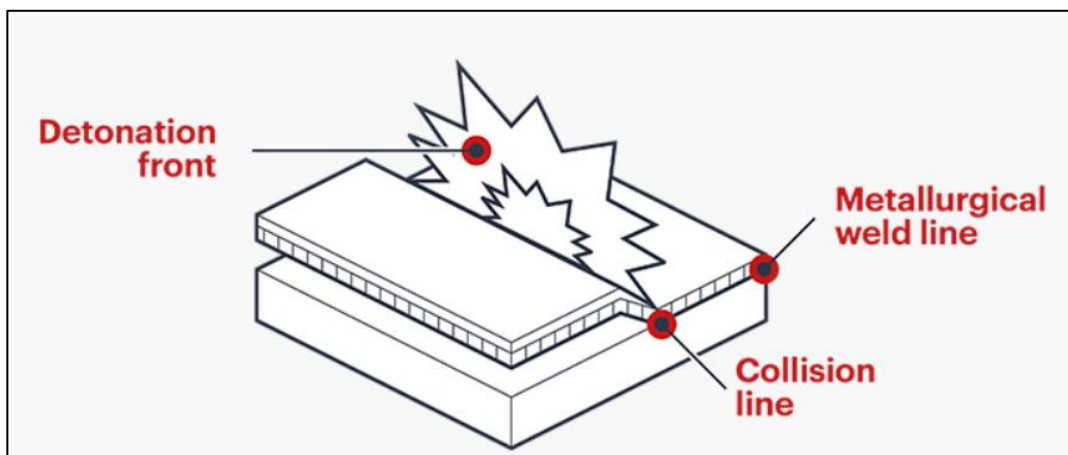


Fig. 1.10 Schematic representation of explosive cladding (triclاد.com, 2022)

Cold roll bonding (CRB) is a solid phase welding process, in which intimate bond between the sheets is established by plastic deformation of the sheet metals (Jamaati, 2010). The schematic illustration of CRB to produce clad sheet materials is shown in Fig. 1.11. In this method, two or more sheets, plates or strips of metals or alloys are stacked one by one together and thereafter passed through a well-established pair of rolls until required deformation is obtained to make an appropriate solid-state bonding between the strips of metals or alloys. The surfaces of sheet metals or alloys which will be bonded to each other, must be properly prepared and cleaned to remove any types of residues or surface layers etc. (Wright, Mohamed). In cold rolled bonding process, due to high pressure at the rollers, a high reduction in the thickness of sheet metals is obtained. The reduction in the sheet thickness can be achieved up to fifty percent or more than fifty percent in a single rolling pass. Due to high reduction in

sheet thickness, a great amount of heat is generated and developed virgin surfaces on the sheet metals get bonded to each other. Generally, to enhance the bond strength between the sheet metals, an annealing process is conducted after the cold rolling because the annealing process is supposed to create a good metallurgical bond at the interface of sheet metals (Luo and Tsuji, 2004). After performing the heat treatment process, the laminated/clad sheets may be further processed into a required shape and size by any conventional manufacturing method. They can be stretched, deep drawn, bent, roll-formed and joined into any required part. At the completion of cold rolled bonding, the laminated composite sheets can be processed further in coil form. The manufacturing of laminated/clad sheet is economically cost-effective and has a high productivity. The principle of cold roll bonding process has been shown in Fig.1.11.

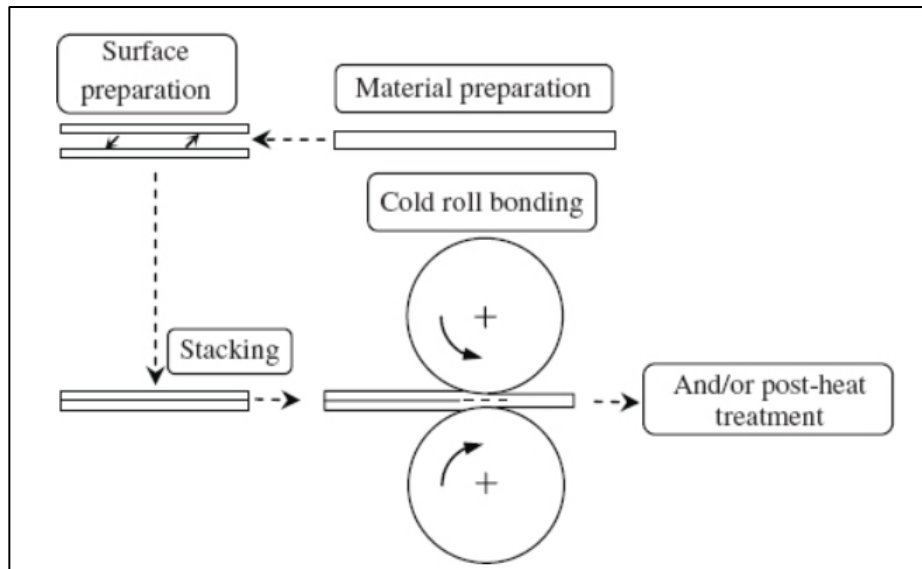


Fig. 1.11 Schematic of cold roll bonding process, (Li et. al., 2008)

The rough surfaces of the sheets to be bonded together facilitate the bonding mechanism by extrusion of softest metal in the crevices on the surfaces which results in atom to atom contact between parent sheets (Abedi, 2015).

Wang et. al (2023) manufactured AlZn4SiPb/Steel laminated sheet by roll bonding technique at room temperature. They used 2.2 mm thickness of AlZn4SiPb and 3.2 mm thickness of low carbon steel for manufacturing of AlZn4SiPb/Steel laminated sheet. Both Al alloy and low carbon steel sheets were taken in the size of 100 mm width and 120 mm length. For AlZn4SiPb alloy and low carbon steel sheets heat treatment has been done so that

deformation of resistance can be reduced during roll bonding. For surface cleaning and preparation of AlZn4SiPb alloy and low carbon steel sheets, wire brush and flap disc with abrasive pad has been used. To remove residual grease both the sheets were immersed into ethyl alcohol for 0.5 hr. To prevent the mismatching of Al alloy and low carbon steel sheets, they used aluminium rivet at the front ends of both the sheets. These riveted sheets were entered into the roll mill and finally rolled at normal environmental conditions. They got 58 percent reduction in thickness at 12 m/min rolling speed. After rolling, they heat-treated the laminated sheet at 350 degrees Centigrade for 60 minutes so that laminated sheet could be returned to the initial state. After heat treatment to improve mechanical properties of laminated sheet, they were further aged at 120 degrees Centigrade for one day in an oil bath furnace. The Manufacturing process for AlZn4SiPb/steel laminated sheet is represented in Fig.1.12

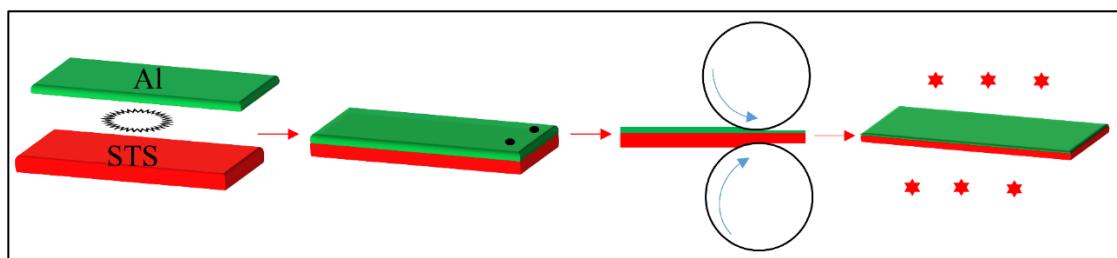


Fig.1.12 Manufacturing process for AlZn4SiPb/steel laminated sheet (Wang, 2023)

The CRB process has several good qualities, especially straight bonding layers and accurate dimension control (Kim, 1997). The growing interest of researchers in lightweight materials and the glorious mechanical and useful physical properties of the clad sheets has led to the remarkable developments in understanding of the forming behaviour of the clad sheets. However, press forming the components of clad sheet metals is a difficult task because their elasto-plastic behaviour is completely different from that of their individual part sheets. The plastic deformation behaviour of a clad sheet depends upon the properties of individual materials, thickness ratio, arrangement of materials in thickness direction, surface properties, bonding parameters, and heat treatment (Kim, 2013-Manesh, 2003, Kim, 2014-Mori, 1996). Especially, their bending and springback characteristics are completely different from those of

monolithic sheets resulting from the inherent modification in their mechanical properties and change in thickness direction (Yilamu, 2010). The most widely manufactured laminated sheets are Al/ferritic stainless steel, Al/Fe, Al/Cu, Ti/ferritic stainless steel, austenitic stainless steel/Al/ ferritic stainless steel, austenitic stainless steel/Al/Cu, Fe/Al/Fe, Al/Mg/Al, Ti/steel/Ti and AZ31/Al/ferritic stainless steel (Tseng, 2010-Kim, 2014).

**1.3.2 2-ply and 3-ply laminate composite of aluminium and stainless steel**

In this present study, 2-ply, and 3-ply laminate composite of aluminium and stainless steel (SS430/AA1050 and SS430/AA1050/SS304) have been used in V-bending for prediction of springback. These two laminates are manufactured by cold roll bonding process. Fig. 1.13 shows when different metals with varied metallic properties are cladded into a single sheet, how the clad sheet metal becomes functional. The composition is made to compensate for the drawbacks of each other while also utilizing each metal's advantageous properties, which together give a distinctive, sophisticated function (Okui et al, 2014).

| CHARACTERISTICS      | Aluminium | Stainless steel |
|----------------------|-----------|-----------------|
| Density              | Low       | High            |
| Thermal Conductivity | High      | Low             |
| Corrosion Resistance | Low       | High            |
| Strength             | Low       | High            |

Fig. 1.13 Representation of mechanical properties by the cladding of SS and Al metal

**1.3.3 Advantages of aluminium/ stainless steel-clad sheets**

- (a) **Weight reduction:** Due to the light weight of aluminium, appreciable weight reduction is achieved in aluminium/ stainless steel-clad Sheets.
- (b) **Scratch resistant:** Stainless steels are the main constituent of Aluminium/ Stainless steel-clad Sheets. They improve the scratch resistant property of the clad sheets

**(c) Thermally conductive:** Aluminium/ Stainless steel-clad sheets are thermally conductive materials. Aluminium provides better heat distribution.

**(d) Ductility:** Aluminium and stainless steels are both good in ductility. Using these materials clad sheets gives excellent ductility.

**(e) Corrosion resistant:** By using stainless steel, clad sheets are able to offer resistance to corrosion.

**(f) Electrically Conductive:** Aluminium and stainless steels are both electrically conductive materials. So clad sheets are highly electrically conductive materials.

**(g) Strong:** Stainless steels are very strong in strength. Stainless steels give good strength to the clad sheets.

#### **1.3.4 Application of aluminium/ stainless steel-clad sheets**

*Truck bumpers:* For the corrosion resistance, dent and scratch resistance bumpers are made from aluminium/stainless clad sheets.

*Cookware:* Cookware made from clad sheets offers better heat distribution, which means consistent cooking performance.

*Iron soleplates:* Iron soleplates are made by the aluminium/ stainless steel-clad Sheets. The even heat distribution of aluminium and scratch resistance of stainless steel make an unbeatable combination.

*Automotive:* Several automotive parts are manufactured by the clad sheet metals, e.g., laminated sheet (SS/Al/SS) for disc brakes. A 3-ply laminated sheet consisting of SS403/Al/SS403 is used for the sliding parts of disc brake which prevents the problems caused by excessive heat generation. This 3-ply SUS 403/Al/SUS 403 clad sheet is widely using in the manufacturing of racing mountain bicycle's disc brake rotor.

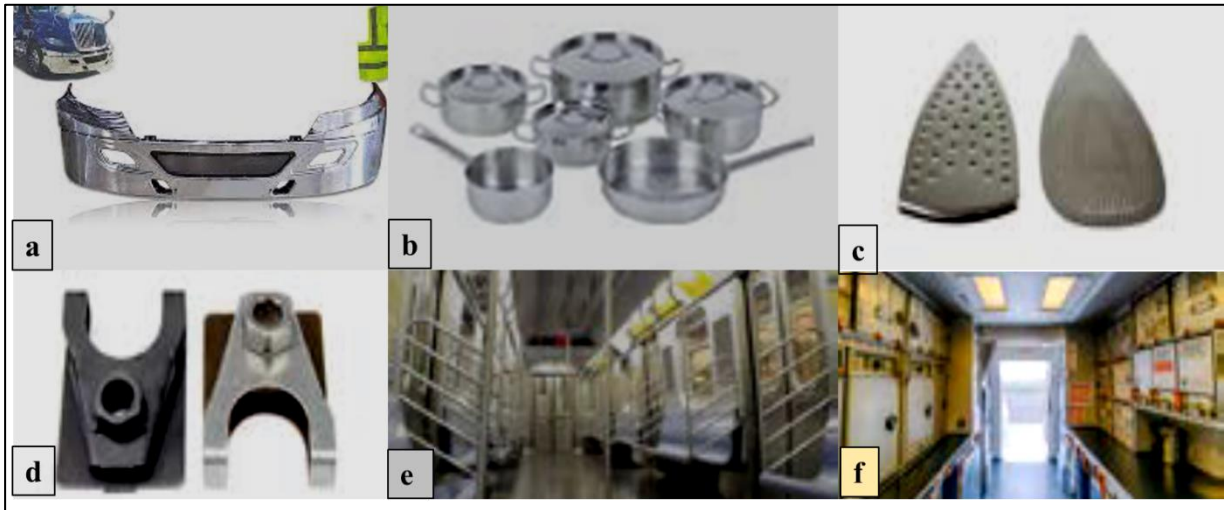


Fig. 1.14 Various components manufactured by using aluminium/stainless steel-clad sheets  
 (a) Truck bumpers (b) Cookware (c) Iron Soleplates (d) Electrical ground Connectors (e) Metro rail  
 Coach (f) Spacecraft chamber (<https://www.emsclad.com>, 2018)

*Rail Transport:* The stainless / aluminium transition strip allows for weight saving aluminium to be used on steel bodies, while the stainless / aluminium optimizes the heat diffusion of HVAC grills and ductwork.

*Aerospace:* Aluminium corrodes heavily when in direct contact with the new generation of composite airframe assemblies. Stainless steel clad to aluminium gives a permanent maintenance-free barrier between the aluminium and the composite materials. So, these clad sheets are being used for several aerospace applications.

In order to identify the research gaps, objectives and challenges, a comprehensive literature survey is done and discussed in the next chapter.

## **CHAPTER 02**

### **LITERATURE REVIEW**

Springback is the most prevalent issue in sheet metal bending operations. Springback occurs due to the recovery of elastic strain thereby resulting in geometrical and dimensional changes in the formed component along with considerable residual stresses. Literature review in this work covers springback analysis of conventional blanks/monolithic sheet, springback analysis for clad sheets, and factors or process parameters influencing springback of metal sheets.

#### **2.1 Springback in conventional blanks/monolithic Sheets**

The springback effect in sheet metal forming is basically a stress driven mechanism. Initial work related to springback with plane stress condition was carried out by Gardiner (1957). Then springback analysis in stretch bending was described by Woo and Marshall (1959). Gau and Kinzel (2001) presented a hardening model and an incremental method, based on isotropy and kinematic hardening to study springback phenomenon in the wipe bending of aluminium strips with plane strain assumption. This new incremental method incorporated the Bauschinger effect in predictions of springback for aluminium sheet undergoing multiple bending. Experimental observations were also made and compared with the predictions. Geng and Wagoner (2002) experimentally and numerically analyzed the draw bend tests incorporating an anisotropic hardening model to study springback phenomenon in aluminium alloys. It was observed that predicted springback results were dependent on both hardening law and plastic anisotropy. The material models based on von-Mises, Hill's quadratic and Barlat's three parameter yield criteria were used in the simulations and presented good agreement. Simulations using Barlat's 1996 yield function showed closer agreement with the experimental results. Cho et al. (2003) conducted a finite element analysis on springback phenomenon in U-



bending of sheet metal and identified major process parameters affecting springback. To achieve this, Lagrangian thermo-elastoplastic FEM was incorporated to simulate U-bending of sheets in plane strain condition. Chongthairungruang et al. (2013) conducted experiments and FE simulations to characterize springback in U-bending of two different dual phase high strength steels of different strengths (JSC780Y and JSC590R) and compared with that of a low carbon steel sheet (JSC270C). Simulations were performed using anisotropic material models according to Yoshida-Uemori kinematic hardening model and Barlat's 2000 yield criteria and Hill's 1948. Between the predicted results and the experimental results, a fair agreement was established. Although material model obeying Yoshida-Uemori proved to be the most accurate among the three, but improved calculation results with improved material model and parameters are still required in industry related problems. The differences in stress distribution between top and the bottom surfaces of the deformed samples of high strength steels affect the side wall curl most significantly. Zhai et al. (2021) used proportional kinematic hardening model for springback prediction of AA6082 in stretch bending. They have performed numerical and experimental investigation and observed good agreement between experimental, analytical, and numerical results. They, also, observed that the proportional kinematic hardening model is better than the classical kinematic hardening model for prediction of springback of aluminium AA6082. They concluded that springback decreased when the tensile force increased. Hai et al (2020) predicted springback of SS400 experimentally and numerically in V-bending process. They used combination of Taguchi method and ABAQUS simulation to find out the important parameters which would highly affect springback. They found optimal values of plate thickness, punch stroke and punch radius for minimum springback. Senol et al (2014) conducted experiments and finite element simulations to determine springback of SS in air-bending. Experimental results were in good agreements with FE simulation results. They also used experimental results in artificial neural network to predict springback. They observed that springback decreased as bend angle increased.

Spathopoulos et al. (2020) concluded that springback was influenced by sheet thickness, material properties, tools geometry and friction, etc. They applied a novel neural network system based on Bayesian regularized backpropagation networks for springback prediction in sheet metal forming processes.

Serban et al. (2013) investigated the possibility of ANFIS- adaptive neuro-fuzzy inference system and ANN- artificial neural networks in springback prediction of free cylindrical bending of sheet metals. Firstly, FEM was used to predict the springback in free cylindrical bending of sheet metals and thereafter these results were applied in the form of training data for ANFIS and ANN. The FEM results were compared with the experimental results and good agreement was obtained between them. They used statistical methods so that the performances of the ANFIS and ANN models could be evaluated. Both the models provided good results close to the experimental values for springback.

Kazan et al. (2009) observed that springback was influenced by a number of variables, including lubrication levels, tooling geometry, sheet thickness, processing parameters and material characteristics. The ANN (artificial neural network) technique was used to construct the springback prediction model for the wipe-bending process. To gather the neural network training data, various numerical simulations utilising the finite element method were carried out. Thus, it is possible to quickly implement springback prediction for the new areas using the learnt neural network, which has undergone numerical testing.

Magar et al (2023) used ANN approach and finite element method to investigate the effect of process parameters i.e. tool travel rate, bend angle and sheet thickness on springback of sheets of C80 and SS304 materials under V-bending. In this paper, three parameters have been considered with 03 levels for each of them. Finally, total 09 experiments ( $L_9$  – orthogonal array) have been conducted. The results of FEM model and ANN model were in good agreement. The optimal values of tool travel rate, bend angle and sheet thickness are obtained 2 mm/s, 80° and 2 mm for sheets of C80 material and for sheets of SS304 material 6 mm/s, 80° and 6 mm respectively.

Wahed et. al (2020) have done investigations on process parameters of bending of Ti-6Al-4V alloy in V-bending operation to get minimum springback. It has been concluded that elevated temperature plays important role among the other process parameter namely holding time, and punch speed to minimize the springback. It has been observed when temperature increases, yield strength decreases. Decreased yield strength reduces the amount of springback. For this study, finite element simulation (Abacus), RSM and experiments have been conducted. The results of finite element simulation (Abacus) and experiments were in good agreement. For getting minimum springback, the optimal values of process parameters of V-bending are holding time: 0.05 min, punch speed: 0.05 mm/s and temperature: 900°C by optimizing the RSM using genetic algorithm.

Şen and Taşdemir (2021) studied the bending behaviour of CP 800 sheet in V-bending operation at normal temperature. In the experiments, 2.5 mm thick sheets of CP800 were used under two different holding times, three different punch radii and four different bending angles. The impact of these process parameters on springback was observed via finite element analysis (FEA) and experimentally. The results of experiments and FEA were in a good agreement. As an outcome of this investigation, springback increased as the punch radius increased and decreased as the die angle increased, further the holding time, however, exhibited only limited influence on springback. Additionally, some bending samples obtained under experimental conditions of  $\alpha = 60^\circ$  and  $r = 2$  mm showed signs of damage.

Karalar and Bayramoğlu (2022) investigated the effect of bending angle and thickness, individually and combinedly on springback of sheets of 1000DP steel. Regression analyses and INOVA were used. Design-Expert software has been applied to record the results. The study revealed two important findings. First, reducing the bending angle or increasing the thickness resulted in a decrease in springback. Second, the analyses indicated that the thickness of the sheet metal had a more significant impact on springback compared to the bending angle.

Rahdiana et al. (2023) have done investigations on springback of the V-bending process for SS304. They have observed that springback of SS304 blank is increased when bending radius increased. They have concluded that springback is proportional to bending radius.

## **2.2 Springback in clad sheets**

A summary of the work done by researchers in the recent years on springback of clad sheets in bending as follows: -

Hino et. al. (2003) studied Al100/SUS430 clad sheet analytically and experimentally in draw bending process. Results showed that the layer-thickness ratio, relative location of the layers, and the stretching force exerted on the laminates, as well as the difference in strength between the layers of component of the clad sheet metals, had a significant impact on the behaviour of springback of clad sheet metals. When the weaker metal is inside the bent of clad sheet metals, the springback is significantly reduced along with increasing stretching force, but when the stronger metal is inside the bent of clad sheets, the stretching force has no effect on the springback. The behaviour of springback of the clad sheet metals resembles that of monolithic sheets when the layer of stronger metal of the clad sheets is suitably thick.

Aghchai et. al. (2008) investigated the formability of two-layer AA1100-SS12 laminated sheet. They used experimental and theoretical approaches to find the FLD of the two-layer AA1100-SS12 sheet. It was also, observed that the 2-ply clad sheet metal had better formability than the formability of AA1100 metal sheet.

Gautam et. al. (2018) studied 3-Ply clad sheet metal (SS430/Al1050/SS304) experimentally and numerically in U-Bending process. They observed that the tensile strength of the clad sheet specimens is the highest at 90° and the ductility is the lowest at 90° to the rolling direction when compared with the specimens of other orientations (0° and 90°). The average plastic strain ratio or normal anisotropy ( $\bar{R}$ ) of the laminated sheet metals was less than one which indicated that it had poor formability. The springback values obtained from the experiments were always

higher than the results obtained from the simulations. The springback was observed to be the highest in the specimen-oriented transverse to the RD (rolling direction).

Mohammadi et. al. (2011) studied prediction of springback of three-layer aluminium/polypropylene/aluminium clad sheets and two-layer aluminium/steel clad sheets. Setting conditions, or variations in thickness of layers and locations relative to one another, were investigated. The results demonstrated that the setting condition and thickness distribution have a significant impact on the bending and behaviour of springback of multi-layer clad sheets. It was found that in Al/PP/Al clad sheets, normalised springback decreases by roughly 25 percents as compared to symmetrical sandwich clad sheets as the bend's inner layer thickens. When the steel layer had the thickest feasible thickness, normalised springback was seen to be reduced in both setup situations (Al/St or St/Al). Furthermore, it is found the strong correlation between FEM and analytical techniques.

Parsa et. al. (2015) studied aluminium/copper clad sheet analytically and numerically in air bending process. Experiments were also conducted to validate analytical results and to study the effect of setting condition, die opening, punch radius and punch stroke on the behaviour of springback. The setting condition (Al/Cu or Cu/Al) was seen to have very small effect, while die opening had a large effect on the springback. On the other side, Al/Cu or Cu/Al setting condition played an important role on thickness variation in the bending of laminated sheet metals. Laminated sheet thinned in the setting condition of Cu/Al (Cu is at inner side and Al is at outer side) and thickened in the case of Al/Cu (Al is at inner side and Cu is at outer side). Springback increased when die opening was incrementally increased, so die opening was established as a key parameter for springback. With an increase in punch stroke, springback also increased. Radius of punch had negligible effect on springback. If copper sheet faced the punch, the thinning happened and if aluminium sheet faced the punch, then clad sheet thickened. Good agreement was seen between numerical and analytical results.

Kagzi et al. (2016) provided the analytical solution for the springback prediction during bimetallic sheet bending. The analytical findings for both setting conditions ( $SS_{in}/Al_{out}$  and  $Al_{in}/SS_{out}$ ) were more in line with the experimental findings.

Patel et. al. (2014) investigated springback behaviour of a laminated stainless steel (SS-304) and aluminium alloy (Al-6101T6) in V-bending process. They observed that the springback behaviour of bi-layered material was strongly influenced by relative location of layer and thickness of stronger/weaker layer of material. When thickness of Al-6101T6 was more than SS-304, springback of a bi-layered strip was less. When thickness of SS-304 was more as compare with Al-6101T6, springback was nearly same as in case of monolithic SS-304

Yilamu et. al. (2010) investigated springback prediction of stainless steel/ aluminum clad sheets. Results showed that the thickness ratios and the setting conditions ( $Al_{in}/SS_{out}$  and  $SS_{in}/Al_{out}$ ) affected the bending behaviour of laminated sheet such as sheet thinning and springback.

Weiss et. al. (2004) performed draw bending tests on SPS (steel/polymer/steel) laminated sheets to determine the effect of interlayer thickness on wall springback of SPS. The draw bending tests indicated that the laminates decreased springback values with increasing interlayer thickness.

Tekaslan et. al. (2008) investigated the impact of sheet thickness and bending angle on the springback in V bending dies. They observed that an increase in the bending angle and sheet thickness, increased the values of springback. Holding the punch longer during the bending operation reduced springback.

Aghchai et. al. (2017) used experimental, theoretical, and finite element methods to investigate the springback behaviour of sandwich sheets made of Al2024, Polyurethane-glass reinforcement, and Al2024. Findings revealed that raising the temperature of process and sandwich sheet core thickness lowered the value of springback in sandwich sheets. The average difference between experimental and FE findings was just 12%, whereas the average difference between experimental and theoretical results was 17%. Springback was reduced by about 22%

and bending force was reduced by nearly 50% when process temperature was raised to 150°C. Change in core thickness from 0.4 to 1.6 mm resulted in a 17% decrease in springback angle and a 38% increase in the needed bending force. In the diagonal direction, the sandwich sheet which was made of diagonal layer of Al2024, experienced the least amount of springback.

Etemadi et. al. (2020) manufactured two ply Al/Cu and three-ply Al/Cu/Al<sub>2</sub>O<sub>3</sub> clad sheets by using accumulative press bonding technique and investigated their springback experimentally. They observed that for both composites, springback decreased when applied strain increased in L-die bending. The composite having higher elastic modulus showed lower value of springback.

Mohammadi et. al. (2015) investigated the springback prediction of sheets that had been laminated with Al3105, polypropylene, and Al3105 and bent in air bending process. For the purpose of confirming the impact of punch stroke, punch radius and die opening, on springback behaviour, experiments, analytical and numerical analysis were conducted. According to the findings, springback rises when punch radius, punch stroke, or die opening increases. The parameter with the greatest influence was determined to be die opening. The springback was calculated on the higher side by the numerical analysis of the air bending process, due to the deficient material model particularly for the polymeric core. According to experimental data, doubling the punch radius, punch stroke and die opening, resulted in an average increase in springback of about 7%, 18%, and 27%, respectively.

Valinezhad et. al. (2019) studied springback behaviour of Cu/Al clad sheet for L-die bending process. They observed that springback decreased with decrement of die radius and clearance. They also observed that sheet placing pattern affected the springback due to different strengths of the sheets and variation of the bending radius.

Etemadi et al. (2020) investigated the impact of the curvatures of die and punch or both in spring-go /springback of 2-ply Al/Cu clad sheets in unique U-bending setups. They observed that in new U-bending setups against regular U-bending setups, curvatures play a very important role in decreasing the spring-go /springback. They achieved a good agreement

between FEM and experimental values of spring-go /springback. They also focused on the thicknesses of Cu and Al as well as the setting conditions of layers. It was observed that springback of Al/Cu was low as compared to Cu/Al. They concluded that the relocation of neutral axis was responsible for the change in springback of Al/Cu or Cu/Al.

Srinivasan and Karthik Raja (2019) done V-bending experiments conducted with Al-Cu clad sheets to gain insights into springback, bend force, and thickness alterations. Various parameters, including sheet thickness, sheet configuration, die angle, die opening, and punch radius, were systematically explored. The findings revealed that smaller die angles, wider die openings, and larger punch radii result in more pronounced springback. Conversely, increasing the die angle, widening the die opening, or reducing the punch radius leads to a decrease in bend force. It was observed that the sheet thickness varies depending on whether Al or Cu is on the outer surface. The Al/Cu setting condition causes thickening, while the Cu/Al setting condition leads to thinning. This variation in sheet thickness significantly impacts both springback and bend force.

## **2.3 Springback influencing factors**

Influencing factors of springback in case of the sheet metal bending are explained below:

### **2.3.1 Modulus of elasticity or Young's modulus (E)**

During unloading, springback is influenced by the material's Young's modulus. When the elastic modulus rises, the amount of springback decreases since the stiffness also rises. It is customary to make the assumption that E stays constant when performing analysis. Yet, experimental studies showed that a material's elastic constants may somewhat alter during plastic deformation. (Bonora et al., 2005; Morestin and Boivin, 1996).



### **2.3.2 Sheet thickness (t)**

The relationship between springback and sheet thickness is inverse in nature, meaning that the greater the sheet thickness, the lower the springback (Tekaslan et al., 2008; Wagoner et al., 2013). This is because during plastic bending, smaller sheets of the same material have a larger proportion of thickness in the elastic range (elastic core) than the thicker sheets.

### **2.3.3 Flow stress ( $\sigma_0$ ) or yield stress and strain hardening exponent**

With a rise in flow stress or yield stress, springback also increases. AHSS-Advanced high strength steels with a high strength to weight ratio are now extensively utilized to make car components as part of attempts to reduce weight and improve fuel economy. Hence, because of their large yield strengths, the springback problem become more serious. High strength steel components exhibit better elastic strain recovery than low strength steel components due to increased elastic recovery caused by higher flow stress, as shown in Fig. 2.1. (a). In Fig. 2.1 (b), two components generated by U-bending and displaying varied springback are constructed of two different steels with the same yield strength (350 MPa) but differing tensile strengths (600 MPa and 450 MPa). The sample of DP350/600 steel with YS of 350MPa and ultimate tensile strength (UTS) of 600MPa exhibits much higher springback in the formed component than that of the other sample of high strength low alloy (HSLA) steel with same yield strength but lower ultimate tensile strength. The strain hardening exponent "n" of the materials that obey the power law of strain hardening also affects springback. During plastic bending, the flow stress rises due to strain hardening phenomenon [ $\sigma = K\varepsilon^n$ ] (Marciniak, 2002) where  $\varepsilon$  is true plastic strain corresponding to flow stress and  $K$  is strength coefficient. Plastic deformation reduces the value of the strain hardening exponent, which causes the flow stress to considerably rise and increases springback since the strain hardening exponent (n) is a measure of a material's workability at room temperature.

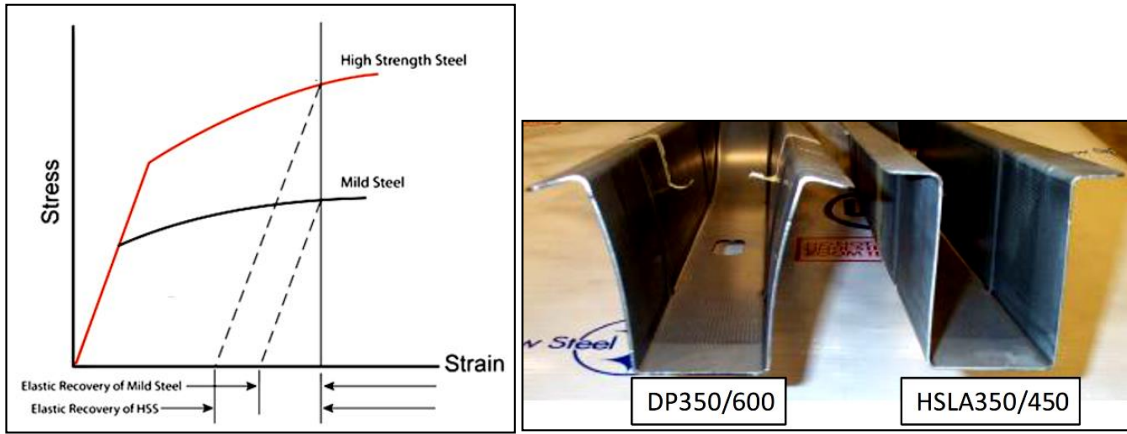


Fig. 2.1 Comparison of (a) elastic recovery in two different steels and (b) springback in U-bending of two different steels (Billur and Altan, 2012)

### 2.3.4 Anisotropy

The mechanical characteristics of sheet metals change depending on the RD (rolling direction). This behaviour of dependence of mechanical characteristics on the orientation is known as anisotropy. The ratio of strain in width ( $\epsilon_w$ ) to the strain in thickness ( $\epsilon_t$ ) is known as the plastic strain ratio, which is used to assess anisotropy in the sheets.

$$\text{Plastic strain ratio } (R) = (\epsilon_w / \epsilon_t). \quad (2.1)$$

Average plastic strain ratio or Normal anisotropy ( $\bar{R}$ ) is given by the equation (Hosford, 2007):

$$\bar{R} = \left( \frac{R_0 + 2R_{45} + R_{90}}{4} \right) \quad (2.2)$$

Anisotropy of a sheet metal is due to the development of crystallographic texture during plastic deformation (cold rolling) and annealing and mechanical fibering (Dieter and Bacon, 1986). During plastic deformation in rolling, significant reduction affects the crystallographic structure of the material hence the anisotropy gets affected. Huge deformation makes polycrystalline sheets to approach single crystal anisotropy and the strength of a single crystal is highly anisotropic, so the polycrystalline sheet also shows high anisotropic behaviour under huge deformation. The reason behind the above-mentioned behaviour is based on the slip system of the BCC lattice structure of the sheet material. The BCC lattice structure possesses a total number of 48 slip system by combining the family of slip directions  $\langle 111 \rangle$  and favourable

slip planes such as  $\{110\}$ ,  $\{112\}$  or  $\{123\}$  together. Due to this nature of the slip systems, deformation of a grain under a stress level depends upon orientation of the grains (Van Boxel, 2010). Anisotropy caused due to mechanical fibering or intergranular substructure is mainly due to preferred alignment of structural discontinuities such as inclusions, voids segregation and phase present in the direction of working (Li et al., 2006). During bending operation, the yielding behaviour of the sheet metal is affected by its anisotropy therefore, more attention is to be given to the orientation of the specimen w.r.t. RD. Higher springback is observed with higher value of normal anisotropy (Verma and Halidar, 2007).

## **2.4 Research gaps and motivation**

### **2.4.1 Research gaps**

After an extensive literature survey, it has been observed that the following issues have not been attempted so far:

1. Several models of pure bending of monolithic sheet materials are available in the literature, but an extensive theory is still lacking on the laminated sheet materials. Anisotropy is not fully explored in most of the analytical models of laminated sheets.
2. Study of springback in laminated composite sheets in V-bending is limited although extensive research on V-bending of monolithic materials has been done in sheet metal forming.
3. Effect of individual sheets on springback of laminate composite of aluminium and stainless steel has not been studied.
4. Orientation of bending with respect to rolling direction is of great significance, especially in laminated sheets, but it has not been well studied so far in laminated sheets.

### **2.4.2 Research objectives**

When aluminium/stainless steel laminated sheets are chosen for manufacturing of automobile components, utensils etc. especially for applications which involve bending during deformation, it is important to choose the design and process variables and the material

properties such that springback is minimized. These additional problems make predictions or determination of springback in the case of Aluminium/Stainless steel laminated sheets more challenging as compared to the conventional sheet metals. In view of the above-mentioned challenges and the research gaps in prediction and compensation of springback of aluminium/stainless steel laminated sheets, objectives of the proposed research have been broadly formulated as below:

1. Characterization of tensile properties of parent sheets and 2-ply and 3-ply laminate composite sheets.
2. Determination of anisotropy of parent sheets and 2-ply and 3-ply laminate composite sheets.
3. Development of analytical model for springback prediction of 2-ply and 3-ply laminate composite sheets after V-bending.
4. Springback issues in bending of 2-ply and 3-ply laminate sheets with varying punch profile radius.
5. FE simulations of springback in V-bending of 2-ply and 3-ply laminate sheets and experimental validation of results predicted by simulations and analytical techniques.

## **CHAPTER 03**

### **DEVELOPMENT OF ANALYTICAL MODEL**

Prediction of springback in 2-ply and 3-ply clad sheets is important in sheet bending. It allows the design engineers to design die and punch incorporating springback compensation as a corrective measure and helps reduce the number of trials on the shop floor. Analytical models are approximate solutions, generally based on certain assumptions made to reduce complexities. In the present work, analytical models for springback prediction in bending of 2-ply and 3-ply clad sheets respectively, have been developed by extending the simple theory of sheet bending under plane strain condition. These analytical models have incorporated the effects of strain hardening and anisotropy to predict the springback behaviour after V-bending of a two-ply and a three-ply sheet. The analytical models, also, discuss the effects of sheet setting on springback during bending operation.

The methodology adopted in the present research work for the development of analytical model for springback prediction in V-bending of 2-ply and 3-ply clad sheets is presented below: -

#### **3.1 Development of the analytical model for 2-ply sheet**

The analytical model has been developed based on the following assumptions to calculate the bending moment in a two-ply sheet positioned in the following two ways during bending:

- (1) The inner layer is of SS430, and AA1050 is the outer layer.
- (2) The inner layer is of AA1050, and SS430 is the outer layer.

Consider a two-ply sheet as shown in Fig. 3.1, with a layer of AA1050 of thickness  $t_1$  at the top and a layer of SS430 of thickness  $t_2$  below the top layer, bent to an angle “ $\theta$ ” and radius of curvature “ $r$ ” measured at an assumed neutral layer NN'. The following assumptions have been made to simplify the analytical model:

- Plane strain condition is assumed as the width 'w' is much larger than the combined thickness ( $t_1 + t_2$ ) of the sheet.
- Bauschinger effect and shifting of the neutral axis (NN') are neglected.
- Both the layers are considered to be elastic-plastic and obey the strain hardening power law.
- Total bending moment and the corresponding springback are achieved from the summation of bending moment of each layer.

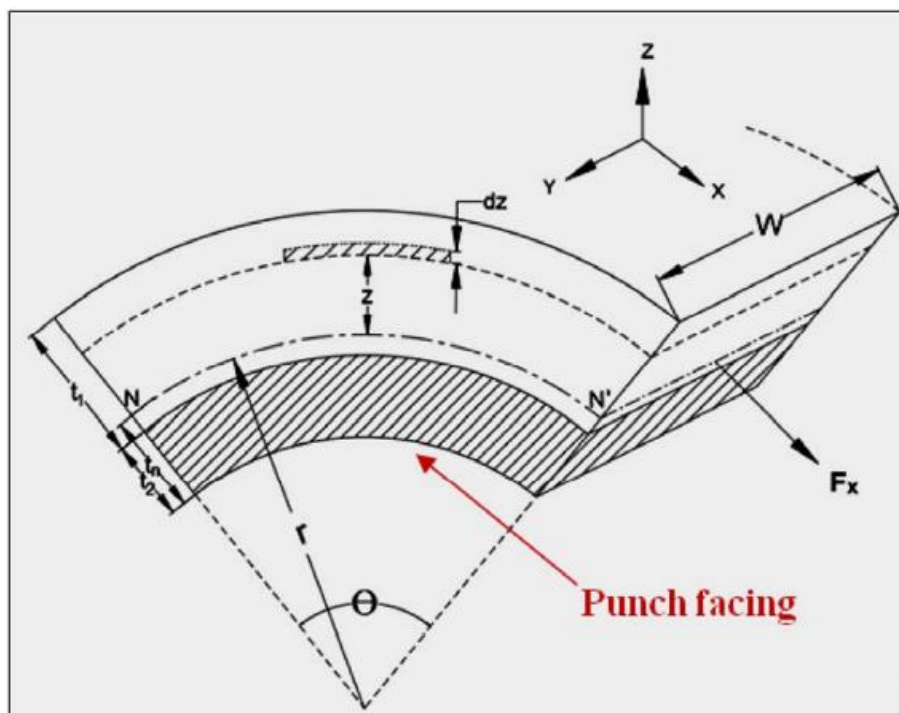


Fig. 3.1 Schematic of plane-strain bending of two-ply sheet

As shown in Fig. 3.1, engineering strain at a distance 'z' from the neutral axis is given by  $\frac{z}{r}$  and as this ratio is small, true strain,  $\epsilon_x \approx \frac{z}{r}$ . Considering an elastic core up to a distance 'ze' from the neutral surface on either side, the true strain in the elastic region is given by

$$\epsilon_x = \frac{z_e}{r} = \frac{\sigma'_0}{E'} \quad (3.1)$$

where  $E'$  is elastic modulus in plane strain condition  $\left(E' = \frac{E}{(1-\nu^2)}\right)$  and  $\sigma'_0$  is flow stress in plane strain condition.

To determine the bending moment,  $M$ , it is assumed that there is no net external force in X-direction, i.e.  $\sum F_x = 0$ . The elemental force  $dF_x$  acting on an elemental strip of area ' $w \cdot dz$ ' along the X-direction is  $dF_x = \sigma_x \cdot w \cdot dz$  and the bending moment is given by

$$dM = \sigma_x \cdot w \cdot z \cdot dz \quad (3.2)$$

Using eq. (3.2), after 'V' bending operation, total bending moment for the whole blank can be obtained as

$$M = M_{layer\ 1} + M_{layer\ 2} \quad (3.3)$$

where,  $M_{layer\ 1}$  and  $M_{layer\ 2}$  are the bending moments of layer\_1 and layer\_2, respectively.

For elastic and plastic regions, the bending moments are calculated separately.

In the elastic region,  $\sigma'_x$  following generalized Hooke's law is given as

$$\sigma'_x = \varepsilon_x \cdot E' = \frac{z}{r} \cdot E' \text{ for } 0 \leq z \leq z_e \quad (3.4)$$

In the plastic region,  $\sigma'_x$  is the flow stress of the material that depends on strain hardening and anisotropic behaviour of the sheet, and so, it is not a constant.

Hill's anisotropic yield function is given as

$$2f(\sigma_{ij}) = F(\sigma_{yy} - \sigma_{zz})^2 + F(\sigma_{zz} - \sigma_{xx})^2 + F(\sigma_{xx} - \sigma_{yy})^2 + 2L\tau_{yz}^2 + 2M\tau_{zx}^2 + 2N\tau_{xy}^2 - 1 = 0 \quad (3.5)$$

Here  $\sigma_{xx}$ ,  $\sigma_{yy}$  and  $\sigma_{zz}$  are the normal stresses in rolling, transverse and through thickness directions, respectively;  $\tau_{xy}$ ,  $\tau_{yz}$  and  $\tau_{zx}$  are shear stresses. If  $\sigma_{0x}$ ,  $\sigma_{0y}$  and  $\sigma_{0z}$  are yield stresses in simple tension along x, y and z directions respectively, it can be shown that

$$\frac{1}{\sigma_{0x}^2} = (G + H), \frac{1}{\sigma_{0y}^2} = (H + F) \text{ and } \frac{1}{\sigma_{0z}^2} = (F + G) \quad (3.6)$$

On simplification, equation (3.6) can be written as

$$2F = \left( \frac{1}{\sigma_{0y}^2} + \frac{1}{\sigma_{0z}^2} - \frac{1}{\sigma_{0x}^2} \right), 2G = \left( \frac{1}{\sigma_{0z}^2} + \frac{1}{\sigma_{0x}^2} - \frac{1}{\sigma_{0y}^2} \right), \text{ and } 2H = \left( \frac{1}{\sigma_{0x}^2} + \frac{1}{\sigma_{0y}^2} - \frac{1}{\sigma_{0z}^2} \right) \quad (3.7)$$

In sheet metal forming, the coefficients F, G, H, and N are generally determined by Lankford-values. Referring to Lankford-values, we define the  $X_\gamma$ ,  $Y_\beta$ , and  $Z_\alpha$  values which are Lankford-

values on the X, Y, and Z plane. Here the X, Y, and Z planes are normal plane to the x, y, and z axis, respectively.

Where,  $\gamma$ ,  $\beta$ ,  $\alpha$  are rotated angle from y, z, and x directions, respectively. By using these values Hill's coefficients are determined as follows:

$$L = \left(\frac{1}{2} + X_{45}\right) \left(\frac{1}{X_0} + \frac{1}{X_{90}}\right) F = \left(\frac{1}{2} + X_{45}\right) \left(1 + \frac{1}{Z_0}\right) H$$

$$M = \left(\frac{1}{2} + Y_{45}\right) \left(\frac{1}{Y_0} + \frac{1}{Y_{90}}\right) F = \left(\frac{1}{2} + Y_{45}\right) \left(1 + \frac{1}{Z_{90}}\right) H$$

$$N = \left(\frac{1}{2} + Z_{45}\right) \left(\frac{1}{Z_0} + \frac{1}{Z_{90}}\right) H$$

where  $F$ ,  $G$ ,  $H$ ,  $L$ ,  $M$  and  $N$  are anisotropic constants.

Using the flow rule associated with the yield criterion, for  $\sigma_{0y} = \sigma_{0z} = 0$ , it can be shown that

$R_0 = \frac{H}{G}$  and  $R_{90} = \frac{H}{F}$ , where  $R_0$  and  $R_{90}$  are the values of plastic strain ratio in rolling and

transverse directions, respectively. The effective stress  $\bar{\sigma}$  and effective strain  $\bar{\epsilon}$  are expressed in terms of  $R_0$  and  $R_{90}$  as follows

$$\bar{\sigma} = \sqrt{\frac{3}{2} \left[ \frac{((1+R_0).R_{90})}{(R_0+R_{90}+(R_0.R_{90}))} \right]} \cdot \sigma_{0x} \quad (3.8)$$

$$\bar{\epsilon} = \sqrt{\frac{2}{3} \left[ \frac{(R_0+R_{90}+(R_0.R_{90}))}{((1+R_0).R_{90})} \right]} \cdot \epsilon_{0x} \quad (3.9)$$

where  $\sigma_{0x}$  and  $\epsilon_{0x}$  are yield stress and yield strain along the rolling direction, respectively. The above equations can be written as  $\bar{\sigma} = C_1 \cdot \sigma_{0x}$  and  $\bar{\epsilon} = C_2 \cdot \epsilon_{0x}$ , where  $C_1$  and  $C_2$  are constants and depend on  $R_0$  and  $R_{90}$ . Considering the strain hardening of the material according to power law  $\bar{\sigma} = K \cdot \bar{\epsilon}^n$ , where  $K$  and  $n$  are strength coefficient and strain hardening exponent, respectively; the effective stress in plane strain bending can be written as follows:

$$\bar{\sigma} = K' \cdot \bar{\epsilon}^n = K' \cdot (C_2 \cdot \epsilon_{0x})^n \quad (3.10)$$

where  $K'$  is strength coefficient in plane strain condition and  $K' = K \left(\frac{4}{3}\right)^{\frac{(n+1)}{2}}$



Therefore,  $\sigma'_x$  in plastic region for an anisotropic material obeying power law of strain hardening is given as

$$\sigma'_x = \frac{K'.c_2^n}{c_1} \cdot \varepsilon_{0x}^n = \frac{K'.c_2^n}{c_1} \cdot \left(\frac{z}{r}\right)^n \quad (3.11)$$

To determine the bending moment, the location of neutral layer of the laminate composite should be known. To achieve this, the two-ply sheet metal is transformed into a single material sheet using "Equivalent Area Method" (EAM) (Jones et. al, 2014). In this technique, one of the materials is selected to be the base material and the area of the other material is adjusted laterally in width so that the equivalent section is transformed into an area of one dominant homogeneous material as shown in Fig.3.2 (a) and Fig. 3.2 (b).

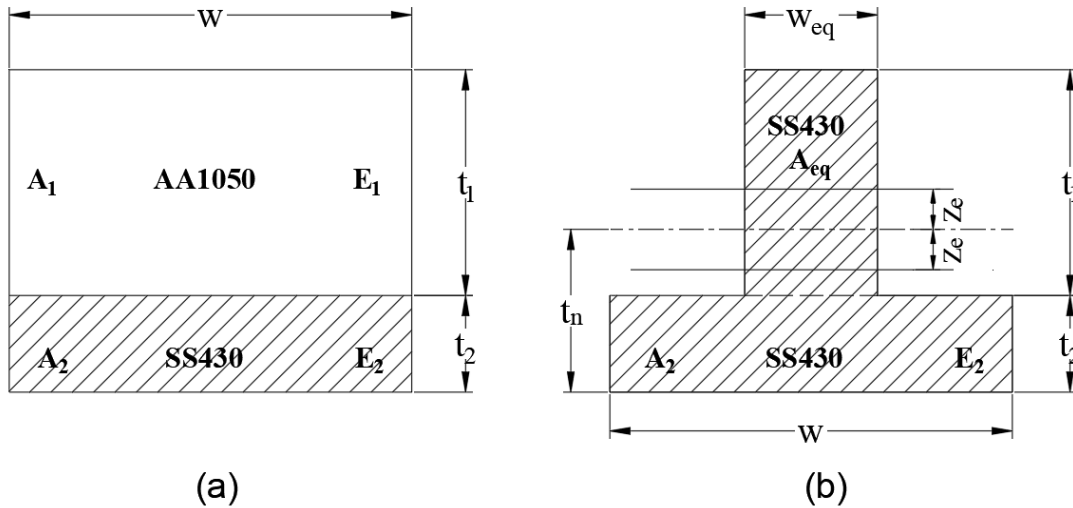


Fig. 3.2 (a) Transverse section of a two-ply sheet AA 1050/SS 430 and (b) Transformed section

Let the thickness of Aluminium layer and steel layer be ' $t_1$ ' and ' $t_2$ ' respectively, having same width equal to ' $w$ ' and length be ' $l$ '. After applying the technique of EAM, let the area of the equivalent section of Aluminium be ' $A_{eq}$ ' with width ' $w_{eq}$ '.

Applying EAM, we get:  $A_{eq}E_2 = E_1A_1$ .

The distance of the neutral axis ' $t'_n$ ' from the bottommost plane of the sheet considering equivalent area is given as below:

$$t_n = \left( \frac{\left(t_2 + \frac{t_1}{2}\right) \frac{E_1}{E_2} A_1 + \frac{t_2}{2} A_2}{A_{eq} + A_2} \right) = \left[ \frac{\left(t_2 + \frac{t_1}{2}\right) \frac{E_1}{E_2} wt_1 + \frac{t_2}{2} wt_2}{\frac{E_1}{E_2} wt_1 + wt_2} \right]$$

$$= \left[ \frac{(2t_2+t_1)E_1t_1+t_2^2E_2}{2(E_1t_1+E_2t_2)} \right] \quad (3.12)$$

Since the position of the neutral layer is known in the form of a general equation given by Eq. (3.12), the procedure for the determination of bending moments of the respective layers of two-ply is explained for the two cases of sheet setting as below:

### 3.1.1 Case-I: Bending of the two-ply sheet with SS430 as the inner layer

Considering a small element of thickness “dz” at a distance of “z” from the neutral axis which is assumed to fall in AA1050 as shown in Fig. 3.3 and applying the procedure to determine the bending moment of each layer using the required integration limits with reference to the neutral axis

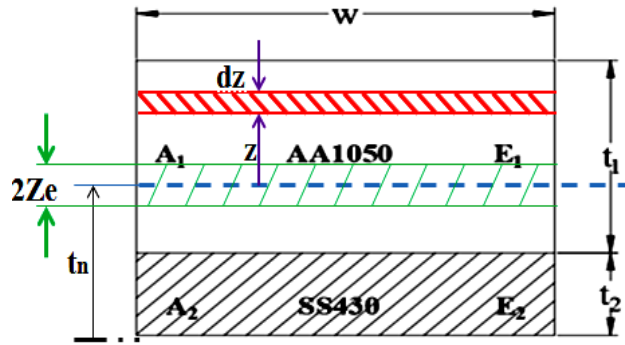


Fig. 3.3 Transverse section of a two-ply sheet with SS430 as the inner layer

Combining elastic and plastic regions, the total bending moment for the layer\_1 ( $M_1^I$ ), i.e., the layer of AA1050, is given by

$$M_1^I = \int_{-(t_n-t_2)}^{(t_n-t_2)} \sigma_{x1} \cdot w \cdot z \cdot dz + \int_{(t_n-t_2)}^{(t_1+t_2-t_n)} \sigma_{x1} \cdot w \cdot z \cdot dz \quad (3.13)$$

The integration limits as shown in Fig. 3.3 for the bending of aluminium layer vary from  $-(t_n-t_2)$  located below the neutral axis till the interface with steel layer and extend up to a limit of  $(t_n-t_2)$  located above the neutral axis but equal in the region as taken below the neutral axis to simplify the integration. Furthermore, the limits of integration for the remaining aluminum layer above the neutral axis vary from  $(t_n-t_2)$  to  $(t_1+t_2-t_n)$ . The first integral part of Eq. (3.13) contains the elastic and plastic regions due to the presence of an elastic core. Therefore, this

part is further expanded in Eq. (3.14) with integration limits for the elastic and plastic region as given below:

$$= \left[ 2 \int_0^{z_e} (\sigma_{x1(elastic)} \cdot w \cdot z \cdot dz) + 2 \int_{z_e}^{(t_n - t_2)} (\sigma_{x1(plastic)} \cdot w \cdot z \cdot dz) + \int_{(t_n - t_2)}^{(t_1 + t_2 - t_n)} (\sigma_{x1(plastic)} \cdot w \cdot z \cdot dz) \right] \quad (3.14)$$

$$= \left[ 2 \int_0^{z_e} \frac{z}{r} \cdot E_1' w \cdot z \cdot dz + 2 \int_{z_e}^{(t_n - t_2)} \left( \frac{K_1' \cdot C_2^n}{c_1} \cdot \left( \frac{z}{r} \right)^n \cdot w \cdot z \cdot dz \right) + \int_{(t_n - t_2)}^{(t_1 + t_2 - t_n)} \left( \frac{K_1' \cdot C_2^n}{c_1} \cdot \left( \frac{z}{r} \right)^n \cdot w \cdot z \cdot dz \right) \right] \quad (3.15)$$

$$= \frac{2w \cdot E_1' \cdot z_e^3}{3r} + \frac{w \cdot K_1' \cdot C_2^n}{c_1 \cdot r^n \cdot (n+2)} \left[ (t_1 + t_2 - t_n)^{(n+2)} - 2(z_e)^{(n+2)} + (t_n - t_2)^{(n+2)} \right] \quad (3.16)$$

The total bending moment for the layer<sub>2</sub>, ( $M_2^I$ ), i.e., the layer of SS430 is given by

$$M_2^I = \int_{(t_n - t_2)}^{t_n} \sigma_{x2} \cdot w \cdot z \cdot dz \quad (3.17)$$

The integration limits with respect to the neutral axis for determination of bending moment for the steel layer vary from  $-(t_n - t_2)$  located below the neutral axis at the interface with aluminum to the bottommost layer of steel, i.e., upto  $-(t_n)$ . In order to simplify the solution, the integration limits with positive signs are considered without affecting the results

$$= \left[ \int_{(t_n - t_2)}^{t_n} (\sigma_{x2(plastic)} \cdot w \cdot z \cdot dz) \right] \quad (3.18)$$

$$= \left[ \int_{(t_n - t_2)}^{t_n} \left( \frac{K_2' \cdot C_2^n}{c_1} \cdot \left( \frac{z}{r} \right)^n \cdot w \cdot z \cdot dz \right) \right] \quad (3.19)$$

$$= \frac{K_2' \cdot C_2^n \cdot w}{r^n \cdot c_1 \cdot (n+2)} \left[ (t_n)^{(n+2)} - (t_n - t_2)^{(n+2)} \right] \quad (3.20)$$

The total bending moment for the Case-I, denoted as  $M^I$ , is given as

$$M^I = \left[ \frac{2w \cdot E_1' \cdot z_e^3}{3r} + \frac{w \cdot K_1' \cdot C_2^n}{c_1 \cdot r^n \cdot (n+2)} \left[ (t_1 + t_2 - t_n)^{(n+2)} - 2(z_e)^{(n+2)} + (t_n - t_2)^{(n+2)} \right] + \frac{K_2' \cdot C_2^n \cdot w}{r^n \cdot c_1 \cdot (n+2)} \left[ (t_n)^{(n+2)} - (t_n - t_2)^{(n+2)} \right] \right] \quad (3.21)$$

Let  $\Delta M$  be the change in the combined bending moment due to the resulting springback after the load is removed. Using the theory of bending, change in combined bending moment  $\Delta M$  is given by

$$\Delta M = E' \cdot I \left( \frac{1}{r} - \frac{1}{r'} \right) \quad (3.22)$$

$$\begin{aligned} &= E'_1 \cdot \left[ I \left( \frac{1}{r} - \frac{1}{r'} \right) \right] + E'_2 \cdot \left[ I \left( \frac{1}{r} - \frac{1}{r'} \right) \right] \\ &= \left[ E'_1 \left[ \frac{wt_1^3}{12} + \left( (wt_1) \cdot \left( t_2 + \frac{t_1}{2} - t_n \right)^2 \right) \right] + E'_2 \left[ \frac{wt_2^3}{12} + \left( (wt_2) \cdot \left( t_n - \frac{t_2}{2} \right)^2 \right) \right] \right] \cdot \left[ \frac{1}{r} - \frac{1}{r'} \right] \end{aligned} \quad (3.23)$$

When the external moment is released, the internal moment must also vanish causing the specimen to unbend elastically. Hence, the net moment will be

$$M^I - \Delta M = 0$$

From Eqs. (3.21) and (3.23) after rearranging we get

$$\begin{aligned} &\left( \frac{1}{r} - \frac{1}{r'} \right) \\ &= \frac{\left[ \frac{2w \cdot E'_1 \cdot z_e^3}{3r} + \frac{w \cdot K'_1 \cdot C_2^n}{C_1 \cdot r^n \cdot (n+2)} \left[ (t_1 + t_2 - t_n)^{(n+2)} - 2(z_e)^{(n+2)} + (t_n - t_2)^{(n+2)} \right] + \frac{K'_2 \cdot C_2^n \cdot w}{r^n \cdot C_1 \cdot (n+2)} \left[ (t_n)^{(n+2)} - (t_n - t_2)^{(n+2)} \right] \right]}{E'_1 \left[ \frac{wt_1^3}{12} + \left( (wt_1) \cdot \left( t_2 + \frac{t_1}{2} - t_n \right)^2 \right) \right] + E'_2 \left[ \frac{wt_2^3}{12} + \left( (wt_2) \cdot \left( t_n - \frac{t_2}{2} \right)^2 \right) \right]} \end{aligned} \quad (3.24)$$

The new radius of curvature ( $r'$ ) after springback is determined from Eq. (3.24)

### 3.1.2 Case-II: Bending of a two-ply sheet with AA1050 as the inner layer

Similarly, considering a small element of thickness “dz” at a distance of “z” from the neutral axis which is assumed to fall in AA1050 as shown in Fig. 3.4 and applying the procedure to determine the bending moment of each layer, as explained before as only the integration limits will change. Combining the elastic and plastic regions, the total bending moment for the layer\_1 ( $M_1^I$ ), i.e., the layer of AA1050, is given by

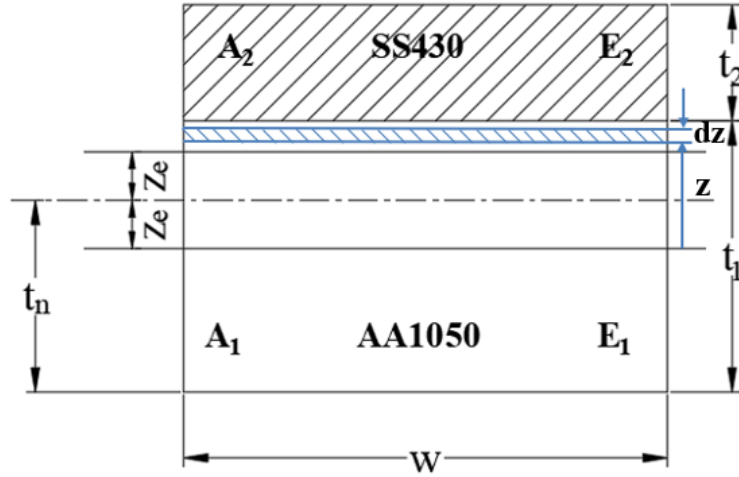


Fig. 3.4 Transverse section of a two-ply sheet with an AA1050 as the inner layer

$$M_1^{II} = \int_{-(t_1-t_n)}^{(t_1-t_n)} \sigma_{x1} \cdot w \cdot z \cdot dz + \int_{(t_1-t_n)}^{(t_n)} \sigma_{x1} \cdot w \cdot z \cdot dz \quad (3.25)$$

The integration limits as shown in Fig. 3.4 for the bending of aluminium in the inner layer vary from  $(t_1 - t_n)$  located above the neutral axis up to the interface with the steel layer and extend up to a limit of  $-(t_1 - t_n)$  located below the neutral axis but equal in the region as taken above to simplify the integration. Furthermore, the limits of integration for the remaining aluminium layer below the neutral layer vary from  $-(t_1 - t_n)$  to  $-(t_n)$  but only the positive sign is considered to simplify the solution. The first integral part of Eq. (3.25) contains the elastic and plastic regions due to the presence of an elastic core. Therefore, this part is further expanded in Eq. (3.26) with integration limits for elastic and plastic regions

$$= \left[ 2 \int_0^{z_e} (\sigma_{x1(elastic)} \cdot w \cdot z \cdot dz) + 2 \int_{z_e}^{(t_1-t_n)} (\sigma_{x1(plastic)} \cdot w \cdot z \cdot dz) + \int_{(t_1-t_n)}^{(t_n)} (\sigma_{x1(plastic)} \cdot w \cdot z \cdot dz) \right] \quad (3.26)$$

$$= \left[ 2 \int_0^{z_e} \left( \frac{z}{r} \cdot E_1' \cdot w \cdot z \cdot dz \right) + 2 \int_{z_e}^{(t_1-t_n)} \left( \frac{K_1' \cdot C_2^n}{C_1} \cdot \left( \frac{z}{r} \right)^n \cdot w \cdot z \cdot dz \right) + \int_{(t_1-t_n)}^{(t_n)} \left( \frac{K_1' \cdot C_2^n}{C_1} \cdot \left( \frac{z}{r} \right)^n \cdot w \cdot z \cdot dz \right) \right] \quad (3.27)$$

$$= \frac{2w \cdot E_1' \cdot z_e^3}{3r} + \frac{K_1' \cdot C_2^n \cdot w}{r^n \cdot C_1 \cdot (n+2)} \left[ (t_1 - t_n)^{(n+2)} - 2(z_e)^{(n+2)} + (t_n)^{(n+2)} \right] \quad (3.28)$$

The bending moment for SS430 denoted as  $M_2^{II}$  in the outer layer is given by

$$M_2^{II} = \int_{(t_1-t_n)}^{(t_1+t_2-t_n)} \sigma_{x2} \cdot w \cdot z \cdot dz \quad (3.29)$$

The integration limits for the bending of steel in the outer layer vary from  $(t_1 - t_n)$  located above the neutral axis at the interface with the steel layer and extend up to a limit of  $(t_1 + t_2 - t_n)$

$$= \left[ \int_{(t_1-t_n)}^{(t_1+t_2-t_n)} (\sigma_{x2(plastic)} \cdot w \cdot z \cdot dz) \right] \quad (3.30)$$

$$= \left[ \int_{(t_1-t_n)}^{(t_1+t_2-t_n)} \left( \frac{K'_2 \cdot C_2^n}{C_1} \cdot \left( \frac{z}{r} \right)^n \cdot w \cdot z \cdot dz \right) \right] \quad (3.31)$$

$$= \frac{K'_2 \cdot C_2^n \cdot w}{r^n \cdot C_1 \cdot (n+2)} \left[ ((t_1 + t_2 - t_n))^{(n+2)} - ((t_1 - t_n))^{(n+2)} \right] \quad (3.32)$$

Total bending moment for the Case-II, denoted as  $M_2^{II}$  is given as

$$M_2^{II} = \left[ \frac{2w \cdot E'_1 \cdot z_e^3}{3r} + \frac{K'_1 \cdot C_2^n \cdot w}{r^n \cdot C_1 \cdot (n+2)} \left[ (t_1 - t_n)^{(n+2)} - 2(z_e)^{(n+2)} + (t_n)^{(n+2)} \right] + \frac{K'_2 \cdot C_2^n \cdot w}{r^n \cdot C_1 \cdot (n+2)} \left[ (t_1 + t_2 - t_n)^{(n+2)} - (t_1 - t_n)^{(n+2)} \right] \right] \quad (3.33)$$

Using theory of bending, change in total bending moment  $\Delta M$  is given as below

$$\Delta M = E' \cdot I \left( \frac{1}{r} - \frac{1}{r'} \right) = \left[ E'_1 \left[ \frac{wt_1^3}{12} + \left( (wt_1) \cdot \left( t_n - \frac{t_1}{2} \right)^2 \right) \right] + E'_2 \left[ \frac{wt_2^3}{12} + \left( (wt_2) \cdot \left( \frac{t_2}{2} + t_1 - t_n \right)^2 \right) \right] \right] \cdot \left[ \frac{1}{r} - \frac{1}{r'} \right] \quad (3.34)$$

When the external moment is released, the internal moment must also vanish causing the specimen to unbend elastically. Using Eqs. (3.33) and (3.34), we get

$$\left( \frac{1}{r} - \frac{1}{r'} \right) = \frac{\left[ \frac{2w \cdot E'_1 \cdot z_e^3}{3r} + \frac{K'_1 \cdot C_2^n \cdot w}{r^n \cdot C_1 \cdot (n+2)} \left[ (t_1 - t_n)^{(n+2)} - 2(z_e)^{(n+2)} + (t_n)^{(n+2)} \right] + \frac{K'_2 \cdot C_2^n \cdot w}{r^n \cdot C_1 \cdot (n+2)} \left[ (t_1 + t_2 - t_n)^{(n+2)} - (t_1 - t_n)^{(n+2)} \right] \right]}{E'_1 \left[ \frac{wt_1^3}{12} + \left( (wt_1) \cdot \left( t_n - \frac{t_1}{2} \right)^2 \right) \right] + E'_2 \left[ \frac{wt_2^3}{12} + \left( (wt_2) \cdot \left( \frac{t_2}{2} + t_1 - t_n \right)^2 \right) \right]} \quad (3.35)$$

To determine the springback in both the cases of sheet setting, the new radius of curvature ( $r'$ ) after springback is determined from Eqs. (3.24) and (3.35), respectively. The change in the bend angle after springback is calculated as

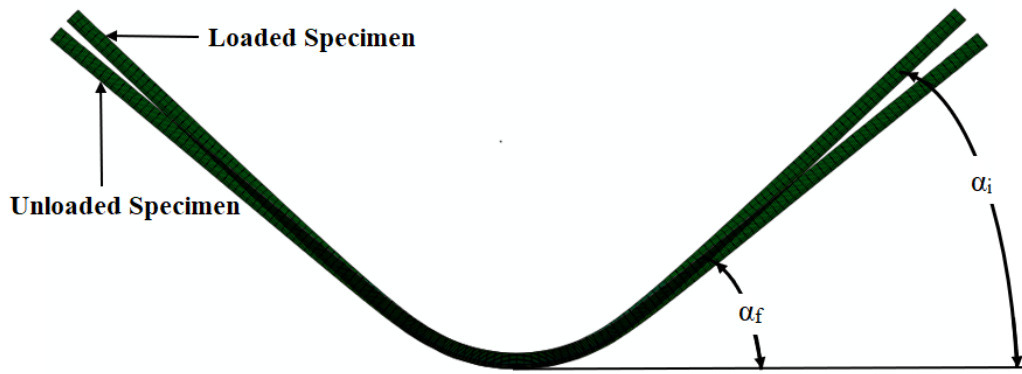


Fig. 3.5 Change in bend angle after springback

Change in the bend angle

$$\alpha_i - \alpha_f = \left(1 - \frac{r}{r'}\right) \alpha_i \quad (3.36)$$

where,  $\alpha_i$  and  $\alpha_f$  are initial and final bend angles as shown in Fig. 3.5. The included bend angle is  $90^\circ$  and is measured on the die, and therefore, the initial bend angle ( $\alpha_i$ ) is  $45^\circ$ .

### 3.2 Development of the analytical model for 3-ply sheet

The present research work is an extension of the study done by Sharma et al. in the development of an analytical model to predict springback incorporating the effects of strain hardening and anisotropy in V-bending of a two-ply clad sheet in which the two layers of different materials and thicknesses are arranged in parallel. Whereas, in the present work, the existing analytical model is redeveloped accordingly to evaluate the springback behaviour of a 3-ply clad sheet metal, comprising of layers of SS304 and SS430 sandwiched with AA1050 layer.

Since the existing analytical model for prediction of springback in bending of two-ply clad sheet incorporating the effects of strain hardening and anisotropy is used in redevelopment of the present analytical model for evaluation of springback in bending of three-ply clad sheet, the assumptions for elastic-plastic material following power law of strain hardening, mainly plane strain condition, neglecting Bauschinger effect, shift in neutral axis and friction at contact

surfaces, remain the same. To determine the bending moment of three-ply clad sheet, two cases of sheet placement on the die during bending are discussed: -

1. SS430 as inner layer and SS304 as outer layer.
2. SS304 as inner layer and SS430 as outer layer.

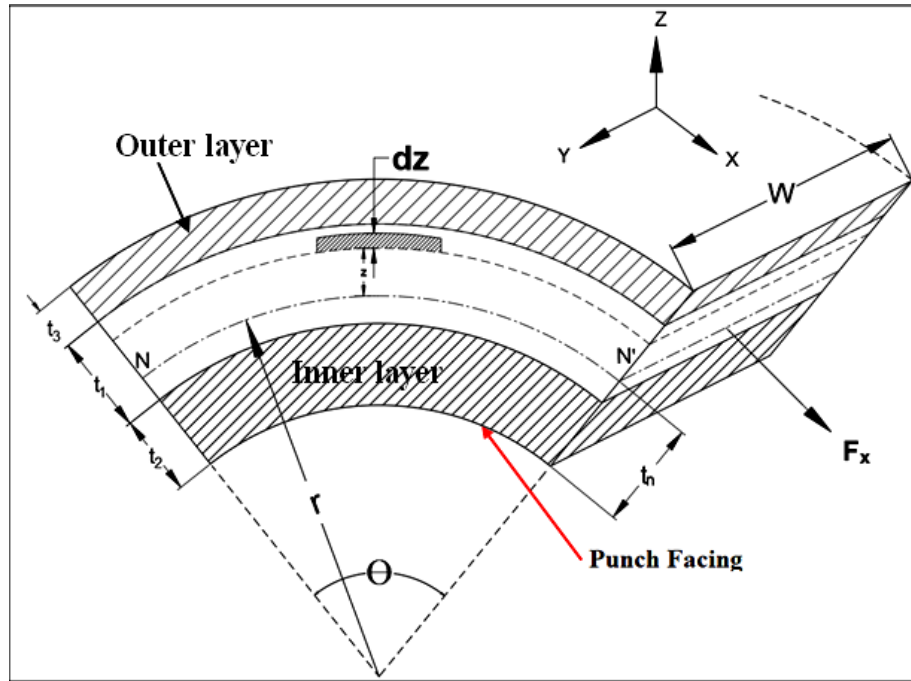


Fig. 3.6 Plane strain bending of a three-ply clad sheet

A schematic diagram of a three-ply clad sheet is shown in Fig. 3.6 considering that an SS304 layer of thickness ' $t_3$ ' at the top and SS430 layer of thickness ' $t_2$ ' at the bottom containing AA1050 layer of thickness ' $t_1$ ' in the middle as a sandwich layer, is bent to an angle ' $\theta$ ' and having a radius of curvature ' $r$ ' with respect to the neutral layer-NN' located at a distance of ' $t_n$ ' from the punch face or the inner layer during bending.

From Fig. 3.6 and Fig. 3.7,  $e_x = \frac{z}{r}$ , where  $e_x$  = engineering strain at ' $z$ ' distance from NN' (neutral axis). Since the ratio  $\frac{z}{r}$  is very small, then true strain  $\epsilon_x \approx \frac{z}{r}$ . Assuming elastic core up to ' $z_e$ ' distance from NN' (neutral axis) on each side as shown in Fig. 3.7. True strain for the elastic zone is given by,

$$\epsilon_x = \frac{z_e}{r} = \frac{\sigma'_0}{E'} \quad (3.37)$$



where,  $\sigma'_0$  is flow stress in plane-strain condition and  $E'$  is modulus of elasticity in plane-strain condition so that  $\left(E' = \frac{E}{(1-\nu^2)}\right)$ , where  $\nu$  is Poisson's ratio and  $E$  is elastic modulus.

Assuming the equilibrium in the direction of bending force, i.e. the x-direction,  $\sum F_x = 0$ . The elemental force  $dF_x$ , is the product of bending stress,  $\sigma_x$ , and the elemental area of strip, i.e.  $(w \cdot dz)$  and the elemental bending moment ( $dM$ ) is given by

$$dM = \sigma_x \cdot w \cdot z \cdot dz \quad (3.38)$$

After bending, the total bending moment,  $M$ , for the three-ply clad sheet can be evaluated as follows:

$$M = M_1 + M_2 + M_3 \quad (3.39)$$

where,  $M_1$ ,  $M_2$  and  $M_3$  are bending moments of layer-1, layer-2, and layer-3, respectively. The bending moments are calculated separately for elastic and plastic zones.

$$\text{In the elastic zone, } \sigma'_x = \varepsilon_x \cdot E' = \frac{z}{r} \cdot E' \text{ for } 0 \leq z \leq z_e \quad (3.40)$$

In the plastic region,  $\sigma'_x$  is flow stress of the material that depends on anisotropy and strain hardening of the sheet and thereby, it is not constant.

Using Hill's anisotropic yield function and the flow rule associated with the criterion, it can be shown that  $R_0 = \frac{H}{G}$  and  $R_{90} = \frac{H}{F}$ , where  $R_0$  and  $R_{90}$  are the values of plastic strain ratio in rolling and transverse directions, respectively. The effective stress  $\bar{\sigma}$  and effective strain  $\bar{\varepsilon}$  are expressed in terms of  $R_0$  and  $R_{90}$  as follows

$$\bar{\sigma} = \sqrt{\frac{3}{2} \left[ \frac{((1+R_0) \cdot R_{90})}{(R_0+R_{90}+(R_0 \cdot R_{90}))} \right]} \cdot \sigma_{0x} \quad (3.41)$$

$$\bar{\varepsilon} = \sqrt{\frac{2}{3} \left[ \frac{(R_0+R_{90}+(R_0 \cdot R_{90}))}{((1+R_0) \cdot R_{90})} \right]} \cdot \varepsilon_{0x} \quad (3.42)$$

where,  $\sigma_{0x}$  and  $\varepsilon_{0x}$  are yield stress and yield strain along the rolling direction, respectively. The effective stress and effective strain can be written as  $\bar{\sigma} = C_1 \cdot \sigma_{0x}$  and  $\bar{\varepsilon} = C_2 \cdot \varepsilon_{0x}$ , where  $C_1$  and  $C_2$  are constants depending on  $R_0$  and  $R_{90}$ . Using the strain hardening power law  $\bar{\sigma} = K \cdot \bar{\varepsilon}^n$ , where  $K$  and  $n$  are strength coefficient and strain hardening exponent, respectively. The effective stress in plane-strain bending can be written as follows:

$$\bar{\sigma} = K' \cdot \bar{\epsilon}^n = K' \cdot (C_2 \cdot \epsilon_{0x})^n \quad (3.43)$$

where  $K'$  is a strength coefficient in plane-strain condition and  $K' = K \left(\frac{4}{3}\right)^{\frac{(n+1)}{2}}$

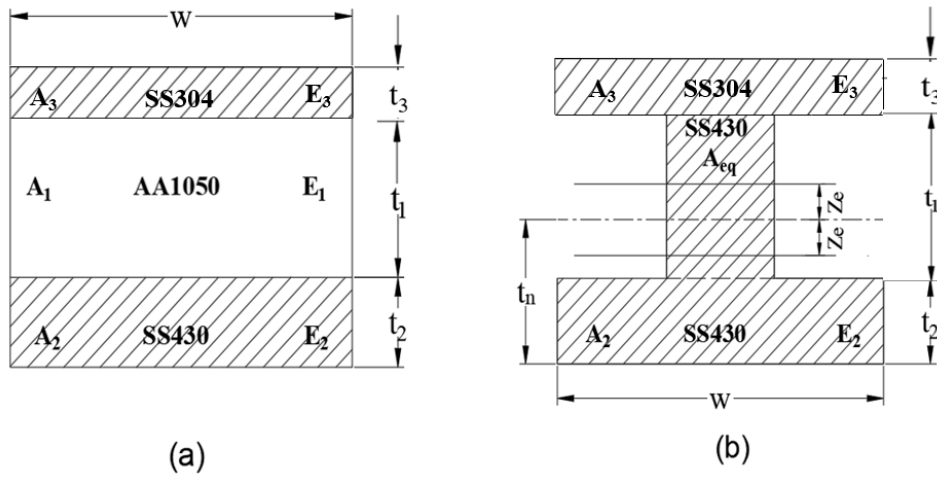


Fig. 3.7 (a) Cross-section of a three-ply clad sheet and (b) Equivalent transformed section

Therefore, flow stress  $\sigma'_x$  in the plastic region for an anisotropic material obeying power law of strain hardening is given as follows:

$$\sigma'_x = \frac{K' \cdot C_2^n}{C_1} \cdot \epsilon_{0x}^n = \frac{K' \cdot C_2^n}{C_1} \cdot \left(\frac{z}{r}\right)^n \quad (3.44)$$

To calculate the bending moment, the position of the neutral layer of clad sheet system during bending, must be determined. To determine the position of neutral layer, the materials of clad sheet are converted into a single material sheet by using Equivalent Area Method (EAM).

In this method, one of the materials is identified as a base material and area of the other material is varied in width, keeping the thickness constant. The transformed area is now considered as an equivalent area as shown in Fig. 3.7 (b).

Here, aluminium is transformed into steel. Let the common width and length of aluminium layer and steel layer be equal to 'w' and 'l', respectively. The thickness of aluminium and steel layer is 't1' and 't2', respectively. After transforming, the width of aluminium becomes 'weq' whereas, the thickness remains constant. The representative equivalent area of aluminium is transformed from 'A1' to 'Aeq'. This implies that:  $E_1 A_1 = A_{eq} E_2$ .

The neutral axis distance ' $t'_n$ ' from the bottommost plane of the sheet considering the equivalent area is given as below:

$$t'_n = \left[ \frac{(2t_2+t_1)E_1t_1+t_2^2E_2+(2t_1+2t_2+t_3)E_2t_3}{2(E_1t_1+E_2t_2+E_3t_3)} \right] \quad (3.45)$$

To determine the springback, required calculations of the bending moment of the layers of three-ply clad sheet is explained below for the two different sheet placement conditions.

### 3.2.1 Case-I: Bending of three-ply sheet with SS430 as the inner layer

A small elemental strip of thickness ' $dz$ ' is considered in the region of AA1050 which is ' $z$ ' distance from neutral axis- NN' as shown in Fig. 3.8.

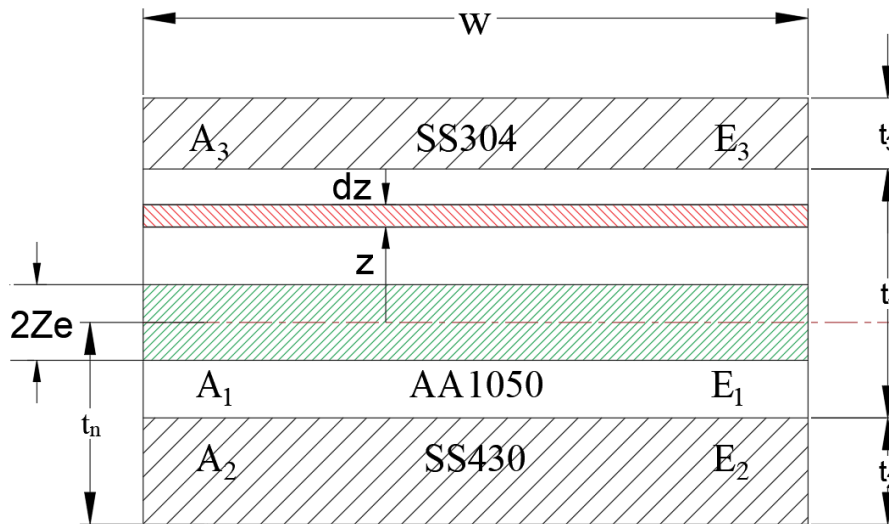


Fig. 3.8 Cross-section of a clad sheet with SS430 as the inner layer

The bending moment of the aluminium layer-1 ( $M_1^I$ ) for elastic-plastic regions is given by

$$M_1^I = \int_{-(t_n-t_2)}^{(t_n-t_2)} \sigma_{x1} \cdot w \cdot z \cdot dz + \int_{(t_n-t_2)}^{(t_1+t_2-t_n)} \sigma_{x1} \cdot w \cdot z \cdot dz \quad (3.46)$$

$$= \left[ 2 \int_0^{z_e} (\sigma_{x1(elastic)} \cdot w \cdot z \cdot dz) + 2 \int_{z_e}^{(t_n-t_2)} (\sigma_{x1(plastic)} \cdot w \cdot z \cdot dz) + \int_{(t_n-t_2)}^{(t_1+t_2-t_n)} (\sigma_{x1(plastic)} \cdot w \cdot z \cdot dz) \right] \quad (3.47)$$

$$= \left[ 2 \int_0^{z_e} \frac{z}{r} \cdot E_1' w \cdot z \cdot dz + 2 \int_{z_e}^{(t_n-t_2)} \left( \frac{K_1' \cdot C_2^n}{C_1} \cdot \left( \frac{z}{r} \right)^n \cdot w \cdot z \cdot dz \right) + \right.$$

$$\int_{(t_n-t_2)}^{(t_1+t_2-t_n)} \left( \frac{K'_1 \cdot C_2^n}{C_1} \cdot \left( \frac{Z}{r} \right)^n \cdot w \cdot z \cdot dz \right) \\ = \frac{2w \cdot E'_1 \cdot z_e^3}{3r} + \frac{w \cdot K'_1 \cdot C_2^n}{C_1 \cdot r^n \cdot (n+2)} \cdot \left[ (t_1 + t_2 - t_n)^{(n+2)} - 2(z_e)^{(n+2)} + (t_n - t_2)^{(n+2)} \right] \quad (3.48)$$

The bending moment ( $M_2^I$ ) of the layer-2 (SS430) for the plastic zone is given by

$$M_2^I = \int_{(t_n-t_2)}^{t_n} \sigma_{x2} \cdot w \cdot z \cdot dz \\ = \left[ \int_{(t_n-t_2)}^{t_n} (\sigma_{x2(plastic)} \cdot w \cdot z \cdot dz) \right] \quad (3.49)$$

$$= \left[ \int_{(t_n-t_2)}^{t_n} \left( \frac{K'_2 \cdot C_2^n}{C_1} \cdot \left( \frac{Z}{r} \right)^n \cdot w \cdot z \cdot dz \right) \right] \quad (3.50)$$

$$= \frac{K'_2 \cdot C_2^n \cdot w}{r^n \cdot C_1 \cdot (n+2)} \left[ (t_n)^{(n+2)} - (t_n - t_2)^{(n+2)} \right] \quad (3.51)$$

Similarly, the bending moment ( $M_3^I$ ) of the layer-3 (SS304) for plastic region is given by

$$M_3^I = \int_{(t_1+t_2-t_n)}^{(t_1+t_2+t_3-t_n)} \sigma_{x3} \cdot w \cdot z \cdot dz \quad (3.52)$$

$$= \left[ \int_{(t_1+t_2-t_n)}^{(t_1+t_2+t_3-t_n)} (\sigma_{x3(plastic)} \cdot w \cdot z \cdot dz) \right] \quad (3.53)$$

$$= \left[ \int_{(t_1+t_2-t_n)}^{(t_1+t_2+t_3-t_n)} \left( \frac{K'_3 \cdot C_2^n}{C_1} \cdot \left( \frac{Z}{r} \right)^n \cdot w \cdot z \cdot dz \right) \right] \quad (3.54)$$

$$= \frac{K'_3 \cdot C_2^n \cdot w}{r^n \cdot C_1 \cdot (n+2)} \left[ (t_1 + t_2 + t_3 - t_n)^{(n+2)} - (t_1 + t_2 - t_n)^{(n+2)} \right] \quad (3.55)$$

Therefore, for the case-I, the total bending moment ( $M^I$ ) is given as follows:

$$M^I = \left[ \frac{2w \cdot E'_1 \cdot z_e^3}{3r} + \frac{w \cdot K'_1 \cdot C_2^n}{C_1 \cdot r^n \cdot (n+2)} \cdot \left[ (t_1 + t_2 - t_n)^{(n+2)} - 2(z_e)^{(n+2)} + (t_n - t_2)^{(n+2)} \right] + \right. \\ \left. \frac{K'_2 \cdot C_2^n \cdot w}{C_1 \cdot r^n \cdot (n+2)} \left[ (t_n)^{(n+2)} - (t_n - t_2)^{(n+2)} \right] + \frac{K'_3 \cdot C_2^n \cdot w}{C_1 \cdot r^n \cdot (n+2)} \left[ (t_1 + t_2 + t_3 - t_n)^{(n+2)} - (t_1 + t_2 - t_n)^{(n+2)} \right] \right] \quad (3.56)$$

For bending a clad sheet to a radius  $r$ , the bending moment as applied to a cross-sectional plane is calculated as above. To initiate the unloading, an equal and opposite bending moment is

applied and the sheet undergoes springback to a new radius  $r'$  and achieves a new equilibrium. It is assumed that the elastic stress distribution is created by the unloading process. The resultant stress distribution is determined by the superposition of elastic–plastic stress distribution caused by the loading process and the elastic stress distribution from the unloading process should not exceed the yield stress for the application of the method of superposition to be valid. Also, it is assumed that bending is occurring about an axis of symmetry and the plane sections remain plane (Burchitz, 2008). For calculating the change of radius of curvature by the unloading process,  $E'I$  is calculated by summing the contribution of all three layers with the second moment of area of the cross-sectional plane about the neutral axis as given in Equation (3.57). Using theory of bending, change in total bending moment  $\Delta M$  after springback is given as below

Using theory of bending, change in total bending moment  $\Delta M$  after springback is given as below

$$\Delta M = E' \cdot I \left( \frac{1}{r} - \frac{1}{r'} \right) \quad (3.57)$$

$$= E'_1 \cdot \left[ I \left( \frac{1}{r} - \frac{1}{r'} \right) \right] + E'_2 \cdot \left[ I \left( \frac{1}{r} - \frac{1}{r'} \right) \right] + E'_3 \cdot \left[ I \left( \frac{1}{r} - \frac{1}{r'} \right) \right] \quad (3.58)$$

$$= E'_1 \cdot \left[ \left( \frac{wt_1^3}{12} + \left( wt_1 \cdot \left( t_2 + \frac{t_1}{2} - t_n \right)^2 \right) \right) \cdot \left[ \frac{1}{r} - \frac{1}{r'} \right] \right] + E'_2 \cdot \left[ \left( \frac{wt_2^3}{12} + \left( wt_2 \cdot \left( t_n - \frac{t_2}{2} \right)^2 \right) \right) \cdot \left[ \frac{1}{r} - \frac{1}{r'} \right] \right] + E'_3 \cdot \left[ \left( \frac{wt_3^3}{12} + \left( wt_3 \cdot \left( t_1 + t_2 + \frac{t_3}{2} - t_n \right)^2 \right) \right) \cdot \left[ \frac{1}{r} - \frac{1}{r'} \right] \right] \quad (3.59)$$

After removing  $M$ , the net moment is zero, it can be shown that  $M^I - \Delta M = 0$ . By using Eq. (3.56) & Eq. (3.59) we can conclude that

$$\left( \frac{1}{r} - \frac{1}{r'} \right) = \frac{\frac{2wE'_1 z_e^3}{3r} + \frac{wK'_1 c_2^n}{C_1 r^n (n+2)} [(t_1+t_2-t_n)^{(n+2)} - 2(z_e)^{(n+2)} + (t_n-t_2)^{(n+2)}] + \frac{K'_2 c_2^n w}{r^n C_1 (n+2)} [(t_n)^{(n+2)} - (t_n-t_2)^{(n+2)}] + \frac{K'_3 c_2^n w}{r^n C_1 (n+2)} [(t_1+t_2+t_3-t_n)^{(n+2)} - (t_1+t_2-t_n)^{(n+2)}]}{E'_1 \left[ \left( \frac{wt_1^3}{12} + \left( wt_1 \cdot \left( t_2 + \frac{t_1}{2} - t_n \right)^2 \right) \right) \right] + E'_2 \left[ \left( \frac{wt_2^3}{12} + \left( wt_2 \cdot \left( t_n - \frac{t_2}{2} \right)^2 \right) \right) \right] + E'_3 \left[ \left( \frac{wt_3^3}{12} + \left( wt_3 \cdot \left( t_1 + t_2 + \frac{t_3}{2} - t_n \right)^2 \right) \right) \right]} \quad (3.60)$$

Equation (3.60) gives the final radius of curvature ( $r'$ ) after springback.

### 3.2.2 Case-II: Bending of three-ply sheet with SS304 as the inner layer

Similarly, a small elemental strip of thickness 'dz' is considered in the region of AA1050 which is 'z' distance from neutral axis- NN' as shown in Fig. 3.9.

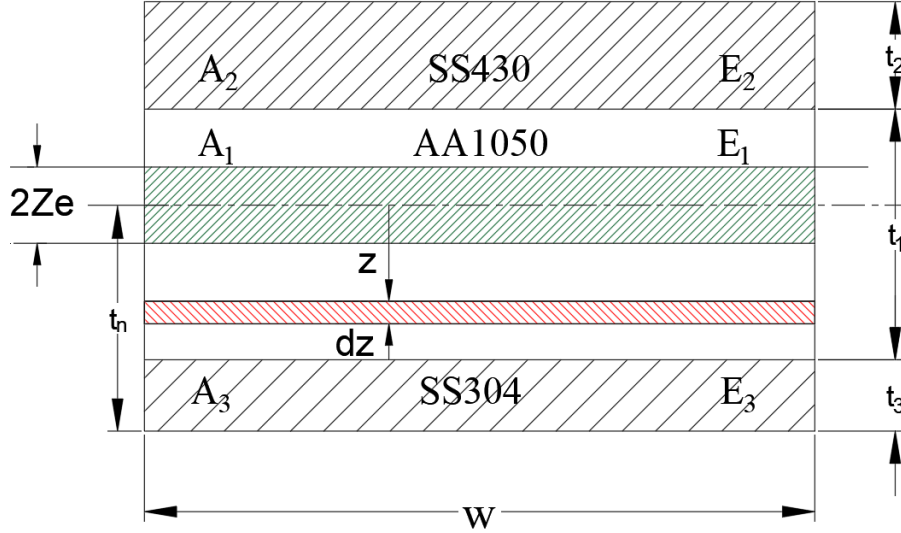


Fig. 3.9 Cross-section of a three-ply clad sheet with a SS304 as the inner layer during bending

The total bending moment of the layer-1 ( $M_1^I$ ) i.e., AA1050 for elastic-plastic regions is given by

$$M_1^I = \int_{-(t_1+t_3-t_n)}^{(t_1+t_3-t_n)} \sigma_{x1} \cdot w \cdot z \cdot dz + \int_{(t_1+t_3-t_n)}^{(t_n-t_3)} \sigma_{x1} \cdot w \cdot z \cdot dz \quad (3.61)$$

$$= \left[ 2 \int_0^{z_e} (\sigma_{x1(elastic)} \cdot w \cdot z \cdot dz) + 2 \int_{z_e}^{(t_1+t_3-t_n)} (\sigma_{x1(plastic)} \cdot w \cdot z \cdot dz) + \int_{(t_1+t_3-t_n)}^{(t_n-t_3)} (\sigma_{x1(plastic)} \cdot w \cdot z \cdot dz) \right] \quad (3.62)$$

$$= \left[ 2 \int_0^{z_e} \left( \frac{z}{r} \cdot E_1' \cdot w \cdot z \cdot dz \right) + 2 \int_{z_e}^{(t_1+t_3-t_n)} \left( \frac{K_1' \cdot C_2^n}{c_1} \cdot \left( \frac{z}{r} \right)^n \cdot w \cdot z \cdot dz \right) + \int_{(t_1+t_3-t_n)}^{(t_n-t_3)} \left( \frac{K_1' \cdot C_2^n}{c_1} \cdot \left( \frac{z}{r} \right)^n \cdot w \cdot z \cdot dz \right) \right] \quad (3.63)$$

$$= \frac{2w \cdot E_1' \cdot z_e^3}{3r} + \frac{K_1' \cdot C_2^n \cdot w}{r^n c_1 \cdot (n+2)} \left[ (t_1 + t_3 - t_n)^{(n+2)} - 2(z_e)^{(n+2)} + (t_n - t_3)^{(n+2)} \right] \quad (3.64)$$

The bending moment of the layer-2 ( $M_2^I$ ) i.e., SS430 layer for plastic region is given by

$$M_2^I = \int_{(t_1+t_3-t_n)}^{(t_1+t_2+t_3-t_n)} \sigma_{x2} \cdot w \cdot z \cdot dz \quad (3.65)$$

$$= \left[ \int_{(t_1+t_3-t_n)}^{(t_1+t_2+t_3-t_n)} (\sigma_{x2(plastic)} \cdot w \cdot z \cdot dz) \right] \quad (3.66)$$

$$= \left[ \int_{(t_1+t_3-t_n)}^{(t_1+t_2+t_3-t_n)} \left( \frac{K'_2 \cdot C_2^n}{C_1} \cdot \left( \frac{z}{r} \right)^n \cdot w \cdot z \cdot dz \right) \right]$$

$$= \frac{K'_2 \cdot C_2^n \cdot w}{r^n C_1 \cdot (n+2)} \left[ (t_1 + t_2 + t_3 - t_n)^{(n+2)} - (t_1 + t_3 - t_n)^{(n+2)} \right] \quad (3.67)$$

The bending moment of the layer-3 ( $M_3^{II}$ ) i.e., SS304 layer for plastic region is given by

$$M_3^{II} = \int_{(t_n-t_3)}^{(t_n)} \sigma_{x3} \cdot w \cdot z \cdot dz \quad (3.68)$$

$$= \left[ \int_{(t_n-t_3)}^{(t_n)} (\sigma_{x3(plastic)} \cdot w \cdot z \cdot dz) \right]$$

$$= \left[ \int_{(t_n-t_3)}^{(t_n)} \left( \frac{K'_3 \cdot C_2^n}{C_1} \cdot \left( \frac{z}{r} \right)^n \cdot w \cdot z \cdot dz \right) \right]$$

$$= \frac{K'_3 \cdot C_2^n \cdot w}{r^n C_1 \cdot (n+2)} \left[ (t_n)^{(n+2)} - (t_n - t_3)^{(n+2)} \right] \quad (3.69)$$

For the case-II, the total bending moment is given as

$$M^{II} = \left[ \frac{2w \cdot E'_1 \cdot z_e^3}{3r} + \frac{K'_1 \cdot C_2^n \cdot w}{r^n C_1 \cdot (n+2)} \left[ (t_1 + t_3 - t_n)^{(n+2)} - 2(z_e)^{(n+2)} + (t_n - t_3)^{(n+2)} \right] + \right. \\ \left. \frac{K'_2 \cdot C_2^n \cdot w}{r^n C_1 \cdot (n+2)} \left[ (t_1 + t_2 + t_3 - t_n)^{(n+2)} - (t_1 + t_3 - t_n)^{(n+2)} \right] + \frac{K'_3 \cdot C_2^n \cdot w}{r^n C_1 \cdot (n+2)} \left[ (t_n)^{(n+2)} - \right. \right. \\ \left. \left. (t_n - t_3)^{(n+2)} \right] \right] \quad (3.70)$$

After springback, using theory of bending, the change in total bending moment  $\Delta M$  is given as

$$\Delta M = E'_1 \cdot \left[ \left( \frac{wt_1^3}{12} + \left( (w \cdot t_1) \cdot \left( t_n - \frac{t_1}{2} - t_3 \right)^2 \right) \right) \cdot \left[ \frac{1}{r} - \frac{1}{r'} \right] \right] + E'_2 \cdot \left[ \left( \frac{wt_2^3}{12} + \left( (wt_2) \cdot \left( t_1 + t_3 + \right. \right. \right. \right. \\ \left. \left. \left. \frac{t_2}{2} - t_n \right)^2 \right) \right) \cdot \left[ \frac{1}{r} - \frac{1}{r'} \right] \right] + E'_3 \cdot \left[ \left( \frac{wt_3^3}{12} + \left( (wt_3) \cdot \left( t_n - \frac{t_3}{2} \right)^2 \right) \right) \cdot \left[ \frac{1}{r} - \frac{1}{r'} \right] \right] \quad (3.71)$$

After removing  $M$ , the net moment is zero. By using Eq. (3.70) & Eq. (3.71) we can conclude that

$$\left(\frac{1}{r} - \frac{1}{r'}\right) = \frac{\left[\frac{2wE_1'ze^3}{3r} + \frac{K_1' C_2^n w}{r^n C_{1,(n+2)}}[(t_1+t_3-t_n)^{(n+2)} - 2(z_e)^{(n+2)} + (t_n-t_3)^{(n+2)}] + \frac{K_2' C_2^n w}{r^n C_{1,(n+2)}}[(t_1+t_2+t_3-t_n)^{(n+2)} - (t_1+t_3-t_n)^{(n+2)}] + \frac{K_3' C_2^n w}{r^n C_{1,(n+2)}}[(t_n)^{(n+2)} - (t_n-t_3)^{(n+2)}]\right]}{E_1' \left[ \left( \frac{wt_1^3}{12} + (wt_1) \cdot \left( t_n - \frac{t_1}{2} - t_3 \right)^2 \right) \right] + E_2' \left[ \left( \frac{wt_2^3}{12} + (wt_2) \cdot \left( t_1 + t_3 + \frac{t_2}{2} - t_n \right)^2 \right) \right] + E_3' \left[ \left( \frac{wt_3^3}{12} + (wt_3) \cdot \left( t_n - \frac{t_3}{2} \right)^2 \right) \right]} \quad (3.72)$$

To obtain springback in both the cases of sheet placements i.e. Case-I and II, the final radius of curvature ( $r'$ ) after the springback is found by Eq. (3.60) and (3.72), respectively.

$$\text{Change in the bend angle, } \alpha_i - \alpha_f = \left(1 - \frac{r}{r'}\right) \alpha_i \quad (3.73)$$

where,  $\alpha_i$  and  $\alpha_f$  are initial and final bend angles. The included bend angle is  $90^\circ$  and is measured on the die and therefore, the initial bend angle ( $\alpha_i$ ) is  $45^\circ$ .

### 3.3 Summary of the chapter

Analytical models are approximate solutions, generally based with certain assumptions taken into considerations to avoid complexities. They enable engineers and manufacturers to predict, control, and optimize bending processes, leading to cost savings, improved product quality, and increased efficiency across a wide range of applications.

In this chapter, analytical models for springback prediction in bending of 2-ply and 3-ply clad sheets respectively, have been developed by extending the simple theory of sheet bending under plane strain condition. These analytical models have incorporated the effects of strain hardening and anisotropy to predict the springback behaviour after V-bending of a two-ply and a three-ply clad sheet. The analytical models, also, discuss the effects of sheet setting on springback during bending operation.

Table 3.1 and Table 3.2 present a comparative analysis of different bending models concerning key parameters and bend characteristics.



Table 3.1 Comparison of analytical models for monolithic sheets

| <b>Bending Models</b>  | Lubhan et al., 1950 | Martin et al., 1966 | Dadras et al., 1982 | Tan et al., 1995 | Zhu et al., 2007 | Zhang et al., 2007 |
|------------------------|---------------------|---------------------|---------------------|------------------|------------------|--------------------|
| <b>Factors</b>         |                     |                     |                     |                  |                  |                    |
| Plane strain condition | √                   | √                   | √                   | √                | √                | √                  |
| Strength coefficient   | -                   | -                   | √                   | √                | -                | √                  |
| Strain hardening       | -                   | -                   | √                   | √                | √                | √                  |
| Anisotropy             | -                   | -                   | -                   | √                | -                | -                  |
| Neutral axis shift     | √                   | √                   | √                   | √                | √                | √                  |
| Bauschinger effect     | -                   | -                   | -                   | √                | √                | -                  |

As per Table 3.1, it was observed that the model proposed by Tan et al. (1995) exhibited superior performance in describing pure bending phenomena compared to the other models. Tan's model offers several advantages, including its consideration of a wide range of relevant parameters, as indicated in Table 3.1.

Table 3.2 Comparison of analytical models of laminated sheets

| <b>Bending Models</b>  | Patel et al., 2014 | Parsa et al., 2015 | Mohammadi et al., 2015 | Kagzi et al., 2016 | Kagzi et al., 2022 | Present Model |
|------------------------|--------------------|--------------------|------------------------|--------------------|--------------------|---------------|
| <b>Factors</b>         |                    |                    |                        |                    |                    |               |
| Plane strain condition | √                  | √                  | √                      | √                  | √                  | √             |
| Strength coefficient   | √                  | √                  | √                      | √                  | √                  | √             |
| Strain hardening       | √                  | √                  | √                      | √                  | √                  | √             |
| Anisotropy             | -                  | -                  | -                      | -                  | √                  | √             |
| Neutral axis shift     | -                  | -                  | -                      | -                  | -                  | -             |
| Bauschinger effect     | -                  | -                  | -                      | -                  | -                  | -             |

Furthermore, Tan's model incorporates the fundamental Ludwik hardening law to account for kinematic hardening and the Bauschinger effect resulting from shifts in the neutral fiber. As per Table 3.2, anisotropy has not been fully explored in the analytical models of clad sheet materials. Kagzi et al. have applied anisotropy in their analytical model of 2-ply clad sheet. They have not tried it for 3-ply clad sheet.

## **CHAPTER 4**

# **SPRINGBACK PREDICTION BY FINITE ELEMENT SIMULATION**

Different analytical and numerical procedures have been in use to study the deformation of a sheet metal during forming process. Of these methods, slab method, upper and lower bound techniques and slip line field theory are some of the standard approaches used for determination of forming loads and limiting deformation. However, these methods suffer from the limitation of low degree of accuracy due to many assumptions that simplify the solution. With the high-speed computing available, sheet metal forming processes can be simulated using FEM (Finite Element Method). FEM discretizes the body into elements and generates simulation equations to find the unknowns at the nodal points. A forming simulation results in nonlinear equations because large deformation involved in the process invokes material and geometric nonlinearities (Fish and Belytschko, 2007). Also, changing boundary conditions and friction at the interfaces between the forming tools and sheet metal induce contact nonlinearities in the problem. Hence Finite Element Method (FEM) requires incremental procedures based on explicit or implicit integration schemes, requiring large computing time.

Prediction of springback helps in the design of the forming tools using springback compensation. Springback prediction and its compensation are a complex problem in the manufacturing of parts from TWBs and clad sheets. FE simulations provide a more economical way of designing dies.

In order to improve springback prediction and reduce the computational cost, Pourboghraat et. al. (1998) developed the membrane/shell method for prediction of springback in draw bending under plane strain condition (two-dimensional). These methods were further extended and improved for springback prediction in bending of anisotropic sheet metals in 3D parts by Yoon et al. (2002) using unconstrained cylindrical bending. Springback was further

studied by many researchers (Lee et al., 2005; Lingbeek et al., 2005; Papeleux and Ponthot, 2002; Thibaud et al., 2002; Wagoner, 2002) to solve challenging benchmark problems to address springback in sheet metal forming. Furthermore, Wagoner et al. (2013) carried out extensive literature survey in his work to address springback compensation by increasing sheet tension and by improved tooling design.

In this present study, springback has been predicted in V-bending of clad sheet metals and parent's sheets by finite element analysis. The methodology of modelling and simulation is presented below.

#### **4.1 About the software**

In the present study, the simulations of sheet bending and springback are performed using ABAQUS (version 6.14-2) software. ABAQUS- Explicit solution procedure is applied for the bending of loading part of simulation as it is faster for the complicated contact problems. The implicit method is used for springback of the unloading part of simulation. Springback simulation is a non-contact problem i.e., the die and punch constraints are removed, thus reducing the non-linearity of the problem. ABAQUS- Implicit (standard) is seen to solve the springback problem faster than the Explicit. So, the bending simulation has been done using the Explicit procedure and thereafter the completed model was exported to ABAQUS- Implicit (Standard).

#### **4.2 Modelling and simulations of bending process**

In the present study, bending process is addressed as a non-linear problem. The material nonlinearity, boundary nonlinearity and geometric nonlinearity are the three types of nonlinearities considered in the simulation of the anisotropic sheet metals, the material is modelled by the power law of strain hardening. Boundary nonlinearity is seen due to the change in the boundary conditions that occurs in the bending process. During bending operation,

initially the sheet metal placed on the die shoulder comes into play. For bending the sheet, the punch makes contact with the upper surface of the sheet metal and the material deforms plastically until the sheet conforms to the shape of the die. Thus, there is a continuous change in boundary conditions during the bending process resulting in non-linearity due to the contact boundary conditions. The third source of nonlinearity is due to the large deflection in the sheet and changes in the geometry of the model during the analysis

ABAQUS-Explicit used for bending simulations finds a solution to the dynamic equation as follows.

$$P - I = M\ddot{u}, \quad (4.1)$$

where  $P$  and  $I$  are externally and internally applied loads, respectively,  $M$  is the nodal mass matrix and  $\ddot{u}$  is the nodal acceleration. This method integrates the equations of motion explicitly through time to find the displacement history. Therefore, at the beginning of the increment at time  $t$ , accelerations are calculated as follows:

$$\ddot{u}_t = (M)^{-1} \cdot (P - I)_t \quad (4.2)$$

The accelerations are integrated with time by a central difference rule that determines the velocities at the middle of the current increment assuming a constant acceleration at that nodal point

$$\dot{u}_{\left(t+\frac{\Delta t}{2}\right)} = \dot{u}_{\left(t-\frac{\Delta t}{2}\right)} + \ddot{u}_t \cdot \left(\frac{\Delta t_{(t+\Delta t)} + \Delta t_{(t)}}{2}\right) \quad (4.3)$$

The velocities are integrated with time to find the displacements at the end of the increment as given below:

$$u_{(t+\Delta t)} = u_{(t)} + \dot{u}_{\left(t+\frac{\Delta t}{2}\right)} \cdot \Delta t_{(t+\Delta t)} \quad (4.4)$$

Thus, the dynamic equilibrium equations provide nodal accelerations at the beginning of the time increment. Knowing accelerations, the velocities and displacements are calculated explicitly through time. Though simulations require many increments, but the cost of an increment of the explicit method is much smaller than that of the implicit method as solving a

global set of equations is avoided. Due to these reasons, ABAQUS-Explicit suits well for a nonlinear analysis.

### 4.3. Numerical simulations of clad sheet

To evaluate the springback results after bending of the 2-ply and 3-ply clad sheet, FE simulations are performed separately for bending and springback using ABAQUS version 6.14-2.

#### 4.3.1 Modelling and meshing

For 2-ply clad sheet, simulations are performed by designing a die and a punch set with a die-profile radius of 17 mm including the clearance for the sheet thickness and a punch profile radius of 15 mm. The clearance between the die and punch neglects the localized compression at the bending region. The included bend angle for the die and punch set is taken as  $90^\circ$  as shown in Fig. 4.1.

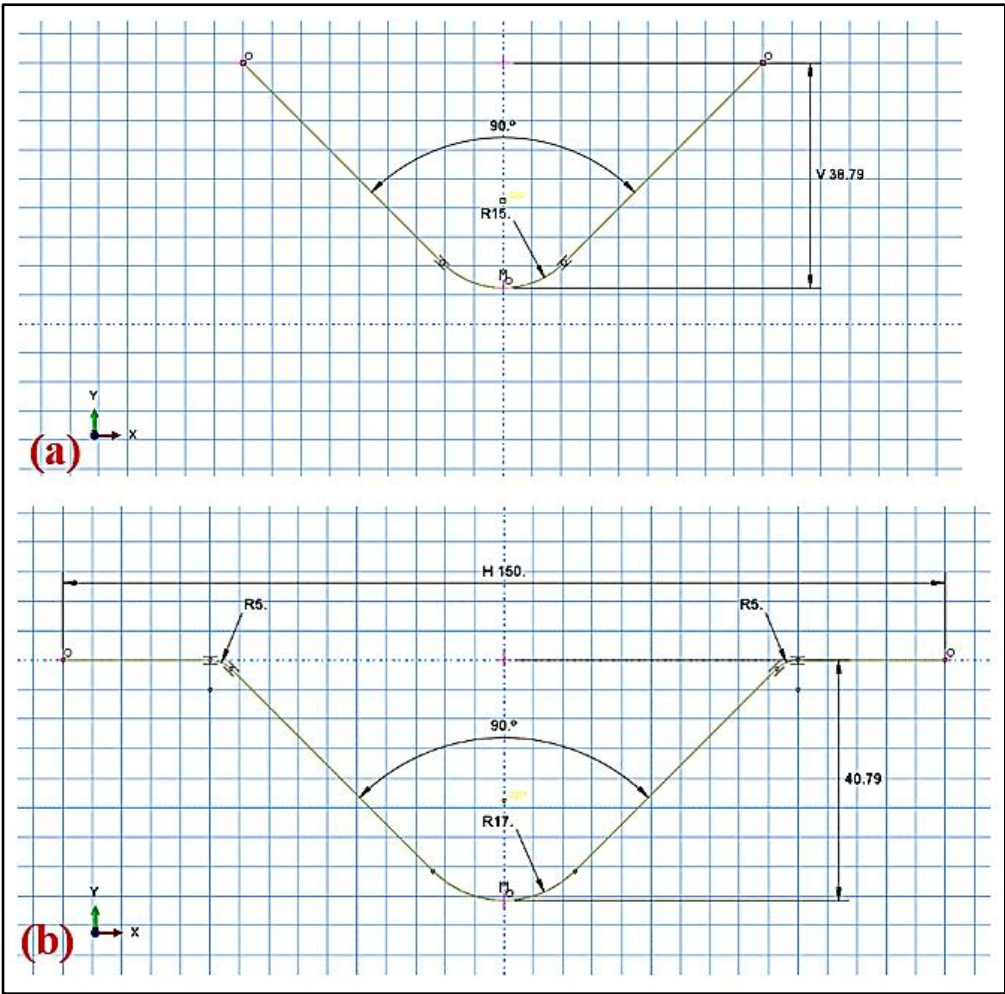


Fig. 4.1 CAD model of (a) Punch and (b) Die for blank of 2-ply clad sheet

The die and punch are modelled as rigid using analytical rigid tools since the rigid surfaces need not be meshed thus reducing the simulation time.

The modelled geometry of the blank is divided longitudinally into two regions of SS430 layer of thickness 0.6 mm and AA1050 layer of 1.4 mm using a partition tool in the software as shown in Fig. 4.2. The meshed model of the blank is shown in Fig.4.3.

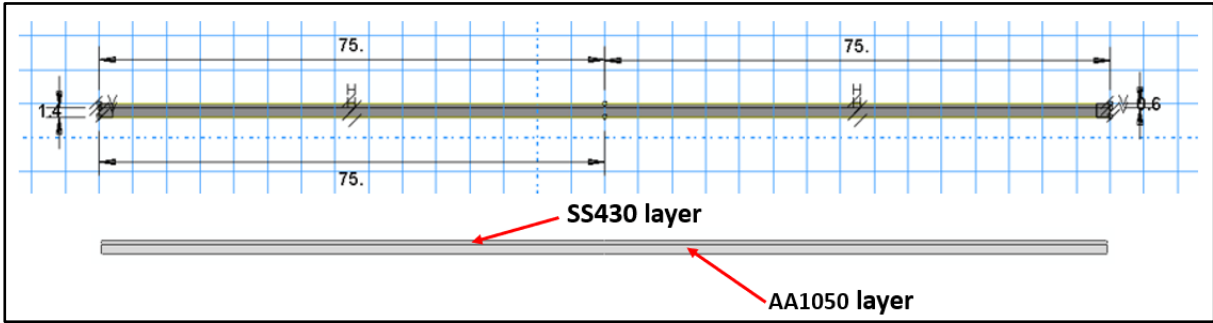


Fig. 4.2 CAD model of blank of 2-ply clad sheet

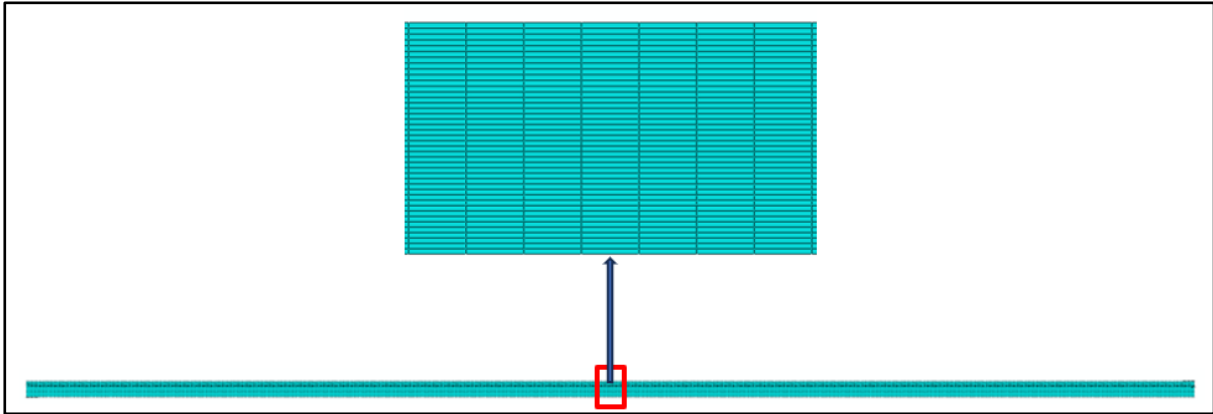


Fig. 4.3 Meshed model of blank of 2-ply clad sheet

In the present research, convergence studies are conducted by gradually increasing the mesh density and observing how the results change. Convergence studies are helpful in determining the optimal mesh size for accurate results. The mesh refining process is continued until the results no longer change significantly.

The details of elements and nodes are given in Table 4.1. The specimen for bending is modelled as deformable with homogeneous solid shell elements i.e., CPE4R plane strain elements which are 4-node bilinear having reduced integration with hourglass control.

Table 4.1 Details of elements and nodes for the simulations of 2-ply clad sheet

| Problem size                        |        |
|-------------------------------------|--------|
| No. of elements                     | 12,600 |
| No. of elements in AA1050           | 9000   |
| No. of elements in SS430            | 3600   |
| No. of nodes                        | 12,945 |
| Total no. of variables in the model | 25,890 |

True stress-true strain data points after plastic yielding for individual materials obtained by uniaxial tension tests of AA1050 and SS430 are used to assign the specific plastic properties of both the materials to the blank. Hill's plasticity model with anisotropy, also known as Hill's yield potential are used in FE modelling to incorporate anisotropy of sheet (Hibbit et. al, 2007).

For the 3-ply clad sheet, simulations are performed by designing a die and a punch set with a die-profile radius of 17.4 mm including the clearance for the sheet thickness and a punch profile radius of 15 mm. The clearance between the die and punch neglects the localized compression at the bending region. The included bend angle for the die and punch set is taken as 90° as shown in Fig.4.4. The die and punch are modelled as rigid using analytical rigid tools since the rigid surfaces need not be meshed thus reducing the simulation time.

The modelled geometry of the blank is divided longitudinally into three regions of SS430 layer of thickness 0.6 mm, AA1050 layer of thickness 1.4 mm and SS304 layer of 0.4 mm using a partition tool in the software as shown in Fig.4.5



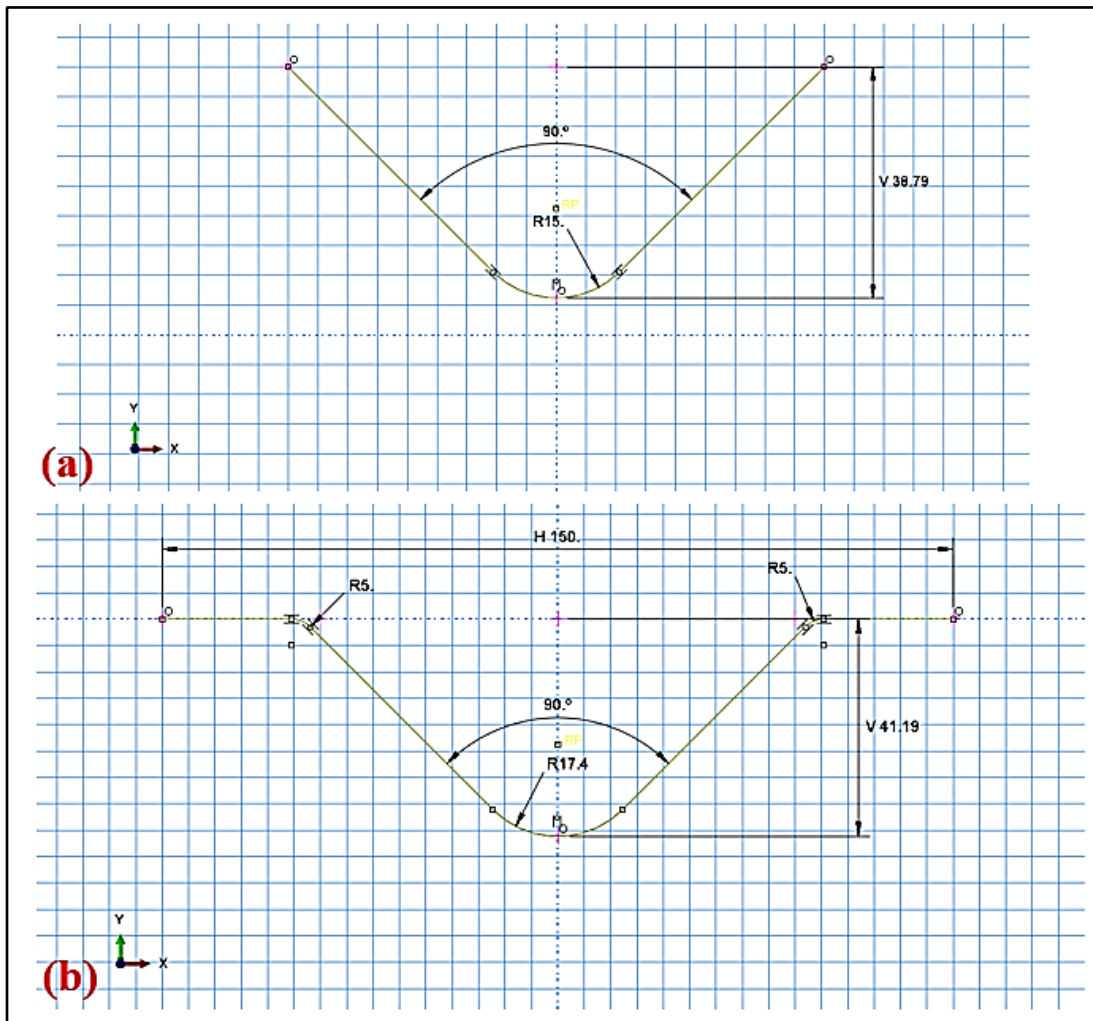


Fig. 4.4 CAD model of (a) Punch and (b) Die for blank of 3-ply clad

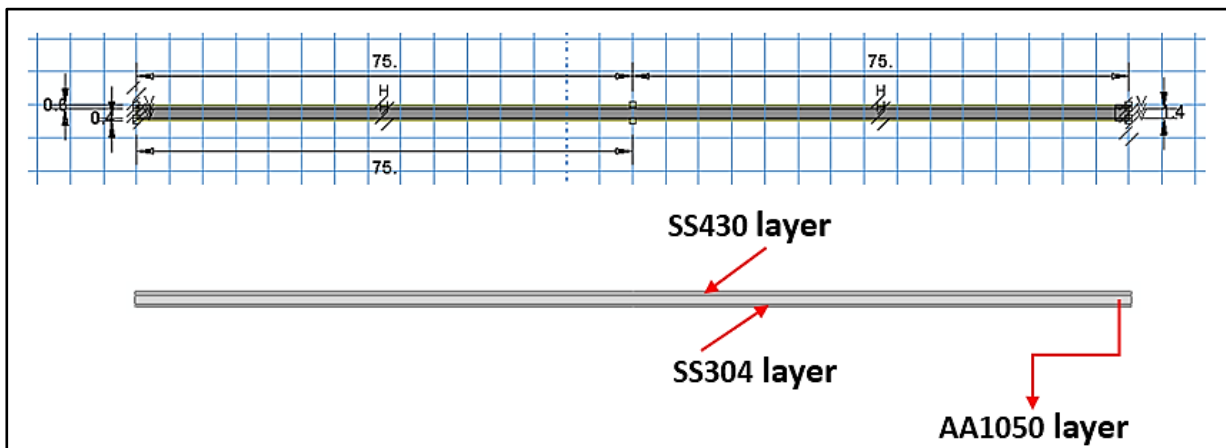


Fig. 4.5 CAD model of blank of 3-ply clad sheet

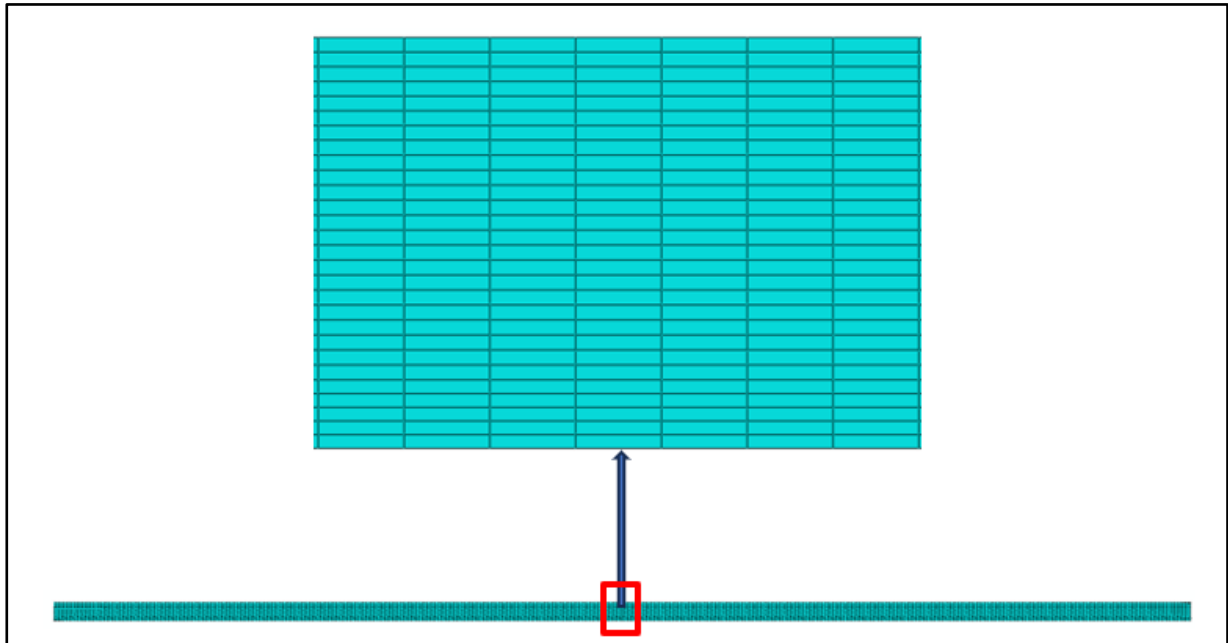


Fig. 4.6 Meshed model of blank of 3-ply clad sheet

The details of elements and nodes are given in Table 4.2.

Table 4.2 Details of elements and nodes for the simulations of 3-ply clad sheet

| Problem size                        |       |
|-------------------------------------|-------|
| No. of elements                     | 8400  |
| No. of elements in AA1050           | 4800  |
| No. of elements in SS430            | 2100  |
| No. of elements in SS304            | 1500  |
| No. of nodes                        | 8731  |
| Total no. of variables in the model | 17462 |

The partitioned layer of SS304 and SS430 are meshed finer due to their lower thickness as compared with a layer of AA1050. The specimen for bending is modelled as deformable with homogeneous solid shell elements i.e., CPE4R plane strain elements which are 4-node bilinear having reduced integration with hourglass control.

True stress-true strain data points after plastic yielding for individual materials obtained by uniaxial tension tests of SS304, AA1050 and SS430 are used to assign the specific plastic properties of all the three materials to the blank. Hill's plasticity model with anisotropy, also known as Hill's yield potential is used in FE modelling to incorporate anisotropy of sheet.

### 4.3.2 Boundary conditions and simulations

In the assembly module, the specimen for bending is placed centrally on the die in such a way that the top surface of the 2-ply sheet faces the punch and is thus, the inner layer as shown in Fig. 4.7. The die and the punch surfaces are defined as the master surfaces and the deformable blank is the slave surface. A pair of different contact properties are established with friction formulated as penalty contact by assigning a coefficient of friction as 0.125 at the interface of die and blank. The friction between the punch and blank interface is taken as 0.05 (Gautam, 2017; Chatti and Hermi, 2011; Papeleux and Ponthot, 2002; Yoon et al., 2002). The bending samples are placed on the die in two ways i.e., in the first case, SS430 is the inner layer and AA1050 is the outer layer whereas in the second case, AA1050 is the inner layer and SS430 is the outer layer.

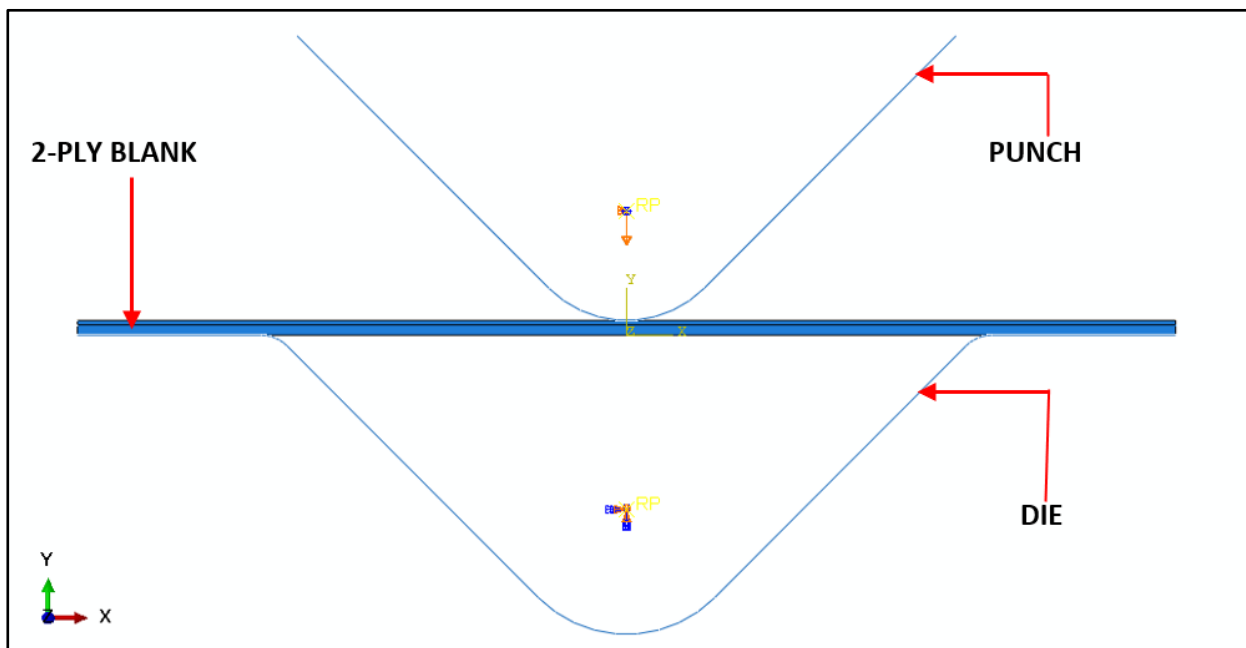


Fig 4.7 Assembly of die, punch, and 2-ply blank

The simulations are done for bending and springback for both the cases of sheet placements on the die to assess the effect of the inner and outer layer on bending and springback. The punch is set with intimate contact with the blank's inner layer. The displacement of the punch is given almost equal to the die depth to avoid any localized compression at the zone of deformation. The die was assigned a boundary condition of 'Encastré' (zero displacement and rotation about

x, y, z). In the final stage of bending simulation, the bend radius is almost equal to the punch radius and the bend angle becomes almost equal to the included angle of the die.

The boundary conditions, adopted in the bending of 2-ply clad sheet has been shown in Fig. 4.8. The fixed and variable parameters used for simulation of bending have been depicted in Table 4.3. All the bending simulations for both the sheet placements on the die are performed using dynamic explicit.

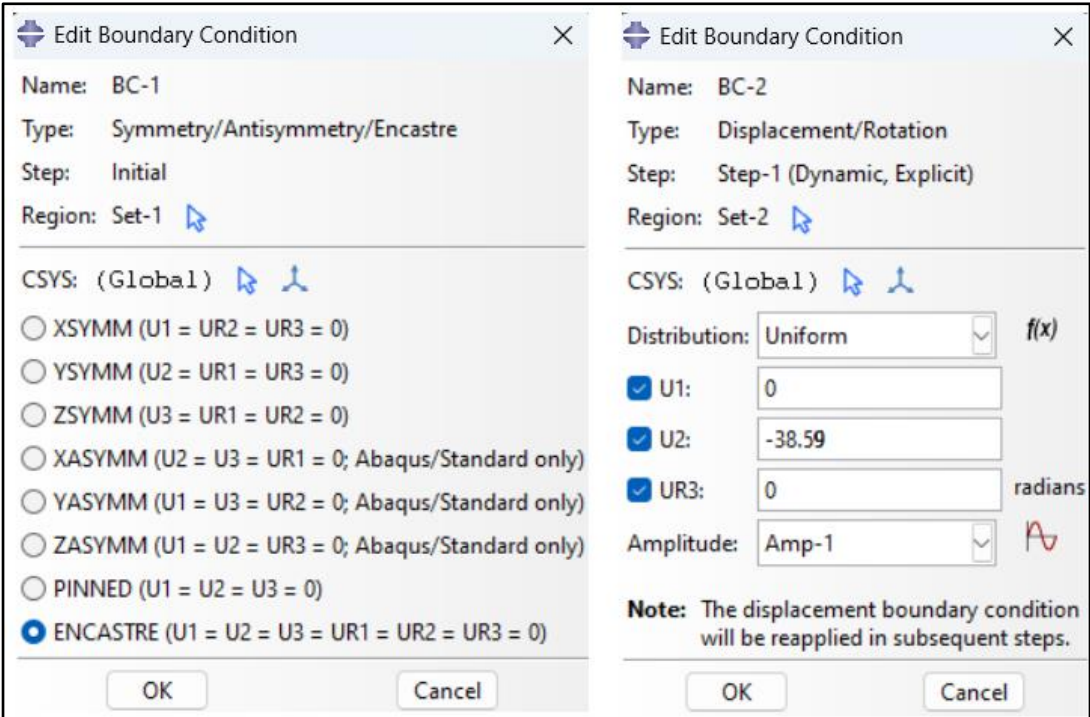


Fig. 4.8 Boundary conditions for simulation of bending of 2-ply blank

To evaluate and capture the results of spring back simulations, the initial output file from the simulated bending process history is utilized after deleting all the constraints in the model of springback. A central node in the blank was assigned a zero velocity so that it remains stationary. Fig. 4.9 and Fig. 4.10 show an overlay plot of loaded and unloaded images after the spring back simulation of a 2-ply and 3-ply specimens respectively.

Table 4.3 List of fixed and variable parameters

| S.No. | Parameter               | Description  | Fixed or Variable |
|-------|-------------------------|--|-------------------|
| 1     | Material properties     | Young's modulus, Poisson's ratio, yield strength, ultimate tensile strength, density, strain hardening coefficient, strength coefficient, plastic strain ratio | Fixed             |
| 2     | Thickness of the sheet  | Thickness of the SS430, AA1050, SS304, 2-ply and 3-ply   | Fixed             |
| 3     | Width of the sheet      | Width of the SS430, AA1050, SS304, 2-ply and 3-ply   | Fixed             |
| 4     | Length of the sheet     | Length of the SS430, AA1050, SS304, 2-ply and 3-ply  | Fixed             |
| 5     | Sheet placement         | Sheet placement with respect to punch and die  | Variable          |
| 6     | Sheet orientation       | Sheet orientation with respect to rolling direction (0°, 45° and 90°)  | Variable          |
| 7     | Bending radius          | Radius of the bend   | Variable          |
| 8     | Coefficient of friction | Friction between blank & die and blank & punch   | Fixed             |
| 9     | Mesh                    | Element Type/Element size and mesh refinement criteria   | Fixed/Variable    |
| 10    | Boundary conditions     | Die encastre/punch displacement  | Fixed/Variable    |

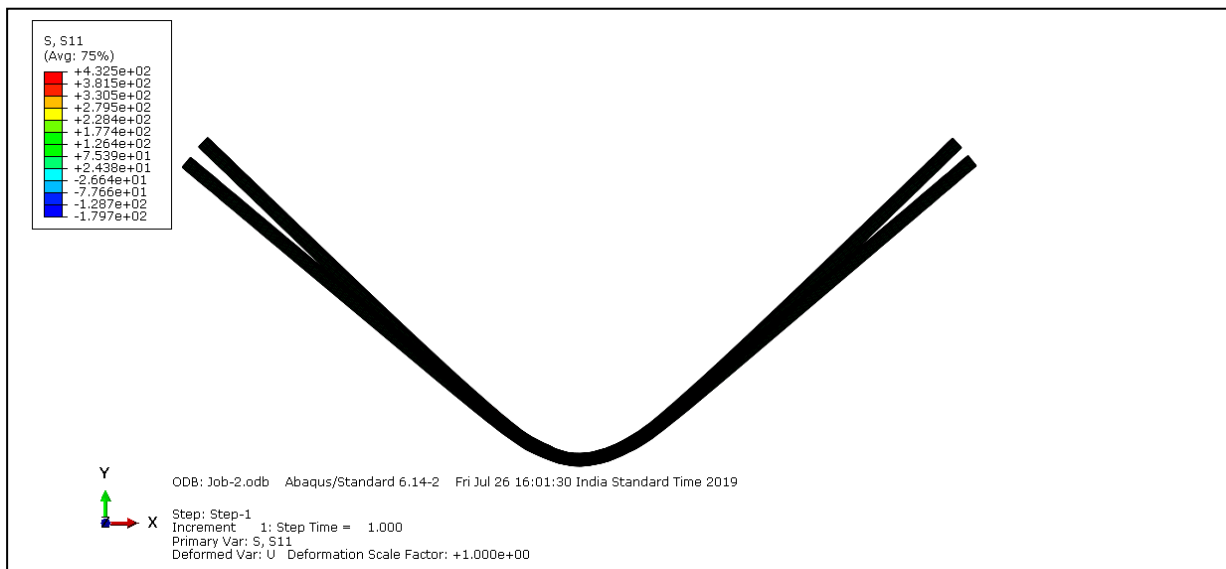


Fig. 4.9 Loaded and unloaded frames after springback of a 2-ply sheet (oriented 45° w.r.t. R.D.) with SS430 as an inner layer for punch radius 15 mm

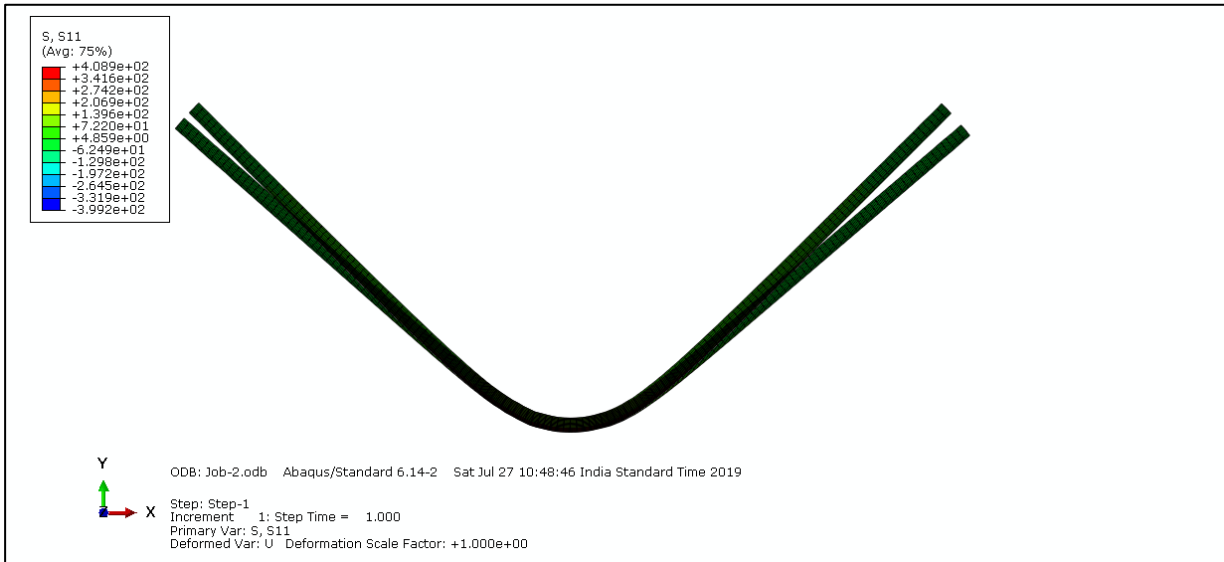


Fig. 4.10 Loaded and unloaded frames after springback of a 2-ply sheet (oriented 45° w.r.t. R.D.) with AA1050 as an inner layer for punch radius 15 mm

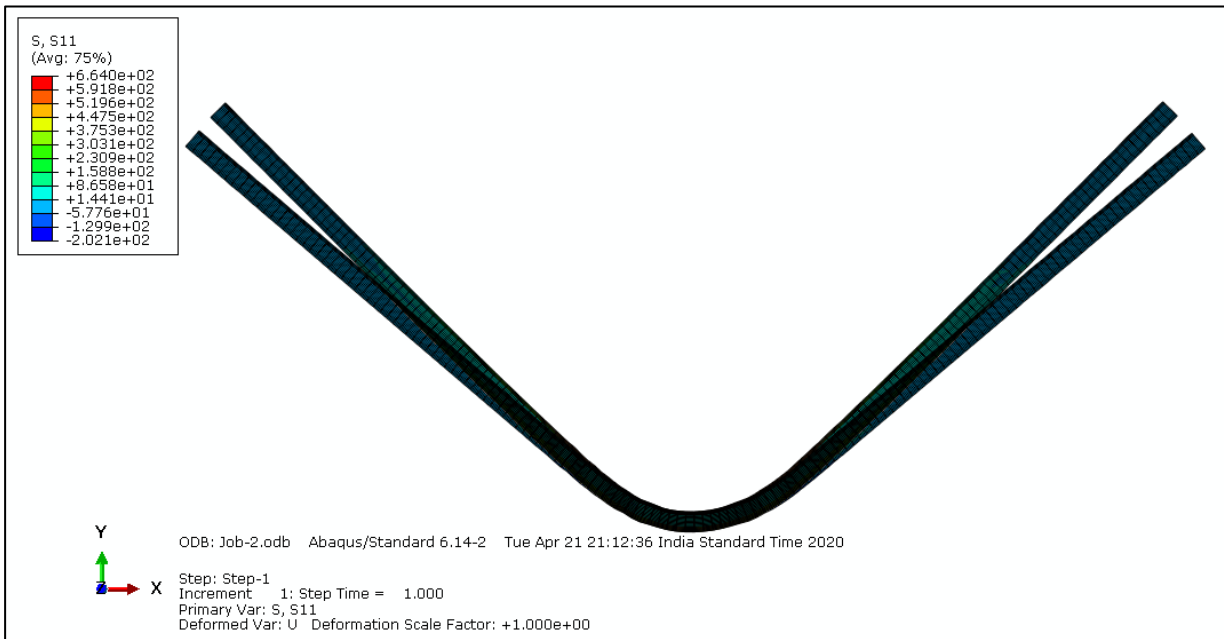


Fig. 4.11 Loaded and unloaded frames after springback of a 3-ply sheet for punch radius 15 mm

The coordinate details of the various nodes are captured individually from the loaded and unloaded frames for springback measurement as depicted in Table 4.4. The final value of springback can be determined by computing the difference between the two carefully recorded coordinates of both the frames in a CAE interface as shown in Fig. 4.11.

Table 4.4 Captured coordinates from loaded and unloaded frames of 2-ply clad blank oriented at 45° w.r.t. R.D. for 15 mm punch radius

| Node ID | Loaded frame (Node history) |               |               | Unloaded frame (Springback) |               |               |
|---------|-----------------------------|---------------|---------------|-----------------------------|---------------|---------------|
|         | X-coordinates               | Y-coordinates | Z-coordinates | X-coordinates               | Y-coordinates | Z-coordinates |
| 5       | -55.57                      | 10.60         | 0             | -57.49                      | 8.61          | 0             |
| 226     | -49.22                      | 4.19          | 0             | -50.82                      | 2.53          | 0             |
| 212     | -38.6218                    | -6.38         | 0             | -40.42                      | -6.83         | 0             |
| 193     | -25.8464                    | -19.07        | 0             | -26.33                      | -19.56        | 0             |
| 179     | -15.7748                    | -28.77        | 0             | -15.91                      | -28.90        | 0             |
| 171     | -8.98664                    | -34.59        | 0             | -9.80                       | -34.05        | 0             |
| 165     | -3.7843                     | -37.15        | 0             | -4.69                       | -36.84        | 0             |
| 3       | 29.53E-03                   | -37.82        | 0             | 48.36E-03                   | -37.82        | 0             |
| 304     | 3.85311                     | -37.26        | 0             | 4.81                        | -36.99        | 0             |
| 300     | 9.01899                     | -34.60        | 0             | 8.29                        | -35.25        | 0             |
| 289     | 16.5325                     | -28.09        | 0             | 16.91                       | -28.57        | 0             |
| 278     | 25.873                      | -19.06        | 0             | 25.24                       | -21.39        | 0             |
| 260     | 36.514                      | -8.49         | 0             | 38.83                       | -9.59         | 0             |
| 243     | 49.2146                     | 4.24          | 0             | 51.66                       | 1.55          | 0             |
| 4       | 55.5702                     | 10.61         | 0             | 58.46                       | 7.45          | 0             |

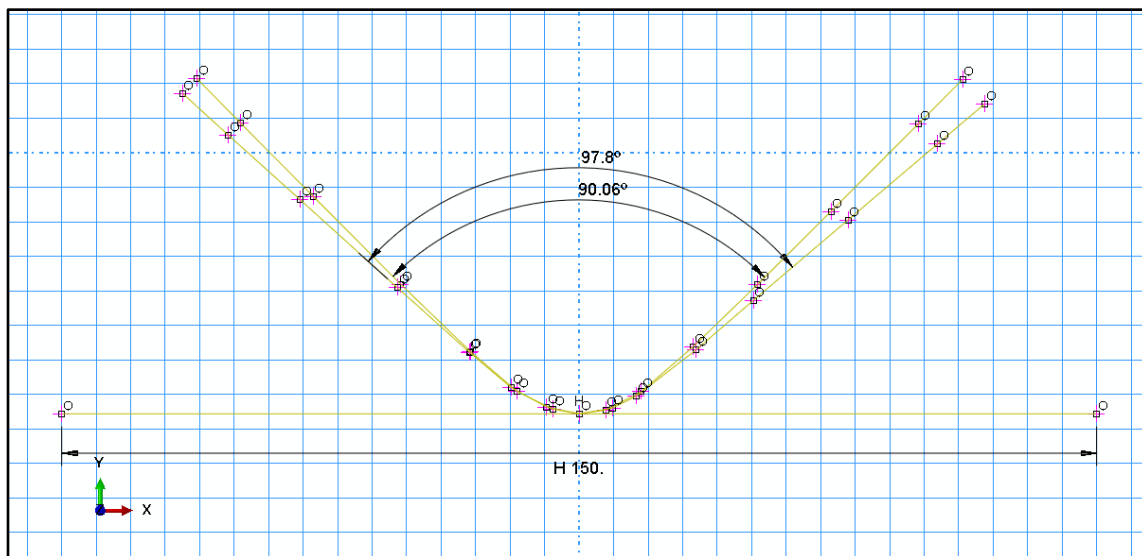


Fig. 4.12 Surfaces of blank plotted using CAE interface before and after springback

For blank of 2-ply clad sheet which is oriented at 45° to the rolling direction and the punch radius is 15 mm, the springback is measured as follows: -

$$\begin{aligned}
 \text{Springback} &= \frac{1}{2} (\text{Included bend angle after springback} - \text{Included bend angle before springback}) \\
 &= \frac{1}{2} (97.8^\circ - 90.06^\circ) \\
 &= 3.87^\circ \text{ (depicted in Table 6.11)}
 \end{aligned}$$

Fig. 4.12 and Fig. 4.13 show an overlay plot of loaded and unloaded images after the spring back simulation of AA1050 and SS430 specimens respectively.

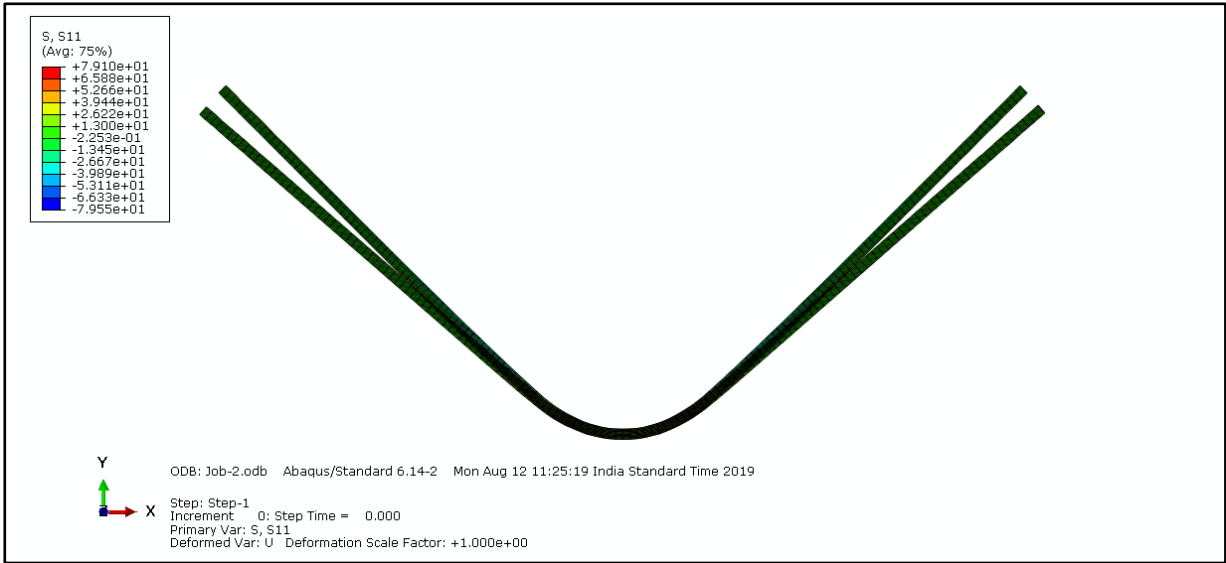


Fig. 4.13 Loaded and unloaded frames after springback of AA1050 specimen (oriented 0° w.r.t. R.D.) for punch radius 15 mm

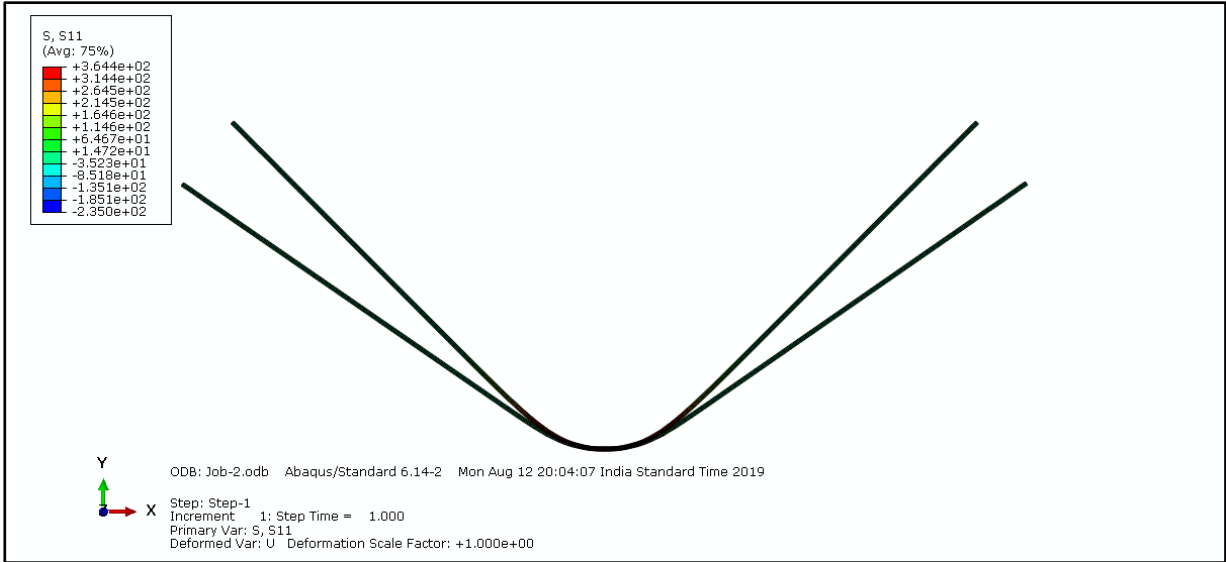


Fig. 4.14 Loaded and unloaded frames after springback of SS430 specimen (oriented 0° w.r.t. R.D.) for punch radius 15 mm

**4.4 Measurement of residual stress numerically**

Obtaining residual stresses numerically in Abaqus software involves a complex process. To get residual stresses through the thickness, firstly Job will be selected. After selecting Job, click on Job Manager then click on Results. After getting the result click on Plot Contours on Deformed



shape. Now there will be two conditions for the deformed blank. The first condition will be for before springback and the second condition will be for after springback. Stresses will be obtained for both conditions, through-thickness from the outer to inner side by following the same procedure. First, the Tool will be selected after that Path and then Create. In the Create path window click continue. Now Edit node list path window opened. In this window add after, is clicked. Now nodes will be selected on the bent blank. After selecting the node point click on done and then OK. Now click on “Create XY- data” and further click on Plot. After getting the plot click on save as XY data-1 and then OK. Now click on “Plug-ins” on the upper bar and click on Excel utilities through tools. After following this step an Excel file with data and a graph can be obtained. This same procedure is followed for the deformed blank after springback. Data and graphs will provide the stress distribution through thickness before and after springback.

## CHAPTER 05

### EXPERIMENTAL PROCEDURE

The different experiments conducted to characterize the properties of Aluminium 1050, SS430, SS304, 2-ply and 3-ply laminated sheets are described in this chapter. The experimental set up fabricated for the characterisation of springback of parent materials and 2-ply and 3-ply laminated composites in V-bending is also described in this chapter.

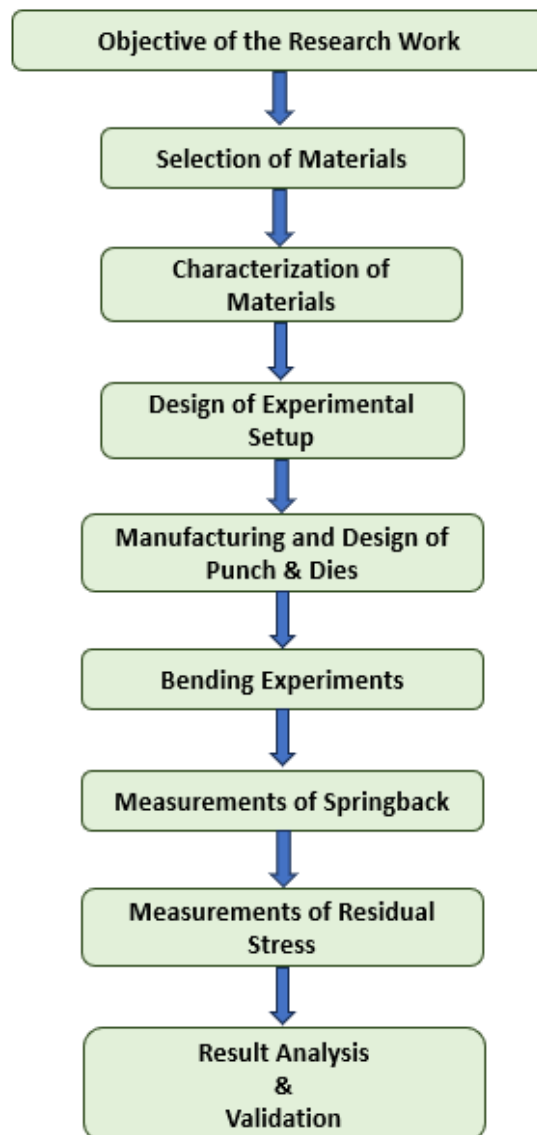


Fig. 5.1 Schematic diagram of the whole experimental plan

## **5.1 Material selection**

Selection of materials in this research work is based on the recent applications of laminated sheets in automotive, aerospace, and electrical industries. In the present research work, a 2-ply and a 3-ply laminate composite of Aluminium and Stainless steel have been used. A 2-ply laminate sheet comprising of layers of a commercially available aluminium AA1050 of thickness 1.4 mm and the other layer of a corrosion and heat resistant ferritic stainless steel SS430 of thickness 0.6 mm is selected and procured in an annealed condition. A 3-ply clad sheet consisting of layers of SS430, AA1050 and SS304 having thickness 0.6 mm, 1.4 mm, and 0.4 mm, respectively is selected for springback characterization and evaluation of residual stress after V-bending. The commercial aluminium AA1050 is clad in between SS430 and SS304 as a sandwich. The layer of SS430 is a corrosion and heat resistant ferritic grade steel whereas SS304 is a standard austenitic grade stainless steel with ability to undergo deep draw without intermediate annealing.

All the layers in the clad sheet were tested for the chemical compositions by spark-based spectroscopy. In this method, a spark is created on the sample which results in rapid heating causing vaporization on its surface which further produces plasma assisted spectrums from the element present in the sample. Then, a machine compares the amount of light from the sample to that of known standards to identify the element, and calculates the quantity of that element.

### **5.1.1 Microstructural examination of 2-ply and 3-ply clad sheets**

#### **5.1.1.1 Sample preparation**

Traditional cutting and shearing processes can adversely affect specimen cross-sections due to plastic deformation, resulting in bevelled surfaces that complicate microstructural examination. To address this issue and obtain flat cross-sectional surfaces conducive to microstructural

analysis, clad sheets meticulously sectioned using a diamond abrasive wheel with the assistance of a coolant.

#### **5.1.1.2 Sample mounting**

The primary objective of mounting the sectioned clad sheet specimens, which varied in thickness combinations, was to facilitate the handling of small-sized, thin samples. A semi-automatic compression-type mounting press was employed to embed the specimens in a 25 mm diameter mould using a thermosetting resin. The mounting press was set to a temperature of 150°C and a pressure of 290 bar. A heating and cooling cycle lasting 5 minutes was utilized to ensure complete setting of the thermosetting resin.

#### **5.1.1.3 Grinding and polishing**

Initial grinding aimed to create a flat surface and eliminate the effects of the sectioning procedure. Consequently, a coarse abrasive grit size of 220, specifically silicon carbide (SiC), was used on the specimen surfaces cut by the diamond abrasive wheel. The emery papers employed for fine grinding followed an ascending order of fineness, with grit sizes of 220, 320, 420, 600, 800, 1000, and 1200. The mounted specimens underwent a final stage of fine polishing using alumina of varying grades to achieve a scratch-free, mirror-like finish. Such a polished surface is essential for accurate microstructural observations in metallographic studies.

#### **5.1.1.4 Etching and microstructure analysis**

Examination of mirror-polished, unetched specimens only reveals a limited number of microstructural features, such as inclusions, cracks, or physical imperfections. Consequently, etching was employed to clearly delineate grain boundaries within the specimens. The aluminium layer after fine diamond polishing is etched with caustic sodium fluoride solution to reveal the grain structure. In order to reveal the microstructure of SS430 and SS304, the

mirror polished surface is etched with a solution containing hydrochloric (5ml) and picric acid (1ml) in ethanol.

### 5.2 Determination of tensile properties and anisotropy

To determine the tensile properties and anisotropy of 2-ply and 3-ply clad sheet metals, the specimens for uniaxial tension test are cut by CO<sub>2</sub>-Laser cutting (TRUMPF: Model-LC3030 with resonator: TLF4000 Turbo) as per ASTM-E8M, as shown in Fig 5.2.

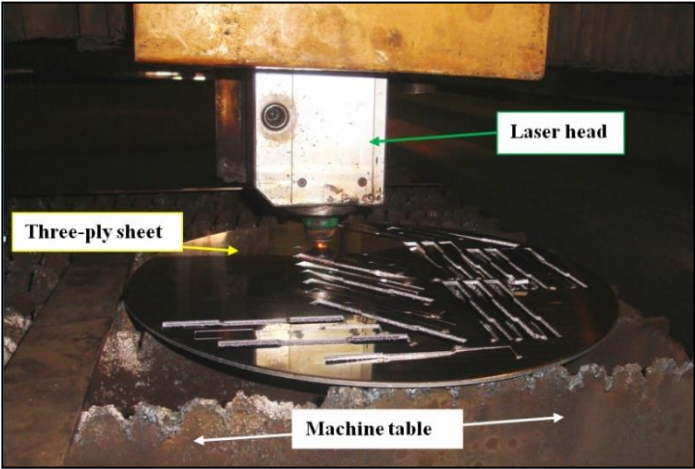


Fig.5.2 Laser cutting of tensile samples in progress

The tensile and anisotropy samples are cut in such a way that its orientation is arranged at 0°, 45° and 90° with respect to the rolling direction of the sheet as shown in Fig. 5.3, Fig. 5.4, Fig. 5.5, Fig. 5.7, Fig. 5.8, Fig. 5.10, and Fig. 5.11 respectively.



Fig.5.3 Tensile samples of 3-ply sheet with different orientations



Fig.5.4 Tensile samples of 2-ply sheet with different orientations

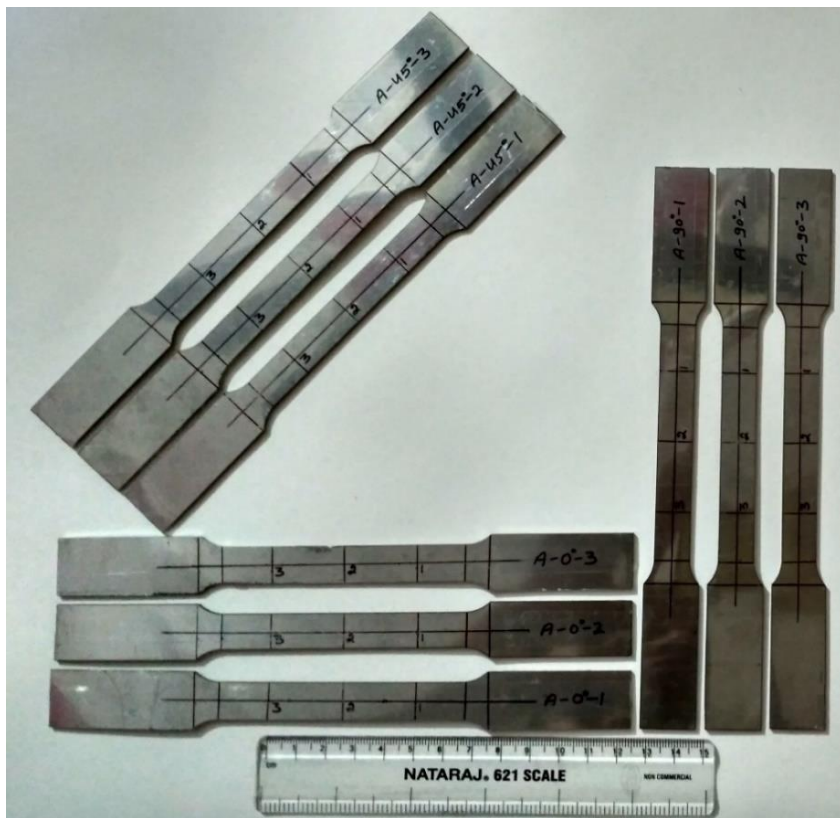


Fig.5.5 Anisotropy samples of 2-ply sheet with different orientations

The tensile samples of steel layers SS430 & SS304 (Fig. 5.7 and Fig 5.8) are claimed from 3-ply clad sheet by dissolving aluminium layer, a required set of the tensile samples are immersed in a glass beaker containing a solution of sodium hydroxide.

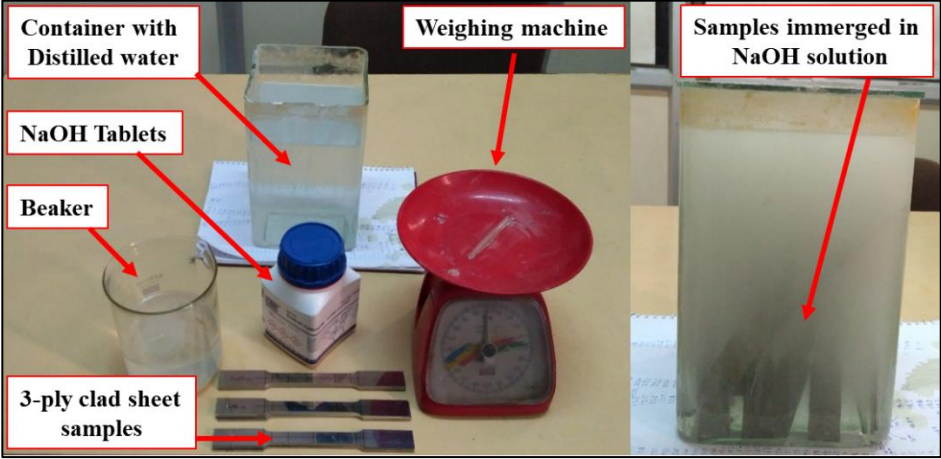


Fig. 5.6 Separation process of SS430 and SS304 from 3-ply sheet by immersing into NaOH Solution



Fig.5.7 Tensile samples of SS430 sheet with different orientations

The process of dissolution of aluminium in sodium hydroxide (Fig. 5.6) takes about three to four weeks of time, although the process can be accelerated by increasing concentration of sodium hydroxide and heating the solution.



Fig.5.8 Tensile samples of SS304 sheet with different orientations

To claim the samples of AA1050 alone from 2-ply sheet, the layer of stainless steel is removed by fine controlled facing operation on a full-sized blank to a predetermined depth equal to the thickness of the SS430 layer as shown in Fig. 5.9. For facing operation Vertical Machine centre (Cosmos Model: CVM 1060Control: Mitsubishi M70Travel: 1050) is used. The facing operation includes two mild steel-holding rings for the placement of 2-ply clad sheet on the milling machine bed. The clad sheet is held around its outer peripheral zone by holding rings which are fixed on the machine bed through mounting plate with the help of fastened screws. The screw joints ensure proper placement of the mild steel-holding rings that eliminates the longitudinal and transversal movement of the clad sheet during the milling operation. The clad sheet is held at its centre with the mounting plate by a nut-bolt joint to restrict the bending of the clad sheet during the interaction of milling tool with the clad sheet.



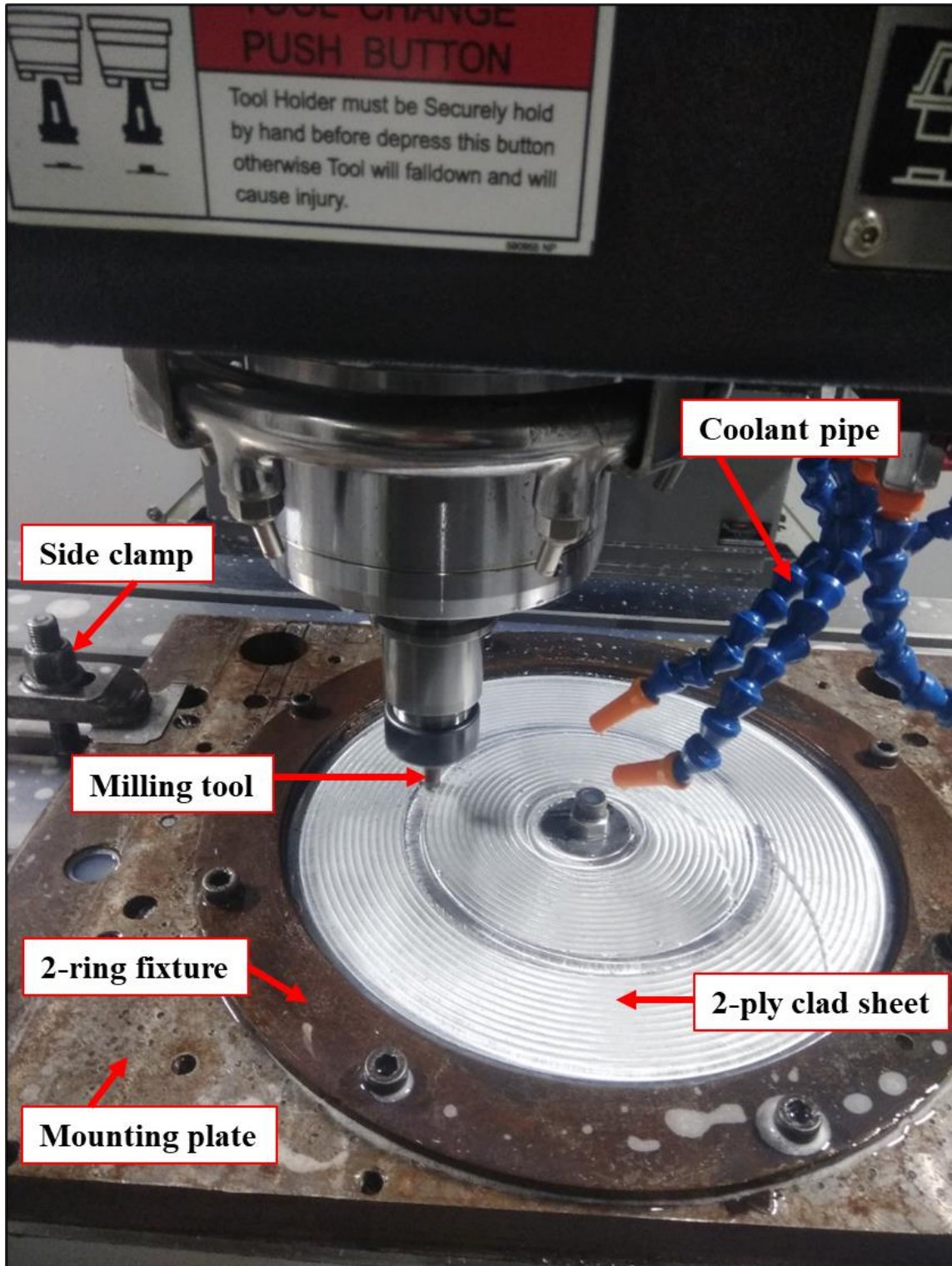


Fig. 5.9 Experimental setup used for removal of SS430 from 2-ply clad sheet

The Fig. 5.10 and Fig 5.11 show the tensile and anisotropic samples of AA1050 sheets respectively.



Fig. 5.10 Tensile samples of AA1050 separated from 2-ply sheet



Fig. 5.11 Anisotropy samples of AA1050 separated from 2-ply sheet

The tensile and anisotropic test samples size of 3-ply, 2-ply, SS430 and SS304 is taken as shown in Fig. 5.12. Due to the limited availability of 2-ply sheets, the tensile and anisotropic test samples of AA1050 layer have been taken in subsized dimensions as shown in Fig.5.13

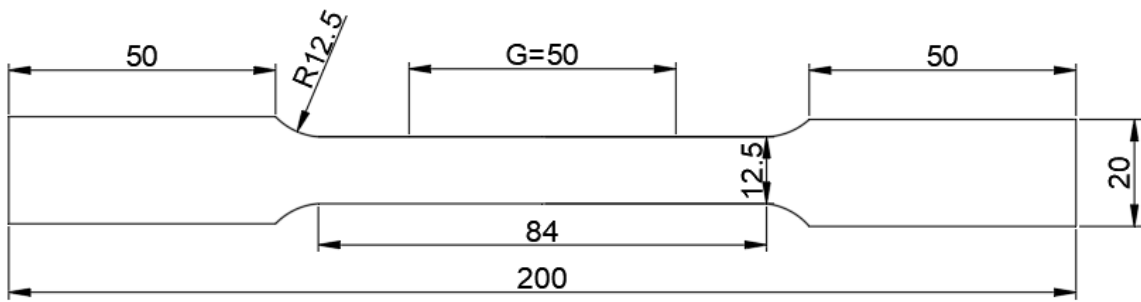


Fig. 5.12 Size description of sample of tensile and anisotropic test (All dimensions are in mm)

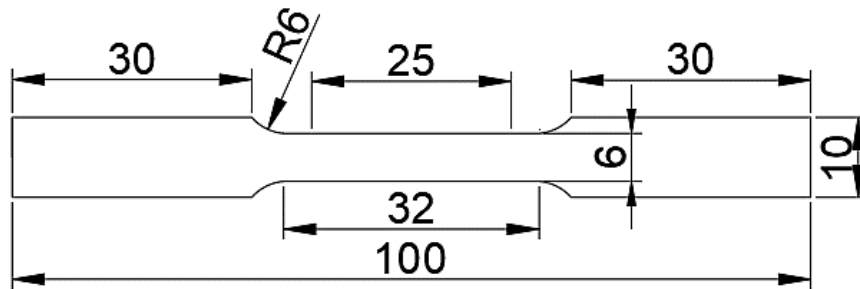


Fig. 5.13 Size description of sub size sample of tensile and anisotropic test for AA1050 (All dimensions are in mm)

All the tensile tests are performed on a 50kN table top UTM (make: Tenius Olsen) with a cross head speed of 2.5 mm/min as shown in Fig 5.14. The tensile test specimen with orientation of 0°, 45° and 90° to the rolling direction (RD) were also tested to properly investigate the normal anisotropy of the 2-ply, 3-ply clad sheet metal and individual parent sheet metal by giving an elongation of 15% to the specimens. Each tensile and anisotropic test is performed thrice to capture the reproducibility of the experimental data points.

From the force-elongation data, true stress-true strain curves as well as  $\ln$  (true stress)- $\ln$  (true strain curves have been plotted.

To convert engineering stress-strain data into true stress-strain data, the following equations have been employed:

$$\sigma \text{ (true stress)} = s (1 + e) \quad (5.1)$$

$$\varepsilon \text{ (true strain)} = \ln (1 + e) \quad (5.2)$$

Where  $s$  represents engineering stress, and  $e$  represents engineering strain

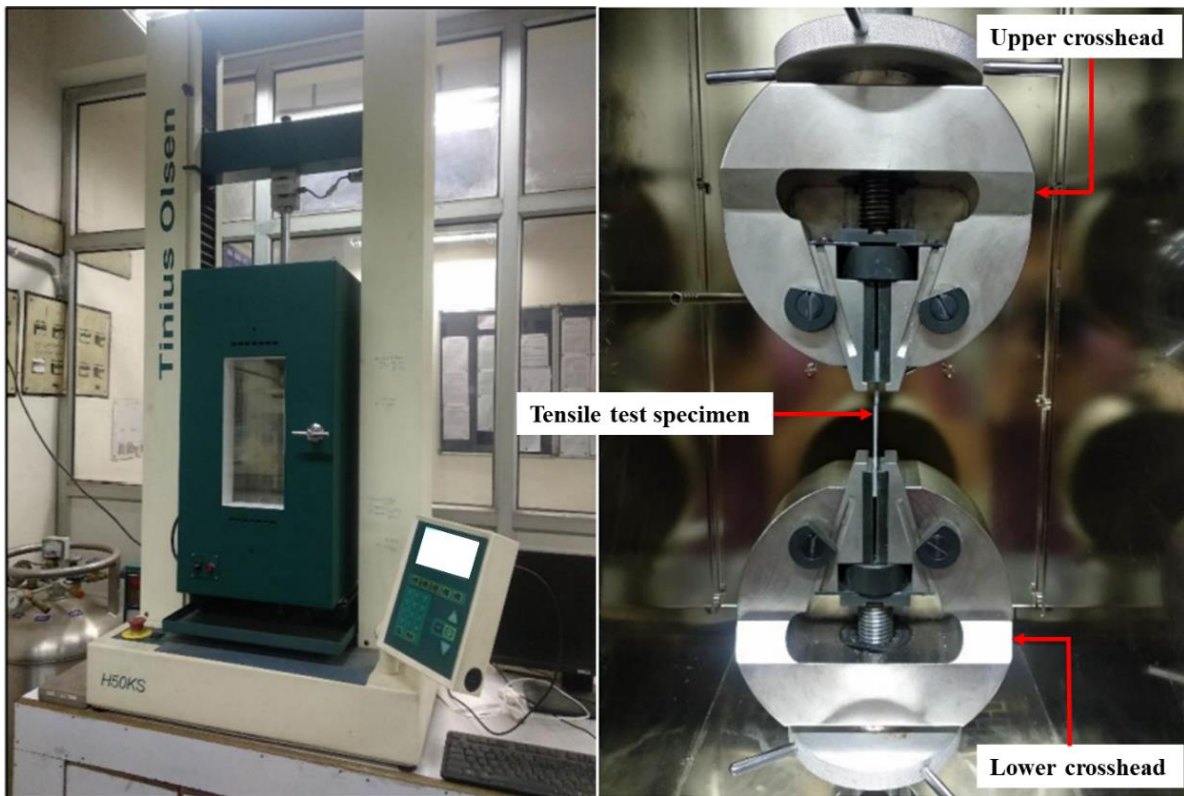


Fig.5.14 Performing tensile test on 50kN table top UTM (make: Tinius Olsen)

As steel and aluminium adhere to the general power law of strain hardening ( $\sigma = K\varepsilon^n$ ), where  $\sigma$  and  $\varepsilon$  denote true stress and true strain respectively, the values of strain hardening exponent ( $n$ ) and strength co-efficient ( $K$ ) have been determined from  $\ln \sigma - \ln \varepsilon$  plots, focusing on data within the uniform plastic deformation range.

The normal anisotropy or the average plastic strain ratio ( $\bar{R}$ ) of the parent steel sheets has also been determined from the uni-axial tension test of specimens oriented at  $0^\circ$ ,  $45^\circ$  and  $90^\circ$  with respect to the rolling direction as per ASTM E517-06. To calculate the  $R$  (plastic strain ratio) value, the tensile specimens were deformed plastically to 15% elongation, and the crosshead was halted automatically using specialized software, Tinius Olsen Horizon, supplied with the testing machine. Measurements of width and gauge length were taken before and after the test using a digital vernier calliper, and the plastic strain ratio was computed in all three directions relative to the rolling direction, as per the following equations:

$$R = \frac{\varepsilon_w}{\varepsilon_t} = \frac{\varepsilon_w}{-(\varepsilon_w + \varepsilon_l)} = \left[ \frac{\ln\left(\frac{w_f}{w_0}\right)}{\ln\left(\frac{l_0 w_0}{l_f w_f}\right)} \right] \quad (5.3)$$

where  $w_0$ ,  $l_0$  are initial width and length,  $w_f$ ,  $l_f$  are final width and length,  $\varepsilon_w$  is true width strain,  $\varepsilon_t$  is true thickness strain and  $\varepsilon_l$  is true longitudinal strain.

The values of plastic strain ratio, determined in three different directions as specified above, were used to calculate normal anisotropy ( $\bar{R}$ ) using the standard formula provided below:

$$\bar{R} = \left( \frac{R_0 + 2R_{45} + R_{90}}{4} \right) \quad (5.4)$$

Here  $R_0$ ,  $R_{45}$  and  $R_{90}$  denote the plastic strain ratio of the specimens oriented at  $0^\circ$ ,  $45^\circ$  and  $90^\circ$  w.r.t the RD (rolling direction). It's important to note that the accuracy of  $\bar{R}$  is highly sensitive to measurement errors, especially in width measurements, and relies on the precision of flatness and squareness of the edges. Therefore, all tensile specimens were meticulously prepared through laser cutting to ensure accurate determination of the plastic strain ratio.

The engineering stress-strain curves are plotted from the data captured for force and displacement using a dedicated HORIZON software. The engineering stress-strain curves are further transformed into plots of true stress- true strain curves. The log-log plot of true stress-true strain values gives the values of strain hardening exponent (n) and strength coefficients (K) using the simple mathematical equation of power law of strain hardening.

ln (true stress)-ln (true strain) plots for the data in uniform plastic deformation region (between YS and UTS) which were used to determine values of strain hardening exponent (n) and strength coefficient (K) of AA1050 using power law of strain hardening are shown in Fig. 5.15. The values of n and K of AA1050 are also given in the Table 6.4.

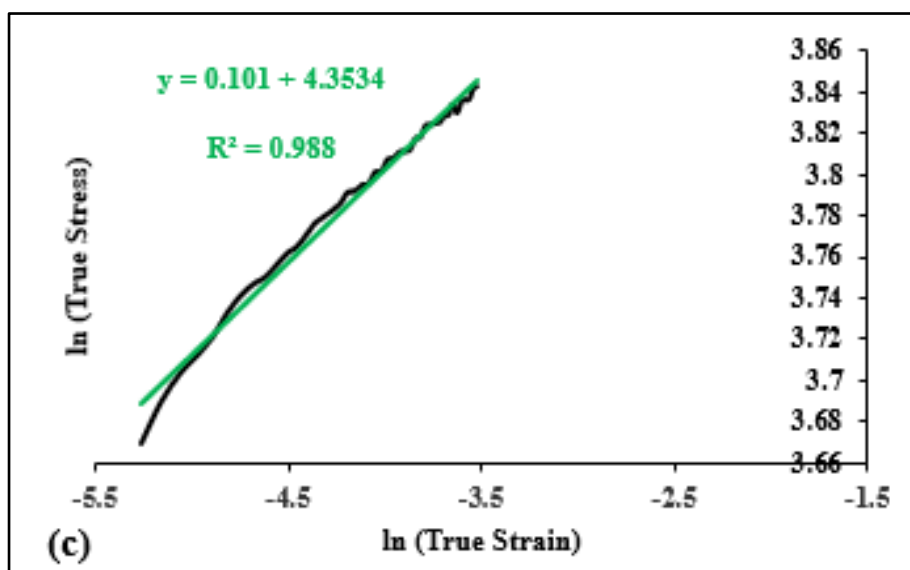
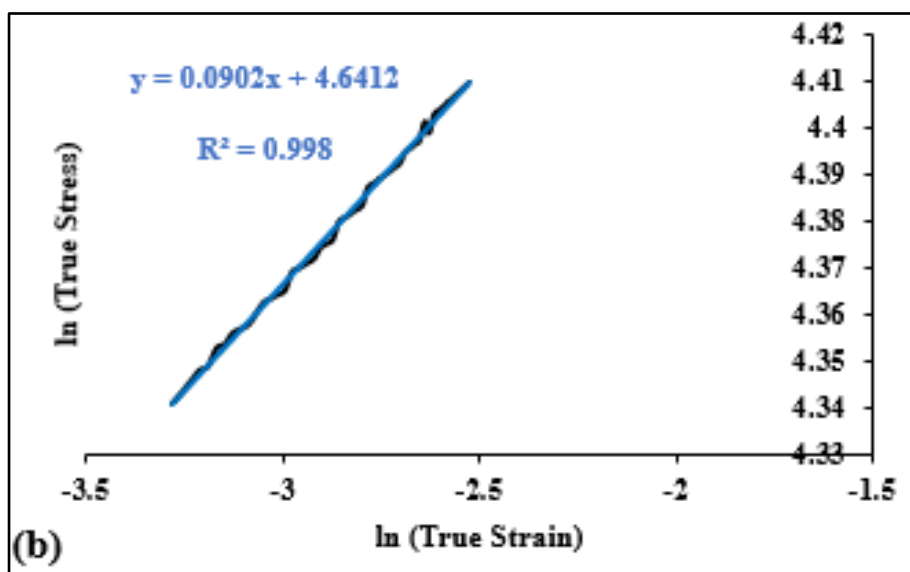
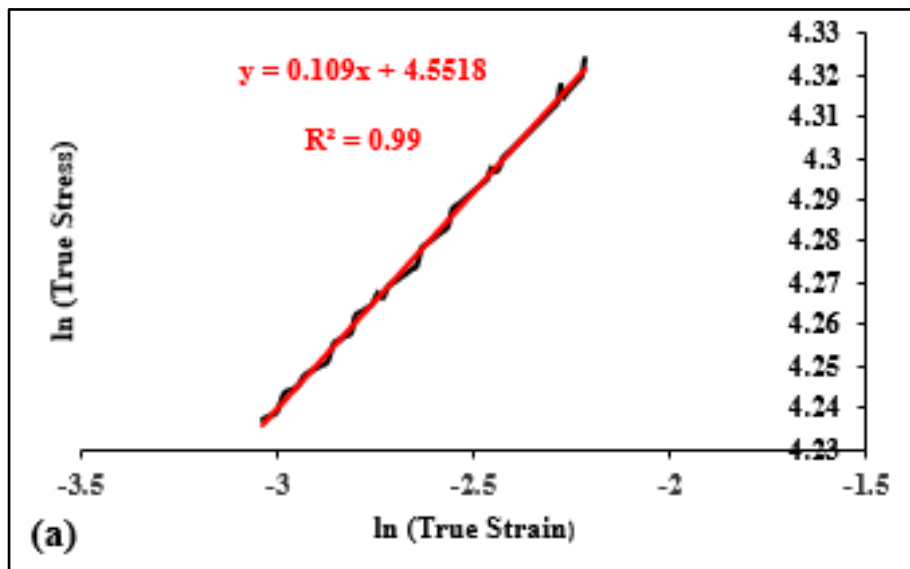


Fig. 5.15 ln (true stress)-ln (true strain) plots of AA1050 at (a) 0°, (b) 45° and (c) 90° to R.D.

The strain hardening exponent which is a measure of ability of the material to strain harden during plastic deformation without necking or fracture, is observed to be lower for AA1050 when compared to SS430 and SS304 as per Table 6.7.

From Fig. 5.15 (a), the value of strain hardening exponent  $n = 0.109 \approx 0.11$  and the value of  $K$  will be  $e^{4.5518} = 94.8$  MPa.

### **5.3 Microhardness measurement**

Microhardness number was measured on the SS304, Al 1050 and SS430 specimens with the help of Duramin 40 Microhardness tester as shown in Fig. 5.16. Vickers method was used to find material hardness using a hardness scale of HV0.05 with 10 seconds of dwell time. A diamond pyramid indenter was used to apply a load of 100-gm.

The process of measuring microhardness comprises loading, dwell period and unloading, followed by the measurement of both the diagonals of the indentation. This microhardness measuring machine has six turrets, two of which are indenters and the rest are objective lenses of different magnifications. Fig. 5.16 also shows an image taken from the camera attached to the head of the instrument.

The table or the bed of the instrument has a computer-controlled screw which is used to produce motion in “X”, “Y” and “Z” directions. So, the specimen is fixed on the table, the starting point for measurement is located by the position offset from the periphery of the specimen.

Then the indenter is brought on to the specimen and the measurement process is started. A line is marked on the specimen to make a set of measurements. The specimen is fixed on the table. The starting point for measurement is located at a position having some offset from the specimen periphery.

Then the indenter is brought down to make indentation on the specimen and the measurements are made.

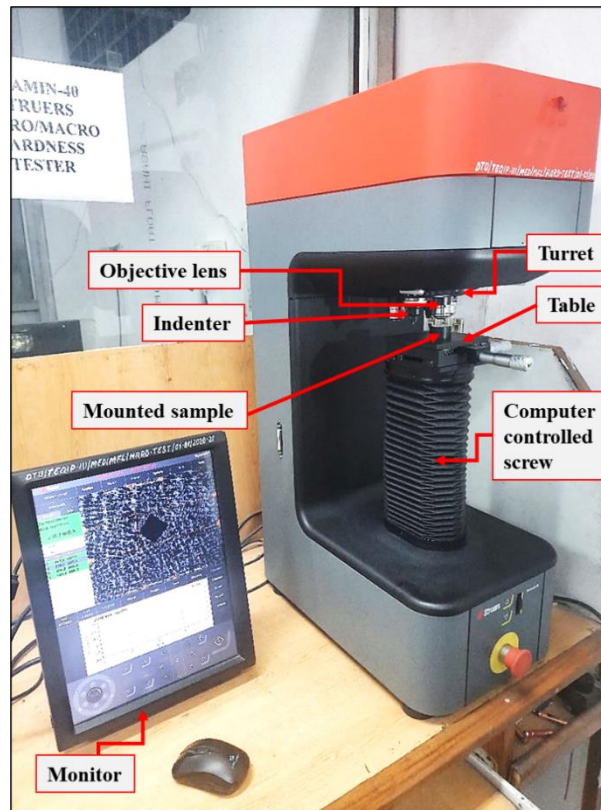


Fig. 5.16 Duramin 40 Microhardness tester

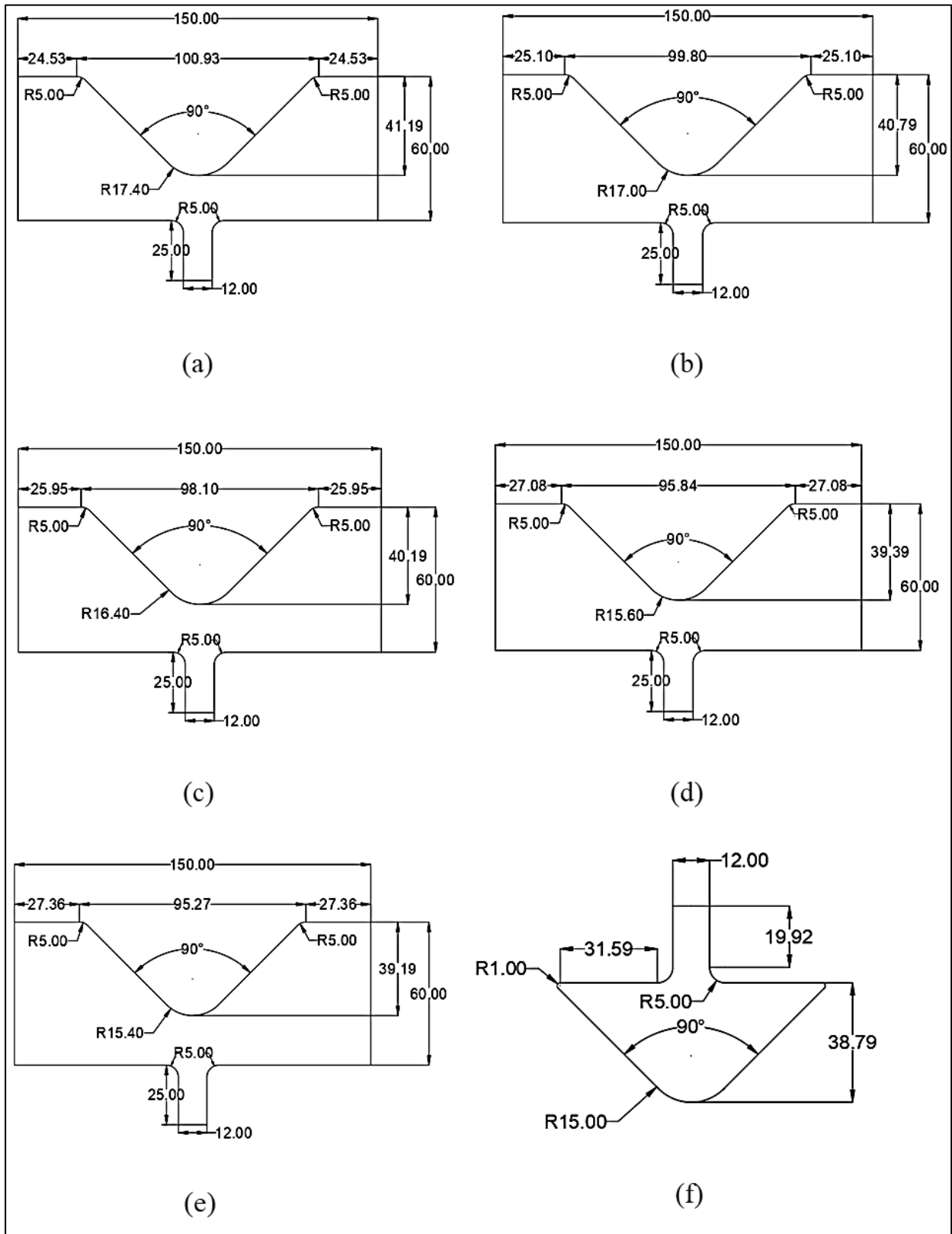
#### 5.4 Determination of springback for clad sheet

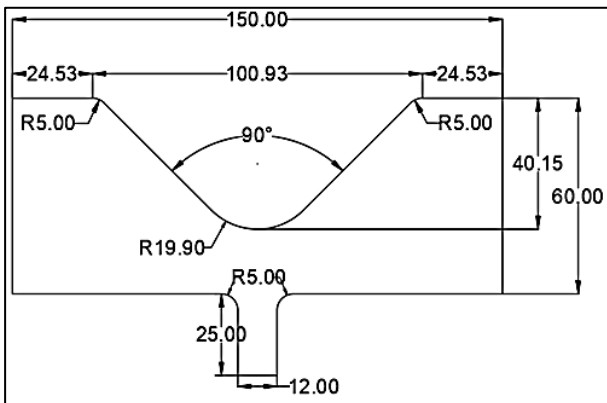
An experimental set up has been created for determination of springback in V-bending. This arrangement includes three sets of V-dies and punches, each having a  $90^\circ$  included angle. The punches are specifically manufactured with radii of 15 mm, 17.5 mm, and 20 mm and dies with corresponding radii and clearances as shown in Fig 5.17 (a) to (r). The clearance was kept equal to the sheet thickness in order to prevent any localized compression at the bottom of the die.

To determine the springback results of 2-ply clad sheet from the bending experiments, a V-bending die and punch set is designed with a die profile radius of 17 mm and a punch profile radius of 15 mm. The included bend angle is  $90^\circ$ . Different die sets of D2 steel, are also designed for individual sheets of thickness 1.4 mm for AA1050 and 0.6 mm for SS430 as the clearance between the die and punch is kept equal to sheet thickness. All the toolings of D2 steel are prepared by wire cut Electric Discharge Machining (EDM) process followed by proper heat treatment. In the case of 3-ply clad sheet, die profile radius of 17.4 mm and a punch profile radius of 15 mm are taken. The punch is designed to be fixed in the wedge grip attached with

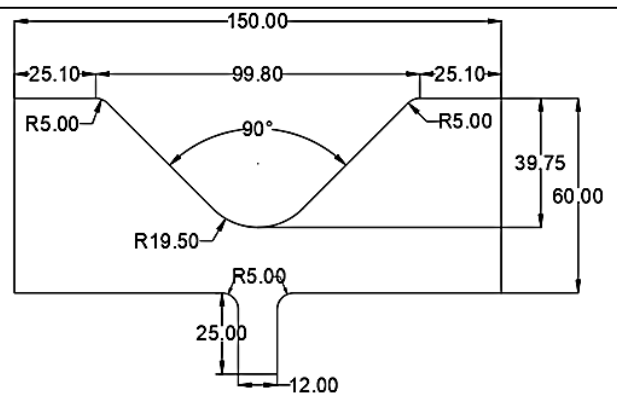


the movable crosshead and the die is firmly secured in a stationary wedge grip located at the bottom of a 50 kN universal testing machine as shown in Fig. 5.18.

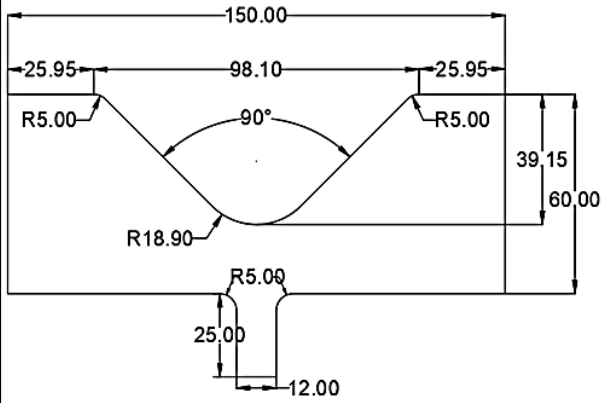




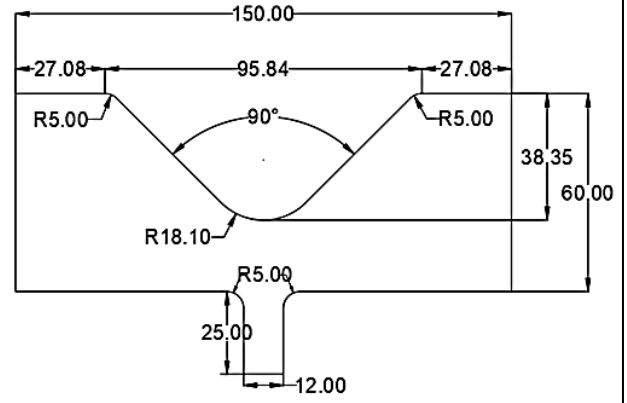
(g)



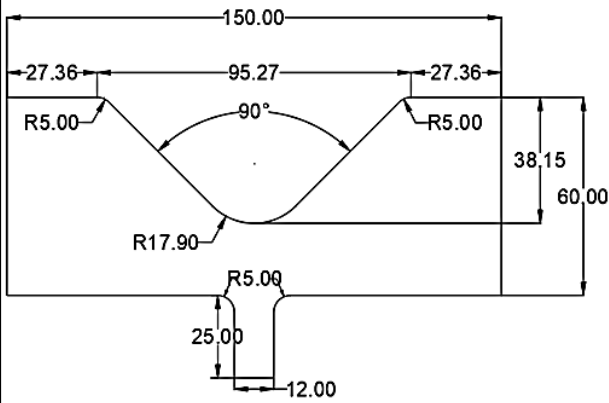
(h)



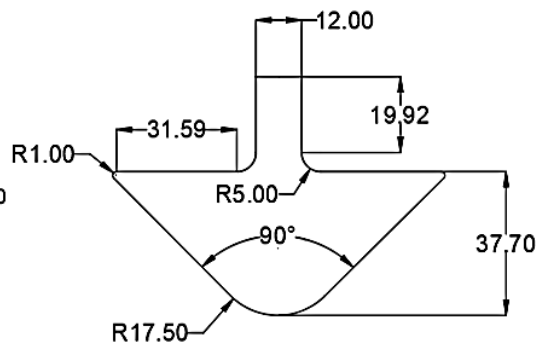
(i)



(j)



(k)



(l)

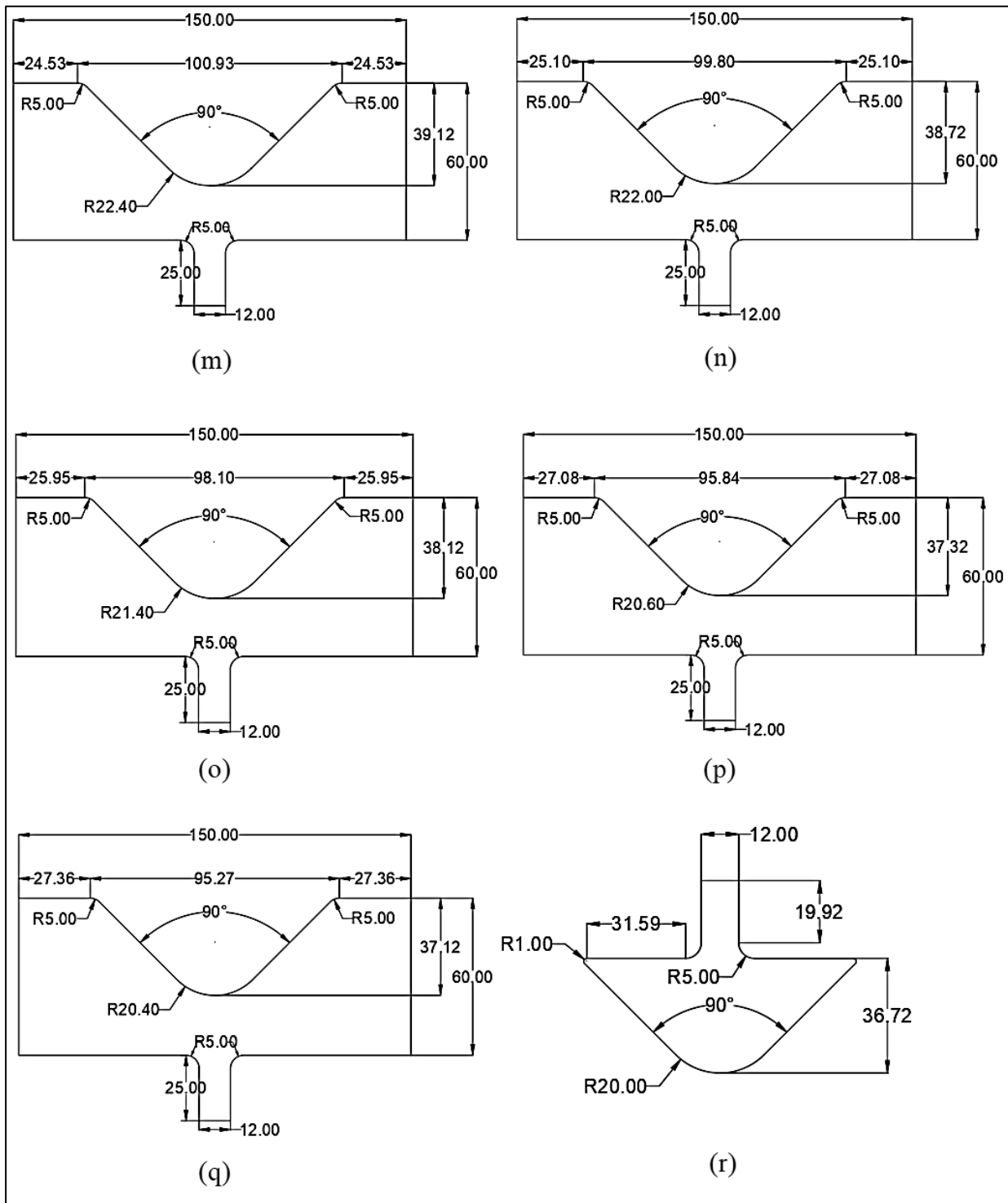


Fig. 5.17 Design of punches and dies for V-bending experiments (dimensions in mm): (a)-(e) Dies for a punch profile radius of 15 mm, (f) Punch with profile radius of 15 mm, (g)-(k) Dies for a punch profile radius of 17.5 mm, (l) Punch with profile radius of 17.5 mm, (m)-(q) Dies for a punch profile radius of 20 mm and (r) Punch with profile radius of 20 mm

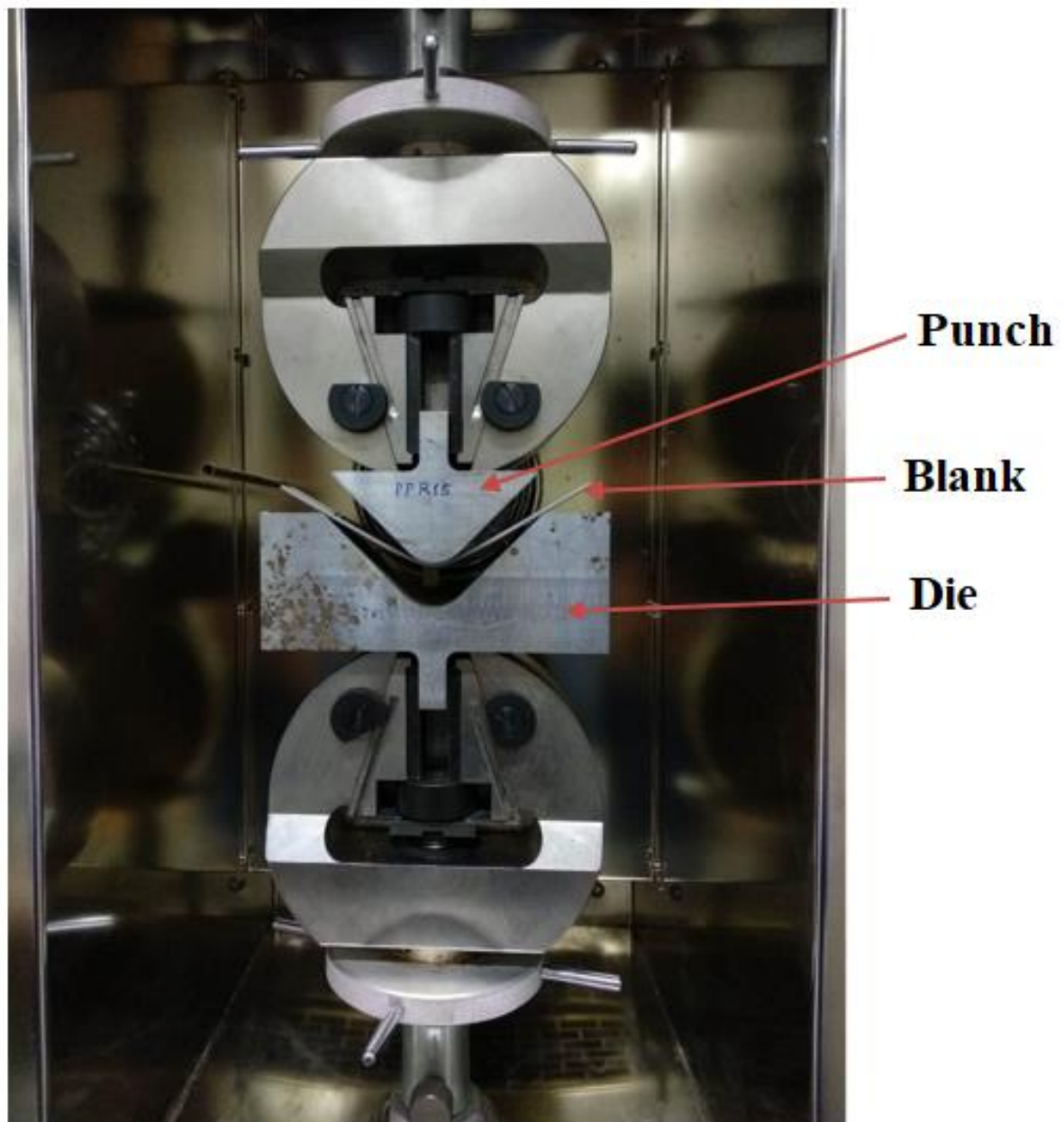


Fig. 5.18 Experimental setup for V-bending operation

The specimens for bending with a dimension of 150 mm x 25 mm are precisely cut from a 2-ply and 3-ply sheet by a wire-cut EDM (Fig. 5.19). Some of the specimens of different orientation ( $0^\circ$ ,  $45^\circ$  and  $90^\circ$  to the rolling direction) for the 2-ply and 3-ply sheet are shown in Fig. 5.20.

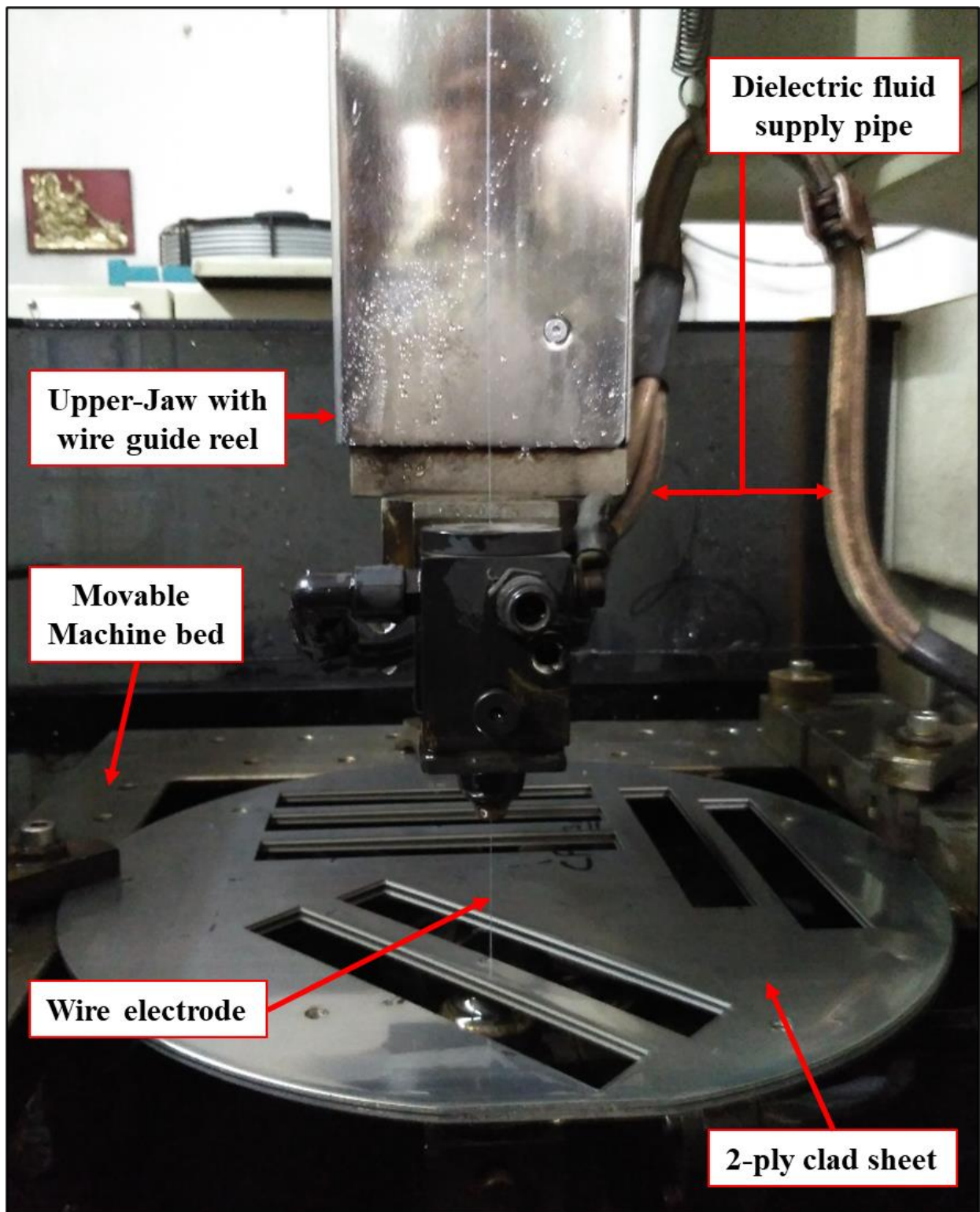


Fig.5.19 Cutting of bending samples on CNC Wire-Cut EDM Machine



Fig.5.20 Bending samples of 2-ply and 3-ply sheet with different orientations

The bending specimens for SS430 and SS304 are taken from the 3-ply sheet by dissolving the aluminium in sodium hydroxide whereas AA1050 specimens are carefully claimed by machining the layer of steel to the depth equal to layer thickness by a facing operation. To determine the effect of sheet setting on bending and springback, the bending experiments are carried out by placing the specimens in two ways. For a 2-ply clad sheet, firstly the stainless-steel layer faces the punch during bending and in the second setting, aluminium layer faces the punch. For a 3-ply clad sheet, in the first setting, the stainless-steel layer (SS430) faces the punch during bending and in the second setting, the stainless-steel layer (SS304) faces the punch. The bending experiments are also carried out for individual sheets to determine the springback characteristics of each. All the bending experiments are carried out with a constant punch speed of 20 mm/min and the punch stroke is kept equal to the depth of the die. Bent

samples of parent sheets, and 2-ply and 3-ply clad sheets have been shown in Fig. 5.21 and Fig. 5.22 respectively.

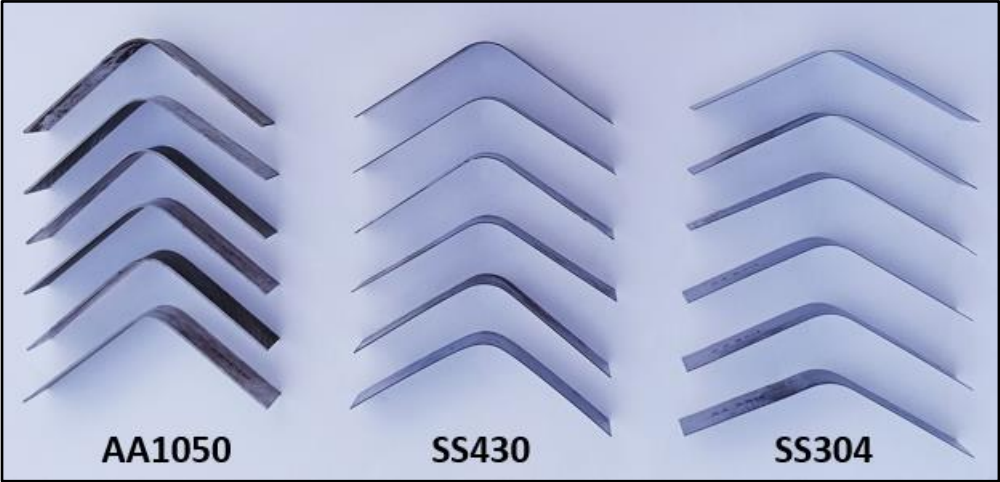


Fig. 5.21 Bent samples of AA1050, SS430 and SS304

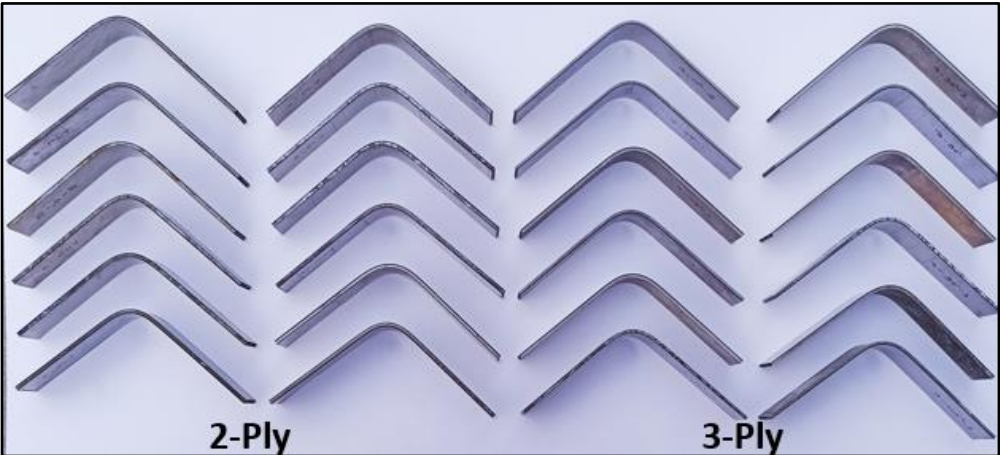


Fig. 5.22 Bent samples of 2-ply and 3-ply clad sheets

The values of included bend angle after bending experiments are determined using a sensor-based vision inspection machine by carefully placing the tested specimens on a magnetic V-block as shown in Fig. 5.23. The sensor of the probing tool is moved manually on both surfaces of the arms of the bending specimens to capture the coordinates with dedicated software and the angle is measured between two flat planes. The included bend angle of the die is predetermined followed by the determination of the final bend angle of the tested specimen

after springback. The angular difference between the initial and final bend angle gives the springback.



Fig. 5.23 Sensor-based vision inspection machine for angle measurement

$$\text{Springback } (\theta_s) = \frac{1}{2} (\theta_f - \theta_i) \tag{5.1}$$

where  $\theta_f$  = Included bend angle of unloaded specimen,

$\theta_i$  = Included bend angle of loaded specimen  $\approx 90^\circ$

**5.5 Measurement of residual stress**

The measurement of the resultant residual stress after springback on inner and outer surfaces of tested clad sheet sample is done by using an X-ray device ( $\mu$ -X360: PULSETEC) mounted on a table as shown in Fig. 5.24(a).

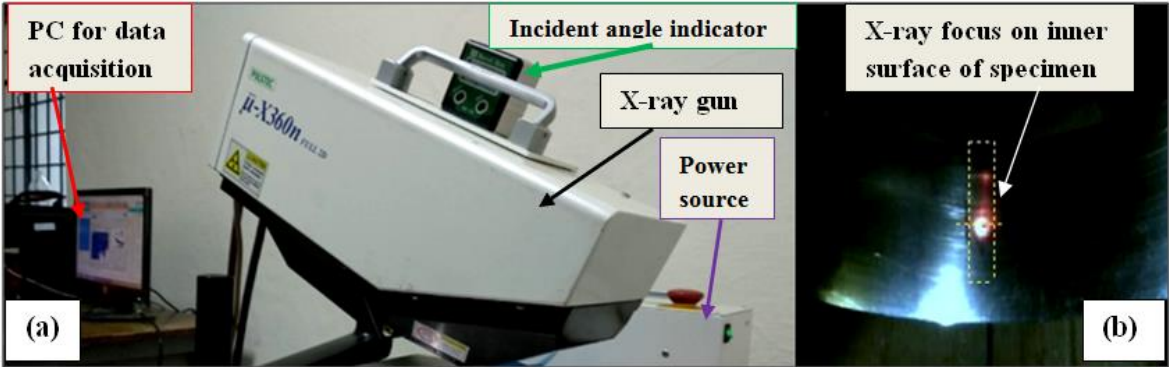


Fig.5.24 (a) Experimental set-up for residual stress measurement using an X-ray machine and (b) Measurement of residual stress in progress



The device is connected with a dedicated data acquisition system software which is used to generate the data in a portable format. For residual stress measurements, specimens after bending experiments of the clad sheet with different sheet placement positions are marked with points on the inner and outer layers along the axis of bending. The samples are placed on a platform below the X-ray sensor gun in such a way that the surface to be evaluated for residual stress is exposed to the X-ray beam. The detector gun of X-ray tube uses a single incident angle measurement using  $\text{Cos}\alpha$  technique which utilizes the Debye ring collected with a single measurement. X-ray beam is incident on the mark on the surface to be assessed establishing a red spot for easy focusing of  $\sim 2$  mm in diameter as shown in Fig. 5.24 (b) and once the focus is set, a green check box appears on the marking. Similar procedure is adopted for a number of points marked on the inner and outer surface of the bend specimens

## **CHAPTER-06**

### **RESULTS AND DISCUSSION**

The results obtained from various experiments conducted to characterize the mechanical properties of 2-ply and 3-ply clad are presented and discussed in this chapter. The characterisation of the mechanical properties of different material like SS430, SS304 and Al1050 is also presented in details.

#### **6.1 Chemical compositions of two-ply and three-ply clad sheet**

##### **6.1.1 Chemical composition of 2-ply clad sheet**

2-ply clad sheet, procured in an annealed condition, is composed of a layer of a commercially available aluminium AA1050 of thickness 1.4 mm bonded to a layer of a corrosion and heat resistant ferritic stainless steel SS430 of thickness 0.6 mm. Both the layers in the clad sheet were tested for the chemical compositions by spark-based spectroscopy. The measurements are seen to match the material specifications for both the layers. The elemental chemical compositions as obtained are given in Table 6.1

Table 6.1 Chemical composition of individual layers of the 2-ply sheet in wt%.

| Clad Sheet metals | Layer thickness (mm) | Cr    | Ni    | Mn    | Si    | P     | Cu     | Ti     | Al   | Fe    |
|-------------------|----------------------|-------|-------|-------|-------|-------|--------|--------|------|-------|
| SS430             | 0.6                  | 16.18 | 0.134 | 0.421 | 0.313 | 0.023 | 0.0200 | 0.0300 | 0.03 | Rest  |
| AA1050            | 1.4                  | 0.002 | 0.005 | 0.002 | 0.061 | 0.002 | 0.0117 | 0.0172 | Rest | 0.296 |

##### **6.1.2 Chemical composition of three-ply clad sheet**

A 3-ply clad sheet consisting of layers of SS430, AA1050 and SS304 having thickness 0.6 mm, 1.4 mm, and 0.4 mm, respectively is selected for springback characterization and evaluation of residual stress after V-bending. The commercial aluminium AA1050 is cladded in between

SS430 and SS304 as a sandwich. The layer of SS430 is a corrosion and heat resistant ferritic grade steel whereas SS304 is a standard austenitic grade stainless steel with an ability to undergo deep draw without intermediate annealing. Spark-based spectroscopy has been used to obtain the chemical compositions of all the three layers of the clad sheet. The chemical compositions of different layers of three-ply clad sheet are given in Table 6.2.

Table 6.2 Chemical composition of individual layers of the 3-ply clad sheet in wt%.

| Layer thickness (mm) | Clad Sheet metals | Cr    | Ni    | Mn    | Si    | P     | Cu     | Ti     | Al    | Fe    |
|----------------------|-------------------|-------|-------|-------|-------|-------|--------|--------|-------|-------|
| 0.4                  | SS304             | 18.13 | 8.471 | 1.238 | 0.518 | 0.025 | 0.229  | 0.0300 | 0.001 | Rest  |
| 1.4                  | AA1050            | 0.002 | 0.005 | 0.002 | 0.061 | 0.002 | 0.0117 | 0.0172 | Rest  | 0.296 |
| 0.6                  | SS430             | 16.18 | 0.134 | 0.421 | 0.313 | 0.023 | 0.0200 | 0.0300 | 0.03  | Rest  |

The main difference between the chemical compositions of 2-ply and 3-ply clad sheets is due to the presence of SS304 in 3-ply clad sheet.

## 6.2 Microstructural analysis of the 3-ply and 2-ply clad sheets

The microstructure of laminated sheets is influenced by the composition, processing, and bonding of the individual layers. The potential differences in microstructure for each of these configurations as follows:

The microstructures of 2-ply and 3-ply clad sheets at a magnification of 600X are shown in Fig. 6.1 and Fig 6.2, respectively. The aluminium layer after fine diamond polishing is etched with caustic sodium fluoride solution to reveal the grain structure. The grains in the microstructure appeared to be distorted due to CRB process of the clad sheet as the layer is subjected to a high degree of plastic deformation. In order to reveal the microstructure of SS430 and SS304, the mirror polished surface is etched with a solution containing hydrochloric (5ml) and picric acid (1ml) in ethanol. The microstructure of SS430 layer shows a fine equiaxed rounded grained structure of ferritic grains with an average grain size of 5 $\mu$ m. The microstructure of SS304 layer shows a fine equiaxed grained structure of single austenitic phase

having an average grain size of  $12\mu\text{m}$  with sharp edged boundaries. The twinned grains with deformation bands parallel to rolling direction are also observed.

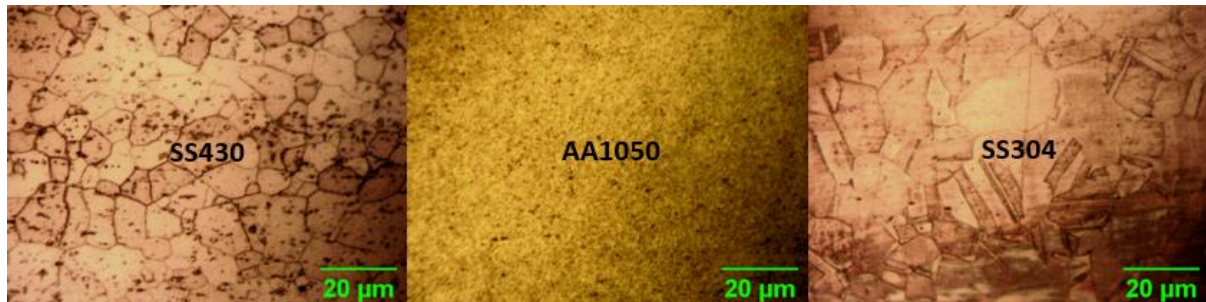


Fig. 6.1 Microstructure of 3-ply clad sheet (SS430/AA1050/SS304) at 600X

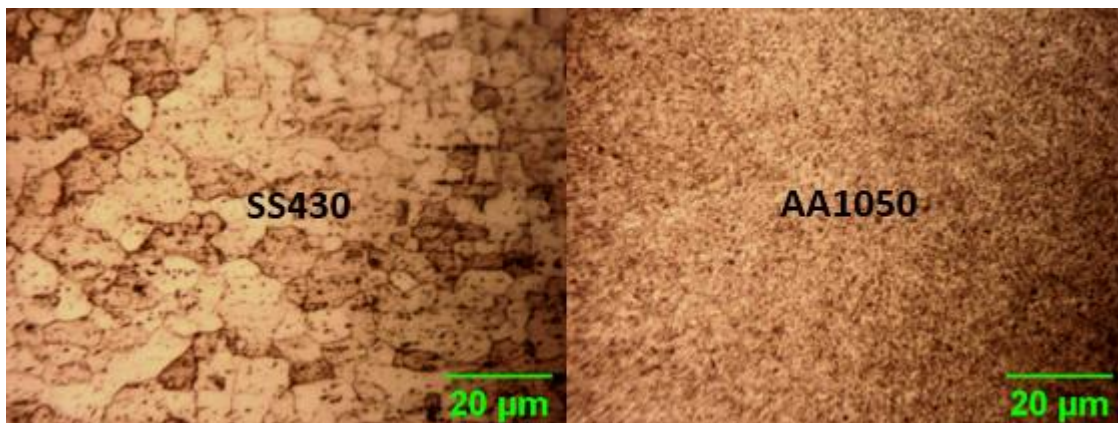


Fig. 6.2 Microstructure of 2-ply clad sheet (SS430/AA1050) at 600X

## 6.3 Tensile properties

### 6.3.1 Tensile properties of 2-ply sheet

Typical tensile properties of a 2-ply clad sheet obtained from uniaxial tension tests of the specimens oriented at  $0^\circ$ ,  $45^\circ$ , and  $90^\circ$  with respect to the rolling direction (RD) are given in Table 6.3. The 0.2% offset yield strength and UTS of the specimens inclined to the rolling direction and measured from the engineering stress-strain plots are observed to be highest followed by the strength of the specimens oriented at transverse and along the rolling direction. These strengths are attributed to the combined strengths of AA1050 and SS430. All the tested samples showed a clearly visible localized wrinkling and warping phenomenon at the zone of

fracture indicating that the difference in plastic strain ratios of both the layers played a key role during this distinctive feature of fracture. The minimum value of the plastic strain ratio is seen in the specimens oriented parallel to the rolling direction followed by the specimens oriented inclined and transverse to the rolling direction. A lower value of the average plastic strain ratio of approximately 0.98 indicates reduced formability of the cladded sheet. The ductility of the 2-ply sheet on an average basis is observed to be very good indicating good formability of the sheet but the specimen oriented at 0° to the rolling direction shows maximum percentage elongation. The values of strain hardening exponent and strength coefficient are determined from the log-log plots of true stress-true strain curves of the tensile data and are found to be approximately 0.2 and 279MPa, respectively. All the tensile specimens of 2-ply showed the initiation of fracture from the aluminium layer which can be attributed to the lower ductility of the AA1050 layer than the ductility of the SS430 layer as evident from Table 6.4 and 6.5.

Table 6.3 Tensile properties of 2-ply sheet

| Specimen's orientation w.r.t. RD | 0.2% Yield Stress (MPa) | Tensile Strength (MPa) | % Elongation | Strain hardening exponent n | Strength coefficient (MPa) K | Plastic strain ratio R |
|----------------------------------|-------------------------|------------------------|--------------|-----------------------------|------------------------------|------------------------|
| 0°                               | 115±2.10                | 162±1.73               | 31.10±3.17   | 0.204                       | 277.7±4.3                    | 0.78                   |
| 45°                              | 117±1.73                | 164±1.50               | 24.12±2.10   | 0.202                       | 282.6±3.0                    | 1.02                   |
| 90°                              | 114±5.65                | 161±4.24               | 25.65±0.21   | 0.203                       | 276.6±7.4                    | 1.11                   |

The tensile properties of AA1050 layer removed from the cladded sheet obtained from uniaxial tension tests of the specimens oriented at 0°, 45°, and 90° with respect to the rolling directions are given in Table 6.4. It is observed that this layer of aluminium is very soft when compared with the yield and tensile strength of the 2-ply sheet metal. The difference between the 0.2% offset yield and tensile strength is approximately 10MPa. The percentage elongation is highest in the specimens oriented at 45° to the rolling direction followed by specimens oriented at 0° and 90° to the rolling direction. The strain hardening exponent is found to be only 0.11 or lower which indicates a lower uniform elongation in the tensile specimens. The average

plastic strain ratio is also much lower than unity and is equal to 0.63 indicating poor formability of AA1050.

Table 6.4. Tensile properties of AA1050 layer

| Specimen's orientation w.r.t. RD | 0.2% Yield Stress (MPa) | Tensile Strength (MPa) | % Elongation | Strain hardening exponent n | Strength coefficient (MPa) K | R    |
|----------------------------------|-------------------------|------------------------|--------------|-----------------------------|------------------------------|------|
| 0°                               | 59±2.12                 | 68±1.97                | 21.81±0.14   | 0.11                        | 94.8±2.91                    | 0.89 |
| 45°                              | 64±1.90                 | 77±2.50                | 22.90±1.36   | 0.09                        | 103.6±2.58                   | 0.49 |
| 90°                              | 57±1.30                 | 62±2.10                | 19.50±0.85   | 0.10                        | 77.7±2.63                    | 0.64 |

The tensile properties obtained from the uniaxial tension tests of the specimens oriented at 0°, 45°, and 90° with respect to the rolling direction of SS430 layer of thickness 0.6 mm retrieved from a 2-ply clad sheet by the dissolution of aluminium, are given in Table 6.5. The yield strength and tensile strength of the sheet is the highest when compared with the strengths of the aluminium layer and 2-ply clad sheet as shown in Fig. 6.3. The percentage elongation of this layer is approximately 29% and the value of strain hardening exponent is 0.23 on an average basis. This layer is responsible for the high strength and ductility of the clad sheet. The normal anisotropy of the steel layer is found to be 0.82 which is again lower than unity.

Table 6.5. Tensile properties of SS430 layer

| Specimen's orientation w.r.t. RD | 0.2% Yield Stress (MPa) | Tensile Strength (MPa) | % Elongation | Strain hardening exponent n | Strength coefficient (MPa) K | R    |
|----------------------------------|-------------------------|------------------------|--------------|-----------------------------|------------------------------|------|
| 0°                               | 269±21.21               | 410±15.87              | 31.51±1.10   | 0.24                        | 749±71.72                    | 0.88 |
| 45°                              | 252±1.50                | 437±17.09              | 27.00±1.60   | 0.23                        | 786±59.60                    | 0.71 |
| 90°                              | 330±14.84               | 445±8.60               | 28.80±1.79   | 0.22                        | 782±44.43                    | 0.98 |

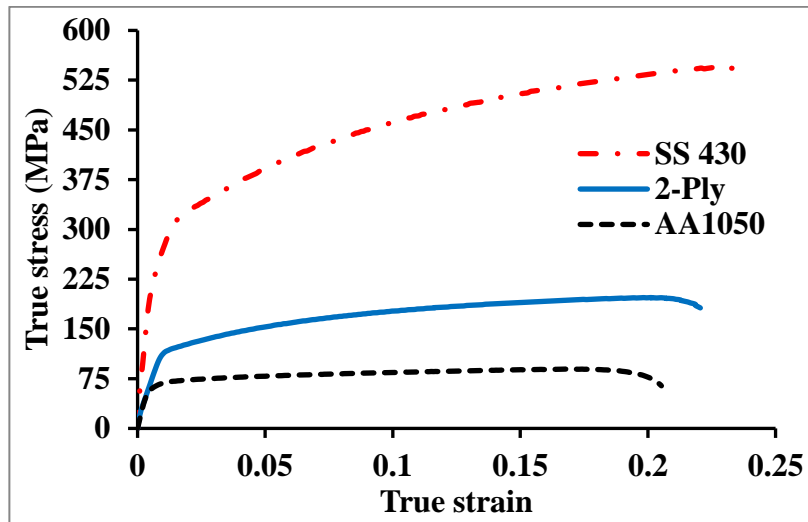


Fig. 6.3 True stress-true strain plots of a 2-ply clad, SS430 and AA1050 sheet samples

### 6.3.2 Tensile properties of 3-ply sheet

The tensile properties of a three-ply sheet tested in uniaxial tension along rolling, transverse, and inclined directions with respect to the rolling direction are summarised in Table 6.6. The yield strength, tensile strength, and strain hardening exponent of the specimens oriented at transverse to the rolling direction are higher than the specimens of the other two orientations w.r.t. the rolling direction. This representative strength of the clad sheet can be attributed to the strength of the individual sheets in a particular direction.

Table 6.6. Tensile properties of a 3-ply clad sheet

| Specimen's orientation w.r.t. RD | Tensile Strength (MPa) | 0.2% Yield Strength (MPa) | % Elongation | Strength coefficient (MPa) K | Strain hardening exponent n | Plastic strain ratio R |
|----------------------------------|------------------------|---------------------------|--------------|------------------------------|-----------------------------|------------------------|
| 0°                               | 219.5±2.12             | 153.5±0.71                | 49.50±4.80   | 400.0±2.83                   | 0.255                       | 0.64                   |
| 45°                              | 228.0±1.41             | 174.0±1.00                | 48.85±1.48   | 398.5±20.5                   | 0.232                       | 0.89                   |
| 90°                              | 237.5±2.12             | 176.0±1.41                | 44.45±0.29   | 437.5±4.95                   | 0.266                       | 0.83                   |

The clad sheet shows higher stretchability in the transverse plane of the blank w.r.t. the rolling direction. The percentage elongation is observed to be highest in the specimens with an orientation of 0° w.r.t. the rolling direction followed by the specimens oriented at inclined and transverse direction w.r.t. the rolling. The normal anisotropy of the clad sheet is observed to be 0.81 indicating decreased formability when compared with that of individual stainless-steel

sheets. The tensile properties of the individual sheets dissociated from a three-ply clad sheet are compiled in Table 6.7. It is observed that the austenitic grade SS304 is the strongest layer in terms of tensile and yield strengths and strain hardening exponent in any direction when compared with that of SS430 and AA1050 layers. The percentage elongation and normal anisotropy of SS304 is the highest which indicates its ability to sustain severe deformation in deep drawing. This layer of steel also shows the highest values of strain hardening exponent in all the directions which indicates excellent uniform elongation before fracture. This SS304 layer does not undergo necking phenomenon and breaks abruptly after specimen experiences maximum force and percentage elongation. It is also observed that the steel layer SS430 possesses appreciable strength and ductility but less than those of the layer SS304 and does not also work harden as much as SS304. Therefore, this steel layer undergoes necking phenomenon and gives clear indication before failure unlike SS304.

Table 6.7. Tensile properties of individual layers

| Specimen's orientation w.r.t. RD | Tensile Strength (MPa) | 0.2% Yield Strength (MPa) | % Elongation | Strain hardening exponent. n | Strength coefficient (MPa), K | R    |
|----------------------------------|------------------------|---------------------------|--------------|------------------------------|-------------------------------|------|
| <b>SS430 layer</b>               |                        |                           |              |                              |                               |      |
| 0°                               | 410                    | 269                       | 31.51        | 0.24                         | 749                           | 0.88 |
| 45°                              | 437                    | 252                       | 27.00        | 0.23                         | 786                           | 0.71 |
| 90°                              | 445                    | 330                       | 28.80        | 0.22                         | 782                           | 0.98 |
| <b>AA1050 layer</b>              |                        |                           |              |                              |                               |      |
| 0°                               | 68                     | 59                        | 21.81        | 0.11                         | 94.8                          | 0.89 |
| 45°                              | 77                     | 64                        | 22.90        | 0.09                         | 103.6                         | 0.49 |
| 90°                              | 62                     | 57                        | 19.50        | 0.10                         | 77.7                          | 0.64 |
| <b>SS304 layer</b>               |                        |                           |              |                              |                               |      |
| 0°                               | 636                    | 289                       | 78.1         | 0.40                         | 1556                          | 0.73 |
| 45°                              | 649                    | 316                       | 75.6         | 0.37                         | 1575                          | 1.41 |
| 90°                              | 690                    | 320                       | 65.0         | 0.36                         | 1666                          | 0.97 |

The strength of the layer AA1050 dissociated from the three-ply sheet is the lowest with poor work hardening exponent and anisotropy when compared with other materials, although this layer has appreciable amount of percentage elongation. In order to have a better visual



assessment of the tensile properties, the true stress-true strain plot for the three-ply sheet is compared with that of the individual layers as shown in Fig. 6.4.

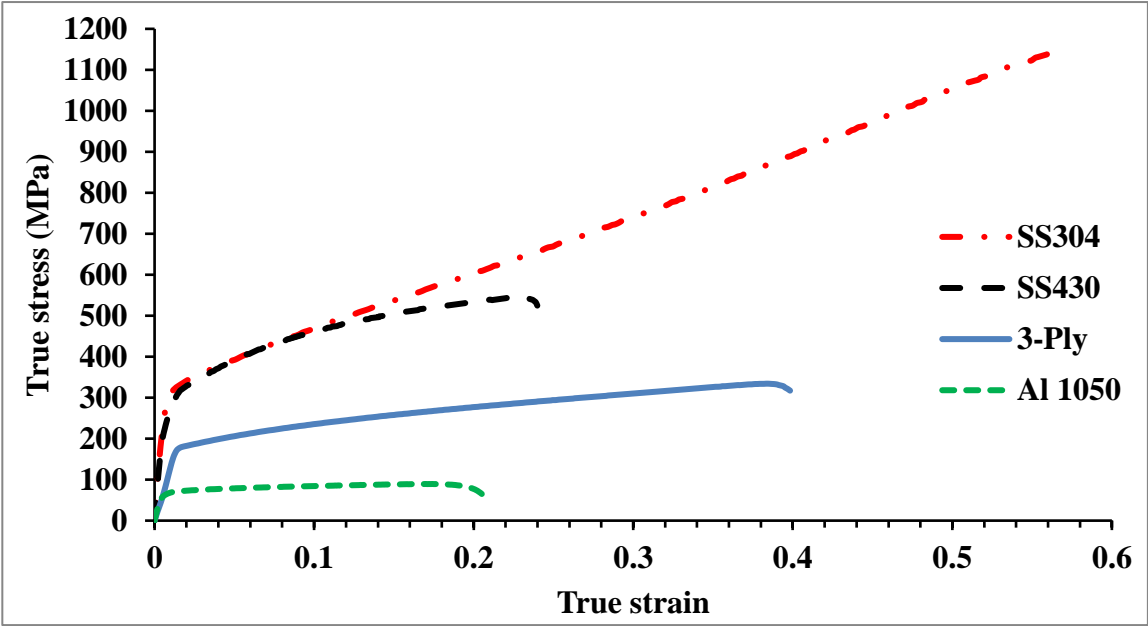


Fig. 6.4 True stress-true strain plots of three-ply clad sheet and individual layers

**6.4 Microhardness**

**6.4.1 Microhardness of 2-ply clad sheet**

The average microhardness of SS430 and AA1050 are 173.50 HV & 32.91 HV respectively. AA1050 layer is very soft as compared to SS430 layer. The average hardness of 2-ply clad sheet is evaluated as 84.03 HV (Table 6.8).

Table 6.8 Microhardness of individual layers of the 2-ply clad sheet

| S.No. | Material | Hardness (HV) | Mean Hardness (HV) |
|-------|----------|---------------|--------------------|
| 1     | AA1050   | 36.54         | 32.91              |
| 2     |          | 34.41         |                    |
| 3     |          | 32.41         |                    |
| 4     |          | 31.50         |                    |
| 5     |          | 31.01         |                    |
| 6     |          | 31.30         |                    |
| 7     |          | 33.19         |                    |
| 8     | SS430    | 173.22        | 173.5              |
| 9     |          | 172.70        |                    |
| 10    |          | 176.95        |                    |
| 11    |          | 171.14        |                    |

### 6.4.2 Microhardness of 3-ply clad sheet

The average microhardness of SS430 and AA1050 are 173.5 HV & 32.91 HV respectively as shown in Table 6.9. The average microhardness of SS304 is 220.05 HV which is more than the hardness of SS430 and AA1050. The average hardness of 3-ply clad sheet is evaluated as 113.18 HV. AA1050 layer is softest among all the layers of 3-ply clad sheet.

The size of the impression of hardness tester is largest and smallest on AA1050 layer and SS304 respectively. It indicates that AA1050 is the softest and SS304 is hardest material in the 3-ply clad sheet. The hardness of SS430 layer lies in between AA1050 and SS304 layers. As per Fig. 6.5, the impression of hardness tester in SS430 & SS304 is fine, sharp and small as compared to AA1050.

Table 6.9 Microhardness of individual layers of the 3-ply clad sheet

| S.No. | Material | Hardness (HV) | Mean Hardness (HV) |
|-------|----------|---------------|--------------------|
| 1     | SS304    | 228.90        | 220.05             |
| 2     |          | 218.91        |                    |
| 3     |          | 212.35        |                    |
| 4     | AA1050   | 36.54         | 32.91              |
| 5     |          | 34.41         |                    |
| 6     |          | 32.41         |                    |
| 7     |          | 31.50         |                    |
| 8     |          | 31.01         |                    |
| 9     |          | 31.30         |                    |
| 10    |          | 33.19         |                    |
| 11    | SS430    | 173.22        | 173.5              |
| 12    |          | 172.70        |                    |
| 13    |          | 176.95        |                    |
| 14    |          | 171.14        |                    |

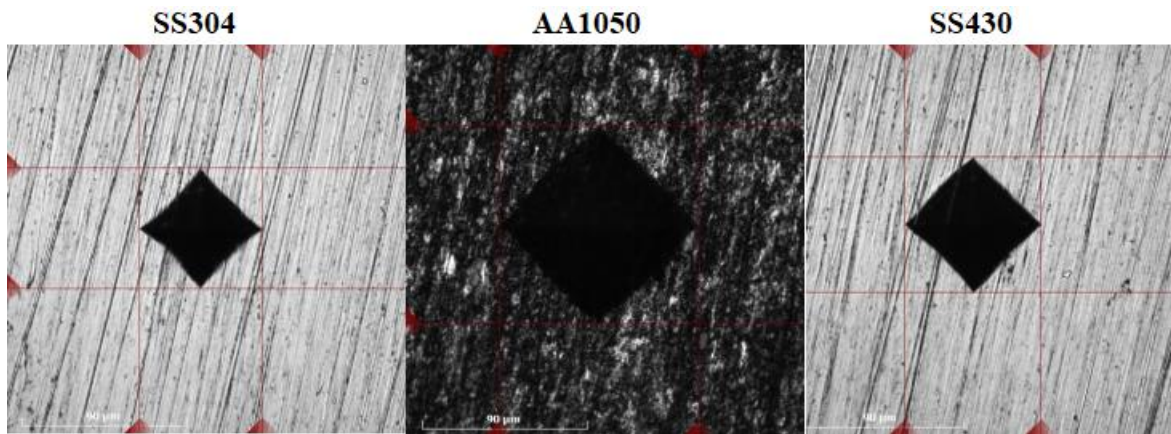


Fig.6.5 Impressions of hardness tester (DURAMIN-40 M1) in SS430/AA1050/SS304 clad sheet

## 6.5 Springback characteristics

### 6.5.1 Springback analysis of 2-ply clad sheet

The springback results after the bending of individual layers of 2-ply clad sheet obtained by experiments, numerical simulations and existing analytical model are given in Table 6.10. Highest springback values are observed in SS430 which could be attributed to its higher strength and smaller sheet thickness. The springback results of AA1050 are also given in Table 6.10. It is observed that the springback values are less than half the values of springback in SS430 which could be attributed to its lower strength and higher sheet thickness. Similar results are predicted by FE simulations and analytical results. Also, the results predicted by FE simulations are closer to the experimental results.

Table 6.10 Springback results of SS430 and AA1050 for punch radius 15 mm

| Individual sheet | Specimen orientation w.r.t. RD (in degree) | Experimental |                | Simulation  |         | Analytical  |         |
|------------------|--|--------------|----------------|-------------|---------|-------------|---------|
|                  |  | (in degree)  | Std. deviation | (in degree) | % error | (in degree) | % error |
| SS430            | 0  | 10.24        | ±0.51          | 10.49       | 2.44    | 11.18       | 9.18    |
|                  | 45   | 11.33        | ±0.59          | 10.60       | 6.44    | 12.24       | 8.03    |
|                  | 90   | 11.42        | ±0.33          | 10.71       | 6.22    | 12.71       | 11.3    |
| AA1050           | 0  | 4.35         | ±0.23          | 4.32        | 0.69    | 3.60        | 17.24   |
|                  | 45   | 4.70         | ±0.13          | 4.50        | 4.26    | 4.21        | 10.43   |
|                  | 90   | 3.99         | ±0.21          | 4.06        | 1.75    | 3.05        | 23.56   |

To determine the simulation results, the coordinate details of the various nodes are captured individually from the loaded and unloaded frames for springback measurement as depicted in Table 6.11. The final value of springback can be determined by computing the difference between the two carefully recorded coordinates of both the frames in a CAE interface as shown in Fig. 6.6.

Table 6.11 Captured coordinates from loaded and unloaded frames of AA1050 blank oriented at 0° w.r.t. R.D. for 15 mm punch radius

| Node ID | Loaded frame (Node history) |               |               | Unloaded frame (Springback) |               |               |
|---------|-----------------------------|---------------|---------------|-----------------------------|---------------|---------------|
|         | X-coordinates               | Y-coordinates | Z-coordinates | X-coordinates               | Y-coordinates | Z-coordinates |
| 1209    | -55.56                      | 10.56         | 0             | -58.30                      | 7.59          | 0             |
| 1213    | -52.74                      | 7.72          | 0             | -55.29                      | 4.95          | 0             |
| 1218    | -49.20                      | 4.21          | 0             | -51.52                      | 1.69          | 0             |
| 1224    | -44.96                      | -38.15E-03    | 0             | -46.99                      | -2.24         | 0             |
| 1230    | -40.72                      | -4.27         | 0             | -42.46                      | -6.17         | 0             |
| 1236    | -36.48                      | -8.52         | 0             | -37.93                      | -10.10        | 0             |
| 1242    | -32.23                      | -12.75        | 0             | -33.39                      | -14.04        | 0             |
| 1248    | -27.97                      | -16.98        | 0             | -28.86                      | -17.97        | 0             |
| 1254    | -23.69                      | -21.18        | 0             | -24.33                      | -21.91        | 0             |
| 1260    | -19.38                      | -25.35        | 0             | -19.80                      | -25.85        | 0             |
| 1266    | -15.03                      | -29.46        | 0             | -15.26                      | -29.76        | 0             |
| 1272    | -10.58                      | -33.45        | 0             | -10.67                      | -33.60        | 0             |
| 1278    | -5.60                       | -36.37        | 0             | -5.62                       | -36.42        | 0             |
| 1282    | -1.92                       | -37.35        | 0             | -1.92                       | -37.35        | 0             |
| 1284    | -13.72E-03                  | -37.46        | 0             | -17.14E-03                  | -37.45        | 0             |
| 1286    | 1.89                        | -37.35        | 0             | 1.89                        | -37.35        | 0             |
| 1290    | 5.57                        | -36.37        | 0             | 5.58                        | -36.40        | 0             |
| 1296    | 10.53                       | -33.43        | 0             | 10.60                       | -33.53        | 0             |
| 1302    | 14.99                       | -29.45        | 0             | 15.18                       | -29.67        | 0             |
| 1308    | 19.34                       | -25.35        | 0             | 19.70                       | -25.75        | 0             |
| 1314    | 23.66                       | -21.18        | 0             | 24.22                       | -21.80        | 0             |
| 1320    | 27.94                       | -16.99        | 0             | 28.74                       | -17.85        | 0             |
| 1326    | 32.21                       | -12.77        | 0             | 33.26                       | -13.90        | 0             |
| 1332    | 36.46                       | -8.54         | 0             | 37.78                       | -9.95         | 0             |
| 1338    | 40.71                       | -4.29         | 0             | 42.30                       | -5.99         | 0             |
| 1344    | 44.94                       | -61.71E-03    | 0             | 46.80                       | -2.06         | 0             |
| 1350    | 49.19                       | 4.18          | 0             | 51.33                       | 1.89          | 0             |
| 1356    | 53.45                       | 8.43          | 0             | 55.86                       | 5.85          | 0             |
| 1359    | 55.54                       | 10.55         | 0             | 58.08                       | 7.83          | 0             |

For blank of AA1050 sheet which is oriented at 0° to the rolling direction and the punch radius is 15 mm, the simulated springback is measured as follows: -

$$\begin{aligned} \text{Springback} &= \frac{1}{2} (\text{Included bend angle after springback} - \text{Included bend angle before springback}) \\ &= \frac{1}{2} (98.68^\circ - 90.04^\circ) \\ &= 4.32^\circ \text{ (depicted in Table 6.10)} \end{aligned}$$

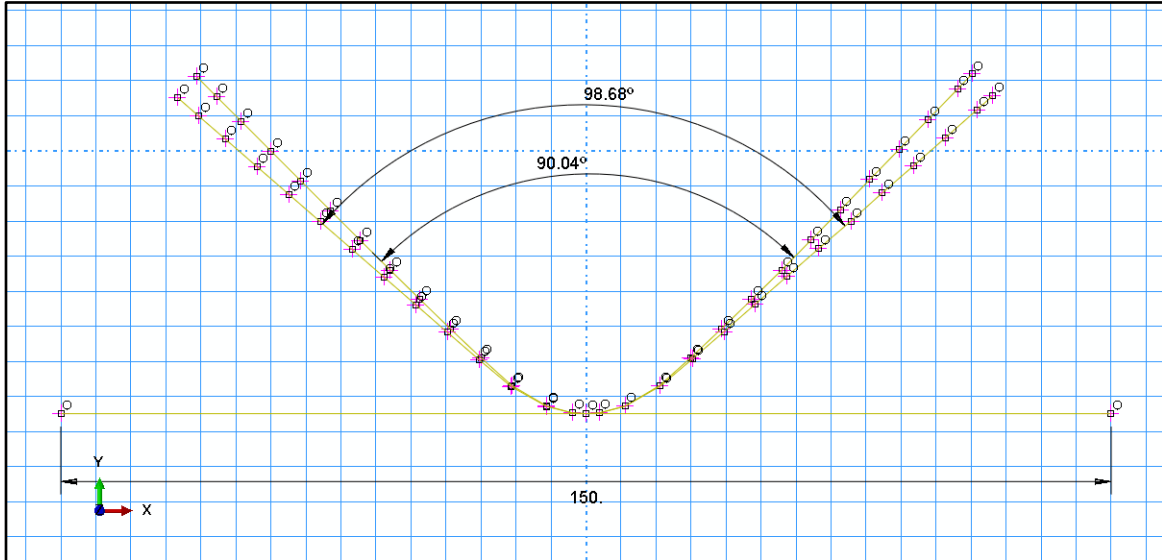


Fig. 6.6 Surfaces of blank of AA1050 (oriented 0° to R.D.) plotted using CAE interface before and after springback

To determine the analytical results of monolithic sheets SS430, SS304 and AA1050 the Eq. (6.1) and Eq. (6.2) have been used to get the value of springback. (Gautam et al. 2017)

$$\frac{1}{r} - \frac{1}{r'} = \frac{\left[ \frac{2}{3} \cdot \frac{w}{r} \cdot E' \cdot z_e^3 + \frac{2 \cdot K' \cdot C_2^n \cdot w}{C_1 \cdot r^n \cdot (n+2)} \left[ \left( \frac{t}{2} \right)^{(n+2)} - z_e^{(n+2)} \right] \right]}{E' \left[ \frac{wt^2}{12} \right]} \quad (6.1)$$

To obtain springback, the final radius of curvature ( $r'$ ) after the springback is found by Eq. (6.1).

$$\text{Change in the bend angle, } \alpha_i - \alpha_f = \left( 1 - \frac{r}{r'} \right) \alpha_i \quad (6.2)$$

where,  $\alpha_i$  and  $\alpha_f$  are initial and final bend angles. The included bend angle is 90° and is measured on the die and therefore, the initial bend angle ( $\alpha_i$ ) is 45°.

The springback results after the bending of samples of a 2-ply sheet obtained by experiments, analytical prediction, and FE simulations are given in Table 6.12. The specimens of 2-ply sheet oriented at 45° to the rolling direction tested with SS430 as inner layer experiences highest springback followed by the specimens oriented at 0° and 90° w.r.t. the rolling direction of the clad sheet which again may be attributed to the tensile strength of the sheet and the combined effects of anisotropy of both the layers at the zone of deformation. The springback results of the tested samples of a 2-ply sheet at different orientations w.r.t. the rolling direction are slightly lower than the springback results of individual sheet samples of AA1050, suggesting that the higher thickness of the layer outweighs the effect of the higher tensile strength of the steel layer. Similar results are observed in the springback values predicted by simulation and analytical models in all the cases.

Also the specimens of the 2-ply sheet with an inner layer of AA1050, oriented at 45° to the rolling direction experience the highest springback followed by the specimens oriented at 0° and 90° w.r.t. the rolling direction as given in Table 6.12 and Fig.6.7.

Table 6.12 Comparison of predicted springback results with experimental in bending operation of a 2-ply sheet for punch radius 15 mm

| Inner layer during bending | Specimen orientation w.r.t. RD (in degree) | Experimental |                | Simulation  |         | Analytical  |         |
|----------------------------|--|--------------|----------------|-------------|---------|-------------|---------|
|                            |  | (in degree)  | Std. deviation | (in degree) | % error | (in degree) | % error |
| SS430                      | 0  | 3.71         | ±0.35          | 3.59        | 3.23    | 4.01        | 8.09    |
|                            | 45   | 3.87         | ±0.31          | 3.74        | 3.36    | 4.47        | 15.50   |
|                            | 90   | 3.69         | ±0.43          | 3.63        | 1.63    | 4.04        | 9.49    |
| AA1050                     | 0  | 3.91         | ±0.41          | 3.81        | 2.56    | 4.12        | 5.37    |
|                            | 45   | 4.12         | ±0.54          | 3.87        | 6.07    | 4.59        | 11.41   |
|                            | 90   | 3.77         | ±0.20          | 3.65        | 3.18    | 4.15        | 10.08   |

Also, similar results are observed in the springback values predicted by simulation and analytical models, although simulation results are closer to the experimental values in all the cases.

In all the cases of springback experiments of specimens of 2-ply with an inner layer of SS430, the springback values are lower than the values obtained with the specimens when the

inner layer is of AA1050. This could be because of the higher tensile strength of SS layer and the effect of higher bending radius experienced by SS layer.

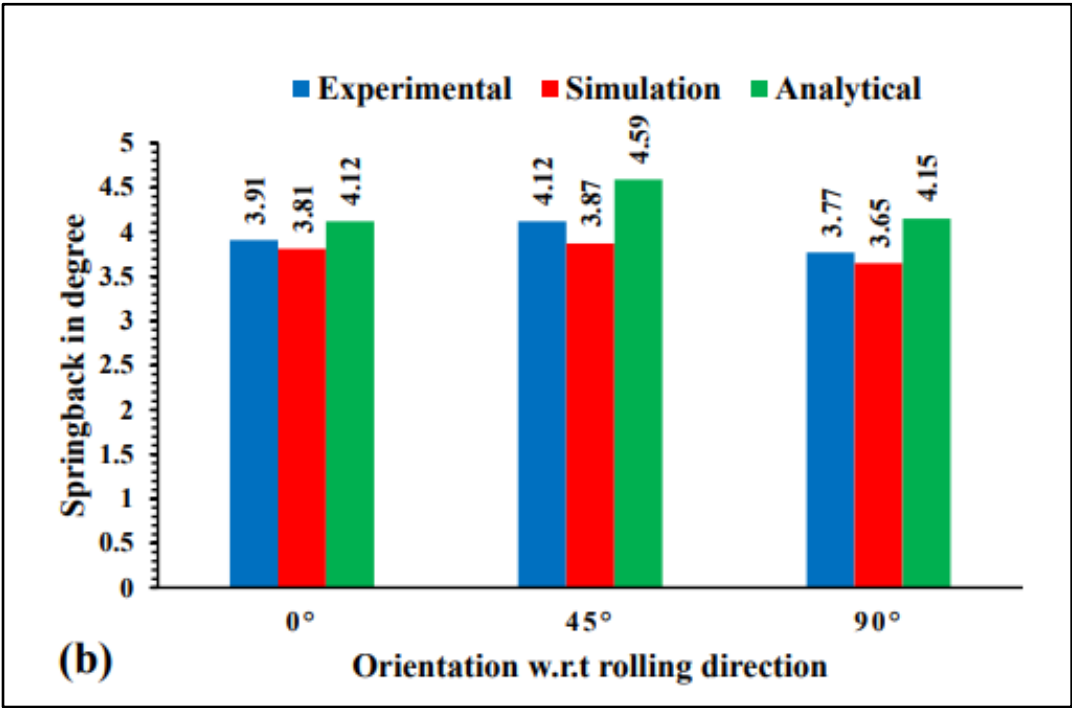
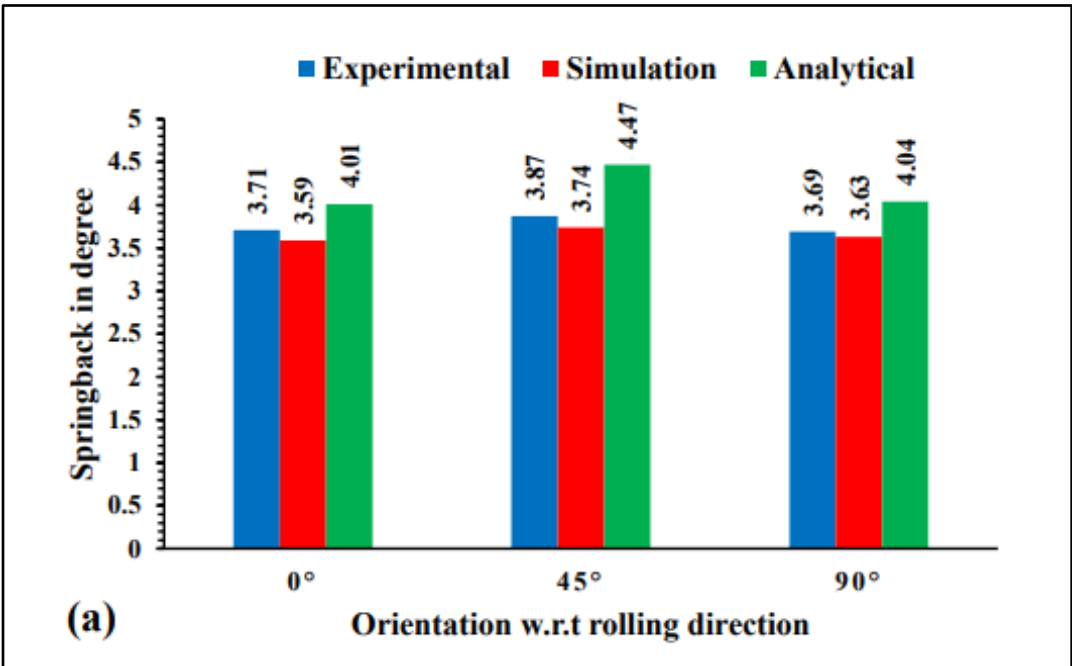


Fig. 6.7 Comparison of predicted springback results with experimental in bending operation of a 2-ply sheet for punch radius 15 mm (a) inner layer SS430 (b) inner layer AA1050

This clearly indicates that the sheet placement affects the springback in the bending operation of a 2-ply sheet. The springback results obtained by the analytical model and simulations are in good agreement with the results obtained by the experiments.

In the analytical model, friction at the interface of punch-blank and die-blank is neglected during bending whereas the friction is considered in simulations. The shift in neutral axis has also not been considered in analytical model and it introduces an error in the calculated bending moment. Moreover, the material model for FEA is more robust as it uses complete plastic stress and strain data whereas the analytical model is based on the single input values of elastic and plastic properties. Therefore, the results predicted by simulations are closer to the experimental results.

#### *Changes in thickness after springback*

From the experimental data it has been observed that the setting condition has a great impact on the shape of the clad sheet. It means that different positions of the weak (AA1050) and strong (SS430) layers of the composite sheet produce different shapes during bending. Sheet thickness changes occur differently during the bending of AA\_in/SS\_out and AA\_out/SS\_in. In all the orientations of sheet for both the sheet-set conditions, the thickness of the sheet is measured with the help of a stereo microscope. To get a sample for thickness measurement, bent clad sheet is cut centrally. After getting sample from the central part of the bent clad sheet, it is mounted in mounting compound followed by dry polishing, wet polishing and etching.

As shown in Fig.6.8 (a), (b) & (c) and Table 6.13, for AA\_in /SS\_out (specimen oriented at 45° to R.D) the sheet thickness increases from 2 mm to 2.23 mm, in contrast, for AA\_out/SS\_in (specimen oriented at 45° to R.D) it decreases from 2 mm to 1.92 mm during bending.

This observation can be explained as follows. Basically, when we observed the bending of AA\_out/SS\_in, then the tensile stress developed in the thick layer of AA1050. Due to this tensile stress, thickness of AA1050 decreases and so, the overall thickness of composite sheet is decreased as shown in Fig. 6.9.



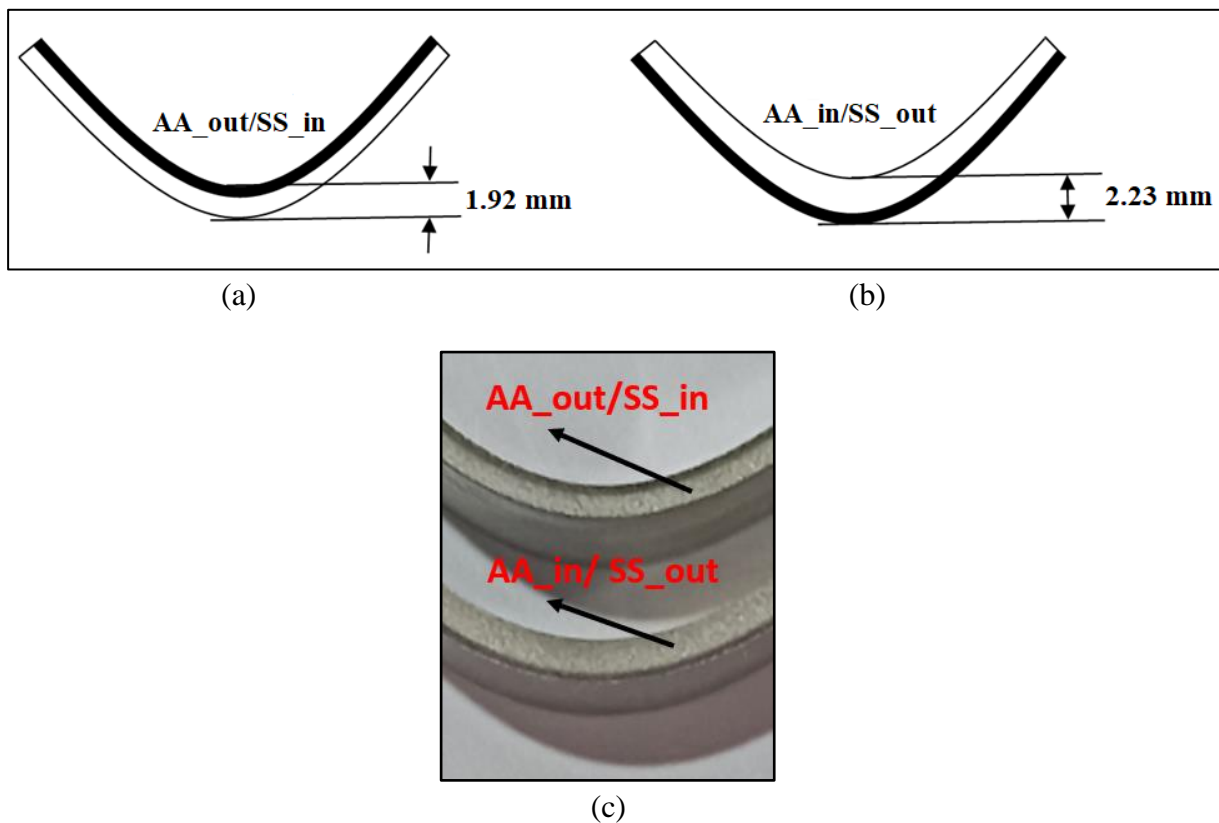


Fig. 6.8 Central part of laminated sheets during V-bending for 45-degree orientation: (a) AA\_out/SS\_in and (b) AA\_in/SS\_out (c) actual image of AA\_out/SS\_in and AA\_in/SS\_out

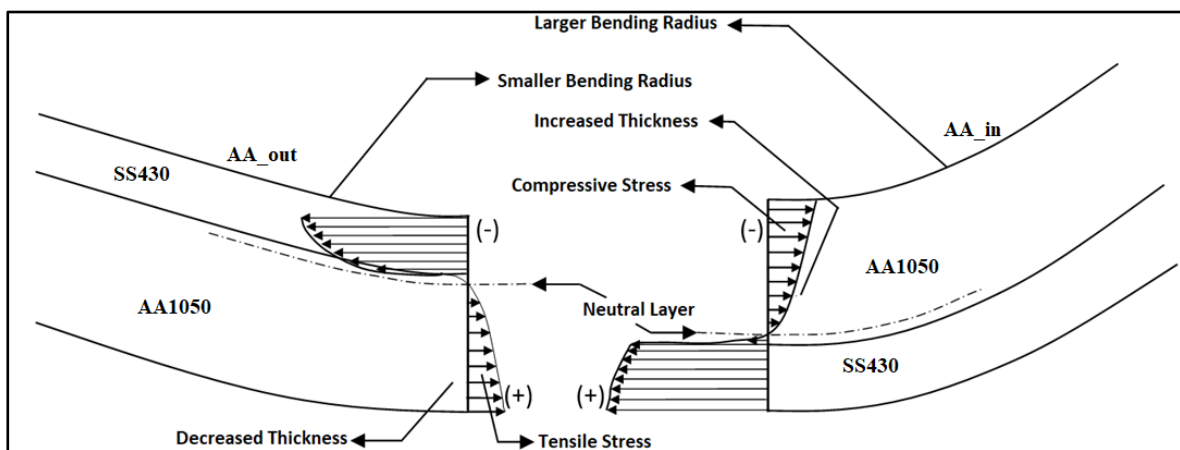


Fig.6.9 Stress distribution in 2-ply sample with varying thickness and bending radius

In contrast during bending of AA\_in/SS\_out, the compressive stress developed in the thick layer of AA1050. Due to this compressive stress, thickness of AA1050 increases and so the overall thickness of composite sheet is increased. Punch load depends on the change in thickness quite significantly. Increased sheet thickness requires increased bending moment so

larger punch load is needed for bending. In the same manner for decreasing thickness smaller punch load is needed.

Table 6.13. Thickness and max punch load for V-bent laminated sheet when punch having 15 mm radius:

| SNo. | Sheet Set-Condition | Orientation w.r.t. Rolling Direction | Thickness before Bending | Thickness after Bending | Maximum Punch load (Newton) |
|------|---------------------|--------------------------------------|--------------------------|-------------------------|-----------------------------|
| 1    | AA_out/SS_in        | 0°                                   | 2 mm                     | 1.95 mm                 | 126.58                      |
| 2    | AA_out/SS_in        | 45°                                  | 2 mm                     | 1.92 mm                 | 123.33                      |
| 3    | AA_out/SS_in        | 90°                                  | 2 mm                     | 1.95 mm                 | 127.02                      |
| 4    | AA_in/SS_out        | 0°                                   | 2 mm                     | 2.20 mm                 | 146.67                      |
| 5    | AA_in/SS_out        | 45°                                  | 2 mm                     | 2.23 mm                 | 148.33                      |
| 6    | AA_in/SS_out        | 90°                                  | 2 mm                     | 2.21 mm                 | 166.67                      |

One more observation has been found that the radius of curvature is small for bending of AA\_out/SS\_in, as compared to AA\_in/SS\_out. Due to this, sharp bending is seen in bending of AA\_out/SS\_in. Experimentally it has been observed that a higher punch load is required in the case of AA\_in/SS\_out as compared to the AA\_out/SS\_in. Highest punch load (166.67 N) is required in the case of AA\_in/SS\_out when the specimen is oriented at 90° to the R.D. This could be attributed to the higher tensile properties of SS430 layer and less thickness coupled with the effect of higher bending radius experienced by SS430 layer.

### 6.5.2 Springback analysis of 3-ply clad sheet

The springback results for bending of individual layers dissociated from a three-ply clad sheet, acquired from experimental technique are shown in Fig. 6.10. The springback values of the layer of SS304 are higher in the specimens-oriented transverse to the rolling direction than that of the values experienced by specimens with an orientation along rolling and inclined direction w.r.t. the rolling direction. The lowest springback is observed in the specimens oriented along the rolling direction. These values of springback may be attributed to the tensile strength of the layer of SS304. The springback values for the layer of SS430 are lower than that of SS304 in

all the specimens due to its lower strength and higher layer thickness. Springback values also show a similar trend for the specimens of different orientations w.r.t. the rolling direction i.e., the higher the tensile strength, the higher is the springback. The strength and thickness of the steel layer plays a key role in the springback values obtained from the experiments. The layer of AA1050, being the softest material in the clad combination, experiences the lowest springback when compared with the values of SS430 and SS304 layers for all the cases.

Table 6.14 and Fig. 6.12 summarises the values of springback of specimens of three-ply clad sheet oriented in three different directions acquired after bending using analytical approach, numerical simulation, and experiments.

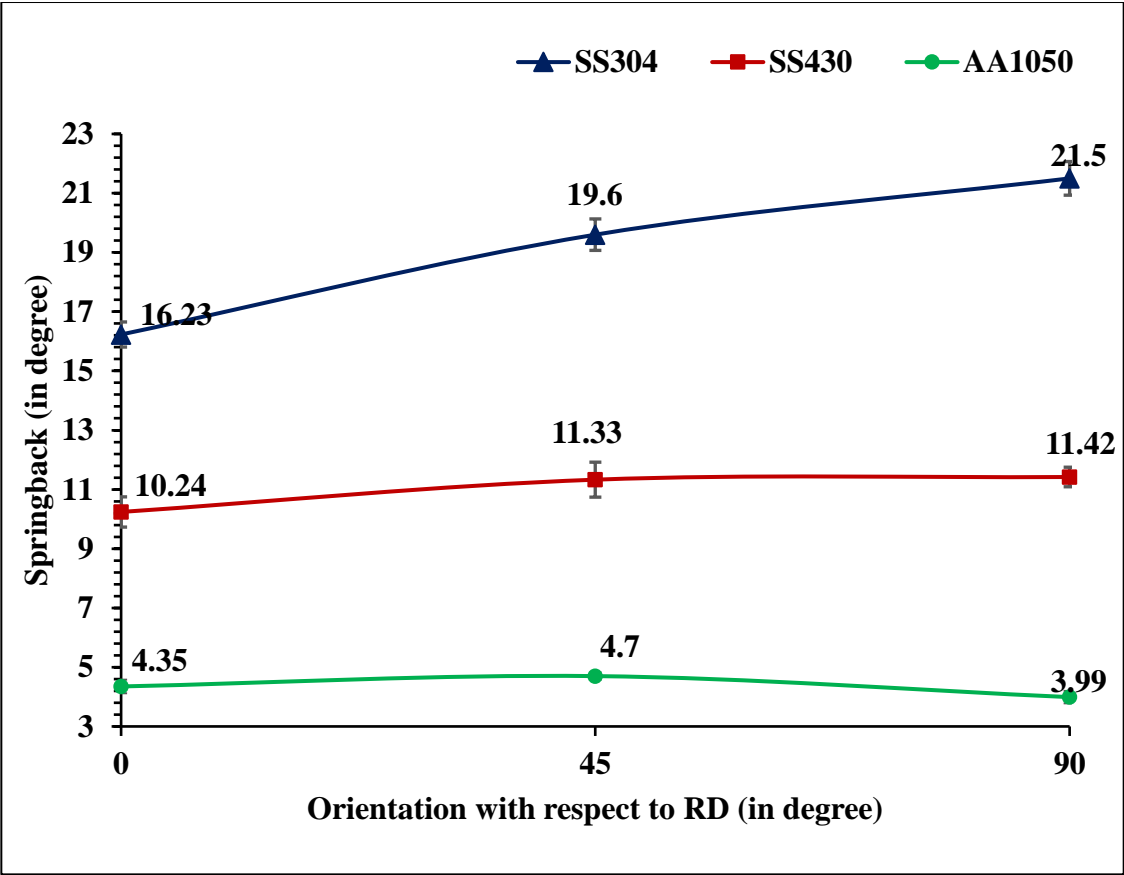


Fig. 6.10 Comparison of experimental values of springback of individual layers for punch radius 15 mm

The samples of the clad sheet which are transverse to the rolling direction, exhibit highest springback values due to the higher tensile strength of the sheet as compared with the results obtained for the other two orientations w.r.t. the rolling direction.

In this case also, strength of the sheet plays a key role in the springback results. These results are close to the springback results obtained from the analytical and simulation models in all the cases.

Table 6.14 also summarises the effect of sheet placement on the springback after bending of a three-ply clad sheet. On comparing the springback results with reference to the specimen's orientations in both the cases of sheet placement, it is observed that the springback values of the clad sheet specimens placed with inner layer of SS304 facing the punch during bending experience slightly higher springback when compared with the values of springback in specimens with inner layer SS430. A small difference between the values of springback can be attributed to the lower thickness and higher strength of layer of SS304 when compared with that of SS430. Also, in the specimens of clad sheet with inner layer of SS304, experience a higher bending radius as shown in Fig.6.11. Hence, the sheet placement plays an important role in the springback phenomenon after bending of a three-ply clad sheet.

The springback results obtained after bending of a three-ply clad sheet by using experimental, analytical and simulations techniques are in good agreement in all the cases of sheet placement, although simulation results are seen to be closer to the experimental results as compared with the analytical results. The nearness of FE simulation results to the experimental results than the analytical results can be attributed to the assumptions in the analytical model i.e. neglecting Bauschinger effect, shift in neutral axis and friction at contact surfaces. Furthermore, the material model used in simulations is more powerful as it is based on complete stress and strain data obtained from tensile experiments whereas analytical model lacks in material data as it is dependent on single values of elastic and plastic properties.

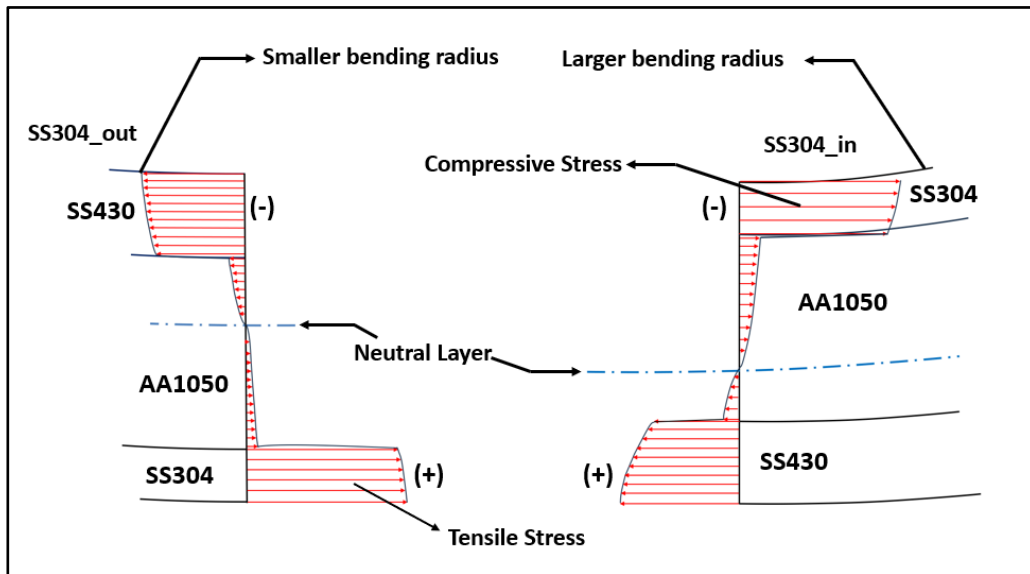
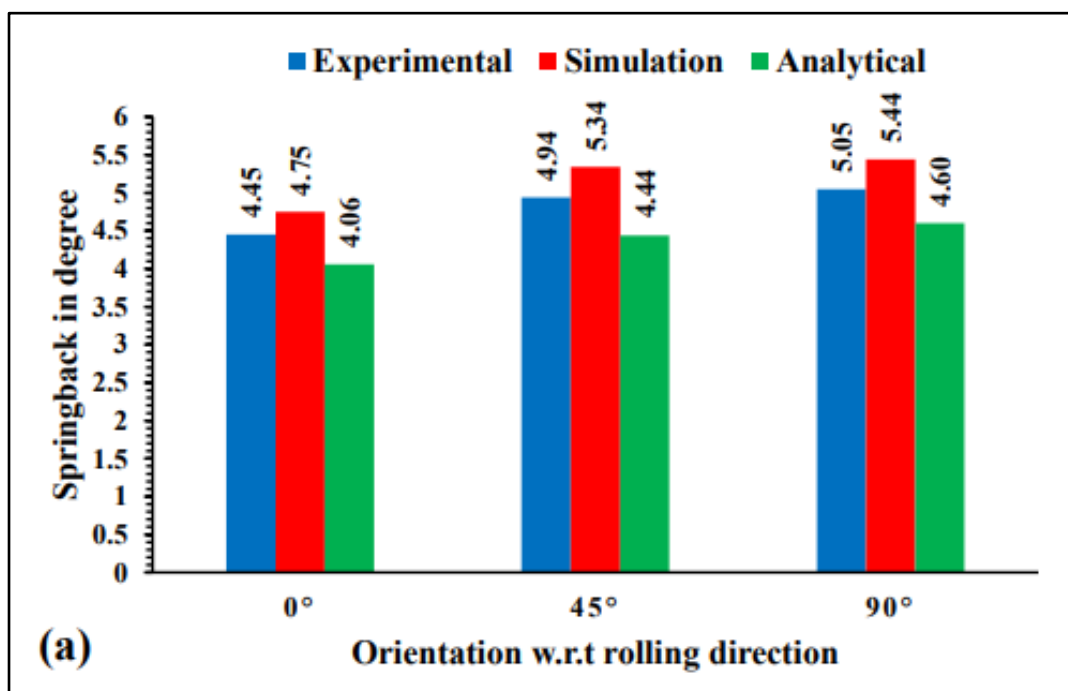


Fig.6.11 Stress distribution in 3-ply sample with varying bending radius

Table 6.14 Springback results of a 3-ply clad sheet for punch radius 15 mm

| Inner layer during bending | Specimen orientation w.r.t. RD (in degree) | Experimental |                | Simulation  |         | Analytical  |         |
|----------------------------|--|--------------|----------------|-------------|---------|-------------|---------|
|                            |  | (in degree)  | Std. deviation | (in degree) | % error | (in degree) | % error |
| SS430                      | 0  | 4.45         | ±0.12          | 4.75        | 6.74    | 4.06        | 8.68    |
|                            | 45   | 4.94         | ±0.18          | 5.34        | 8.19    | 4.44        | 10.02   |
|                            | 90   | 5.05         | ±0.23          | 5.44        | 7.82    | 4.60        | 8.86    |
| SS304                      | 0  | 4.51         | ±0.22          | 4.67        | 3.66    | 4.08        | 9.43    |
|                            | 45   | 5.01         | ±0.20          | 5.21        | 4.09    | 4.47        | 10.79   |
|                            | 90   | 5.15         | ±0.25          | 5.39        | 4.66    | 4.63        | 10.15   |



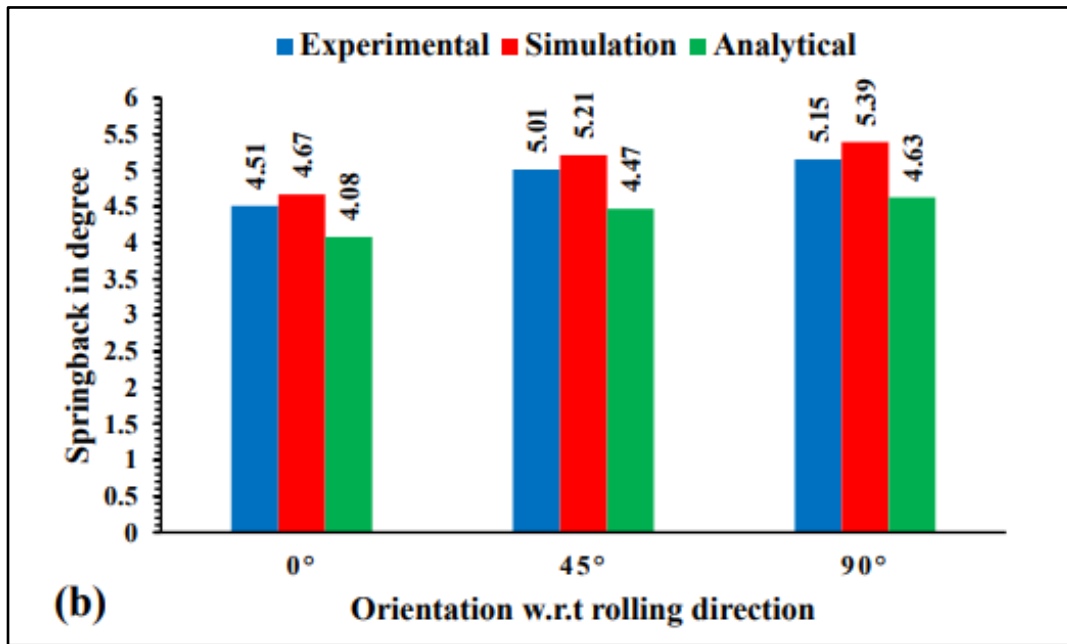


Fig. 6.12 Springback results of a 3-ply clad sheet for punch radius 15 mm (a) inner layer SS430 and (b) inner layer SS304

### 6.5.3 Springback analysis for varying punch radius

The values of springback w.r.t varying punch profile radius (PPR), after the bending of 2-ply clad sheet (AA1050/SS430) obtained by experiments and numerical simulations are given in Table 6.15. When punch corner radius is increased from 15 mm to 17.5 mm and 17.5 mm to 20 mm then values of springback also increased significantly in all the cases. It is observed that the higher punch corner radius is responsible for higher springback value. The experimental results show that the punch radii have significant effect on springback behaviour of the laminated sheet. The springback results obtained by simulations are seen to be in good agreement with the results obtained by experiments.

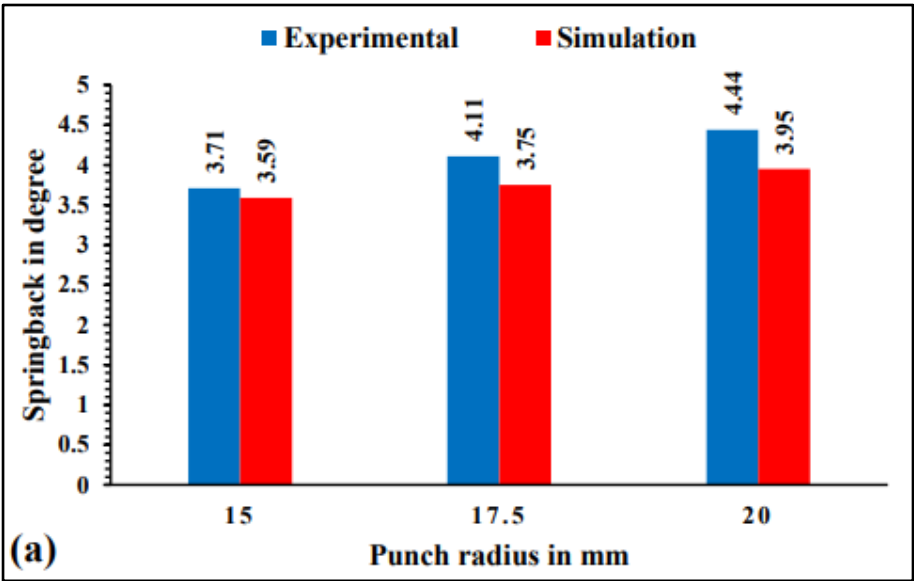
For all the punch corner radii (15 mm, 17.5 mm, and 20 mm) the specimens of 2-ply clad sheet labelled as AA\_out/SS\_in (i.e., SS430 facing the punch) and AA\_in/SS\_out (i.e., AA1050 facing the punch) oriented at 45° to the rolling direction indicate highest springback than the specimens which are oriented at 90° and 0° w.r.t. the rolling direction. Highest springback obtained is 4.58° and 4.88° in the case of AA\_out/SS\_in and AA\_in/SS\_out respectively for the specimens which are oriented at 45° to rolling direction as shown in Fig.

6.13 and Fig.6.14. Also, similar results are observed in the springback values predicted by FE simulation.

In all the cases of springback experiments of specimens of 2-ply clad sheets labelled as AA\_out/SS\_in, the springback values are lower than the values obtained with the specimens labelled as AA\_in/SS\_out. This is due to higher tensile properties of SS430 layer and higher bending radius experienced by SS430 layer. It is observed that the sheet setting conditions play a key role during bending of a 2-ply laminated sheets for all the punch corner radii.

Table 6.15 Experimental and simulated springback results of a 2-ply clad sheet for varying punch radius

| Inner layer during bending |     | Punch radius 15 mm |            |         | Punch radius 17.5 mm |            |         | Punch radius 20 mm |            |         |
|----------------------------|-----|--------------------|------------|---------|----------------------|------------|---------|--------------------|------------|---------|
|                            |     | Exp.               | Simulation | % error | Exp.                 | Simulation | % error | Exp.               | Simulation | % error |
|                            |     | (in degree)        |            |         | (in degree)          |            |         | (in degree)        |            |         |
| SS430                      | 0°  | 3.71               | 3.59       | 3.23    | 4.11                 | 3.75       | 8.76    | 4.44               | 3.95       | 11.04   |
|                            | 45° | 3.87               | 3.74       | 3.36    | 4.44                 | 3.92       | 11.71   | 4.58               | 4.15       | 9.39    |
|                            | 90° | 3.69               | 3.63       | 1.63    | 4.15                 | 3.81       | 8.19    | 4.49               | 4.05       | 9.80    |
|                            |     | Punch radius 15 mm |            |         | Punch radius 17.5 mm |            |         | Punch radius 20 mm |            |         |
| AA1050                     | 0°  | 3.91               | 3.81       | 2.56    | 4.28                 | 3.99       | 6.78    | 4.56               | 4.17       | 8.55    |
|                            | 45° | 4.12               | 3.87       | 6.07    | 4.54                 | 4.11       | 9.47    | 4.88               | 4.31       | 11.68   |
|                            | 90° | 3.77               | 3.65       | 3.18    | 4.33                 | 3.91       | 9.70    | 4.63               | 4.11       | 11.23   |



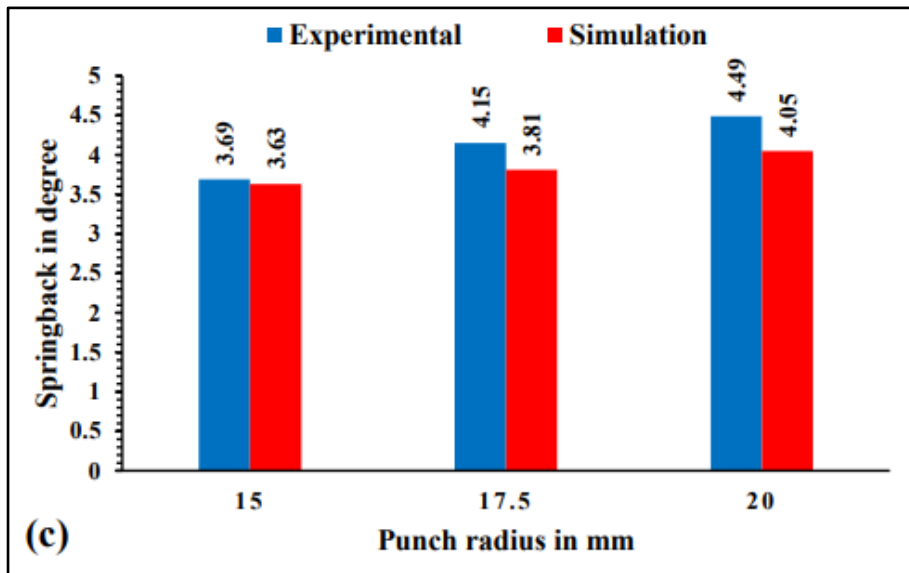
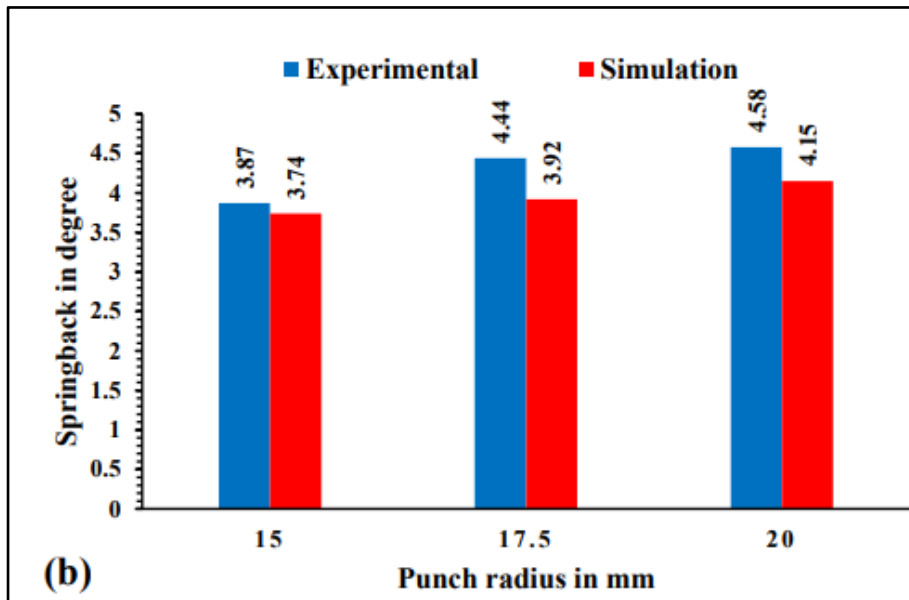
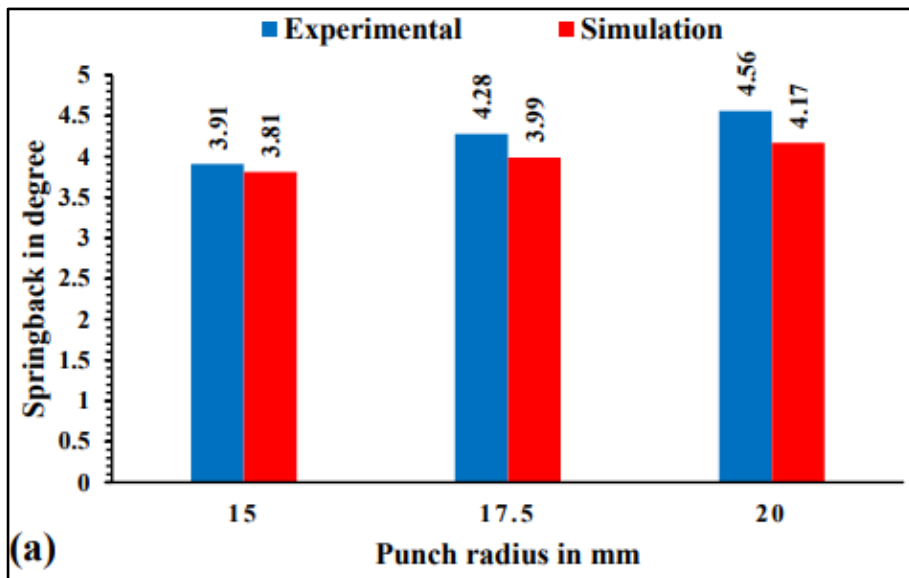


Fig. 6.13 Experimental and simulated springback results of a 2-ply clad sheets, oriented at (a) 0°, (b) 45° and (c) 90° for varying punch radius when SS430 taken as an inner layer





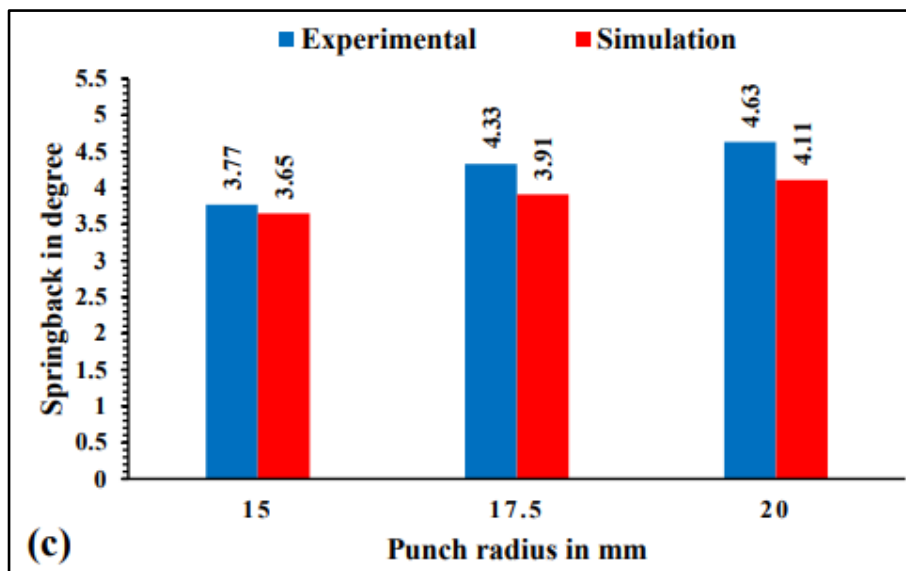
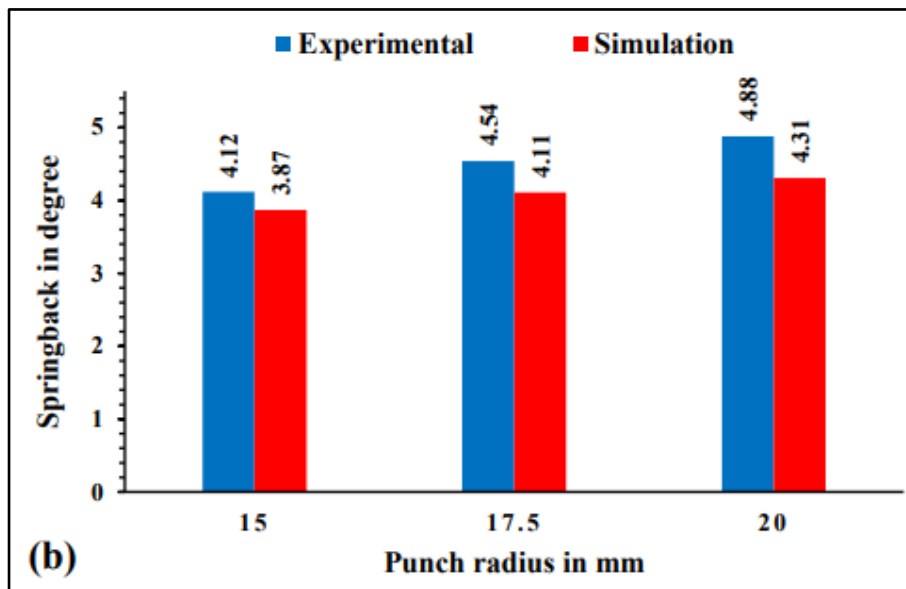


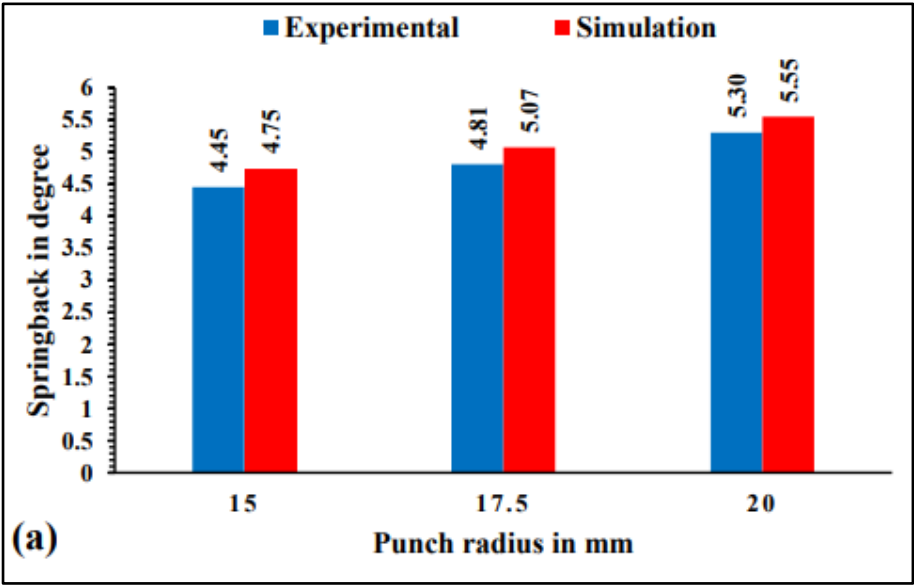
Fig.6.14 Experimental and simulated springback results of a 2-ply clad sheets, oriented at (a), 0°, (b) 45° and (c) 90° for varying punch radius when AA1050 taken as an inner layer

The springback results for various bending radii (punch profile radii) after the bending of 3-ply sheet by experiments, numerical simulations, and analytical model are given in Table 6.16 and Table 6.17. The specimens of 3-ply sheet oriented at 90° to the rolling direction tested with SS304 as inner layer experience highest springback followed by the specimens oriented at 0° and 45° with respect to the rolling direction of the clad sheet which again may be attributed to the tensile strength of the sheet and the combined effects of anisotropy of all the layers at the zone of deformation. Highest springback values are obtained for 20 mm punch profile radius

(PPR) whereas lowest springback values are obtained for 15 mm punch profile radius as shown in Fig. 6.15, Fig 6.16, Fig. 6.17, and Fig. 6.18.

Table 6.16 Numerical and Experimental springback results of a 3-ply sheet for varying bending radius

| Inner layer during bending |     | Punch radius 15 mm |            |         | Punch radius 17.5 mm |            |         | Punch radius 20 mm |            |         |
|----------------------------|-----|--------------------|------------|---------|----------------------|------------|---------|--------------------|------------|---------|
|                            |     | Exp.               | Simulation | % error | Exp.                 | Simulation | % error | Exp.               | Simulation | % error |
|                            |     | (in degree)        |            |         | (in degree)          |            |         | (in degree)        |            |         |
| SS430                      | 0°  | 4.45               | 4.75       | 6.74    | 4.81                 | 5.07       | 5.41    | 5.3                | 5.55       | 5.11    |
|                            | 45° | 4.94               | 5.34       | 8.10    | 5.32                 | 5.59       | 5.08    | 5.8                | 6.09       | 5.36    |
|                            | 90° | 5.05               | 5.44       | 7.72    | 5.48                 | 5.71       | 4.20    | 6                  | 6.32       | 4.98    |
|                            |     | Punch radius 15 mm |            |         | Punch radius 15 mm   |            |         | Punch radius 15 mm |            |         |
| SS304                      | 0°  | 4.51               | 4.67       | 3.55    | 4.89                 | 5.17       | 5.73    | 5.4                | 5.61       | 4.08    |
|                            | 45° | 5.01               | 5.21       | 3.99    | 5.41                 | 5.74       | 6.10    | 6                  | 6.19       | 3.86    |
|                            | 90° | 5.15               | 5.39       | 4.66    | 5.61                 | 5.84       | 4.10    | 6.1                | 6.45       | 5.56    |



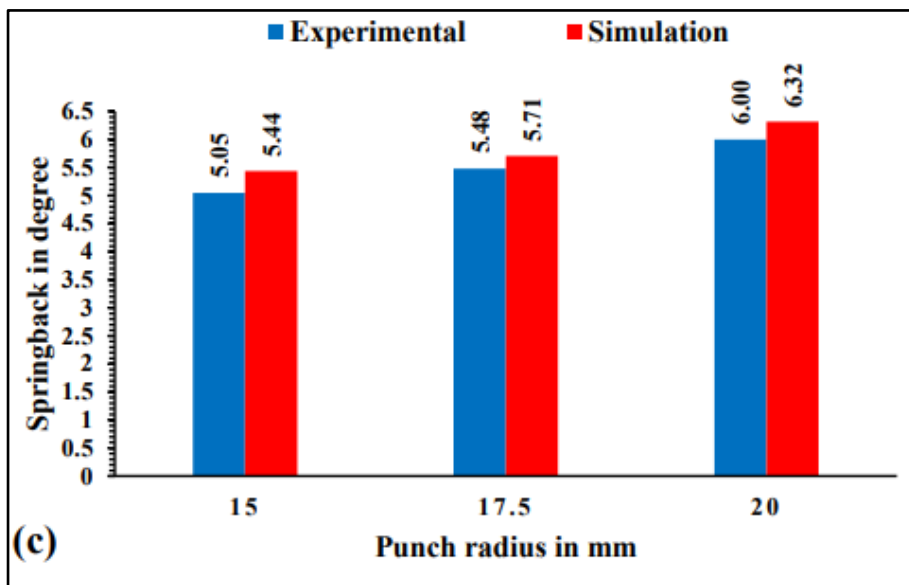
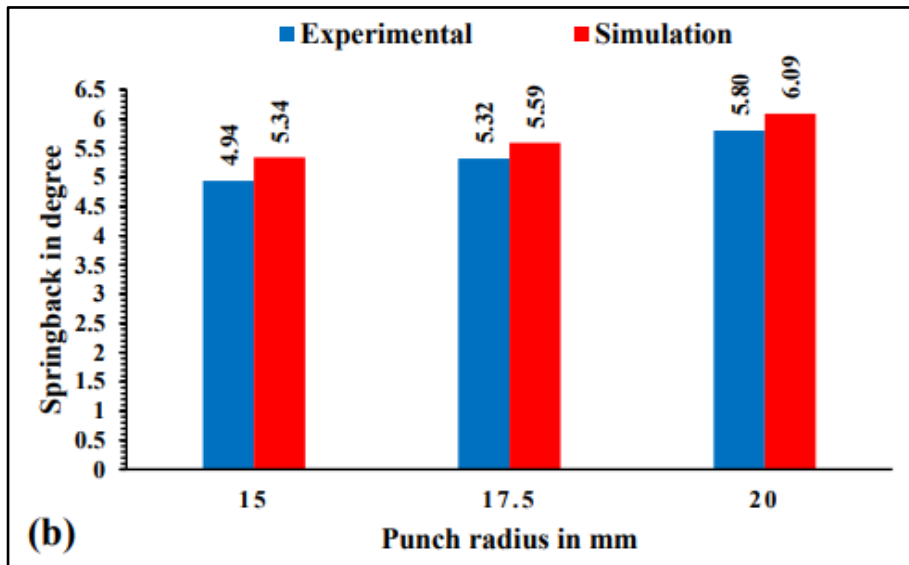
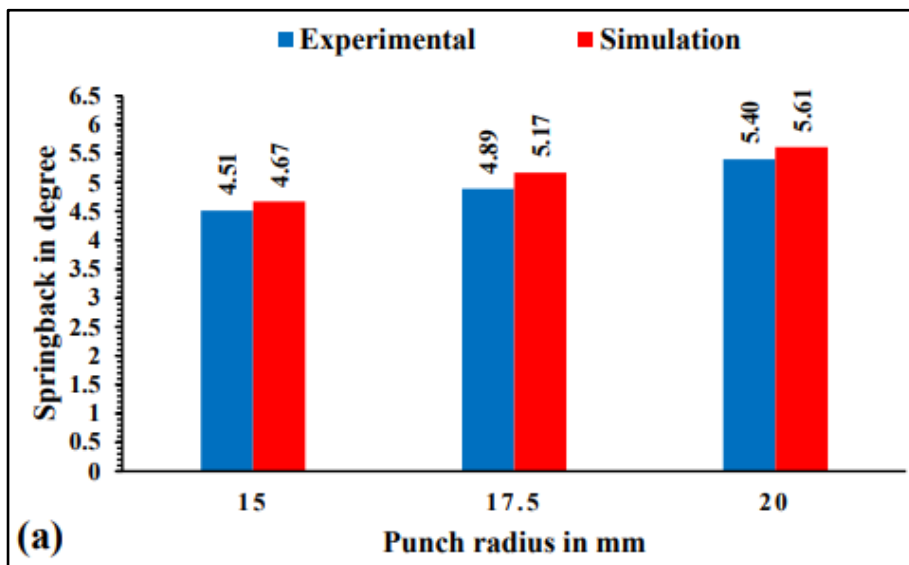


Fig.6.15 Experimental and simulated springback results of a 3-ply clad sheet, oriented at (a) 0°, (b) 45° and (c) 90° for varying punch radius when SS430 taken as an inner layer



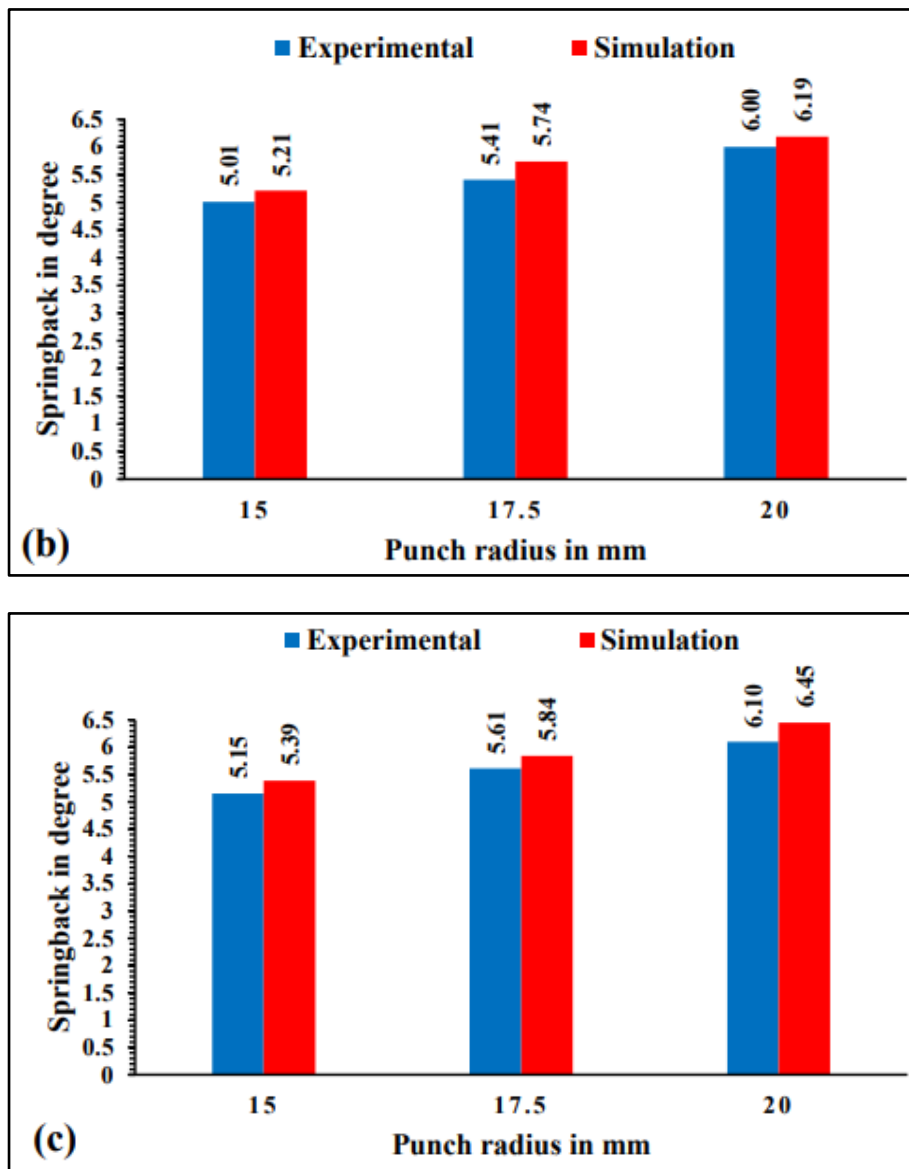
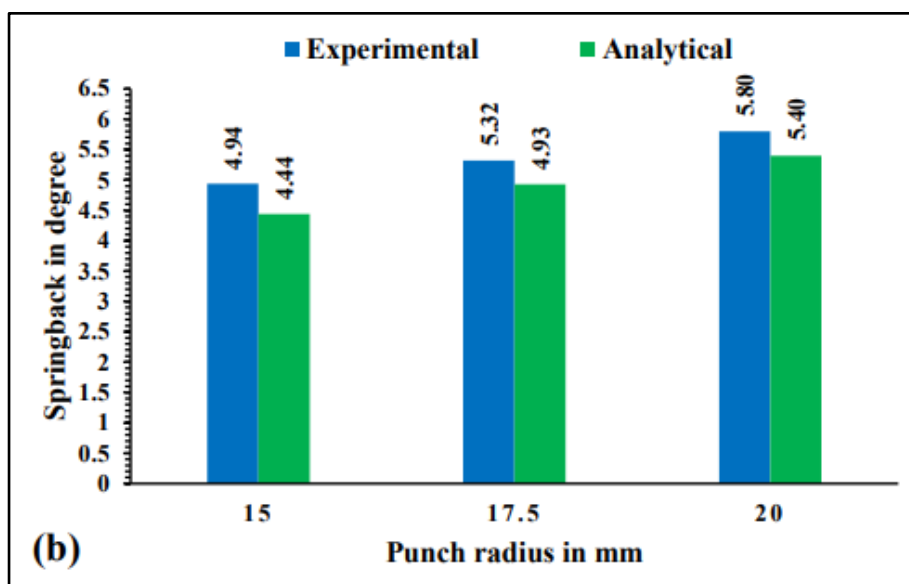
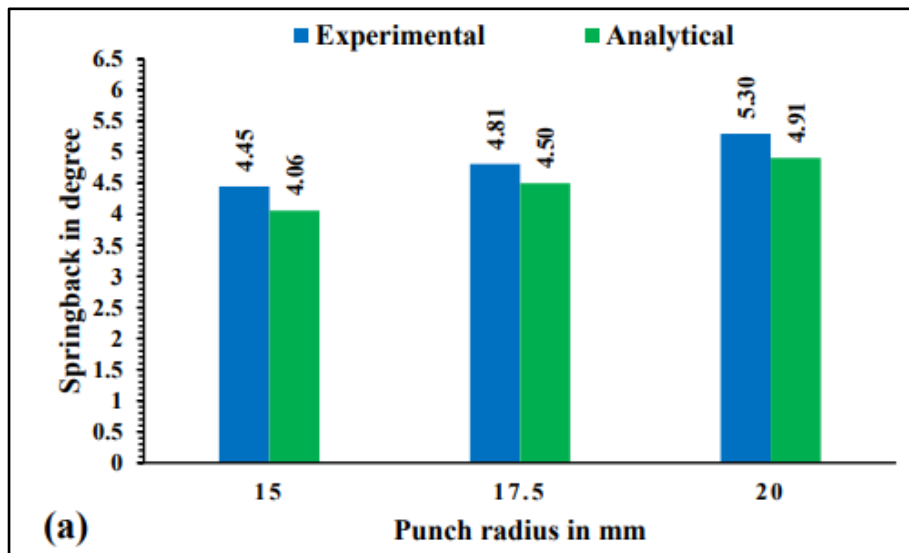


Fig.6.16 Experimental and simulated springback results of a 3-ply clad sheet, oriented at (a) 0°, (b) 45° and (c) 90° for varying punch radius when SS304 taken as an inner layer

Similar results are observed in the springback values predicted by simulation and analytical models in all the cases. Springback values are increased with increase in the punch profile radius. Springback can be minimized by taking small punch radius. Sheet setting conditions also affect springback a lot. Almost in all the cases higher springback values are obtained when SS304 is inner layer during bending which can attributed due to higher bending radius and higher strength of SS304 as compared to SS430.

Table 6.17 Analytical and experimental springback results of a 3-ply sheet for varying bending radius

| Inner layer during bending |     | Punch radius 15 mm |      |         | Punch radius 17.5 mm |      |         | Punch radius 20 mm |      |         |
|----------------------------|-----|--------------------|------|---------|----------------------|------|---------|--------------------|------|---------|
|                            |     | Exp.               | Ana. | % error | Exp.                 | Ana. | % error | Exp.               | Ana. | % error |
|                            |     | (in degree)        |      |         | (in degree)          |      |         | (in degree)        |      |         |
| SS430                      | 0°  | 4.45               | 4.06 | 8.76    | 4.81                 | 4.50 | 6.44    | 5.3                | 4.91 | 7.01    |
|                            | 45° | 4.94               | 4.44 | 10.12   | 5.32                 | 4.93 | 7.33    | 5.8                | 5.40 | 6.57    |
|                            | 90° | 5.05               | 4.60 | 8.91    | 5.48                 | 5.08 | 7.30    | 6                  | 5.55 | 7.81    |
|                            |     | Punch radius 15 mm |      |         | Punch radius 17.5 mm |      |         | Punch radius 20 mm |      |         |
| SS304                      | 0°  | 4.51               | 4.08 | 9.53    | 4.89                 | 4.52 | 7.57    | 5.4                | 4.93 | 8.53    |
|                            | 45° | 5.01               | 4.47 | 10.78   | 5.41                 | 4.96 | 8.32    | 6                  | 5.42 | 9.06    |
|                            | 90° | 5.15               | 4.63 | 10.10   | 5.61                 | 5.10 | 9.09    | 6.1                | 5.58 | 8.67    |



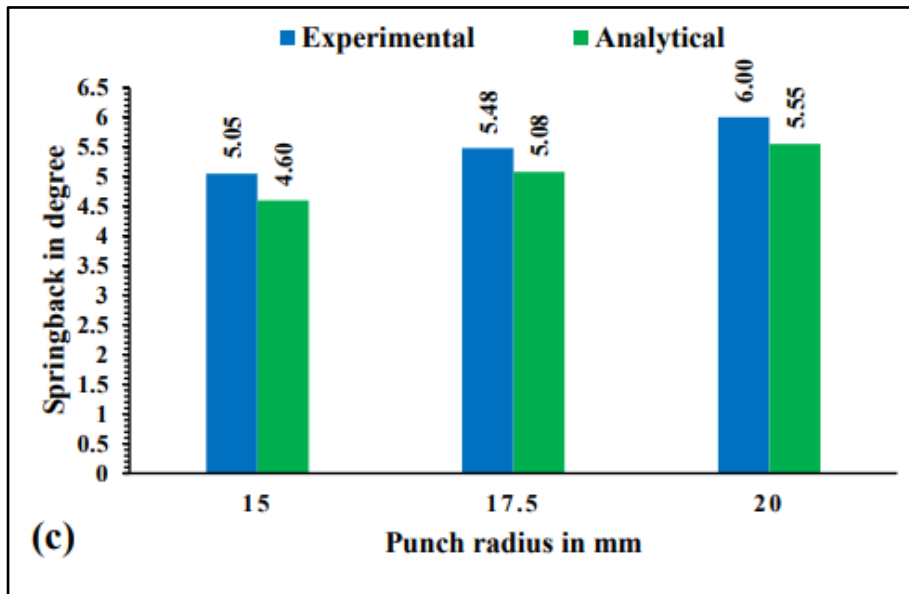
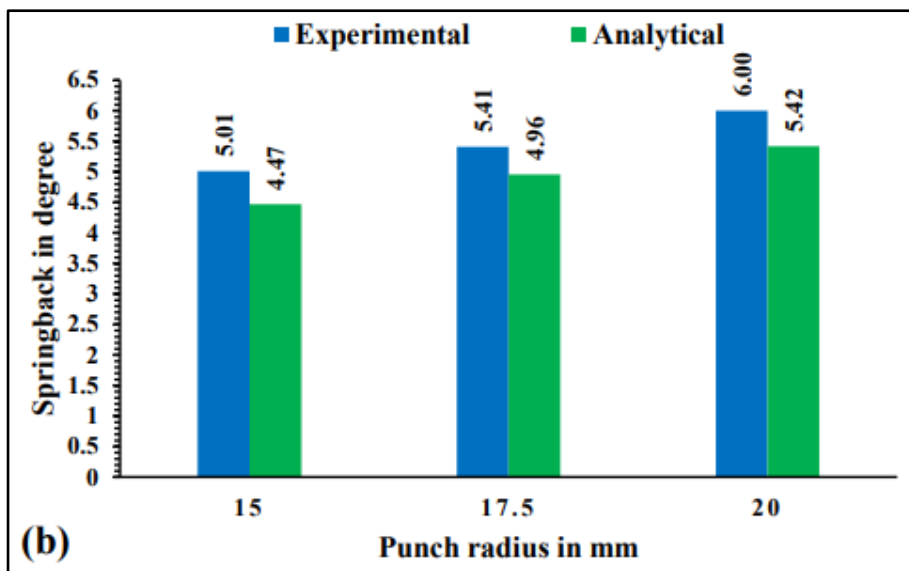
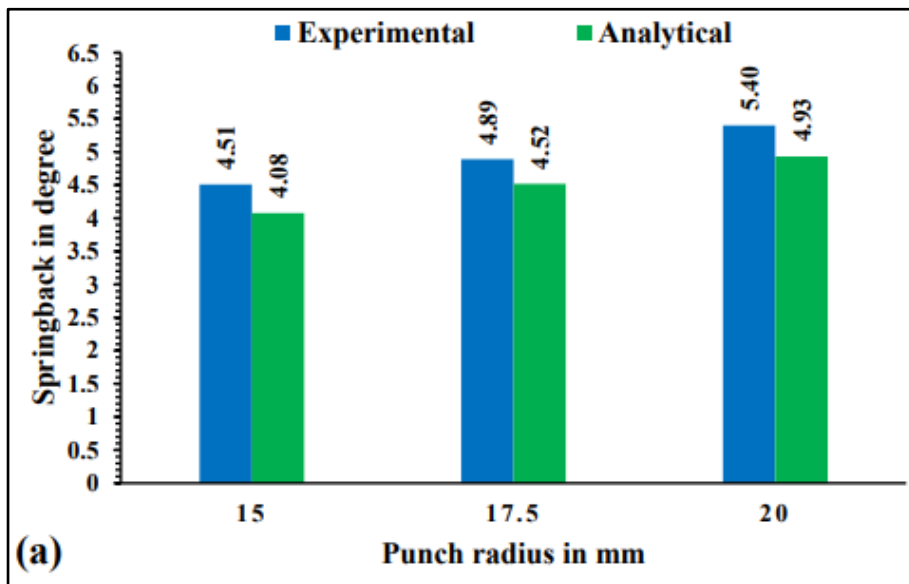


Fig.6.17 Experimental and analytical springback results of a 3-ply sheet oriented at (a) 0°, (b) 45° and (c) 90° for varying punch radius when SS 430 taken as an inner layer



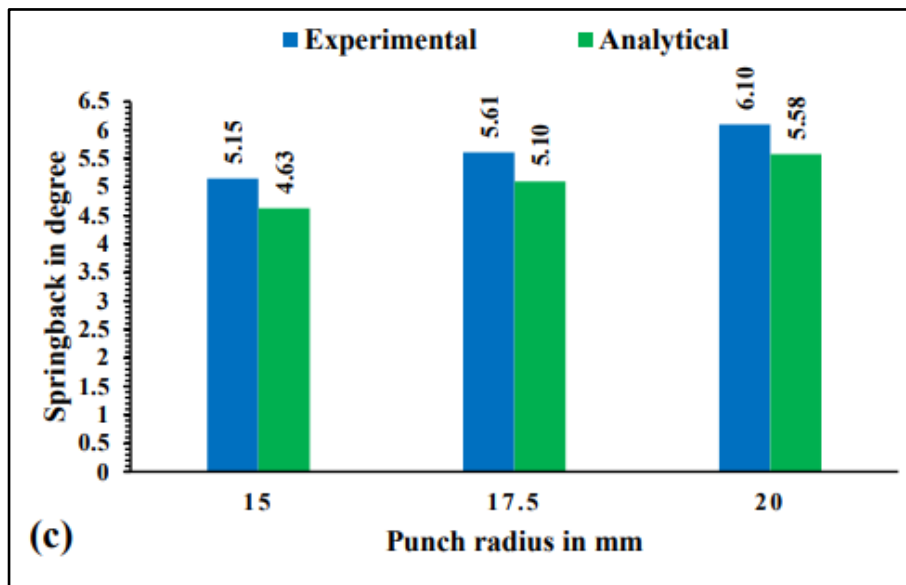


Fig.6.18 Experimental and analytical springback results of a 3-ply sheet oriented at (a) 0°, (b) 45° and (c) 90° for varying punch radius when SS 304 taken as an inner layer

### 6.6 Distribution of longitudinal and residual stress through the thickness for 2-ply clad sheet

The results for the variations of longitudinal stress through the thickness before and after springback as obtained from the simulations for the two different cases on the basis of inner layer during bending of specimens along the rolling direction are presented in this section.

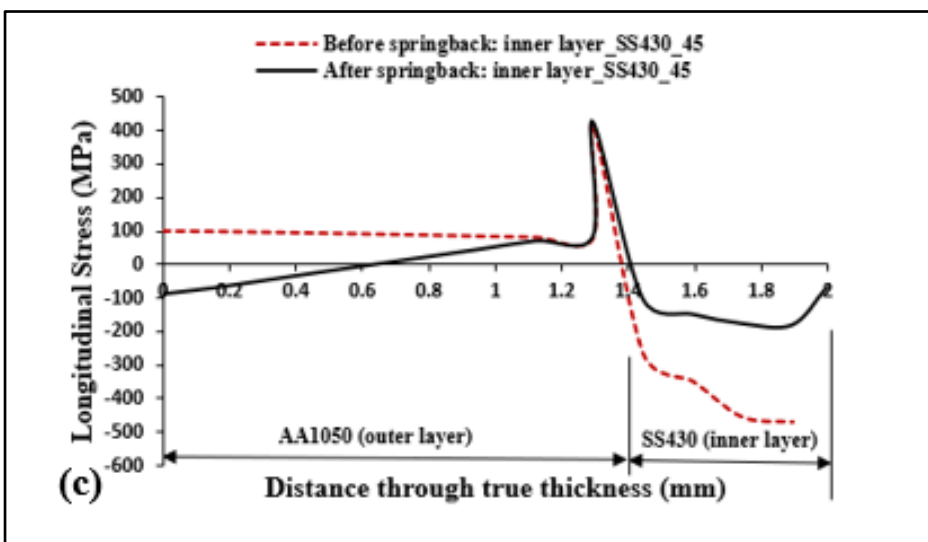
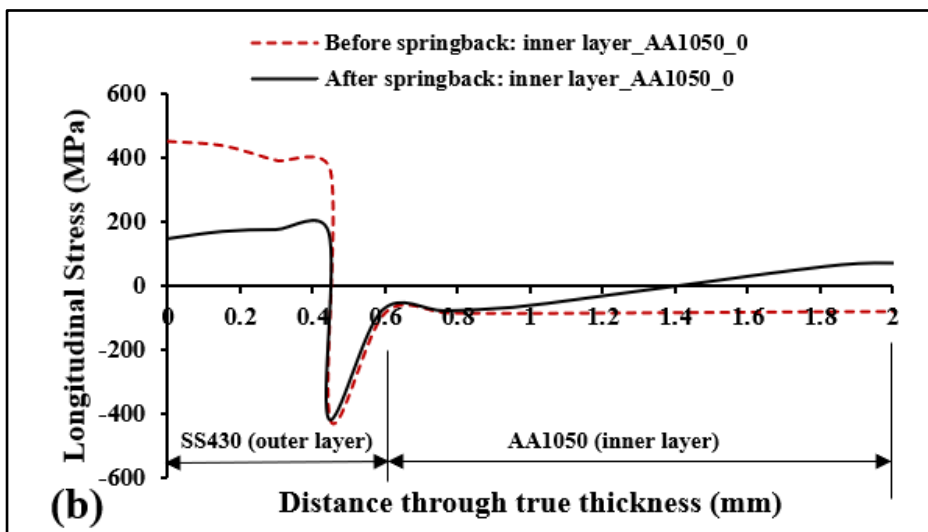
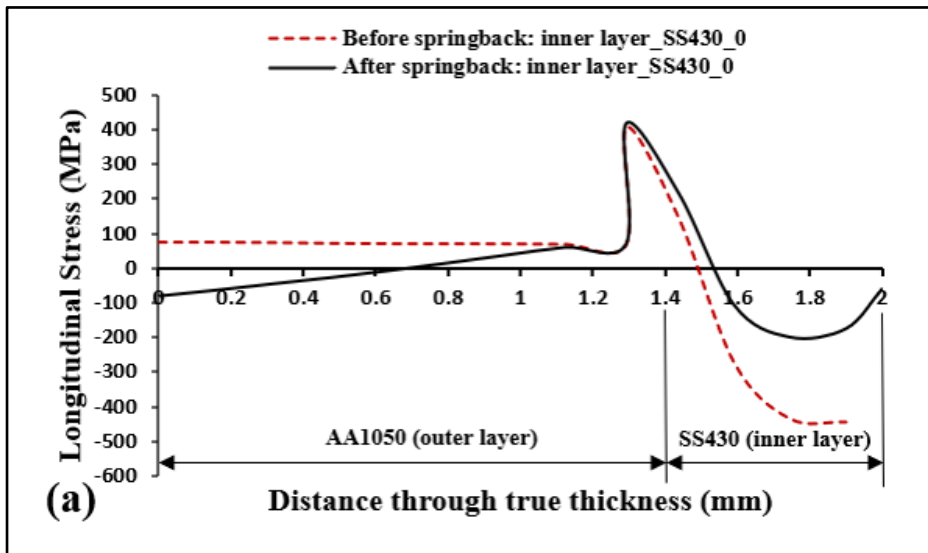
In the case of inner layer of SS430 during bending before springback, as shown in Fig. 6.19(a), the longitudinal stress is nearly uniformly distributed in the outer layer of AA1050 over a thickness of 1.2 mm which suddenly drops and then rises to a maximum of approximately 407MPa (tensile stress) at the interface and then abruptly drops in the region of SS430 after neutral axis at 1.5 mm of thickness and reaches a maximum compressive stress of 442MPa in the inner layer.

The Fig. 6.19(a) also shows the variation of residual stress after springback. It is observed that the residual stress which is initially compressive in nature, gradually reduces to zero and changes from compression to tension at half the way of the thickness in the aluminium sheet and remains roughly unaltered upto a linear distance of 1.2 mm through thickness from the outermost layer. The variation of residual stress at the interface exhibits increasing and decreasing trend till it reaches to zero in steel layer at a linear distance of 1.56 mm from the

outermost layer. The residual stress in the steel sheet remains compressive in nature though dropping significantly to a value of -60MPa at the innermost layer. This shows that the thinner sheet is constrained from undergoing complete springback by the thicker sheet and hence the residual stress in the thinner sheet is compressive even after springback.

In the case of inner layer of AA1050 as shown in Fig. 6.19(b), the variation of longitudinal stress and residual stress show a nearly opposite pattern when compared to the case of inner layer of SS430. The longitudinal stress decreases gradually from 449MPa to 389MPa up to a thickness of 0.46 mm in steel layer and drops suddenly to zero at the neutral axis located at 0.46 mm from the outermost layer of steel and then rises to a maximum compressive stress of 419MPa. The longitudinal stress is nearly uniformly distributed throughout the inner layer of aluminium sheet thickness up to the innermost layer which is in the contact with punch surface. The figure also shows the variation of residual stress after springback. It is observed that the residual stress drops by more than half than that of the bending stress but remains tensile in nature in the thickness of outer layer of SS430 and drops abruptly to zero at a linear distance of 0.45 mm from the outermost layer of steel which is in contact with the die surface. It is also observed that the residual stress near the interface remains compressive in nature and drops to 60MPa at the interface and then varies with a gradually decreasing trend to zero at a distance of 1.4 mm from the outermost layer. At a thickness distance of 1.4 mm, the residual stress changes its sign and becomes tensile in nature and increases gradually to a maximum value of 68MPa at the innermost layer.





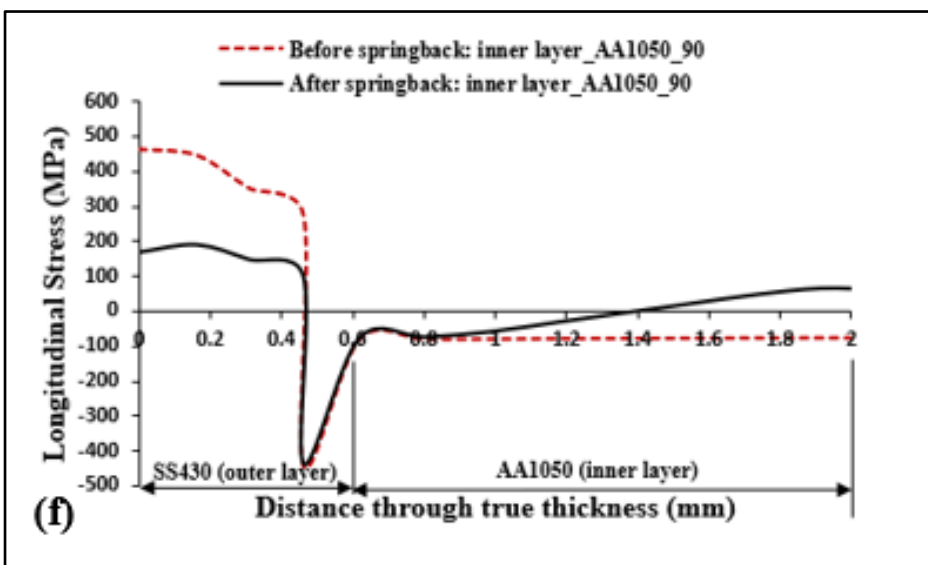
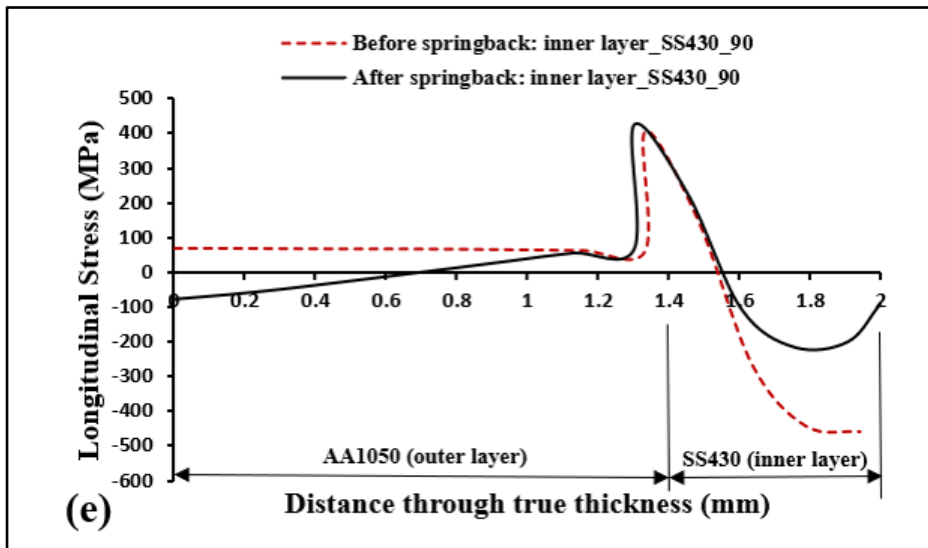
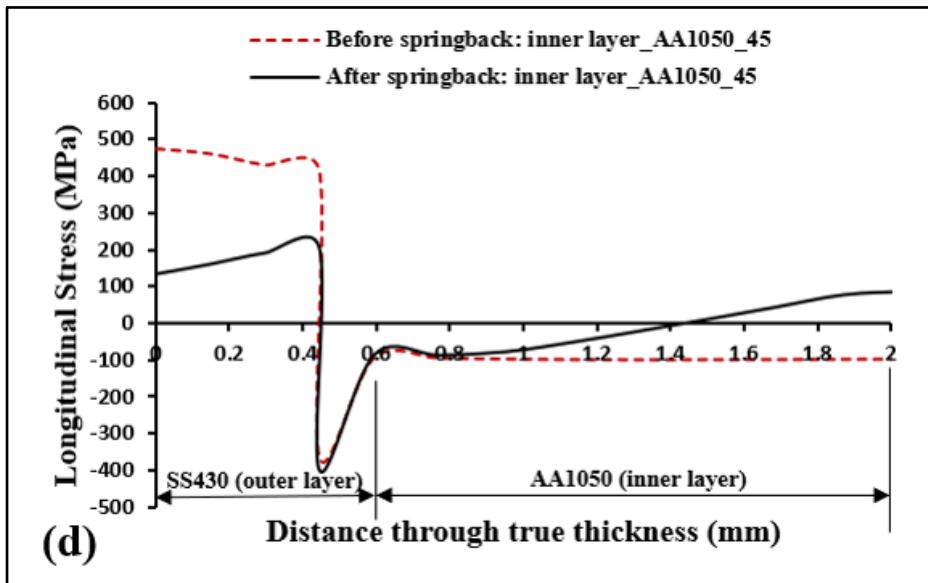
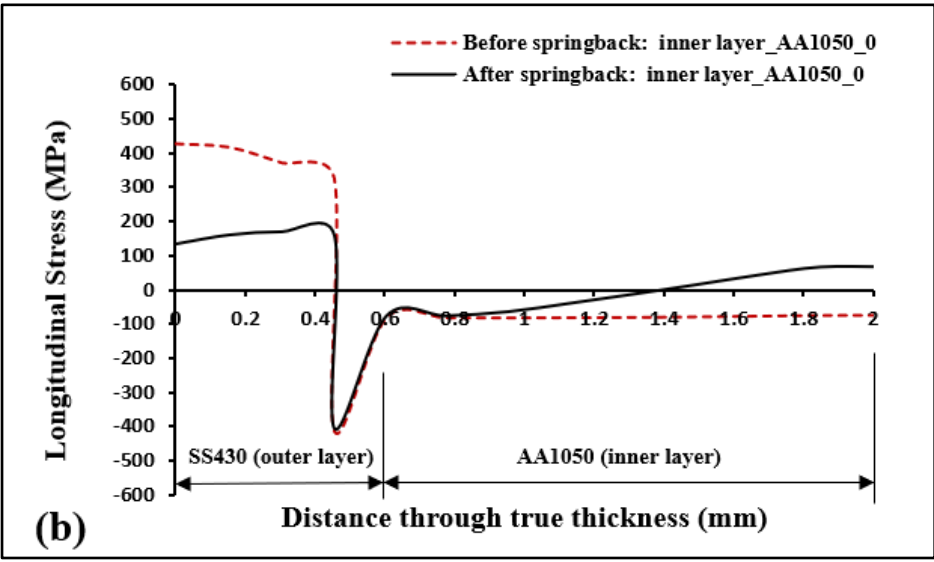
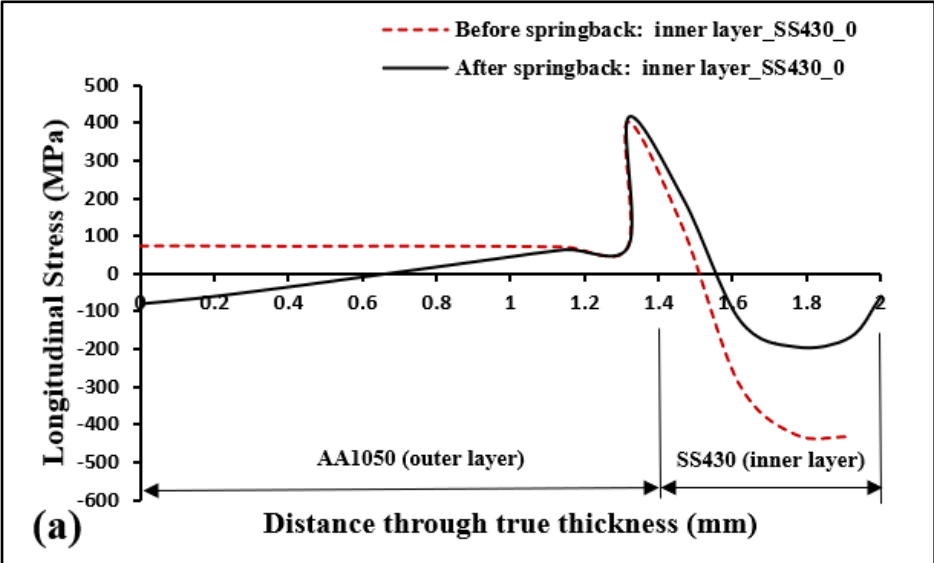
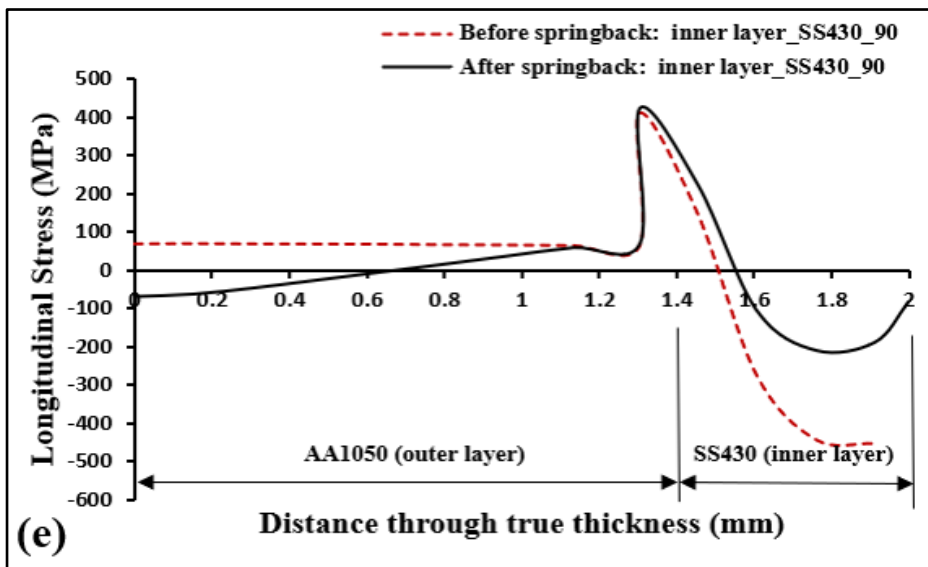
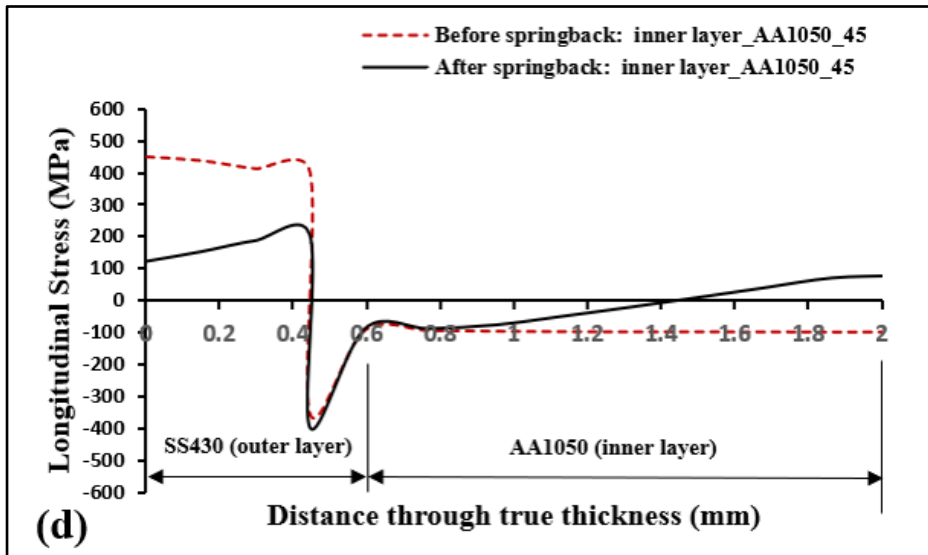
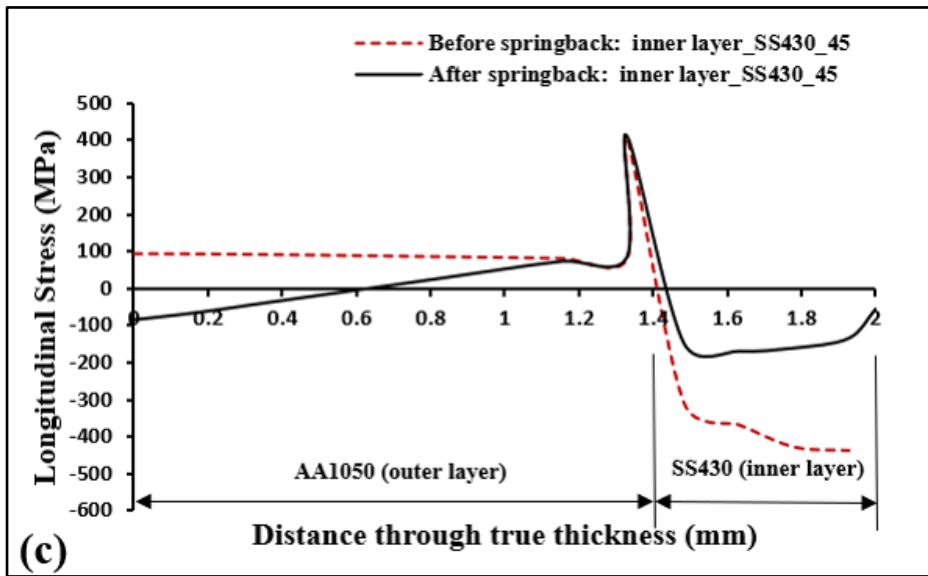


Fig. 6.19 Variation of longitudinal and residual stress through thickness (a), (c) and (e) with SS430 as inner layer; and (b), (d) and (f) with AA1050 as inner layer for three different orientations at 15 mm punch profile radius

In this case also, it may be concluded that the thinner sheet is constrained from undergoing complete springback by the thicker sheet and hence the residual stress in the thinner sheet is still tensile in nature even after the springback.

Similar results from simulations are observed for the specimens with orientation of 45° and 90° to the rolling direction. The similar simulation has been done for 17.5 mm and 20 mm punch profile radius as shown in Fig. 6.20 and Fig. 6.21 respectively.





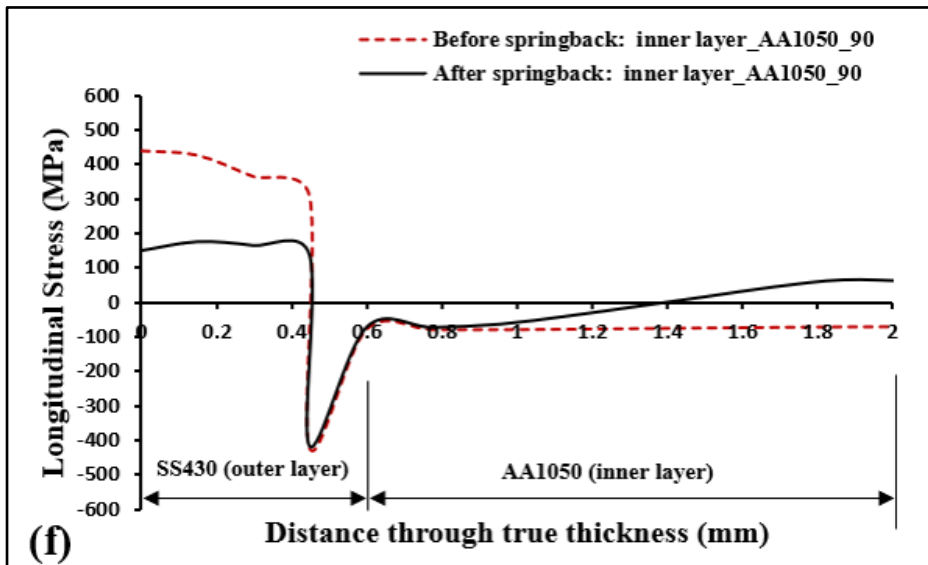
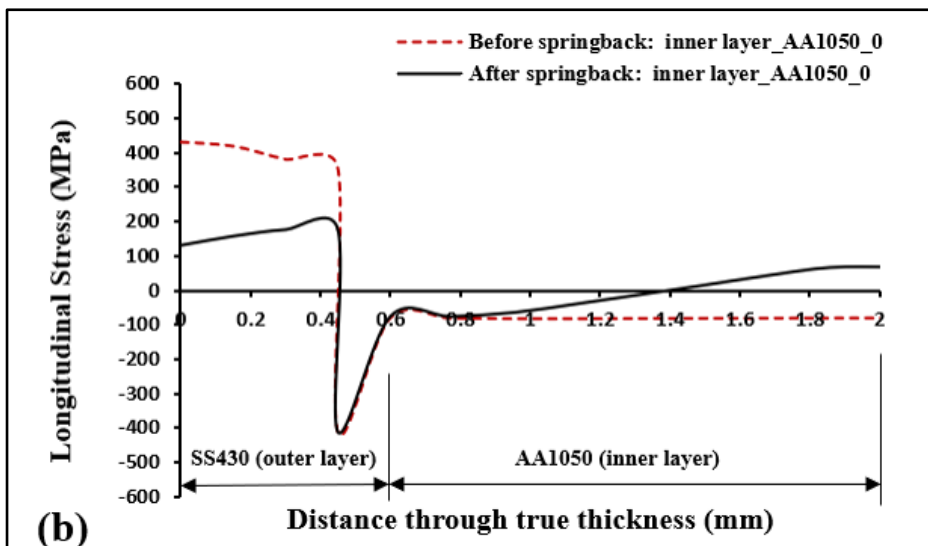
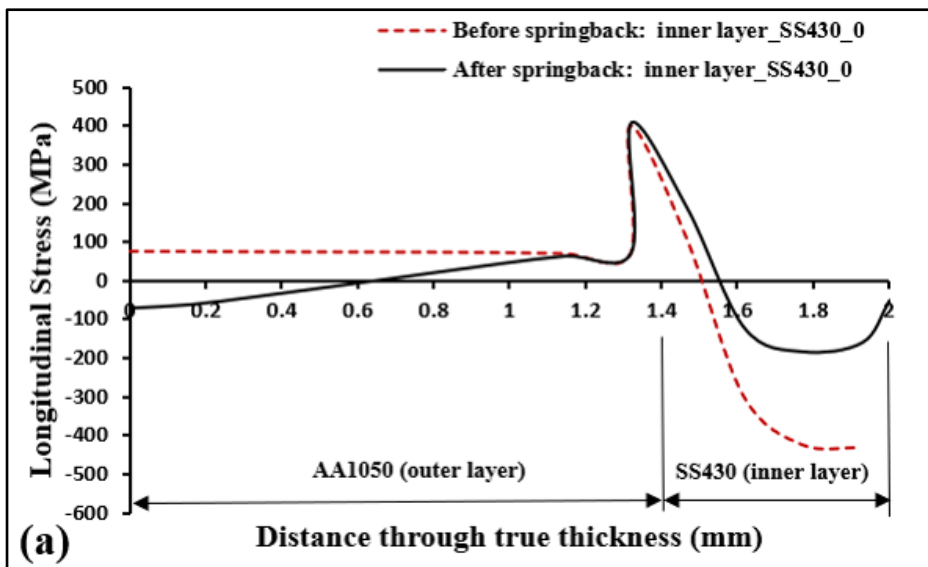
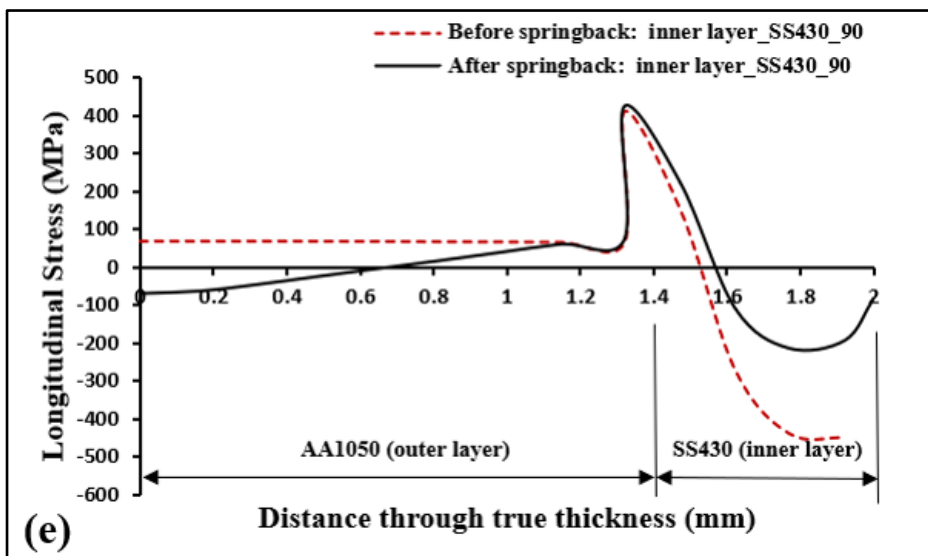
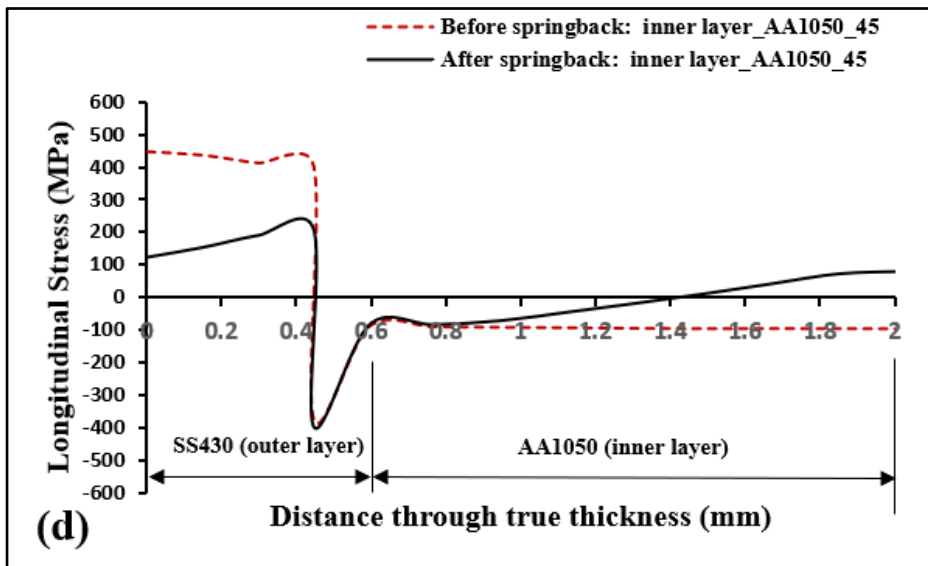
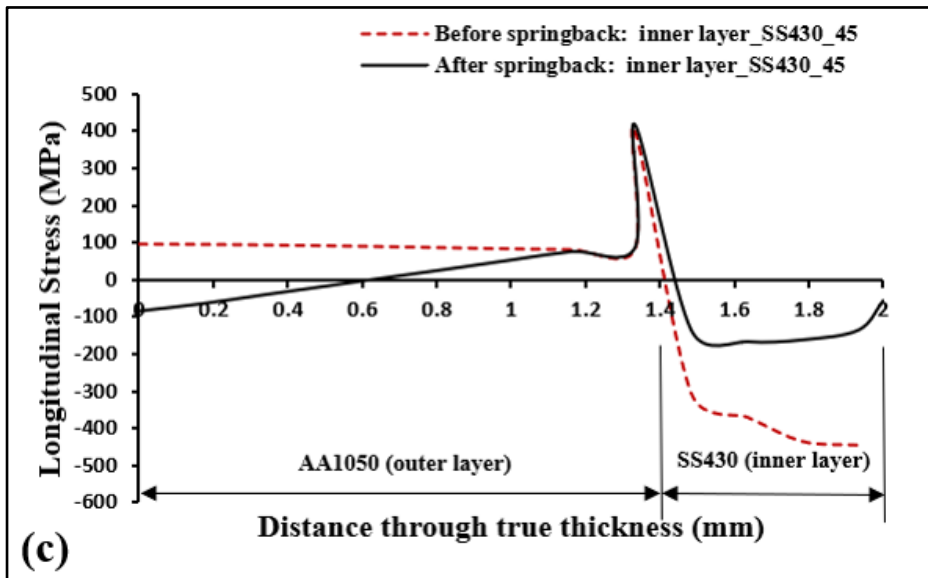


Fig.6.20 Variation of longitudinal and residual stress through thickness (a), (c) and (e) with SS430 as inner layer; and (b), (d) and (f) with AA1050 as inner layer for three different orientations at 17.5 mm punch profile radius





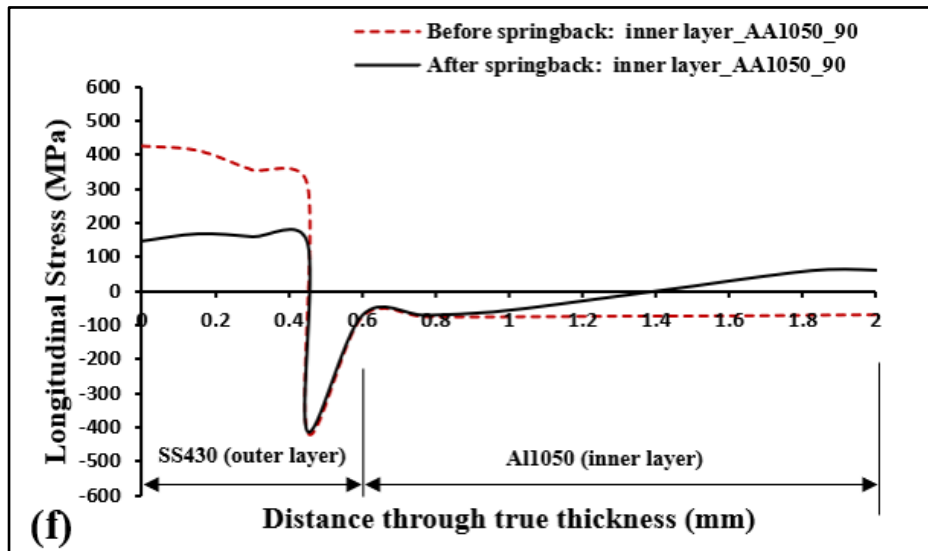


Fig.6.21 Variation of longitudinal and residual stress through thickness (a), (c) and (e) with SS430 as inner layer; and (b), (d) and (f) with AA1050 as inner layer for three different orientations at 20 mm punch profile radius

### 6.7 Distribution of longitudinal and residual stress through the thickness for 3-ply clad sheet

Table 6.18 summarizes the results of residual stress acquired by experiments and simulations of the specimens oriented in three different directions w.r.t. the rolling direction of 3-ply clad sheet after springback for both the cases of sheet settings.

In the case of bending of clad sheet with inner layer of SS304, the inner layer is in compression and outer layer is in tension. After springback, it is observed that the innermost layer always shows the tensile residual stress although small in magnitude whereas the outermost layer is always set with a higher value of compressive residual stress in all the specimens. This indicates that the outermost layer of SS430 is able to undergo complete springback whereas the thinner layer of SS304 is still slightly constrained due to adjoining layer of higher thickness.

In the other case of bending specimens of clad sheet with inner layer of SS430, the inner layer is in compression and outer layer is in tension. After springback, ideally inner layer should be having tensile residual stress and outer layer the compressive residual stress but it is observed that both the layers i.e., innermost and outermost layers always show tensile residual stress in all the specimens. This indicates that the innermost layer of SS430 is able to undergo complete

springback and hence shows tensile residual stress whereas the thinner layer of SS304 is not able to undergo complete springback and remains constrained due to adjoining layer of higher thickness.

In both the cases of sheet settings, the results of longitudinal stress after the springback predicted by FE simulations agree with the experimental results except for a few cases.

Table 6.18 Comparison of experimental and simulation results for 3-ply clad sheet

| Inner layer during bending | Specimen orientation w.r.t. RD (in degree) | Residual stress (MPa) |            |             |            |
|----------------------------|--|-----------------------|------------|-------------|------------|
|                            |  | SS304-layer           |            | SS430-layer |            |
|                            |  | Experiment            | Simulation | Experiment  | Simulation |
| SS304                      | 0  | 14                    | 16.68      | -113        | -118.32    |
|                            | 45   | 12                    | -4.28      | -120        | -122.40    |
|                            | 90   | 36                    | 33.37      | -111        | -114.12    |
| SS430                      | 0  | 92                    | 77.48      | 141         | 148.67     |
|                            | 45   | 64                    | 77.09      | 166         | 174.84     |
|                            | 90   | 56                    | 68.54      | 176         | 182.90     |

The variation of longitudinal stress through the thickness of the clad sheet before and after springback, acquired from the FE simulations of the bending specimens oriented with three different orientations w.r.t. the rolling direction and for both the cases of sheet placements, are shown in Fig. 6.22 (a)-(f). In Fig. 6.22, it is observed that the longitudinal stress through the thickness of the clad sheet varies in increasing and decreasing manner in all the cases of bending and springback simulations.

In the case of bending simulations with SS430 as the inner layer, the outer layer of SS304 in contact with the die undergoes a higher value of bending stress of approximately 780MPa which decreases slightly through the thickness of the layer of SS304 and abruptly falls to a minimum value at the layer interface with AA1050 as shown in Fig.6.22 (a). The magnitude of longitudinal stress through the thickness of aluminium layer remains lowest and changes its

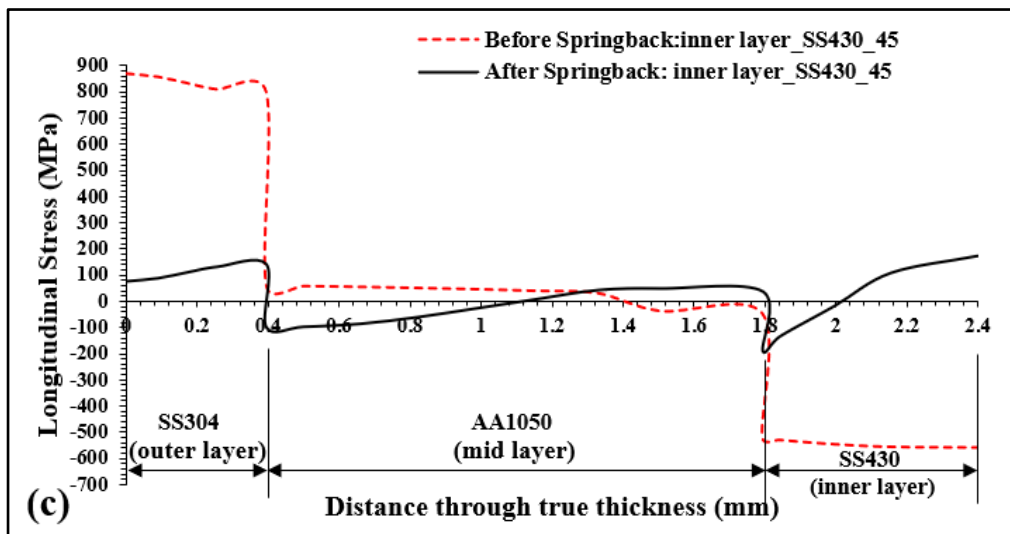
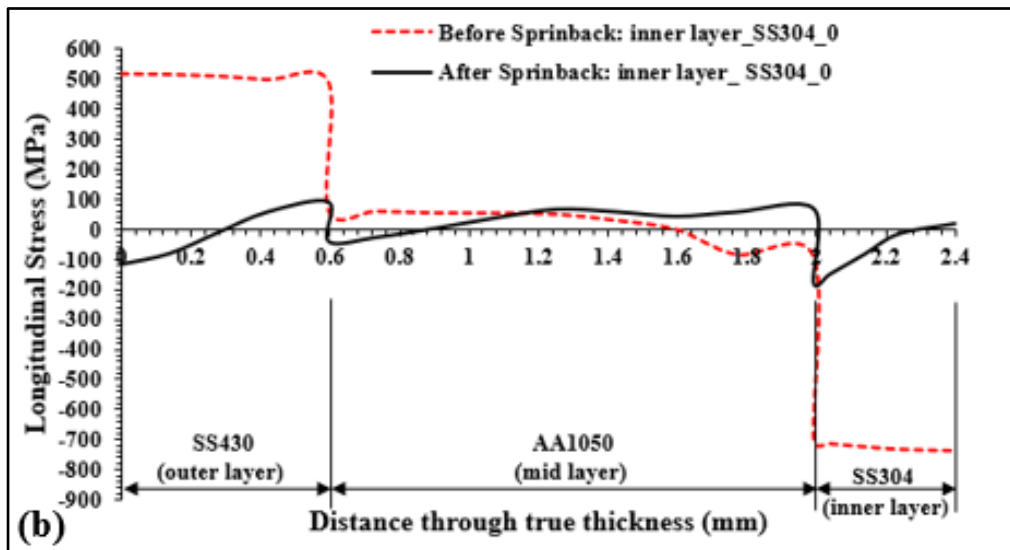
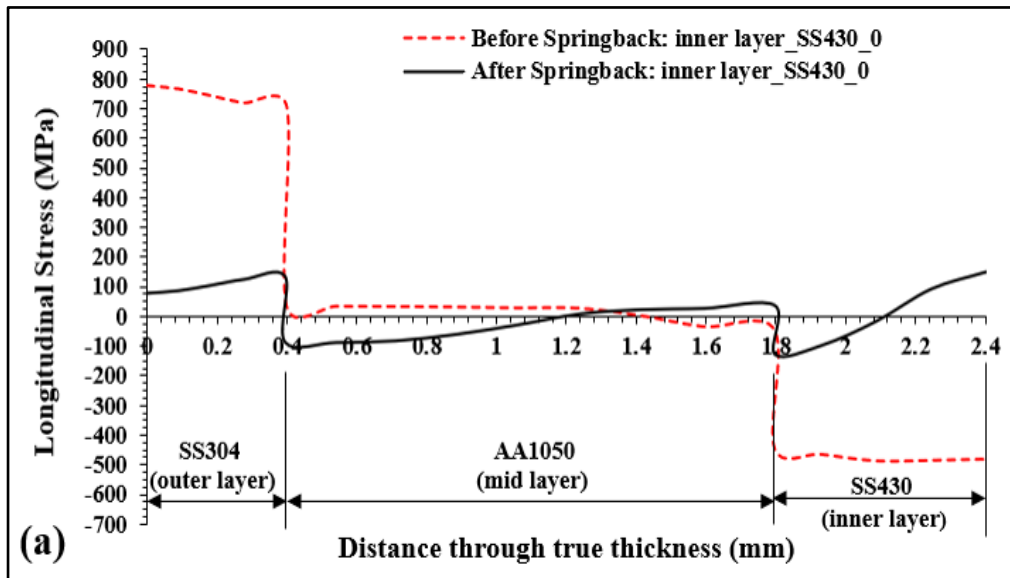


sign from tension to compression when the neutral axis is reached at approximately 1.4 mm indicating a shift in the neutral axis towards the compression side i.e. the inner layer of the clad sheet. After this, the longitudinal stress traverses in compression towards the layer interface of aluminium with SS430 and increase to a value of approximately 443MPa and remains almost constant till the innermost layer is reached at sheet-punch interface. After springback simulation, as soon as the punch is retracted, the longitudinal residual stress rearranges its distribution through thickness of layer of SS430 and varies almost linearly from tension to compression till the interface with aluminium layer is reached. This indicates that this layer of SS430 has undergone springback completely. The residual stress changes its sign at the interface of SS430-AA1050 from compression to tension and decreases almost linearly and once again changes its sign from tension to compression at a distance equal to the clad sheet thickness of 1.2 mm and remains in compression till an interface layer with SS304 is reached. In the layer of SS304, the residual stress rises to a maximum value in tension and then decreases linearly through the thickness to a value of approximately 77MPa (at die-sheet interface) but remains in tension only. This stress state indicates that this layer of SS304 is still in tension even after springback although the value decreases significantly when compared to that of the value before springback. This phenomenon of tensile residual stress in the thinner steel layer after springback can be attributed to the smaller thickness of the layer and constraining effect of the adjoining thicker aluminium layer.

In the other case of bending and springback simulations with SS304 as inner layer, the layer of SS430 in contact with the die, undergoes a value of bending stress of approximately 510MPa which remains almost constant through the thickness in the layer of SS430 and abruptly falls to a minimum value at the interface layer with the layer of AA1050 as shown in Fig.6.22 (b). The magnitude of longitudinal stress through the thickness of aluminium layer remains lowest and changes its sign from tension to compression when the neutral axis is reached at a distance of approximately 1.6 mm from the outermost layer indicating a shift in

the neutral axis towards the compression side. After this, the longitudinal stress traverses in compression towards the interface layer of aluminium with the layer of SS304 and increases to a value of approximately 711MPa and remains almost constant till the innermost layer is reached at sheet metal-punch interface. After springback, as soon as the punch is retracted, the longitudinal residual stress rearranges itself through the thickness of layer of SS304 and varies almost linearly from tension to compression till the interface with aluminium layer is reached. This indicates that this layer of steel i.e. SS304 has not undergone springback completely due to the constraining effect of thicker aluminium layer. The residual stress changes its sign at the interface of SS304-AA1050 from compression to tension and decreases almost linearly and changes its sign at a clad sheet thickness of 0.9 mm and remains in compression till an interface layer with SS430 is reached. The residual stress decreases almost linearly in magnitude after springback and changes its sign from tension to compression at a distance of approximately 0.3 mm from the die-sheet interface. This stress state indicates that this outer layer of SS430 has undergone springback completely although the value of stress decreases significantly in the outermost layer when compared to that of the value before springback. This phenomenon of tensile and compressive residual stress in the thicker outermost steel layer after springback shows that this layer of SS430 is not affected by constraining effect of adjoining thicker aluminium layer and hence participates significantly in the overall springback of the clad sheet when compared with the other case of bending with SS304 as outermost layer.

Almost similar results are observed for the bending and springback simulations of specimens with the orientation of  $45^\circ$  and  $90^\circ$  w.r.t. the rolling direction of the clad sheet as shown in Fig. 6.22 (c)-(f).



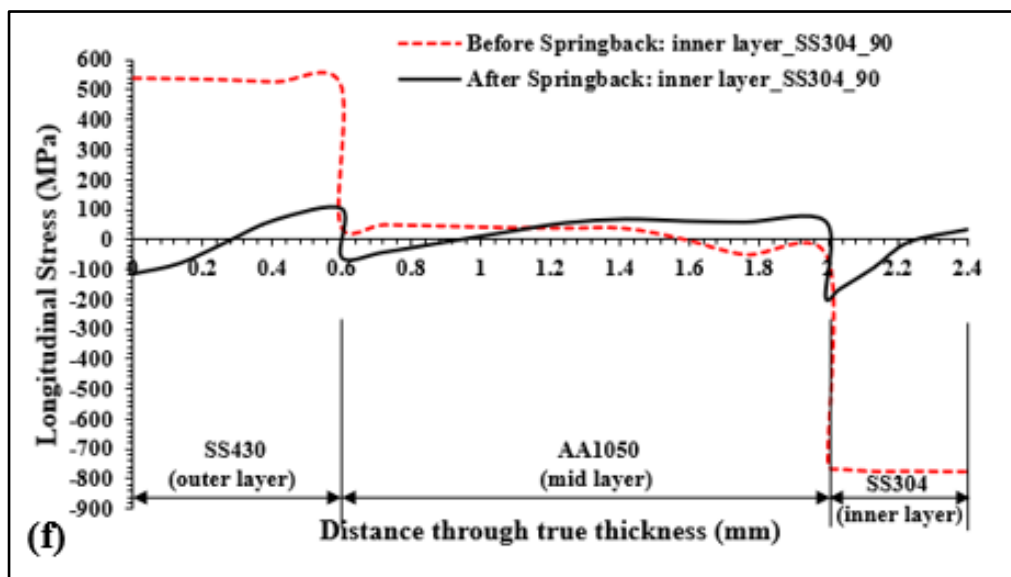
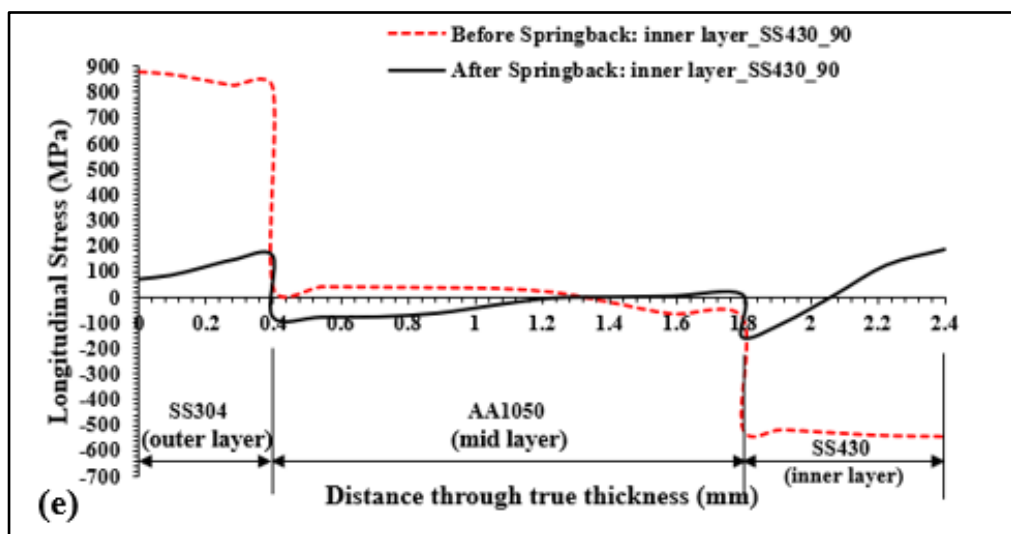
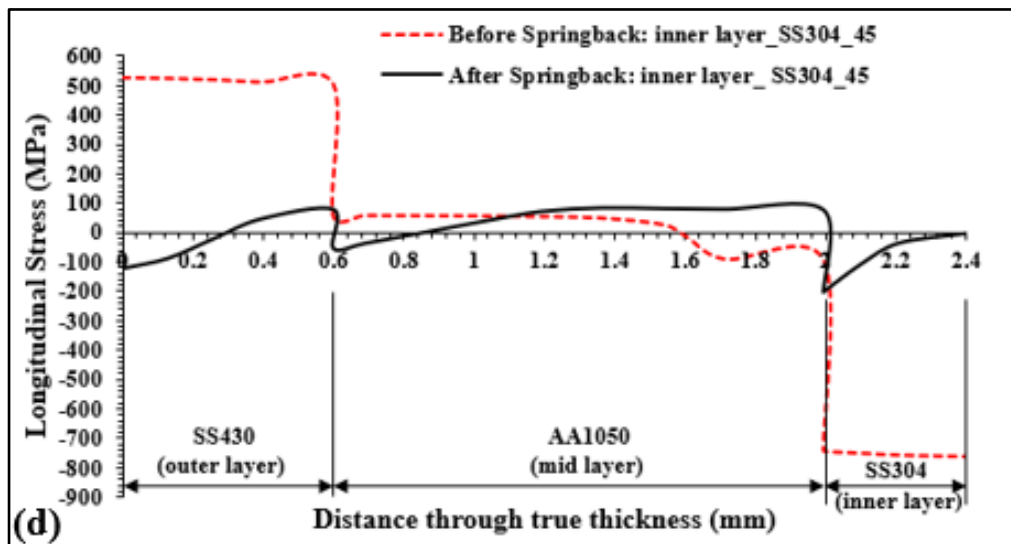
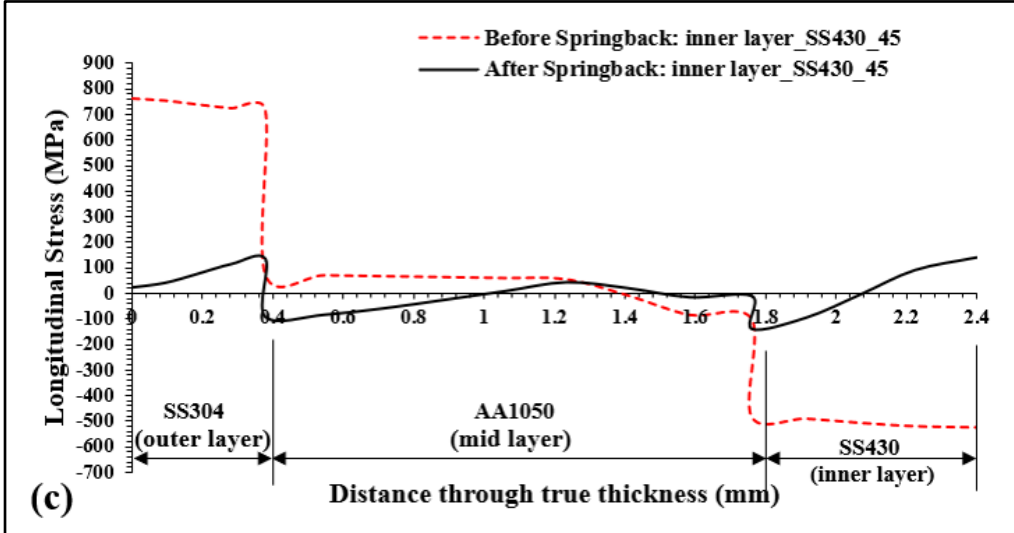
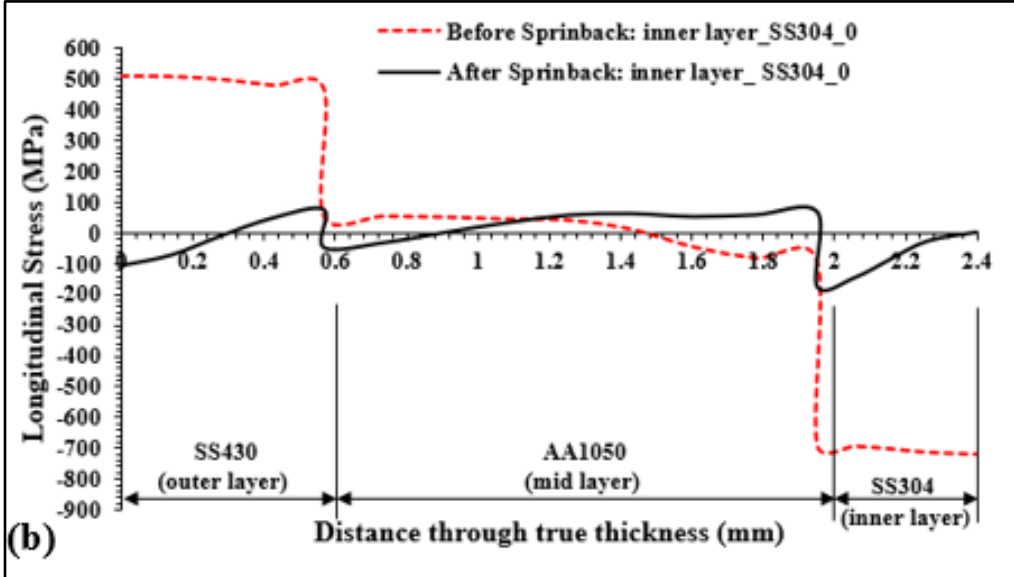
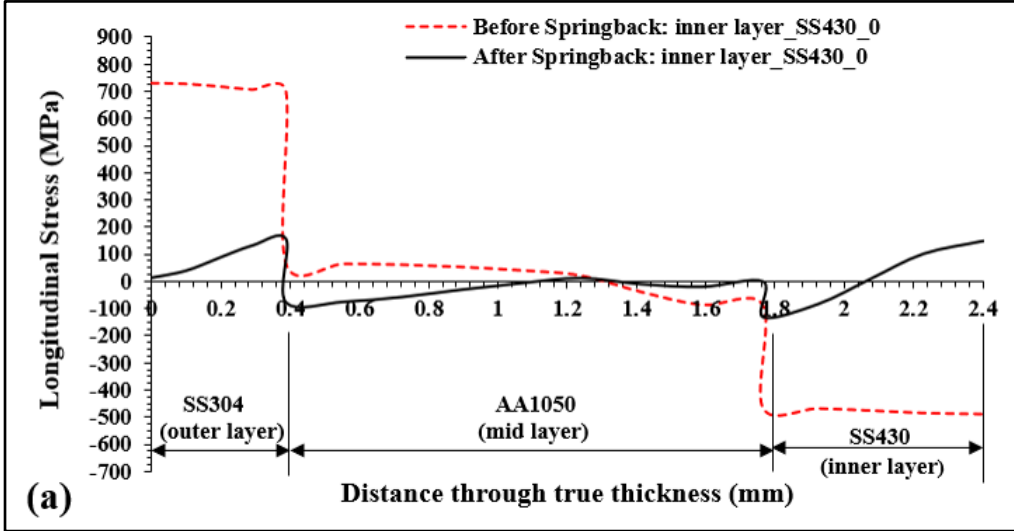


Fig. 6.22 Distribution of longitudinal and residual stress through thickness (a), (c) and (e) with SS430 as inner layer; (b), (d) and (f) with SS304 as inner layer for three different orientations at 15 mm punch profile radius

The similar simulation has been done for 17.5 mm and 20 mm punch profile radius as shown in Fig. 6.23 and Fig. 6.24 respectively.



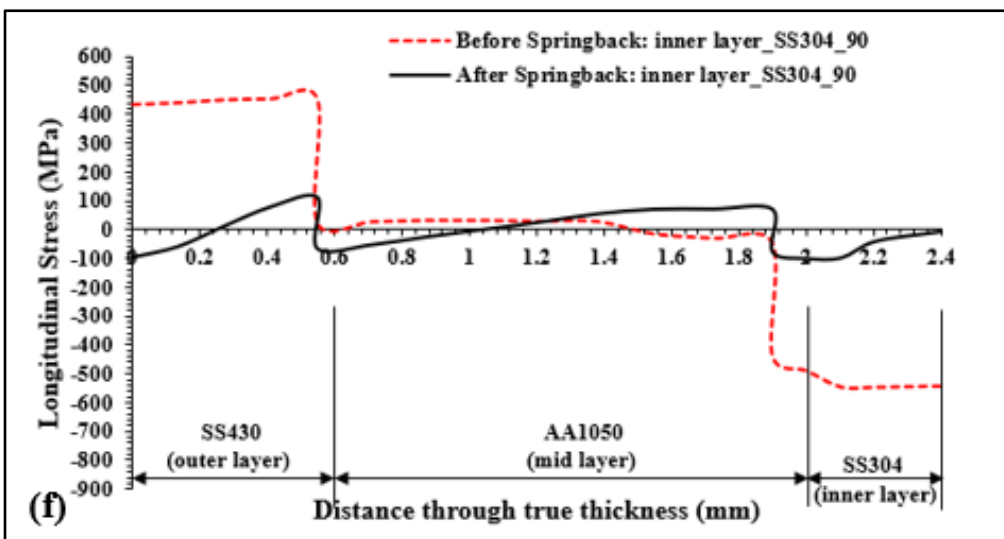
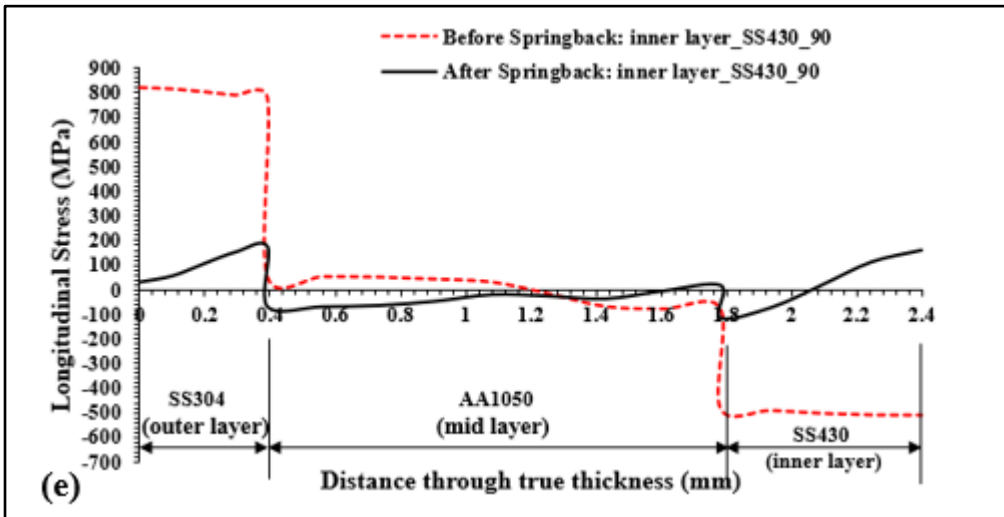
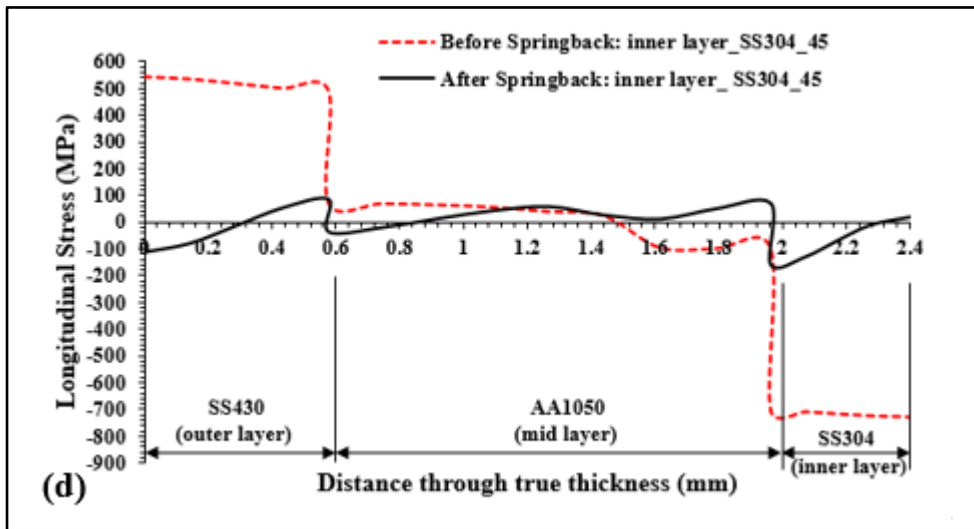
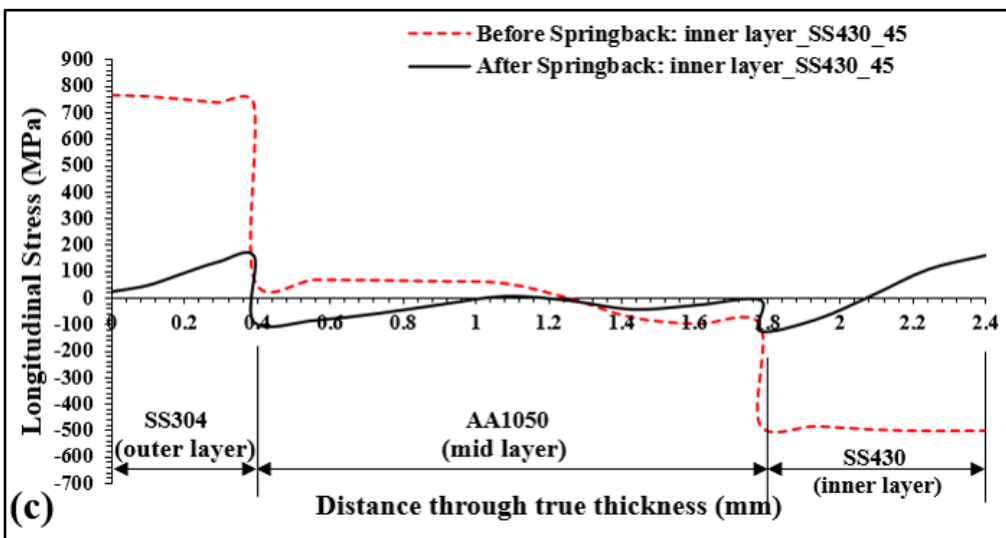
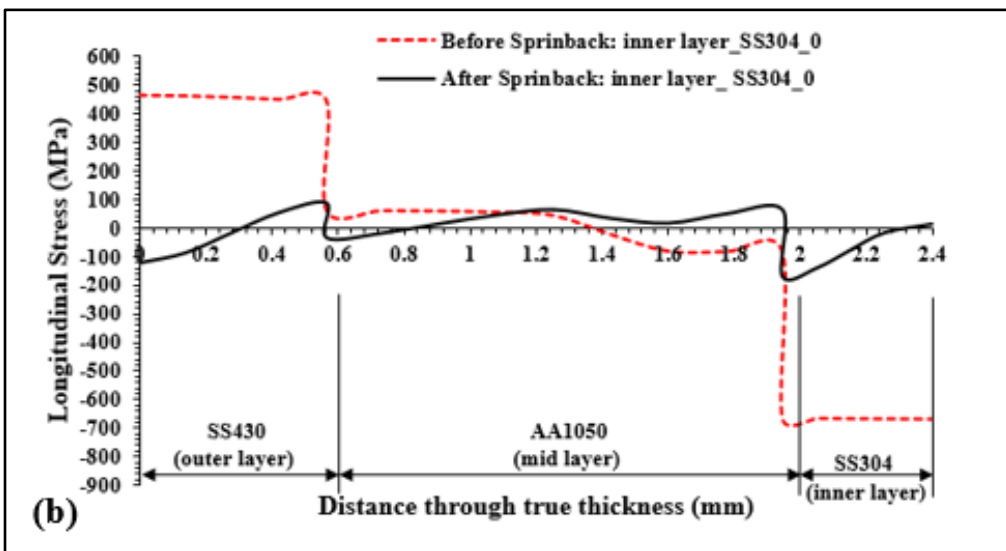
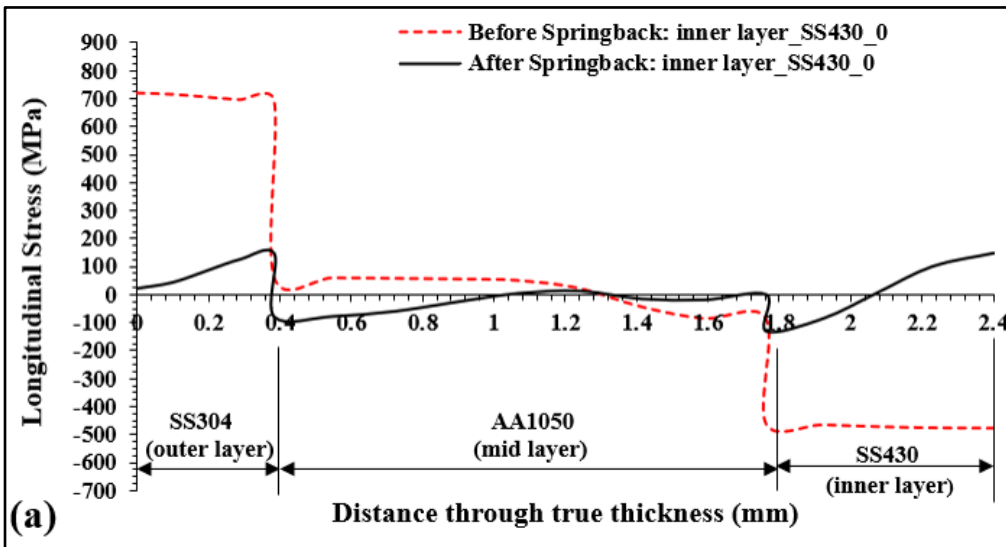


Fig. 6.23 Distribution of longitudinal and residual stress through thickness (a), (c) and (e) with SS430 as inner layer; (b), (d) and (f) with SS304 as inner layer for three different orientations at 17.5 mm punch profile radius



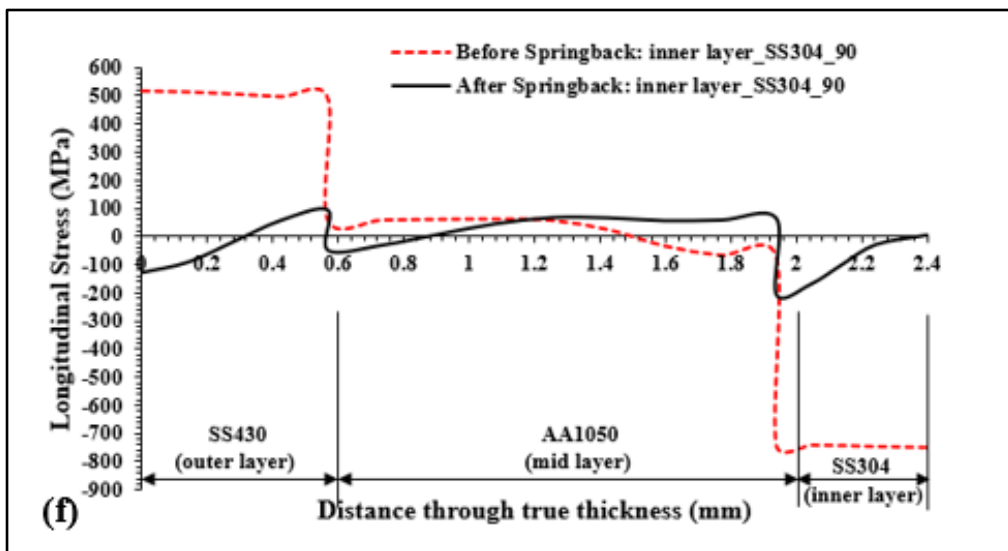
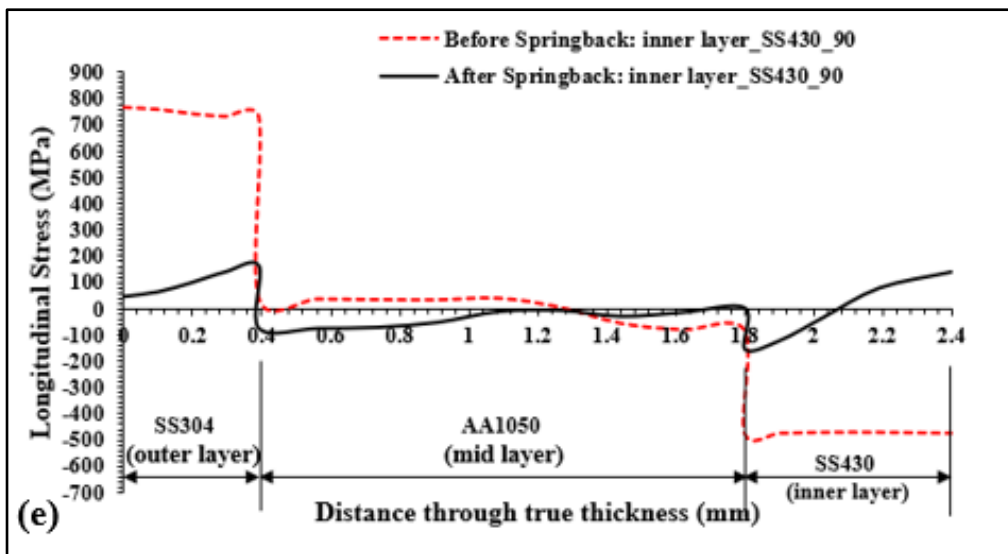
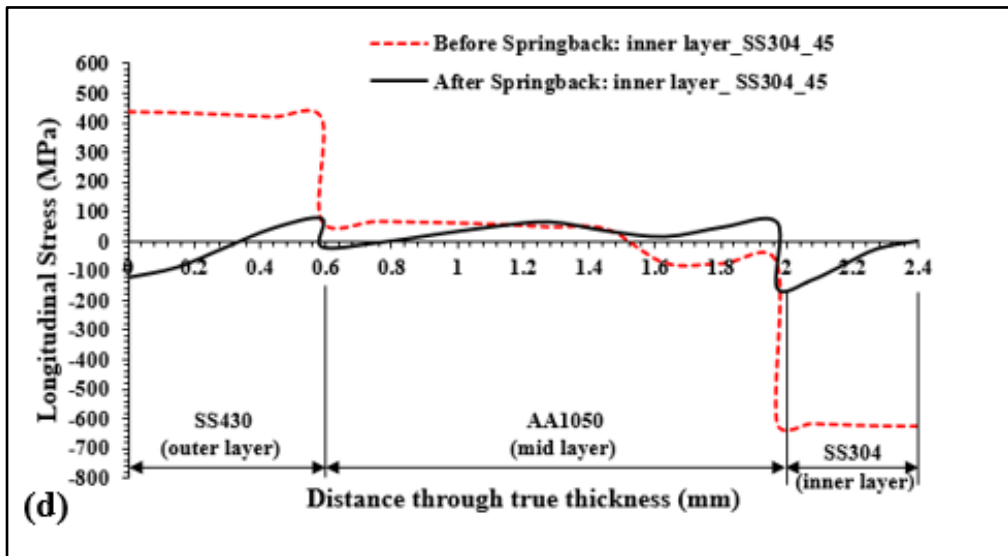


Fig. 6.24 Distribution of longitudinal and residual stress through thickness (a), (c) and (e) with SS430 as inner layer; (b), (d) and (f) with SS304 as inner layer for three different orientations at 20 mm punch profile radius



## **6.8 Industrial significance of the present research work**

Experimental, analytical, and numerical studies on the springback of 2-ply and 3-ply laminate composites consisting of aluminium and stainless steel have significant industrial significance.

*Springback Prediction and Control:* Understanding and predicting the springback behaviour of laminate composites is crucial for achieving accurate dimensional control in sheet metal components. Experimental studies provide real-world data on the actual springback, while numerical simulations help in predicting and optimizing the springback behaviour. By combining experimental and numerical approaches, design engineers and manufacturers can gain insights of the springback characteristics of these specific laminate composites and develop strategies to control and minimize springback, thereby improving the quality of the final product.

*Process Optimization:* Experimental, analytical, and numerical studies allow for the optimization of the forming parameters during manufacturing. By studying the springback behaviour of 2-ply and 3-ply laminate composites, manufacturers can identify the optimal process parameters, such as bending angles, tooling design, and material combinations, to reduce springback and achieve the desired dimensional accuracy. This optimization leads to increased process efficiency, reduced scrap rates, and improved productivity.

*Material Selection and Design:* Experimental studies help in evaluating the mechanical properties and behaviour of 2-ply and 3-ply laminate composites. By testing different material combinations and laminate configurations, design engineers can identify the most suitable materials and designs that exhibit reduced springback and improved structural integrity. This knowledge aids in efficient material selection and design decisions, ensuring that the laminate composites meet the desired performance requirements while minimizing springback related issues.

*Cost and Time Savings:* Springback can lead to dimensional inaccuracies and shape deviations, resulting in additional manufacturing steps, such as post-bending corrections or rework. By conducting experimental and numerical studies on 2-ply and 3-ply laminate composites,

manufacturers can gain insights into the springback behaviour early in the product development process. This knowledge allows for pre-emptive adjustments in the manufacturing process, reducing the need for costly and time-consuming corrective measures, ultimately saving both time and resources.

*Quality Assurance:* Understanding the springback behaviour of laminate composites helps in ensuring consistent product quality. By conducting experimental tests and numerical simulations, manufacturers can establish quality control standards and specifications to ensure that the final products meet the required dimensional tolerances. This improves customer satisfaction, reduces product rejection rates, and enhances the overall reliability and reputation of the manufacturing process.

*Advancements in Composite Materials:* Composite materials, such as laminate composites of aluminium and stainless steel, are increasingly used in various sheet metal forming industries due to their lightweight, high strength, and corrosion resistance. Studying the springback behaviour of these specific laminate composites contributes to the overall knowledge and understanding of composite material behaviour. This knowledge can be applied to the development of new composite materials and the improvement of existing ones, leading to advancements in material science and engineering.

**6.9 Other people's work and discussion**

There has been a significant amount of research on the V-bending of sheet of monolithic materials and clad sheets. Some studies and findings have been described in Table 6.18.

Table 6.19 Comparison of bending and springback studies

| S.No. | Reference           | Materials           | Methodology                      | Key Findings  |
|-------|---------------------|---------------------|----------------------------------|---|
| 1     | Kagzi et al. (2022) | Al/SS430 clad sheet | Analytical Method (included with | The outcomes of this model have been compared with both an isotropic model and experimental data. |

|   |                     |                        |  |   |
|---|---------------------|------------------------|--|---|
|   |                     |                        | anisotropy and strain hardening) validated by experimental procedure | Notably, the inclusion of anisotropy yielded an improvement of 0.3% in results, particularly for cases involving smaller bend radii. The disparity between isotropic and anisotropic conditions becomes much more pronounced when dealing with larger bend radii. At a bend radius of 600 mm for a bimetallic plate with a thickness of 1.56 mm, the percentage difference in the unloaded radius increases to approximately 50% when considering anisotropy. |
| 2 | Lafta et al. (2020) | Al/Cu bimetallic sheet | Experimental, Simulation and ANNOVA Analysis                         | A strong alignment between experimental findings and numerical simulations observed. The setting condition $Cu_{in}/Al_{out}$ offers lower value of springback as compared to $Cu_{out}/Al_{in}$ during V-bending. The value of springback is increased when the radii of the punch and die are increased; on the contrary, it is decreased when the thickness of the sheet increases.  |
| 3 | Wang et al. (2019)  | Al/Ni clad sheet       | Experimental   | They have observed an increase in springback angle when the bending   |

|   |                     |       |  |  |
|---|---------------------|-------|--|--|
|   |                     |       | And Numerical Analysis   | angle decreases from 120° to 60°, even when using the same placement method and annealed specimens. When employing Cu/Ni, it results in a reduction in the thickness of the clad foil along the punch's fillet. Conversely, when Ni/Cu is employed, there is an increase in the thickness of the clad foil.  |
| 4 | Trieu et al. (2023) | SS400 | Experimental And Numerical Analysis                                    | A good agreement between experimental findings and numerical simulations (ABAQUS 6.13 software) have been observed.  |
| 5 | Hai et al. (2020)   | SS400 | Experimental And Numerical Analysis (ABAQUS) along with Taguchi Method | A good agreement between experimental findings and numerical simulations have been observed. Moreover, this study employs a combination of ABAQUS simulation and the TAGUCHI method to compute and select the most effective parameters for V-bending SS400 steel sheets. the key factor influencing the springback angle of V-bending products is identified, and optimal values are determined, including a punch stroke of H = 18 mm, a plate |

|  |  |  |  |   |
|--|--|--|--|---|
|  |  |  |  | thickness of $t = 7$ mm, and a punch radius of $R = 40$ mm. |
|--|--|--|--|---|

Kagzi et al. (2016) present an analytical model for predicting springback in bending of bimetallic sheets. The model is based on logarithmic strain distribution across the thickness and thickness change during bending. The authors validate their model using experimental results and study the variation of springback with changes in material properties and layer thickness. The analytical results for the Alin/SSout and SSin/Alout cases agree with the experimental results and the thickness changes evaluated under unloaded conditions are also closer to the experimental results in both cases.

Kagzi et al. (2022) have observed an essential factor influencing the springback behaviour of clad materials is their anisotropy, a property that must be accounted for to achieve more accurate springback predictions. Efforts have been made to incorporate the influence of anisotropy into the analytical model outlined in existing literature (Kagzi, 2016). The mathematical modelling endeavour achieved success through the incorporation of several enhancements into the mathematical model initially presented by Yuen [83]. These enhancements encompassed the integration of factors such as strain hardening, logarithmic strain distribution, and the consideration of anisotropic effects. The objective is to enhance the precision of springback predictions for bimetallic plates. The outcomes of this model have been compared with both an isotropic model and experimental data. Notably, the inclusion of anisotropy yielded an improvement of 0.3% in results, particularly for cases involving smaller bend radii.

The disparity between isotropic and anisotropic conditions becomes much more pronounced when dealing with larger bend radii. At a bend radius of 600 mm for a bimetallic plate with a thickness of 1.56 mm, the percentage difference in the unloaded radius increases to approximately 50% when considering anisotropy. Thus, it becomes evident that accounting for anisotropy is of paramount importance, particularly in scenarios involving larger bend radii.

Lafta et al. (2020) investigated the impact of various process parameters on springback in Al/Cu bimetallic sheets during V-bending. These parameters encompassed sheet thickness, punch and die radii, and strain rates. They observed that the relative positioning of the Al and Cu (setting conditions) significantly influenced springback, as evidenced both experimentally and through numerical simulations. In general, they observed a strong alignment between experimental findings and numerical simulations. The setting condition  $Cu_{in}/Al_{out}$  offers low value of springback as compared to  $Cu_{out}/Al_{in}$  during V-bending. The value of springback is increased when the radii of the punch and die are increased; on the contrary, it is decreased when the thickness of the sheet increases. To ascertain the relative contributions of these process parameters to spring back, they conducted an ANOVA analysis. This statistical analysis revealed that bimetallic sheet thickness, punch and die radii were statistically significant, with a P-value less than 0.05, signifying their substantial influence on springback. In contrast, strain rate was found to be a less significant factor.

Wang et al. (2019) studied on springback of Cu/Ni clad sheet in the V-bending process experimentally and numerically both. They have observed an increase in springback angle when the bending angle decreases from  $120^\circ$  to  $60^\circ$ , even when using the same placement method and annealed specimens. When employing Cu/Ni, it results in a reduction in the thickness of the clad foil along the punch's fillet. Conversely, when Ni/Cu is employed, there is an increase in the thickness of the clad foil. This phenomenon can be attributed to the dominance of transverse compressive stress when the stronger Ni layer is positioned on the interior.

Trieu et al. (2023) introduce an innovative methodology for accurately predicting the springback tendencies in V-bending processes using SS400 steel sheets under elevated temperatures. The study relies on a comprehensive dataset of tensile tests to determine parameters for both pure isotropic and kinematic hardening laws at various temperatures, which are critical inputs for Finite Element Method (FEM) simulations. While using either pure isotropic or kinematic hardening laws in isolation has limitations, especially at elevated

temperatures, they recommend a hybrid approach to create robust predictive models within the ABAQUS 6.13 software. To overcome this challenge, they propose a novel method that utilizes the ratios of flow stress curves between elevated and room temperatures as a function of equivalent strain to derive combined hardening law parameters. A thorough comparison between simulation and experimental results confirms the model's effectiveness in predicting springback during the V-bending of SS400 steel sheets, particularly under elevated temperatures. This innovative approach enhances the understanding of material behaviour at high temperatures and improves predictive capabilities for designing and optimizing complex V-bending processes.

Hai et al. (2020) have investigated how different punch strokes, corresponding to various bending angles, impact the springback angle in the V-bending process using 6 mm thick SS400 sheet steel. To validate the experimental findings, finite element analysis (FEA) utilizing ABAQUS software is employed. To simulate the springback in V-bending, the deformed results of the V-shaped sheet from a dynamic forming simulation in Abaqus/Explicit are imported into Abaqus/Standard, followed by a static analysis to calculate the springback. The simulation studies reveal variations in the initial bending angle and the springback angle after releasing the bending force, with consideration of isotropic and kinematic hardening models. Consequently, a combined hardening model is proposed to reconcile the discrepancies between predicted results and experimental observations. Furthermore, this study explores the impact of parameters such as sheet thickness, punch radius, and punch stroke on the springback angle's behavior, with the objective of identifying optimal input parameters through the Taguchi method. The samples are cut along the rolling direction, and a series of experimental tests are conducted for comparison with numerical simulation results. The study evaluates the springback effect under different punch strokes corresponding to bending angles of 90°, 123.5°, and 150°. A comprehensive FEA study is conducted with the assistance of ABAQUS software. Notably, it is observed that as the bending angle of the sheets increases, the springback angle also rises, ranging from 2.46° to 5.92° for the specified bending angles. The alignment between

experimental and simulation outcomes demonstrates the suitability of ABAQUS software for predicting springback in V-bending SS400 steel sheets.

Moreover, this study employs a combination of ABAQUS simulation and the TAGUCHI method to compute and select the most effective parameters for V-bending SS400 steel sheets. Through FEM simulation, the key factor influencing the springback angle of V-bending products is identified, and optimal values are determined, including a punch stroke of  $H = 18$  mm, a plate thickness of  $t = 7$  mm, and a punch radius of  $R = 40$  mm.

Wasif et al. ((2020) have designed experimental setup to investigate the effects of width, thickness, bend angle and machine tool parameters on the springback, in JSC440 and JSC590 high strength steel, during the V-bending process. The optimal combination of parameters for the minimum springback in V-bending of JSC440 and JSC590 steels was evaluated. Analysis of variance (ANOVA) was performed to analyze the magnitude of influence of these parameters on the springback. Using the experimental results, analytical models for the prediction of springback for the combinations of blank thickness, width, bend angle, and machine tool parameters were developed. Their analytical model includes quadratic equations to predict the springback

The results revealed that in V-bending of JSC440, thickness and width are the dominant factors influencing the springback, whereas in JSC590 steel, an insignificant change in springback is observed with the change in width of the blank. However, the thickness of the steel sheet and bend angle significantly influence the springback in JSC590 steels.

Zhang et al. (2007) introduce an analytical model, founded on Hill's yielding criterion and plane strain conditions, to accurately predict V-bending sheet springback. This model incorporates several factors, such as contact pressure, the length of the bending arm between the punch and die, transverse stress, neutral surface displacement, and sheet thickness reduction. The analytical model's predictions reveal that contact pressure and transverse stress significantly impact springback, especially when the bending ratio (the ratio of punch radius to sheet thickness) is less than five. A shorter length of the bending arm results in greater



springback due to decreased contact pressure. The influence of neutral surface displacement on springback is less pronounced than that of contact pressure and diminishes with increasing bending ratio. However, this research highlights that the effect of sheet thickness reduction on springback can be disregarded. Comparative analysis with finite element method (FEM) simulation results demonstrates that the analytical model's predictions closely align with FEM simulations.

Mulidrán et al. (2021) have observed that the simulation outcomes of TRIP steel in V-bending revealed a strong correlation between experimental and numerical data, particularly when employing a combination of the Hill48 and Barlat yield criteria in conjunction with the Ludwik hardening law. This correlation was notably evident when a calibration force ( $F$ ) of 900 N was applied.

Xie (2013) employed a finite element model to analyze the air bending process. Experimental tests are conducted using ST12 materials to validate the finite element model results. The comparative analysis demonstrates that the numerical model accurately predicts springback in 2D draw bending. Key conclusions from this study include springback in the air bending process increases with punch displacement, friction coefficient and punch radius.

Dametew et al. (2017) examined various factors, including sheet metal thickness, sheet metal type (Aluminium, copper, mild steel, and High-strength steels), friction, tool radius, and tool shape to assess their influence on springback. The empirical results revealed that increasing the sheet metal thickness from 0.8 mm to 4.5 mm resulted in a reduction of springback by 16%. It was observed that as the sheet metal's strength increased, springback also increased. Consequently, materials with higher yield strength exhibited greater springback after unloading. Substituting Aluminium sheet metal for high-strength sheet metals led to a significant reduction in springback, approximately 56%. Reducing the tool radius contributed to a decrease in springback. Increasing the friction coefficient from 0.01 to 0.50 resulted in a 52% increase in springback.

Panthi et al. (2010) adopted an innovative approach incorporating a total-elastic–incremental-plastic (TEIP) algorithm suitable for handling large deformations and substantial rotational problems within an indigenous Finite Element software. This software was employed to predict springback in a typical sheet metal bending process. The findings revealed that the degree of springback increases as the sector angle is increased. Friction between the blank and the tool has a negligible effect on springback. Springback exhibits an increase with higher yield stress and greater strain hardening, but conversely decreases as Young's modulus increases.

### **6.10 Limitations of present research work**

Experimental, analytical, and numerical studies on the springback of 2-ply and 3-ply laminate composites consisting of aluminium and stainless steel have certain limitations. Here are some common limitations associated with these studies:

*Simplified Assumptions:* Both Numerical and analytical models rely on certain assumptions to simplify the complex behaviour of the laminated composites. These assumptions may not fully capture all the real-world complexities, such as variations in material properties, interfacial effects, or non-linear behaviour, potentially leading to deviations between predicted and actual springback behaviour. Springback predicted by FE simulations are closer to the values obtained by experimental work than that predicted by proposed analytical model. This could be attributed to the assumption of plane strain condition and neglecting neutral axis shift and Bauschinger effect in the analytical model. Also, the material model used in FE simulations is more robust as it uses complete plastic stress and plastic strain data, whereas analytical model is based on the input values of elastic and plastic material properties.

*Material Property Variations:* Clad composites often exhibit variations in material properties due to the presence of dissimilar layers such as aluminium and stainless steel. Experimental studies rely on the assumption of uniform properties within the laminate, which may not accurately represent the true material behaviour. This can result in discrepancies between the predicted and actual springback.

*Interface Effects:* The interaction between the layers in laminate composites can have a significant impact on the springback behaviour. Analytical and numerical models often simplify or neglect the interfacial effects, assuming perfect bonding or neglecting interlayer slip. However, interfacial phenomena can influence the overall springback response, potentially leading to differences between predicted and observed behaviour.

*Complexity of the Bending Process:* Bending process involves various parameters, such as stresses during bending, shift in neutral axis, bending angle, tooling design, and material combination, which influences springback. Analytical and numerical models attempt to capture these complexities, but the accuracy of the predictions may be limited due to uncertainties in these parameters or the assumptions made in the models.

*Sensitivity to Modelling Parameters:* Numerical models, such as finite element analysis, require the selection of various modelling parameters, including mesh density, boundary conditions, and material properties. The accuracy of the results obtained from numerical simulations is dependent on these parameters, and an improper selection or variation in these parameters can lead to discrepancies between predicted and observed springback behaviour.

*Validation Challenges:* Experimental validation of springback behaviour in laminate composites can be challenging due to the difficulties in measuring and characterizing the complex deformations involved. Obtaining accurate and reliable experimental data for validation purposes can be time-consuming and costly.

Despite these limitations, experimental, analytical, and numerical studies provide valuable insights and aid in understanding the springback behaviour of laminate composites. They form a foundation for process optimization, design improvements, and control strategies. It's important to acknowledge these limitations and consider them when interpreting and applying the results of such studies.

## CHAPTER 07

### CONCLUSIONS AND FUTURE RESEARCH SCOPE

#### 7.1 Summary

The first chapter of the thesis is introductory in nature. It includes a brief introduction to sheet metal forming, sheet metal forming operations, especially bending, sheet metal forming defect-springback, manufacturing methods of clad sheet metals, advantages, and applications of clad sheets. The second chapter includes a literature review related to the springback of different monolithic materials and clad sheets. This chapter also discusses the springback influencing factors and presents research gaps and proposed research objectives. The third chapter deals with the methodology adopted for the development of analytical models for springback prediction in V-bending of 2-ply (SS430/AA1050) and 3-ply (SS430/AA1050/SS304) clad sheets, in detail. This chapter, also, includes the effect of sheet setting conditions on springback behaviour in analytical models of 2-ply and 3-ply clad sheets. The Fourth Chapter describes the development of FE simulation procedures for the prediction of springback of 2-ply (SS430/AA1050) and 3-ply (SS430/AA1050/SS304) clad sheets. FE simulations for bending and springback also involve the effect of sheet setting conditions on the prediction of springback of both 2-ply and 3-ply clad sheets. The fifth chapter presents the methodology of all experimental procedures. Different experiments for tensile properties, anisotropy and hardness measurements etc. which are conducted to characterize the properties of AA1050, SS430, SS304, 2-ply and 3-ply laminated sheets are described in this chapter. The experimental setup fabricated for the removal of the SS430 layer from a 2-ply (SS430/AA1050) clad sheet and the setup for springback characterization of parent materials and 2-ply and 3-ply laminated composites in V-bending is also described in this chapter. In the sixth chapter, the results of various experiments conducted to characterize the mechanical properties of 2-ply and 3-ply

clad sheets are presented and discussed. The mechanical properties of different material like SS430, SS304, and Al1050 are also presented in detail. This chapter also describes the results of springback experimentally, numerically, and analytically in detail. The seventh chapter concludes the entire research work and projects the future research scopes for further study.

## **7.2 Conclusions**

In the present study, analytical, experimental, and numerical methods are employed to investigate the springback behaviour of two layered laminated sheet metals made of AA1050 and SS430 and three-layered laminated sheet metals made of AA1050 sandwiched between sheets of SS430 and SS304. Investigations are also conducted into how sheet setting conditions affects the springback behaviour of laminated sheet metals during V- bending. Using experimental and FE simulation methods, the residual stresses that arise on outer and inner surfaces of the bending samples are examined. Several experiments have been conducted for characterization of mechanical properties of AA1050, SS430, SS304, 2-ply and 3-ply clad sheets.

The major findings of this research study can be summarized as

1. The values of tensile strength, ductility, and strain hardening exponent of 2-ply sheet lie in between the properties of individual layers of AA1050 and SS430. In both the cases of placement of the 2-ply sheet during bending, the specimens oriented at 45° to the rolling direction experience the highest springback followed by the specimens oriented at 0° and 90° with respect to the rolling direction (RD) which may be attributed to the higher tensile strength of the 2-ply sheet and the combined effect of anisotropy of both the layers at the zone of deformation.
2. The springback results for the samples of the 2-ply sheet are slightly lower than the springback results of individual sheet samples of AA1050, suggesting that the higher thickness of the sheet outweighs the effect of the tensile strength of the steel layer in the samples.

3. In all the cases of springback experiments of a 2-ply sheet with AA1050 as inner layer, the springback values are higher than the values obtained with the specimens with SS430 as an inner layer which can be attributed to the higher tensile strength of steel and higher bending radius experienced by it in the outer layer during bending.
4. The variation of stress through thickness, after springback, obtained by simulations shows that the thinner sheet is constrained from undergoing complete springback by the thicker sheet, and hence, the residual stress in the thinner sheet remains of the same nature as that of bending stress although substantially reduced in magnitude.
5. During bending of 2-ply sheet, thickness of specimens is decreased in the case of the AA\_out/SS\_in and increased in the case of AA\_in/SS\_out.
6. The springback results obtained by experiments, simulations and analytical models are in good agreement for 2-ply clad sheets.
7. The tensile strength, yield strength and strain hardening exponent of the specimens of 3-ply clad sheet oriented at transverse direction of the RD are higher than that of the specimens with other two orientations w.r.t. the RD. This representative strength of the clad sheet can be attributed to the strength of the individual sheets in a particular direction.
8. The samples of the 3-ply clad sheet which are transverse to the RD, exhibit highest springback values due to the higher tensile strength of the sheet when compared with the results acquired for the other two orientations w.r.t. the RD. These results are close to the springback results obtained from simulation and analytical methods.
9. On comparing the springback results with reference to the specimen's orientations in both the cases of sheet placements, it is observed that the springback values of the 3-ply clad sheet specimens placed with inner layer of SS304 during bending experience slightly higher springback when compared with the values of springback in specimens with inner layer of SS430.
10. The springback results obtained after bending of the 3-ply clad sheet by using experimental, analytical and simulations techniques are in agreement in all the cases of sheet placements,

although simulation results are closer to the experimental results than that of the analytical results. The nearness of simulation results to the experimental results than the analytical results can be attributed to the assumptions in the analytical model and the material model.

11. In the case of bending of clad sheet with inner layer of SS304, after springback, it is observed that the innermost layer always shows the tensile residual stress, whereas the outermost layer is set with a higher value of compressive residual stress in all the specimens. This indicates that the outermost layer of SS430 is able to undergo complete springback, whereas the thinner layer of SS304 is still slightly constrained due to adjoining layer of thicker aluminium.

12. In both clad sheets (2-ply and 3-ply), springback can be reduced by reducing the bending radius/punch profile radius. The present study confirms that the springback can fairly be controlled by taking optimal value of bending radius/punch profile radius.

### **7.3 Future research work**

There are some issues that can be addressed in future: -

1. In the present research, 2-ply AA1050/SS430 and 3-ply SS430/AA1050/SS304 laminated sheets have been used in V-bending. In future research, different clad sheets can be used as these sheets are widely used in various applications in the different industries. In place of V-bending, U-bending, draw bending can be studied in future.

2. In the present investigations, FEA, analytical and experimental approaches have been included for prediction of springback. Artificial neural network (ANN), RSM, Taguchi etc. optimization methods are also the potential fields for the future research.

3. Springback influencing parameters like sheet setting conditions, punch radii have been taken in the present research work. Other important parameters like punch force, thickness ratios, die opening angle can be included in the future research.

4. During bending, thickness of metal strip is changed but in present study, analytical models are developed with assumption of constant strip thickness throughout the bending. Thus, analytical model may also be modified by incorporating thickness change during bending.
5. Further, the present study can be extended to address spring back compensation during the bending operation of clad sheets (such as 2-ply, 3 ply clad sheets etc.).



## REFERENCES:

- 1 Abedi R., Akbarzadeh A., 2015. Bond strength and mechanical properties of three-layered St/AZ31/St composite fabricated by roll bonding. *Materials & Design* 88, 880-888.
- 2 Aghchai A Jalali, Shakeri M, Dariani B Mollaei, 2008. Theoretical and experimental formability study of two-layer metallic sheet (Al1100/St12). *Proceedings of the Institution of Mechanical Engineers, Part B: Journal of Engineering Manufacture* 222, 1131-1140.
- 3 Aghchai A. Jalali, Abolghasemi Amirali, Moradkhani Behrooz, Tajik Morteza, 2017. Experimental, theoretical and numerical investigation of springback behaviour of Al/composite/Al sandwich sheet. *Journal of Sandwich Structures and Materials* 19(6), 1-20.
- 4 B. Osgurg, G. Lengfeld, O. S., 2012. Innovation and globalization as a factor of success for global hot stamping growth. In: Liewald, M. (Ed.), *New Developments in Sheet Metal Forming*. pp. 79-92
- 5 Banabic, D., 2010. *Sheet Metal Forming Processes: Constitutive Modelling and Numerical Simulation*. Springer, Berlin.
- 6 Billur, M., Altan, T., 2012. Challenges in forming advanced high strength steels. *Proceedings of New Developments in Sheet Metal Forming*, 285-304.
- 7 Bonora, N., Gentile, D., Pirondi, A., Newaz, G., 2005. Ductile damage evolution under triaxial state of stress: theory and experiments. *International Journal of Plasticity*, 21, 981-1007.
- 8 Buang M.S., Abdullah S.A. and Saedon J., 2015. Effect of Die and Punch Radius on Springback of Stainless-Steel Sheet Metal in the Air V-Die Bending Process. *Journal of Mechanical Engineering and Sciences (JMES)* 8, 1322-1331.

- 9 Burchitz IA. Improvement of springback prediction in sheet metal forming, 2008. University of Twente, PhD thesis. Rotterdam, The Netherlands.
- 10 Chatti, S., Hermi, N., 2011. The effect of non-linear recovery on springback prediction. *Computers & Structures* 89, 1367-1377
- 11 Cho, J.R., Moon, S.J., Moon, Y.H., Kang, S.S., 2003. Finite element investigation on springback characteristics in sheet metal U-bending process. *Journal of Materials Processing Technology* 141, 109-116.
- 12 Chongthairungruang, B., Uthaisangsuk, V., Suranuntchai, S., Jirathearanat, S., 2013. Springback prediction in sheet metal forming of high strength steels. *Materials & Design* 50, 253-266.
- 13 Custompartnet.com, accessed in May, 2018.
- 14 Dadras, P. and Majlessi, S.A. 1982. Plastic bending of work hardening materials', *Transactions of the ASME*, vol. 104, 224-230.
- 15 Dametew AW and Gebresenbet T, 2017. Study the Effects of SpringBack on Sheet Metal Bending using Mathematical Methods. *Journal of Material Sciences & Engineering*, Vol. 5(6).
- 16 Dieter, G.E., Bacon, D., 1986. *Mechanical metallurgy*. McGraw-Hill New York.
- 17 Dilip Kumar K, Appukuttan KK, Neelakantha VL, Naik PS, 2014. Experimental determination of spring back and thinning effect of aluminum sheet metal during L-bending operation. *Materials and Design*, 56, 613-619.
- 18 Donaldson, C., LeCain, G.H., Goold, V., Ghose, J., 2012. *Tool design*. Tata McGraw-Hill Education.
- 19 Etemadi E, Naseri A, Valinezhad M., 2020. Novel U-bending designed setups for investigating the springback/spring-go of two-layer aluminum/copper sheets through experimental tests and finite element simulations. *Proceedings of the*

- Institution of Mechanical Engineers, Part L: Journal of Materials: Design and Applications, Vol. 234 (8), pp. 1142-1153.
- 20 Etemadi E, Rahmatabadi D, Hosseini S.M, Hashemi R.,2020. Experimental investigation of springback phenomenon through an L-die bending process for multi-layered sheets produced by the accumulative press bonding technique. Proc. Inst. Mech. Eng. Part L J. Mater. Des. Application, 234, 1550–1559.
- 21 Fish, J., Belytschko, T., 2007. A first course in finite elements. John Wiley & Sons.
- 22 Gardiner FJ., 1957. The springback of metals. Transaction of ASME 79, pp.1-9.
- 23 Gau, J.-T., Kinzel, G.L., 2001. A new model for springback prediction in which the Bauschinger effect is considered. International Journal of Mechanical Sciences 43, 1813-1832.
- 24 Gautam Vijay, Sharma Pankaj and Kumar D. Ravi, 2018 Experimental and Numerical Studies on Springback in U-Bending of 3-Ply Cladded Sheet Metal. Materials Today Proceedings, 5: 4421-4430.
- 25 Gautam, V., and Kumar, D. R., 2017, "Experimental and numerical investigations on springback in V-bending of tailor-welded blanks of interstitial free steel," Proceedings of the Institution of Mechanical Engineers, Part B: Journal of Engineering Manufacture, 232 (12) p
- 26 Geng, L., Wagoner, R.H., 2002. Role of plastic anisotropy and its evolution on springback. International Journal of Mechanical Sciences 44, 123-148.
- 27 Hai Vuong Gia, Nguyen Minh Thi Hong and Nguyen Duc Toan, 2020. A study on experiment and simulation to predict the springback of SS400 steel sheet in large radius of V-bending process, Materials Research Express, 7, 016562.
- 28 He Xiaofan, Dong Yinghao, Li Yuhai, Wang Xiangming, 2018. Fatigue crack growth in diffusion-bonded Ti-6Al-4V laminate with unbonded zones. International Journal of Fatigue, Vol. 106, pp. 1-10.

- 29 Hibbit, Karlsson, and Sorensen, 2007. ABAQUS/Standard Analysis User's Manual, Hibbit, Karlsson, Sorensen Inc.
- 30 Hino Ryutaro, Goto Yoshihiro and Yoshida Fusahito, 2003. Springback of sheet metal laminates in draw-bending. *Journal of Materials Processing Technology* 139, 341-347.
- 31 Hosford, W.F., Cadell, R. M., 2007. *Metal forming- Mechanics and Metallurgy*. Cambridge University Press.
- 32 <https://www.emsclad.com>, 2018
- 33 Jamaati R., Toroghinejad M.R., 2010. Effect of friction, annealing conditions and hardness on the bond strength of Al/Al strips produced by cold roll bonding process. *Materials & Design* 31(9), 4508-4513.
- 34 Jones, R. M., 2014. *Mechanics of Composite Materials*, CRC Press, Philadelphia, PA.
- 35 Kagzi Shakil A., Gandhi Anish H., Dave Harshit K., Raval Harit K., 2016. An analytical model for bending and springback of bimetallic sheet. *Mechanics of Advanced Materials and Structures* 23(1), 80-88.
- 36 Kagzi Shakil A. & Raval H. K., 2022. Mathematical modelling to predict springback in bimetallic material including material anisotropy during bending, *Advances in Materials and Processing Technologies*, DOI: 10.1080/2374068X.2022.2118905.
- 37 Kalpakjian Serope and Schmid Steven R., 2014. *Manufacturing engineering and technology*. New Delhi, Pearson Publications.
- 38 Kalpakjian, S., Schmid, S.R., Kok, C.-W., 2008. *Manufacturing processes for engineering materials*. Pearson-Prentice Hall.
- 39 Karalar Mert and Bayramoğlu Melih, 2022. Combined impacts of thickness and bending angle on springback of 1000DP steel sheets. *Advances in Materials and Processing Technologies*, 693-698

- 40 Kartik T and Rajesh R, 2017. Effect of Punch Radius and Sheet Thickness on Springback in V-die Bending. *Advances in Natural and Applied Sciences* 11(8), 178-183.
- 41 Kazan, Recep, Firat, Mehmet and Tiryaki, Aysun Egrisogut, 2009. Prediction of springback in wipe-bending process of sheet metal using neural network. *Materials & Design*, Vol.30(2), pp.418-423.
- 42 Kim I.K., Hong S.I., 2014. Mechanochemical joining in cold roll-cladding of tri-layered Cu/Al/Cu composite and the interface cracking behavior. *Materials & Design* 57, 625-631.
- 43 Kim I.K., Hong S.I., 2013. Effect of component layer thickness on the bending behaviors of roll-bonded tri-layered Mg/Al/STC clad composites. *Materials & Design* 49, 935-944.
- 44 Kim J.K, Xi Yu Tong., 1997. Forming and failure behaviour of coated, laminated and sandwiched sheet metals: a review. *Journal of Materials Processing Technology* 63(1-2), 33-42.
- 45 Lafta Hameed D., Shahab Ayad F. and Ahmed Shadi Bakr, 2020. Experimental and Numerical Study the Effect of Process Parameters on Springback of Al/Cu Bimetallic Sheet in V- Bending Process. *International Journal of Mechanical & Mechatronics Engineering*, Vol. 20 (1), 35-47.
- 46 Lee, M.-G., Kim, D., Kim, C., Wenner, M.L., Chung, K., 2005. Springback evaluation of automotive sheets based on isotropic–kinematic hardening laws and non-quadratic anisotropic yield functions, part III: applications. *International Journal of Plasticity* 21, 915-953.
- 47 Li Long, Nagai Kotobu and Yin Fuxing, 2008. Progress in cold roll bonding of metals. *Science and Technology of Advanced Materials*, Vol. 9 (2), pp.1-11.

- 48 Li, Z., Winther, G., Hansen, N., 2006. Anisotropy in rolled metals induced by dislocation structure. *Acta Materialia* 54, 401-410.
- 49 Lingbeek, R., Huétink, J., Ohnimus, S., Weiher, J., 2005. Iterative springback compensation of numisheet benchmark# 1. *AIP Conf. Proc.* 778, 328-333.
- 50 Lubahn, J.D. and Sachs, G.1950. Bending of an ideal plastic metal. *Transactions of the ASME*, vol. 72, 201-208.
- 51 Luo JG, Acoff VL, 2004.Using cold roll bonding and annealing to process Ti/Al multi-layered composites from elemental foils. *Materials Science and Engineering: A.*, Vol. 379, pp. 164-172.
- 52 Magar Varsha M. and Agrawal Naveen, 2023. Process parameter optimization for springback in steel grade sheet materials under V-bending using FEM and ANN approach. *Ironmaking & Steelmaking*, Taylor & Francis.
- 53 Manesh H.D., Taheri A.K., 2003. Bond strength and formability of an aluminum-clad steel sheet. *Journal of Alloys and Compounds* 361(1–2), 138-143.
- 54 Marciniak, Z.D., JL;Hu,SJ, 2002. *Mechanics of Sheet Metal Forming*, second edition ed. Butterworth Heinemann.
- 55 Martin, G. and Tsang, S. (1966). The plastic bending of beams considering die friction effects. *Journal of Engineering for Industry*, vol. 88, 237-250.
- 56 Mohamed H A. and Washbush J., 1975. Mechanism of solid-state pressure welding. *Weld. Res. Suppl.* 9.
- 57 Mohammadi S. V., Parsa M. H., Aghchai A. Jalali, 2011. Effect of the thickness distribution and setting condition on springback in multi-layer sheet bending. *International Journal of Engineering, Science and Technology* 3(4), 225-235.
- 58 Mohammadi SV, Parsa MH, Aghchai A Jalali, 2015. Simplified Springback Prediction in Al/PP/Al Sandwich Air Bending. *Journal of Sandwich Structures and Materials*, 17(3), 1-21.

- 59 Morestin, F., Boivin, M., 1996. On the necessity of taking into account the variation in the Young modulus with plastic strain in elastic-plastic software. *Nuclear Engineering and Design* 162, 107-116.
- 60 Mori T., Kurimoto S., 1996. Press-formability of stainless steel and aluminum clad sheet. *Journal of Materials Processing Technology* 56(1), 242-253.
- 61 Mulidrán Peter, Spišák Emil, Tomáš Miroslav, Majerníková Janka and Varga Ján, 2021. The Effect of Material Models in the FEM Simulation on the Springback Prediction of the Trip Steel, *ACTA METALLURGICA SLOVACA*, Vol. 27 (3), 103-108.
- 62 Okui Toshiyuki, Yonemitsu Yoshihisa, Yoshida Kentarou. 2014. Development of Metal Clad Sheets and Strips. *Nippon Steel & Sumitomo Metal Technical Report No. 106*.
- 63 Panthi S.K., Ramakrishnan N., Ahmed Meraj, Singh Shambhavi S., Goel M.D., 2010. Finite Element Analysis of sheet metal bending process to predict the springback. *Materials and Design*, 31, 657-662.
- 64 Papeleux, L., Ponthot, J.-P., 2002. Finite element simulation of springback in sheet metal forming. *Journal of Materials Processing Technology* 125–126, 785-791.
- 65 Parsa Mohammad Habibi, Mohammadi Seyed Vahid, Mohseni Ehsan, 2015. Thickness change and springback of cold roll bonded aluminum/copper clad sheets in air bending process. *Proceedings of the Institution of Mechanical Engineers, Part B: Journal of Engineering Manufacture*, 1-15.
- 66 Patel Chintan K., 2014. Investigation of spring back behaviour of SS-304 steel and its bi-layer material in v bending. *Mechanical Engineering: An International Journal (MEIJ)*1(2), 43-52.

- 67 Pourboghrat, F., Chung, K., Richmond, O., 1998. A hybrid membrane/shell method for rapid estimation of springback in anisotropic sheet metals. *Journal of applied mechanics* 65, 671-684.
- 68 Rahdiana et al. (2023) have done investigations on springback of the V-bending process for SS304. They have observed that springback of SS304 blank is increased when bending radius increased. They have concluded that springback is proportional to bending radius.
- 69 Şen Nuri and Taşdemir Vedat, 2021. Experimental and numerical investigation of the springback behaviour of CP800 sheet after the V bending process. *Advances in Materials and Processing Technologies*, 811-818.
- 70 Senol Ozgu, Esat Volkan and Haluk Darendeliler, 2014. Springback analysis in air bending process through experiment based artificial neural networks. *Procedia Engineering, Elsevier*, 81, 999-1004.
- 71 Serban, FM, Balci, Nicolae, Achimaş, Gheorghe and Cristea, Ciprian, 2013. Research Concerning the Springback Prediction in the Bending Operations. *Advanced Engineering Forum*, Vol. 8-9, pp 490-499
- 72 Siegert, K., Wagner, S., 1994. Stretch forming. TALAT Lecture 3703.
- 73 Srinivasan R. and Karthik Raja G., 2019. Experimental study on bending behaviour of aluminium-copper clad sheets in V-bending process. *Mechanics & Industry*, 20 (6).
- 74 Tan, Z., Persson, B. and Magnusson, C. 1995. Plastic bending of anisotropic sheet Metals. *International Journal of Mechanical Sciences*, vol. 37, 405-421.
- 75 Tekaslan, Ö., Gerger, N., Şeker, U., 2008. Determination of springback of stainless steel sheet metal in “V” bending dies. *Materials & Design* 29, 1043-1050.
- 76 Thibaud, S., Boudeau, N., Gelin, J., 2002. On the Influence of the Young Modulus Evolution on the Dynamic Behaviour and Springback of a Sheet Metal Forming



- Component. Proceedings of NUMISHEET 2002, Jeju Island, Korea, Vol.1, 149-154.
- 77 Trieu Q.H., Vuong G.H. and Nguyen D.T., 2023. Predictive Modeling of SpringBack Behaviour in V-bending of SS400 Steel Sheets under Elevated Temperatures Using Combined Hardening Laws, *Applied Sciences*, 13, 10347.
- 78 [triclاد.com](http://triclاد.com), accessed in December, 2022.
- 79 Tseng H.C., Hung C., Huang C.C., 2010. An analysis of the formability of aluminum/copper clad metals with different thicknesses by the finite element method and experiment. *The International Journal of Advanced Manufacturing Technology* 49(9-12), 1029-1036.
- 80 Tsuji N, Ito Y, Saito Y. and Minamino Y., 2002. Strength and ductility of ultrafine grained aluminum and iron produced by ARB and annealing. *Scripta materialia*, Elsevier, 47(12) pp. 893-899.
- 81 Valinezhad M, Etemadi E and Hashemi R, 2019. Experimental and FE analysis on springback of copper/aluminum layers sheet for a L-die bending process. *Materials Research Express*, 6 (11), 1-13.
- 82 Van Boxel, S., 2010. Anisotropic Work-Hardening and Strain Path Effects in an AlMn Alloy. Grenoble INP.
- 83 Verma, R.K., Haldar, A., 2007. Effect of normal anisotropy on springback. *Journal of Materials Processing Technology*, 190, 300-304.
- 84 Wagoner, R., 2002. Fundamental aspects of springback in sheet metal forming, Proceedings of the 5<sup>th</sup> International Conference and Workshop on Numerical Simulation of 3D Sheet Forming Processes, Verification of Simulation with Experiment, NUMISHEET 2002, Jeju Island, Korea, Vol.1, 13-19.
- 85 Wagoner, R.H., Lim, H., Lee, M.-G., 2013. Advanced Issues in springback. *International Journal of Plasticity* 45, 3-20.

- 86 Wahed M.A., Gupta A.K., Gadi V.S.R, K. Supradeepan, Singh S.K., Kotkunde N., 2020. Parameter optimisation in V-bending process at elevated temperatures to minimise springback in Ti-6Al-4V alloy. *Advances in Materials and Processing Technologies*, Vol 6, 350-364.
- 87 Wang Chuanjie, Wang Shan, Wang Shuting, Chen Gang Chen and Zhang Peng, 2019. Investigation on Springback Behaviour of Cu/Ni Clad Foils during Flexible Die Micro V-bending Process, *metal*, 9, 892-903.
- 88 Wang Pengju, Zhong Ning, Tu Liyue, Hong Weiming, Lv Yanming, Chen Yonghong, Sun Jian, Luo Caiyong, Chen Zejun and Tang Qian, 2023. Fabrication of AlZn4SiPb/Steel Clad Sheets by Roll Bonding: Their Microstructure and Mechanical Properties, *Crystals*, 13(2).
- 89 Wasif Muhammad, Iqbal Syed Amir and Karim Muhammad Tufail Hassan, 2020. Experimental Analysis and Prediction of Springback in V-bending Process of High-Tensile Strength Steels. *Transactions of the Indian Institute of Metals*, 73, p.p 285–300.
- 90 Weiss M, Rolfe BF, Dingle ME, 2004. The influence of interlayer thickness and properties on springback of SPS-(steel/polymer/steel) laminates. *Steel Grips* 2, 445–449.
- 91 Woo, D. M. and Marshall, J., 1959. Springback and Stretch Forming of Sheet Metal. *The Engineer*, Vol. 28, pp. 135-136.
- 92 Wright P K, Snow D A. and Tay C K., 1975. Interfacial conditions and bond strength in cold pressure welding by rolling. *Metals Technology*, Vol. 5, pp. 24-31.
- 93 Yilamua K., Hino R., Hamasaki H. and Yoshida F, 2010. Air bending and springback of stainless-steel clad aluminum sheet. *Journal of Materials Processing Technology* 210, 272-278.

- 94 Yoon, J.W., Pourboghrat, F., Chung, K., Yang, D.Y., 2002. Springback prediction for sheet metal forming process using a 3D hybrid membrane/shell method. *International Journal of Mechanical Sciences*, 44, 2133-2153.
- 95 Yuen WYD, 1996. A Generalized solution for the prediction of springback in laminated strip. *Journal of Material Processing Technology*, 61(3), 254–264.
- 96 Xie, Li, 2013. Effects of Air Bending Parameters on Spingback Using Finite Element Analysis. *Applied Mechanics and Materials*, Vol. 423-426, 978-983.
- 97 Zhai Ruixue, Zhao Zhuangkun, Yang Jianhao, Ma Bangbang and Yu Gaochao, 2021. Analytical Prediction of Stretch-Bending Springback Based on the Proportional Kinematic Hardening Model. *Symmetry*, 13, 2389.
- 98 Zhang Dong-juan, Cui Zhen-shan, Chen Zhi-ying and Ruan Xue-yu, 2007. An analytical model for predicting sheet springback after V-bending, *Journal of Zhejiang University SCIENCE A*, 8(2), 237-244.
- 99 Zhu, H.X. 2007. Large deformation pure bending of an elastic plastic power-law - hardening wide plate: analysis and application. *International Journal of Mechanical Sciences*, vol. 49, pp. 500-514.

## **PUBLICATIONS BASED ON THE PRESENT WORK**

The followings are the publications in journals and conferences based on the present work.

### **International Journals: -**

1. Sharma Pankaj Kumar, Gautam Vijay, and Agrawal Atul Kumar, 2021. Analytical and Numerical Prediction of Springback of SS/Al-Alloy Cladded Sheet in V-bending. Journal of Manufacturing Science and Engineering, Vol. 143, 031011-1, **ASME (I/F-4.0)**
2. Sharma Pankaj Kumar, Gautam Vijay, and Agrawal Atul Kumar, 2021. Experimental and numerical investigation of springbuck and residual stress in bending of a three-ply clad sheet. Proc IMechE Part L: Journal of Materials: Design and Applications, Vol 235 (12), pp. 2823–2838, **SAGE (I/F-2.4)**.
3. Sharma Pankaj Kumar, Gautam Vijay and Agrawal Atul Kumar. 2022. Investigations on Effect of Bending Radius on Springback Behaviour of Three-Ply Clad Sheet. Materials Today: Proceedings, Vol 62 (3), 1651-1657, **Elsevier**.
4. Sharma Pankaj Kumar, Gautam Vijay and Agrawal Atul Kumar, 2023. Effect of punch profile radius and sheet setting on springback in V-bending of A 2-ply sheet. Advances in Materials and Processing Technologies, Vol 9(2), pp. 416-424, **Taylor & Francis**.
5. Gautam Vijay, Sharma Pankaj, and Kumar D. Ravi, 2018. Experimental and numerical studies on springback in U-bending of 3-ply cladded sheet metal, Materials Today: Proceedings Vol 5 (2), 4421-4430, **Elsevier**.

### **International Conferences: -**

1. Sharma Pankaj Kumar, Gautam Vijay, and Agrawal Atul Kumar. Investigations on Effect of Bending Radius on Springback Behaviour of Three-Ply Clad Sheet. International Conference on Recent Advances in Modelling and Simulation Techniques in Engineering and Sciences (RAMSTES-2021), held at Manipal University Jaipur, India during December 08-10<sup>th</sup>, 2021.

2. Sharma Pankaj Kumar, Gautam Vijay, and Agrawal Atul Kumar, 2022. Effect of punch profile radius and sheet setting on springback in V-bending of A 2-ply sheet. 2<sup>nd</sup> International Conference on Industrial and Manufacturing Systems (CIMS-2021), held at Punjab Engineering College, Chandigarh, India during 11-13<sup>th</sup> November 2021.

## BIO DATA

Mr. Pankaj Kumar Sharma was born in Uttar Pradesh on 1<sup>st</sup> July 1981. He did B. Tech and M.Tech in Mechanical Engineering from U.P. Technical University, Lucknow (presently AKTU, Lucknow) in 2004 and 2014, respectively. He is currently working as an Assistant Professor in the Department of Mechanical Engineering, RKGIT, Ghaziabad. He is pursuing Ph.D from Delhi Technological University, India since July 2016 under the guidance of Prof. Vijay Gautam and Prof. Atul Agrawal. He has more than eighteen years of teaching experience in leading institutions of Delhi NCER region, like RKGIT Ghaziabad, NIET Greater Noida, IMSEC Ghaziabad & Indian Institute of Packaging Delhi. He has also worked as an Assistant Engineer in Bhushan Steel Ltd., Ghaziabad (presently TATA Steel Ltd.). His research interest includes mechanics, reinforcement-based composites and forming of laminated composites. He has published more than ten papers in national and international journals/conferences.

He has received research award of one lakh rupees (Premier Research Award) from Delhi Technological University, Delhi in the year of 2022 for his paper titled on “Analytical and Numerical Prediction of Springback of SS/Al-Alloy Cladded Sheet in V-bending”, Journal of Manufacturing Science and Engineering, Vol. 143, 031011-1, **ASME (I/F-4.0)**